NATIONAL TECHNICAL UNIVERSITY OF ATHENS
SCHOOL OF NAVAL ARCHITECTURE & MARINE ENGINEERING
DIVISION OF MARINE ENGINEERING

Diploma Thesis

Tribological Study of the Stern Tube Bearing of Marine Vessels

Rossopoulos Georgios Nikitas

Thesis Committee:

Supervisor:	**C.I. Papadopoulos, Assistant Professor NTUA**
Members:	**L. Kaiktsis, Associate Professor NTUA**
	G. Papalambrou, Assistant Professor NTUA

Athens, March 2018

ΕΘΝΙΚΟ ΜΕΤΣΟΒΙΟ ΠΟΛΥΤΕΧΝΕΙΟ
ΣΧΟΛΗ ΝΑΥΠΗΓΩΝ ΜΗΧΑΝΟΛΟΓΩΝ ΜΗΧΑΝΙΚΩΝ
ΤΟΜΕΑΣ ΝΑΥΤΙΚΗΣ ΜΗΧΑΝΟΛΟΓΙΑΣ

Διπλωματική Εργασία

Τριβολογική Μελέτη Πρυμναίου Εδράνου Χοάνης Πλοίων

Ρωσσόπουλος Γεώργιος Νικήτας

Εξεταστική επιτροπή:

Επιβλέπων:	**Χ.Ι. Παπαδόπουλος, Επίκουρος Καθηγητής ΕΜΠ**
Μέλη:	**Λ. Καϊκτσής, Αναπληρωτής Καθηγητής ΕΜΠ**
	Γ. Παπαλάμπρου, Επίκουρος Καθηγητής ΕΜΠ

Αθήνα, Μάρτιος 2018

Table of Contents

Acknowledgements

This work marks the end of my undergraduate studies in the School of Naval Architecture and Marine Engineering of NTUA, therefore I would like to express my gratitude to all those people who supported me during the past five years.

First of all, I would like to thank my family for their support and trust towards me in my entire student life. Their strength and faith in my success has helped me successfully overcome every obstacle I faced. Additionally I feel indebted for all the sacrifices they have done for me, in order to give me the chance to educate myself.

Furthermore I would like to thank from the bottom of my heart my supervisor, Dr. Christos Papadopoulos, for being an excellent collaborator, a mentor and a tutor at the same time. His assistance was of great importance not only for the completion of the present thesis but also for my personal development.

Special thanks goes to Dr. Christos Leontopoulos from ABS, whose mentoring introduced to me the field of Shaft Alignment and Tribology and intrigued me for this particular thesis. His contribution to this work and also his trust towards me, has been of great importance and thereof I am in great debt.

I would also like to thank Mr. L. Kaniaros from Anangel Maritime Company for his kind mentoring during my internship and for the chance that he gave me to explore for the first time the Shaft Alignment issue.

I would also like to thank Sotiris Nanopoulos for his help with programming and for all the useful insight and guidance he provided during the first steps of my work.

Last but not least I would like to thank my friends and classmates for their friendship and encouragement throughout our studies in NTUA. All these experiences and memories would never be the same, if I had been alone.

Abstract

Friction is one of the most important causes of energy losses in mechanical systems. In ships, substantial friction losses are present in the propulsion system, both in the engine and in the shaft arrangement. A proper shaft alignment should be attained in order not only to minimize these losses but also in order to avoid catastrophic failures. Journal bearings are mechanical components used to support the radial loads of rotating shafts. During operation, a thin lubricant film is created and maintained hydrodynamically between the shaft and the bearing, minimizing friction losses and preventing metal to metal contact. Performance of journal bearings is commonly quantified in terms of minimum lubricant thickness, friction losses and maximum pressure of the lubricant. All the above change substantially at different operating conditions (radial load, shaft rotational speed, lubricant viscosity). The stern tube bearing supports the weight of the overhanged propeller, as well as all transient hydrodynamic loads due to propeller operation; thus special attention must be applied during its design.

In this research project, the optimum geometric parameters of a double slope aft stern-tube bearing are sought, for (a) maximizing the contact area between the bearing and the propeller shaft, and (b) minimizing the maximum local pressure exerted on the bearing surface. Here, the aft stern-tube bearing is modeled parametrically; apart from generic geometric parameters (L/D ratio, diameter, clearance, misalignment angle), additional geometric design parameters of the bearing are the two slope angles of the bearing surface and the longitudinal length of each sloped region. The computational approach used in the present study evolves from the solution of the Reynolds differential equation, which describes the phenomenon of hydrodynamic lubrication in the oil domain between the shaft and the bearing. To this end, custom software developed at NTUA is used.

Apart from geometric optimization of the bearing, it is essential to couple the design of the stern tube bearing with a shaft alignment calculation tool, which will conclude to the exact geometry of the shaft at the position of the stern tube. An accurate calculation of shaft geometry during operation will result into better modeling of the fluid film and more accurate design of the double slope bearing, especially during transient loading, commonly applied to this type of bearings. This coupling also provides specific solutions based on the shaft alignment plan and not only the loading of the bearing itself.

At first, the geometry of the lubrication film should be computed for a double-slope journal bearing. Then, the geometry is fed to the Reynolds equation solver, which yields bearing operational parameters (load, eccentricity, attitude angle, maximum pressure, etc.). The system is coupled to a general purpose optimizer to calculate the optimum geometry based on a fitness function. Maximum film thickness, minimum pressure or minimum friction losses are the deciding parameters used in the fitness function. These calculations can be performed for various external loads, L/D ratios and rotational speeds of the shaft.

The optimized results are utilized to generate a 3D map of design variables leading to optimal bearing performance. Based on the above solution process, conclusions are drawn concerning the design geometry of the bearing for a given shaft alignment and can be deciding factor on weather a double-slope geometry is more beneficial than a single slope one. Last but not least, this method provides the optimum solutions for variable loading of the bearing, if that is required by the user.

Σύνοψη

Η τριβή είναι η συνηθέστερη και πιο σημαντική αιτία ενεργειακών απωλειών σε ένα μηχανικό σύστημα. Στο σύστημα πρόωσης πλοίων, σημαντικές απώλειες λόγω τριβής παρουσιάζονται τόσο στη κύρια μηχανή όσο και στο αξονικό σύστημα. Η κατάλληλη ευθυγράμμιση του αξονικού συστήματος είναι απαραίτητη για την ελαχιστοποίηση των απωλειών αυτών, και για την αποφυγή καταστροφών ή φθορών. Τα ακτινικά έδρανα είναι μηχανολογικά τεμάχια που χρησιμοποιούνται για την παραλαβή των ακτινικών φορτίων ενός άξονα. Κατά τη λειτουργία, ένα λεπτό φιλμ λιπαντικού δημιουργείται και συντηρείται με υδροδυναμικό τρόπο μεταξύ του άξονα και του εδράνου, ελαχιστοποιώντας τις απώλειες λόγω τριβής και αποτρέποντας την επαφή μεταξύ των μετάλλων. Η απόδοση των ακτινικών εδράνων συνήθως ποσοτικοποιείται με βάση το ελάχιστο πάχος του λιπαντικού, τις απώλειες τριβής και τη μέγιστη πίεση λιπαντικού. Όλα τα παραπάνω αλλάζουν σημαντικά υπό διαφορετικές καταστάσεις λειτουργίας (ακτινικό φορτίο, ταχύτητα περιστροφής, ιξώδες λιπαντικού). Το πρυμναίο έδρανο χοάνης στηρίζει το βάρος της προεξέχουσας έλικας, καθώς και όλα τα μεταβατικά υδροδυναμικά φορτία λόγω της λειτουργίας της, επομένως χρειάζεται ιδιαίτερη μέριμνα κατά την σχεδίασή του.

Στην παρούσα μελέτη, αναζητούνται οι βέλτιστες παράμετροι γεωμετρίας για ένα πρυμναίο έδρανο χοάνης με διπλή κλίση, με στόχο (α) τη μεγιστοποίηση της ενεργού επιφάνειας επαφής μεταξύ άξονα και εδράνου, (β) την ελαχιστοποίηση της τοπικής πίεσης στο σημείο επαφής. Το πρυμναίο έδρανο χοάνης μοντελοποιείται παραμετρικά: πέρα από τα γενικά γεωμετρικά χαρακτηριστικά (λόγος L/D, διάμετρος, χάρη άξονα, γωνία απευθυγράμμισης) επιπλέον χαρακτηριστικά σχεδίασης του εδράνου είναι οι δύο τιμές κλίσης και η εγκάρσια θέση του σημείου αλλαγής κλίσης. Η υπολογιστική μεθοδολογία προκύπτει από την επίλυση της διαφορικής εξίσωσης του Reynolds, η οποία περιγράφει το φαινόμενο της υδροδυναμικής λίπανσης στην περιοχή μεταξύ άξονα και εδράνου. Η επίλυση της εξίσωσης Reynolds πραγματοποιείται με χρήση υπάρχοντος λογισμικού που έχει αναπτυχθεί στο ΕΜΠ.

Πέρα από τη γεωμετρική βελτιστοποίηση του εδράνου, είναι σημαντικό να συνδεθεί η σχεδίασή του με κάποιο εργαλείο ευθυγράμμισης άξονα, το οποίο θα προσδιορίζει την ακριβή (καμπύλη) μορφή του άξονα στη θέση όπου τοποθετείται το πρυμναίο έδρανο χοάνης. Ο προσδιορισμός της ακριβούς γεωμετρίας του άξονα θα οδηγήσει σε ακριβέστερη μοντελοποίηση της γεωμετρίας του λιπαντικού φιλμ και της γεωμετρίας εδράνου με διπλή κλίση, ειδικά σε κατάσταση μεταβατικών φορτίσεων που επιβάλλονται συνήθως σε τέτοιο τύπο εδράνων. Αυτή η σύνδεση προσφέρει συγκεκριμένες λύσεις με βάση το εκάστοτε σχέδιο ευθυγράμμισης και όχι μοναδικά με βάση τη φόρτιση του εδράνου.

Κατά την επίλυση, υπολογίζεται η γεωμετρία του φιλμ λιπαντικού στο έδρανο με τη διπλή κλίση. Έπειτα η γεωμετρία αυτή αποτελεί στοιχείο εισόδου στην επίλυσή της εξίσωσης Reynolds, μέσω της οποίας υπολογίζονται οι παράμετροι λειτουργίας του εδράνου (φορτίο, εκκεντρότητα, μέγιστη πίεση, κλπ.). Οι παραπάνω υπολογιστικοί αλγόριθμοι συνδυάζονται με εργαλείο βελτιστοποίησης γενικής χρήσης, το οποίο υπολογίζει τη βέλτιστη γεωμετρία με βάση μια αντικειμενική συνάρτηση. Οι στόχοι της βελτιστοποίησης θα είναι η μεγιστοποίηση του ελάχιστου πάχους λιπαντικού και η ελαχιστοποίηση της πίεσης, ή των απωλειών λόγω τριβής. Οι υπολογισμοί αυτοί μπορούν να επαναληφθούν για διάφορες τιμές εξωτερικών φορτίσεων, λόγων L/D και ταχυτήτων περιστροφής του άξονα.

Τα αποτελέσματα θα συνθέσουν έναν τρισδιάστατο πίνακα από τον οποίο μπορούν να υπολογίζονται οι παράμετροι σχεδίασης, για τιμές εντός του εύρους υπολογισμών. Σύμφωνα με την παραπάνω μέθοδο επίλυσης, προκύπτουν συμπεράσματα σχετικά με τη γεωμετρία σχεδίασης του εδράνου, με δεδομένο σχέδιο ευθυγράμμισης, και ελέγχεται η αναγκαιότητα σχεδίασης του εδράνου με διπλή κλίση έναντι των σχεδιάσεων με απλή κλίση. Τέλος, η παρούσα μέθοδος μπορεί να υπολογίσει τη βέλτιστη σχεδίαση εδράνου, ακόμα και για ακραίες μεταβολές της φόρτισης του εδράνου.

Table of Figures

List of Tables

Nomenclature

B	bearing width [m]: $B=\pi \cdot D$
c	bearing clearance [m]: $c= R_1-R_2$
D	bearing diameter [m]: $D=2 \cdot R$
D_{MJ}	journal diameter [m]
e, ε	eccentricity [m], dimensionless eccentricity: $\varepsilon = \frac{e}{c}$
F, F^*	friction force [N], dimensionless friction force: $F^* = F \cdot h_{min} / (U \cdot \eta \cdot B \cdot L)$
F_{CR}	Crosshead bearing force [N]
F_X, F_Z	external bearing load - x-axis component [N], external bearing load - z-axis component [N]
h	lubricant film thickness [m]
h_{max}, h_{min}	maximum film thickness [m], minimum film thickness [m]
k	convergence ratio: $k = \frac{h_{max}}{h_{min}} - 1$
L	bearing length [m]
l_{MJ}	main journal length [m]
m_{MJ}	main journal mass [kg]
m_P	piston system mass [kg]
N	shaft rotational speed [rps]
O_B,O_S	bush center [m], shaft center [m]
P	total external force $P = \sqrt{P_x + P_z}$
p, p_{max}	pressure [Pa], maximum pressure [Pa]
P_X, P_Z	Journal bearing force, x- component [N], Journal bearing force, z- component [N]
p_c, p_0	cavitation pressure [Pa], boundary conditions pressure [Pa]
Q_I, Q_L	inlet flow rate [m^3/s], outlet flow rate [m^3/s]
q_x , q_y	lubricant inlet flow rate per unit length [m^2/s], lubricant outlet flow rate per unit width [m^2/s]
R	bearing radius [m]

R_1, R_2	bush radius [m], shaft radius [m]
S	Sommerfeld number
t	time [sec]
U	rotor linear velocity [m/s]
U_1, U_2	x-axis stator speed [m/s], x-axis rotor speed [m/s]
u	x-axis fluid velocity [m]
V_1, V_2	y-axis stator speed [m/s], y-axis rotor speed [m/s]
v	y-axis fluid velocity [m]
W, W^*	total hydrodynamic force [N] dimensionless hydrodynamic force: $W^* = W \cdot h_{min} / (U \cdot \eta \cdot B \cdot L)$
W_X, W_Z	x-axis hydrodynamic force component [N], z-axis hydrodynamic force component [N]
w	z-axis fluid velocity [m]
x	x-axis coordinate [m]
y	y-axis coordinate [m]
z	z-axis coordinate [m]
η	fluid dynamic viscosity [Pa·s]
θ	hydrodynamic film angle [degrees]
θ_c	contact angle [degrees]
μ	friction coefficient: μ= F/W
ρ, ρ_C, ρ_{ST}	lubricant density [kg/m^3], lubricant density at cavitation pressure p_c [kg/m^3], steel density [kg/m^3]
τ_x, τ_y	shear stress in x direction [Pa] shear stress in y direction [Pa]
ϕ	attitude angle [degrees]
ω	angular velocity [s^{-1}]

1 Introduction

1.1 Historical - Literature Review

High efficiency has become a “must” for modern shipping. Proposed solutions and trends are inevitably affecting the shafting system. Most common trends in the modern shipbuilding of ocean going merchant vessels according to Šverko (2010), are the following:

- Larger vessels, with optimized, and therefore more flexible hull structure,
- High-powered engines of very low RPM, thus requiring larger shaft diameters,
- Optimized cargo-carrying capacity and minimized engine room space, making shafting short and rigid,
- Optimized propulsion train and engines for low fuel consumption, resulting in low shaft speeds and large propeller diameters (increasing propeller efficiency).

Unfortunately, with all the benefits achieved by structural optimization, the shafting alignment bears some unfavorable consequences for the following reasons:

- With an optimized more flexible hull, the propulsion system becomes more sensitive to hull deflections, which should be accounted for during shaft alignment,
- The low shaft speed and the heavy loads from a big shafting/propeller results in more load exerted and more pronounced misalignment on the bearings,
- The production of the vessel in mega-blocks makes it difficult to control the alignment accuracy, particularly the misalignment angle inside the aft stern tube bearing.

Several failures of the shafting system have been reported and specifically, emphasis has been put on the severity of stern tube bearing failures in modern VLCCs and ULCCs, which may lead to loss of propulsion and vessel immobilization. This has drawn the attention of major classification societies and thereof the Elastic Shaft Alignment has been introduced by both ABS and BV, in order to improve the Shaft Alignment standards. In their work, Devanney and Kennedy (2003) had underlined the drastic deterioration of tanker newbuilding standards in the decade preceding their publication, and the corresponding effect on the reliability of the shafting system. The authors claimed that the main reason of this failure is the design of propulsion shafts with decreased diameters, followed by improper shafting alignment. They suggested that (a) hull deflections should be thoroughly taken into account for a range of loading conditions of the ship, (b) the engine room structure should be reinforced, to minimize additional offset of the bearings, and (c) time varying loads on the stern tube bearing and heat dissipation in the lubricant domain should be considered.

The most sensitive component in the propulsion shafting system, according to Šverko (2010) is the aft stern tube bearing, which is exposed to heavy static and dynamic propeller loads exerted to the bearing surface by the propeller shaft. Of key importance, are the remarks he made in 2006 about the stern tube bearing, based on calculation examples computed with the shaft alignment software developed by American Bureau of Shipping (ABS). He supports that the maximum absolute bearing-shaft misalignment allowed is 0.3 mrad, beyond which point, slope boring should be applied at the stern tube bearing. Recent trends and failures as analyzed above have shown that in several cases single slope is insufficient and double slope geometry should be implemented in order to achieve minimum load on the bearing and acceptable safety factors.

1.2 Goals of the Present Study

The main goal of this research project is to calculate the optimum geometry of a double slope bearing and improve its design for safety and durability improvement.

Secondary goals are:

1. Calculation of the equilibrium between the bent shaft under external loads and the required curvature of the bearing, in order to achieve optimal lubrication film,
2. Optimization of the double slope geometry according to the external load distribution,
3. Correlation of optimal double-slope geometric parameters (slope ratios and widths) with the operation parameters (Load, L/D and RPM),
4. Generation of a trustworthy and user friendly tool for engineers in order to quickly solve similar problems with slope bearings, without requiring much processing power.

Considering the methodology of this research, it is essential to clarify how several calculations will be performed and which basic assumptions are made. Assuming hydrodynamic lubrication in the bearing, it is decided to use a solver for the Reynolds equation, which has been developed at the section of Marine Engineering of NTUA. Prior to that, an add-on executable should be compiled in order to properly modify the geometry of the bearing so as to consider double slope geometry. Optionally, the geometry can be modified by introducing more than two slopes, for further research and development. In order to couple the shaft alignment with the bearing design we shall calculate the actual elastic line of shaft using an existing software (ShaftAlign) also developed at NTUA.

As input for our calculation geometry (CalcGeom) add-on, three parameters will be used: two slope angles, a1 and a2, and position of slope change (as a percentage of bearing length L). Additionally we shall include the actual inclination of the shaft within the bearing, calculated from ShaftAlign. The result will be the actual lubrication film of the bearing. Processing the results yields the equilibrium of the shaft bearing system and the actual load distribution of the bearing. Then, a general purpose optimizer based on genetic algorithms will be used to determine the optimum geometry for a set of (dimensionless) external loads, L/D ratios and RPM. As deciding parameters for the fitness function of the optimizer, maximum film thickness, minimum pressure or minimum friction losses may be used. Based on the optimum solutions, diagrams of the optimal input (design) parameters will be generated. From these diagrams valuable information for optimal design can be extracted. Both the optimizer and the fitness function included are developed at NTUA.

Last but not least several case studies will be carried out in order to evaluate the necessity of the double slope geometry, compare single and double slope designs and propose a double slope design for a given set of system parameters, such as bearing load, bearing length/diameter and lubricant.

2 Shaft Alignment

2.1 Definition

In conventional cargo ships the propulsion system consists of a large (2-stroke) marine engine coupled to the propeller. In small vessels, two or four “smaller” (4-stroke) engines drive the propeller through a gearbox, where as in passenger vessels more than one propellers are installed. What is common in every system is the means of power transmission from the main engine(s) to the propeller(s), which is called the ‘’shafting system’’. In most cases it comprises of three parts: the crankshaft, an intermediate shaft and the propeller shaft. These are supported by different kinds of bearings, according to requirements of each installation. The crankshaft, which is heavily loaded from the main engine, is supported by several crankshaft bearings, typically matching the number of the main engine’s cylinders plus one. The intermediate bearing carries the least amount of vertical loading and therefore is typically supported by one or two intermediate bearings. The propeller shaft is usually supported by two stern tube bearings or one large stern tube bearing and an intermediate bearing. The aft stern tube bearing is also heavily loaded due to the propeller loads and usually is quite long, with L/D ratios around two (2). It is evident that severe power losses may occur within this transmission system therefore special care must be applied during design procedure.

Shaft alignment is the process to determine the parameters of the shafting system.

When shaft alignment is completed, the number and type of all support points is decided and they are placed at a specific longitudinal and vertical position. Especially for vertical position a pre-established reference line is defined. Additionally, the angle at which bearings will be positioned in relation to the reference line in order to minimize the shaft/bearing misalignment. The type/ dimensions of the bearings is decided in order to support the shaft load adequately both in cold and running conditions. Conclusively the reaction forces at the support points are calculated for the conditions above and it is verified that these reactions are within acceptable limits.

Proper shaft alignment can minimize the stress of the shaft and therefore the power losses of the system. Working within acceptable limits is essential for both bearings and shaft in order to achieve longer system life span, less wearing and fatigue and no system failures that put the ships safety and operability at risk. In the case of coupling with a gearbox, a proper alignment reduces the wear of the gear teeth and protects the gearbox from catastrophic failures. Last but not least, proper shaft alignment can be very beneficial for reducing maintenance and repair costs.

2.1.1 “Static” and “Running” Condition

During ship’s lifecycle there are two types of conditions that the ship encounters. It can be either anchored or in sea-going condition. These conditions stress the shaft quite differently but both are of significant importance for the Shaft Alignment procedure.

In **static** conditions:

- The main engine (ME) is not running.
- No thrust is produced from the propeller, therefore no additional bending moment is accounted for.

- Shaft is not rotating, therefore no twisting is calculated.
- At the support points (bearings) vertical motion is acceptable within the limits of diametrical clearance.
- The shaft is stationary, therefore hydrodynamic lubrication is not active (no fluid film can be sustained between shaft and bearing).
- Only the static loading of the shaft is accounted, e.g. gravitational forces, vertical loads at bearings and loads applied mechanically on the shaft.

On the other hand in **running** condition (also called dynamic or sea-going):

- The ME is running, thus producing significant additional vertical loads and vibrations on the crankshaft bearings.
- The ME is in hot condition, therefore it is subject to thermal expansion, which affects the vertical offset of all crankshaft bearings.
- The propeller is producing thrust, which is usually eccentric to the shaft-line, thus applying additional bending moment to the shaft.
- Shaft is rotating, which helps to develop a fluid film at the support bearings, lifting the shaft above the lower half of the bushing.
- Any misalignment between the bearing and the shaft will result in a slight shift of the conceived single-point support position of the shaft along the bearings' length.

In the present work, the main objective of the study is the running condition, where a fluid film is developed and shaft is bent. To be more specific, in sea-going conditions the aft stern tube bearing, which is the main topic of this thesis, will be loaded, and the shaft within the length of the bearing will be modeled bent based on this load and the position of the single-point support (along the bearings' length). The vertical motion within the bearings' clearance is governed by the principle of hydrodynamic lubrication. Calculations will not be done for static condition, although they can easily be added given more information about the overall shaft alignment plan.

2.1.2 Influence Factors

In order to better understand the shaft alignment process, the concept of influence factors will be explained. In a shaft alignment plan, several support points are placed longitudinally and at specific vertical offsets from the reference line. It is evident that changing this vertical offset will result to an altered distribution of the reaction forces amongst all bearings. In order to evaluate the correlation between support points, influence factors are used. They are a measure of change in reaction force of a bearing, while the number and longitudinal position of all bearings is constant and the vertical offset of one of the bearings is changed. The influence factors have an underlying concept of superposition that is valid in this case because the vertical offset imposed is much smaller than the longitudinal distance between supports.

The influence factor of bearing i on bearing j is a measure of the change in reaction force of bearing j, caused by a unit vertical offset of bearing i.

As such, it can be calculated as:

$$\sigma_{ij} = \frac{W_{ij} - W_j^0}{y_i}$$

Where:

- σ_{ij} is the influence factor of bearing i on bearing j,
- W_{ij} is the reaction force of bearing j when bearing i has moved vertically by an amount of y_i,
- W^o_j is the reaction force of bearing j, while all bearings have zero vertical offsets (i.e., straight-line).

Using the formula above, it is very simple to predict the reaction force of each bearing, for a set of vertical offsets, when all influence factors have been calculated.

Influence factors can be very useful in works like the present one, where one of the bearings (e.g. aft stern tube bearing) is specifically examined. Furthermore they are a good measure of sensitivity in the shafting plan to external disturbances. Ship's motion and loading can result to different vertical offsets which should not cause devastating conditions at the loading of the bearings. Therefore small values of the influence factors signify a less sensitive system, where on the contrary large influence factors identify a system with great risk of bad alignment caused by a small change in vertical bearing offsets.

2.2 Regulations for Design and Analysis

Regulations regarding shaft alignment of rotating machinery, such as the prime mover of a ship, are more or less homogenous between IACS classes. Most common general requirements are the following:

- A detailed shaft alignment plan, illustrating all considerations taken and all assumptions made must be submitted for approval,
- The results of the analysis carried out prior to plan implementation must be shared with the class,
- Analyses must be carried out for various ship operating (hot/cold) and loading (Ballast Arrival, Full Load Departure, etc.) conditions, taking the corresponding hull deformations and main engine thermal expansion into account,
- Stern tube slope must be thoroughly investigated under any alignment plan, and single, or even multi-slope, boring must be applied whenever necessary, to prevent excessive shaft misalignment,
- Bearing reactions should be within allowable limits,
- The details and procedures followed during the implementation of the plan must be available to the class reviewer,
- All the above must be checked and verified through testing by the class.

Additionally, it has been recognized that accurate alignment of the stern tube bearing is crucial in order to avoid the occurrence of bearing failure problems. In the case where slope boring or bearing inclination is applied, specific regulations are also given. Below, we will further analyze some of the above requirements that are closely related to our work.

2.2.1 Reaction forces

Allowable bearing reaction forces are defined by a series of requirements. First of all, bearings must be in contact with the shaft at the bottom half of their geometry. Reaction forces are defined as "positive" if the statement above is true. Secondly, reaction forces must be within a range of acceptable limits. Typical upper limit for the mean pressure in white metal bearings is 0.8 MPa and 0.6 MPa for composite anti-friction materials. The limit definition for maximum pressure varies in deferent classes, NK sets the limit at 40MPa and Bureau Veritas links reaction forces to lubricant film thickness and sets a limit at 30 μm of minimum film thickness (correlated to the roughness of the material). On the other hand, ABS does not set a specific limit, requires although only positive reactions and instructs that at least 10% of the allowable load to be present at any condition of the vessel in order to prevent unloading due to unaccounted-for disturbances.

ABS also notes the following:

> "Reaction loads are not the only criteria that are important for alignment acceptance. Relative misalignment between the shaft and the bearings has at least the same importance."

Concerning the verification of the reaction forces through testing, large deviations are allowed (±20% deviation) between prescribed calculations and measured reactions, due to significant amount of uncertainty. In all cases, the measured reactions take precedence over calculations.

2.2.2 Deflection Curve

The most modern class regulations contain information concerning this curve. To be more specific, ABS guidance notes on propulsion shafting alignment mention:

"Relative misalignment between the bearing and the shaft may be evaluated from information defined by deflection curvature. Deflection curvature defines the angle of the shaft inclination at each node of the system. This angle is measured from the theoretical zero alignment angle."

Furthermore, there are guides concerning cases were hull deflections are accounted for and mentions that if the misalignment angle is found excessive, slope boring or inclination of the bearing may be required. For this scope it is important to present in detail what 'bearing misalignment' actually is.

Bearing misalignment between shaft and bearings is a very important parameter to check as we mentioned before. It is practically the inclination of the shaft, within the length of the bearing. The stern tube bearing, due to its long length, requires special attention but other supports points should not be overlooked. Bureau Veritas instructs in the elastic shaft alignment regulations that the stern tube bearing should be modeled at least as a five support points system, in order to accurately describe the bearing misalignment at the entire bearing length. The limitations set for the maximum angle of misalignment between the shaft and the bearing bushing are relative to its dimensions. This angle must not exceed the ratio of the radial clearance over the bearing length, which practically prevents shaft from contacting the bearing bottom. If calculations prove otherwise, slope boring or bearing inclination must be applied to the bearing bush. Some classes actually mention that, especially for the stern tube bearing, a multiple slope boring can be applied for extreme cases. In this thesis we will focus on the study and optimization of a two-slope boring arrangement. The difference between slope boring and bearing inclination will be further analyzed shortly after.

A two-slope boring arrangement is depicted in the following figure:

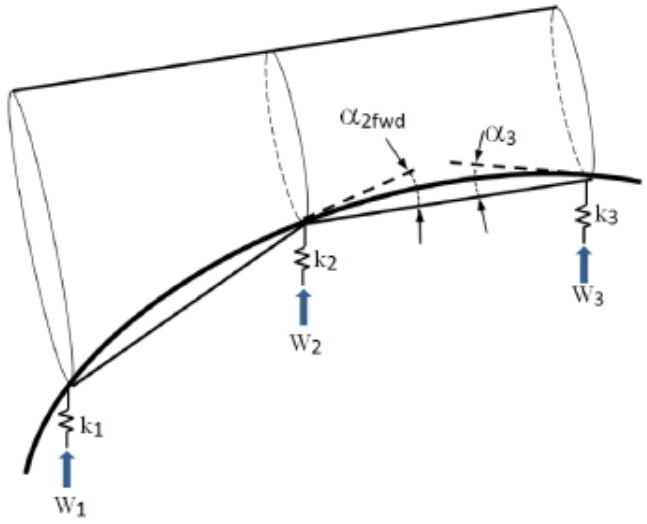

Figure 2-1: SHAFT BEARING WITH TWO-SLOPE BORING

2.2.3 Slope Boring/ Bearing Inclination

Slope boring or bearing inclination is adopted as a practice to prevent excessive edge loading of the tail shaft bearing and distribute the load as evenly as possible along the bearing length. Usually, either of these practices are conducted when the misalignment angle exceeds the value of 0.3 mrad. A quick summary of the reasons, why this can be the case, at the stern tube bearing is as follows:

- Propeller loads result in large bending deformation at the tail shaft.
- Shaft's bending reduces the area of static contact with the bearing.
- The central axes of the bearing and the shaft are misaligned due to the shaft's deformation and the bearing's offset position.
- Relative misalignment causes further area reduction at either one of the bearing's edges.
- Large variation of loads during the whole range of the vessel's operating conditions.

Slope boring or bearing inclinations are processes, where the aft stern tube bearing center line (and sometimes the forward stern tube bearing as well) is inclined to reduce misalignment between the bearing shell and the curved shaft. Both methods are applied before the shafts are out in place.

As defined by ABS in [7]:

"Slope boring is a process where the bearing shell is machined so as to ensure that the center line of the bearing's inner bore is misaligned to the desired angle (defined by shaft alignment analysis). To allow provision for slope boring, the inner bearing diameter is initially pre-machined to the smaller diameter. The special boring machine is then attached to the stern block and aligned so as to match the required misalignment angle. Machining is then conducted by boring through the bearing in several passes, if required. Multiple passes may be necessary when larger amounts of bearing material are to be taken away because of a danger of bearing material overheating, as well as to ensure required machining tolerances."

Disadvantages of this method are that it: is a slow and sensitive process, requires specially designed equipment and that the machining precision may be reduced on lengthy bearings.

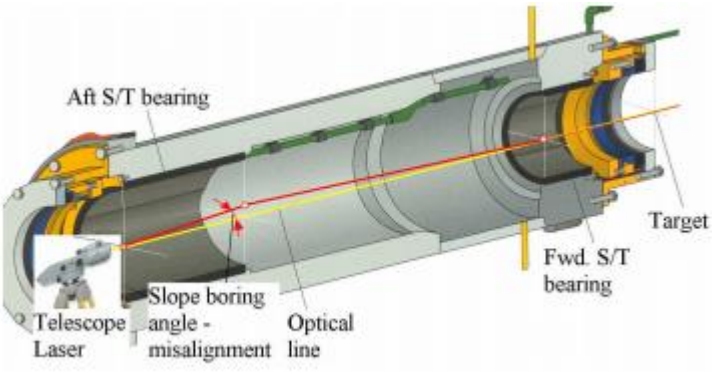

Figure 2-2: SLOPE BORING ARRANGEMENT [7]

Bearing inclination is another process, where instead of machining the bearing after installation, the bearing is machined to its final diameter and placed inclined into the stern block. In this case the bearing's casing is fixed to the stern block by epoxy resign, rather than shrink fit. The major disadvantage of this method is that there can only be one inclination and therefore the benefit for different running conditions and load distributions is significantly lower.

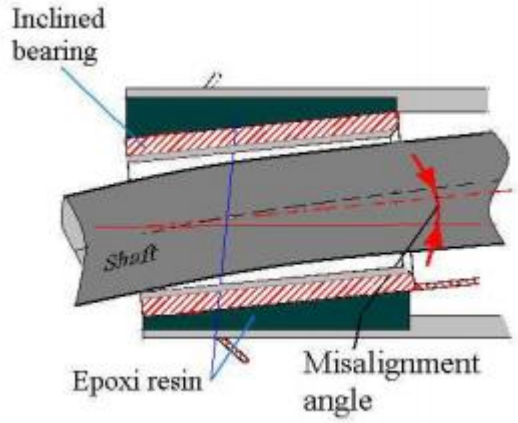

Figure 2-3: BEARING INCLINATION [7]

In both cases the greatest challenge is to find an optimum alignment for a variation of loading conditions, which is very hard to be done. One methodology that can be applied here is, to design for one condition, for example the laden condition, and check that this design results in acceptable bearing loading in other conditions, for example ballast condition or static condition. This basic concept will we follow in this present work.

Another methodology, proposed by ABS in [7] is as follows:

"The misalignment-slope will vary with change in the loading condition of the vessel and the environmental condition (temperature in particular) around and inside the vessel. Therefore, it is more important to predict the trend of misalignment-slope-change than to define one optimum angle which will ideally suit only one alignment condition. When alignment is calculated, the trend of the misalignment angle change is to be observed, and the slope should be defined so as to ensure that slope change will not deteriorate the bearing condition to the point of unacceptable bearing loads. The condition is to be acceptable for all different vessel loadings."

2.2.4 Single or Two Point Contact

The common practice for shaft analysis, is to model each bearing as a single reaction contact point. After 2015, advanced requirements made by several major classes have brought to the spotlight the two or multi- point modeling of bearings. This may be very useful, especially in the study of the stern tube bearing, because it enables multi-contact calculations, instead of assuming a single contact point. Normally, a contact point represents the position of the assumed bearing reaction. The location of the contact point will define the "contact intensity", but more importantly the slope between the shaft and the bearing's bush. There has been some controversy on whether two point contact is actually realistic, since it is very rare to find actual running conditions where two point contact exists. However with two point contact it is easier to make preliminary calculations and verify acceptance criteria in a case. To this extent, ABS and BV have made significant progress trying to model the contact between bearing and shaft bush as proposed respectively is presented here:

ABS in [7]utilizes the area contact in the ABS Stern Tube Bearing Evaluation program in order to evaluate the contact area and bearing condition when the shaft does not rotate or rotates at very low speeds (before the oil film develops). Alternatively, it is recommended to use the single point contact approach, as well as to consider the contact point at D/3 (one third of shaft diameter) distance from the after bearing edge.

BV in [9] proposes that the aftermost bearing, due to its large L/D ratio, is modeled with at least five supporting points in order to have detailed results at each section of the bearing for the chosen elasto-hydrodynamic calculation method.

In the specific case of ESA modeling of the stern tube bearing, the two-point contact is equally valid, but only if the single point contact is verified first and if the slope boring is defined for the single point solution. To verify the two point method, the front-edge contact point is removed and a single point case is studied. If the single point contact is not satisfactory, the two point analysis should not be accepted as valid. It is evident that the single contact point study is inevitable, therefore in this work the single contact point method will be primarily used. It is possible though, due to the double slope modeling of the aft stern tube bearing bush, to result into a case where two point contact is inevitable. Only at that time, two contact point model will be used in order to maximize the contact area and result to minimum pressure on the bearing bush. The results will be verified with the equivalent single contact point model as well.

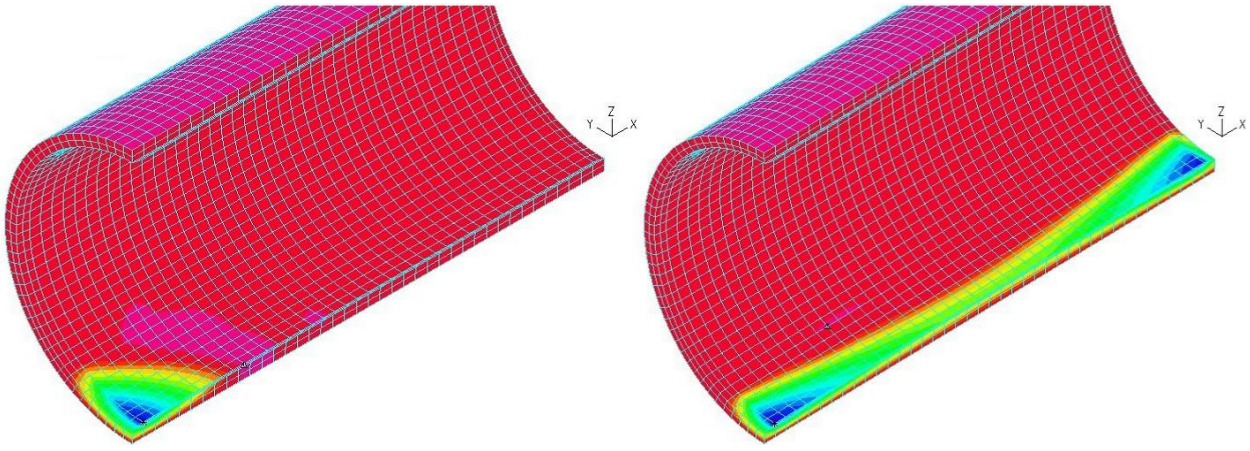

Figure 2-4: SINGLE AND TWO CONTACT POINT MODELS [7]

2.2.5 Documentation and Results Verification

As a result of all the above mentioned regulations, the list of items requested, by major classes to be submitted for approval are the following:

- Drawings of shafting arrangement and auxiliary systems
- General description of calculation model
- Assumptions
- List of investigated calculation conditions
- Input parameters
- Detailed results
- Conclusions
- Shaft alignment model
- Hull flexibility model
- Hull relative deformations
- View of FE model of aft part of ship structure
- Detailed alignment procedure

Further clarifying the above mentioned “Detailed results” the documents requested to be submitted for Elastic Shaft Alignment (ESA) [9] are:

In static conditions:	In running conditions:
Reaction distribution between shaft bearings	
Reaction distribution along effective length of aft bush bearing	
Shaft location inside bearings	
Static contact pressure on anti-friction material	Oil film pressure
Squeezing of anti-friction material	Oil film thickness

Table 2-1: RESULTS TO BE SUBMITTED FOR ESA ACCORDING TO BV

The verification of the above mentioned parameters should include:

- Influence coefficient matrix
- Bearing reactions
- Deflection curvature
- Stern tube bearing slope boring requirements
- Angular inclination at the main gear wheel (if applicable)
- Shear forces and bending moments
- Allowable loads on all bearings

2.3 Shaft Alignment Procedure

Following the aforementioned procedures to design, analyze and report the desired shaft alignment plan, the executable part of the alignment process takes place. The desired alignment is performed according to the requirements of the designer. There is no uniform procedure and most of the times it depends on the shipbuilder's practices, experiences and production schedule. Even though the validity of each approach can't be judged, classes have set a few examples of shaft alignment procedures, which if followed properly, can result to high success probability. For every shaft alignment proposal, safety and practicality are the most important characteristics. In the following section several key parameters of proper shaft alignment procedure will be analyzed.

2.3.1 Preliminary Calculations

First and foremost, a set of preliminary calculations must take place in order to choose accurately the number and longitudinal position of the support points. A basic "straight-line" calculation of the reaction forces will take place, in order to make an estimation for the system's influence factors and shaft deformations. The bearing vertical offsets are set to zero in the first step, but further on they should be redefined, in order to achieve an acceptable distribution of reaction forces. The loading capacity of each bearing should never be exceeded. It is also advised, to avoid extensive shaft inclination and aim for minimum shaft/bushing misalignment. This is often hard to be achieved, especially in the area of the stern tube bearing. At these cases, solutions such as slope boring or bearing inclination are advised according to previous sections. The next step is the application and evaluation of the shaft alignment plan.

2.3.2 Application

According to major classes, the application of shaft alignment is not expected to start before the vessel stern blocks are fully welded and all of the heavy structures are in place. The first step is to establish a reference line for the positioning of bearings, shafts, gearbox and main engine. The several methods to set the reference line will be further analyzed in the following section (Measurements). In this stage, several temporary support points may be used. When shafts are positioned in place, the propeller.is also connected, usually accompanied with a load applied in the forward end of the tail shaft in order to hold it in contact with the forward stern tube bearing before assembly. In this stage it is common practice to measure the Sag and Gap values to verify compliance with appropriate, analytically obtained values. It is essential to ensure correct and accurate Sag and Gap values between shaft segments. At this stage, the bearing- shaft misalignment is evaluated and corrective actions are taken. In many cases, readjustment of the intermediate shaft bearing offset may be necessary. At the end of the process, when the shafts are coupled, extensive testing and measurement of the system parameters is performed in order to match the actual reaction forces with their calculated values found in pre- alignment stage. Several corrective actions may be taken to rectify such inequalities. Further verification of the alignment condition should proceed with the vessel afloat. On a waterborne vessel, it is more difficult to ensure compliance with the calculated alignment, since the bearing reactions significantly differ from the analytical predictions due to the hull deflections.

ABS includes in [7] that: "It is desired to conduct as much of the alignment procedure as possible while the vessel is in the dry dock. Accordingly, if plausible, the reaction verification and the bearing-shaft contact condition should be verified when the vessel is in the dry dock. By doing so, the shipyard can ensure very good control of the alignment procedure against the analysis. It is again important to highlight that the issue of controlling the alignment is in direct relation to the completion of the structural work of the vessel."

Nevertheless, it is general policy of the classification societies to accept any procedure that result in a satisfactory solution. In the following figure, the Sag and Gap alignment process is presented.

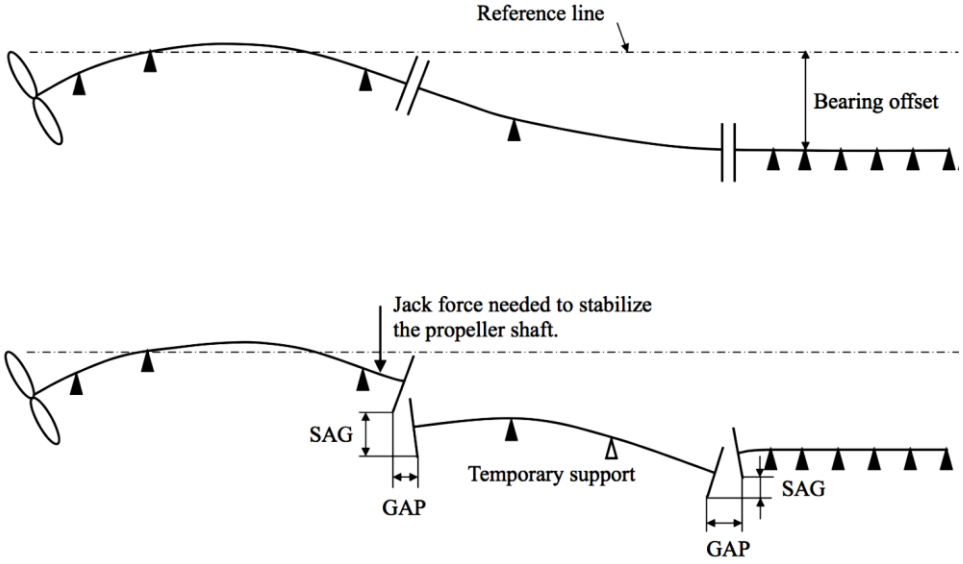

Figure 2-5: SAG AND GAP ALIGNMENT PROCESS [29]

Other significant stages of the alignment procedure or calculations that have to do with the hull stiffness, the main engine, the gear and the vibration analysis, which **will not** be thoroughly analyzed in this work but are essential for proper alignment, are:

- Hull Girder Deflections
- Engine bedplate pre-sagging
- Crankshaft deflection measurement
- Gear contact evaluation (if applicable)
- Gear-shaft bearings reaction measurements
- Lateral Vibration (Whirling) Calculations
- Engine chock calculations
- Maintenance or repair practices
- Bearing wear down issues

2.4 Measurements

2.4.1 Sag and Gap Values

As mentioned at ABS's guidance notes on propulsion shafting alignment [7]:

"Sag and Gap is a shaft alignment method, commonly used to verify the preassembly condition of the propulsion shafting in new construction and repairs."

It is a simple and fast method that requires no special equipment, but it has questionable accuracy. This method is used only as an additional check but has many advantages for the first steps of the preassembly stage. During preassembly, all segments that make up the shafting system, are placed onto their respective support bearings uncoupled. In this state the flanges are hanging freely and a significant amount of force needs to be applied in order to position them at the desired vertical and horizontal offset for coupling. Additionally, after decoupling a shafting system, flanges should be positioned at specific vertical and horizontal distances. SAG and GAP are the parameters of such a measurement. SAG is the vertical distance between the top (or bottom) edges of each flange and GAP is the horizontal distance between facing flange edges, or between the upper and lower edge of each flange. The following figure illustrates some possible arrangements and how SAG and GAP values are measured.

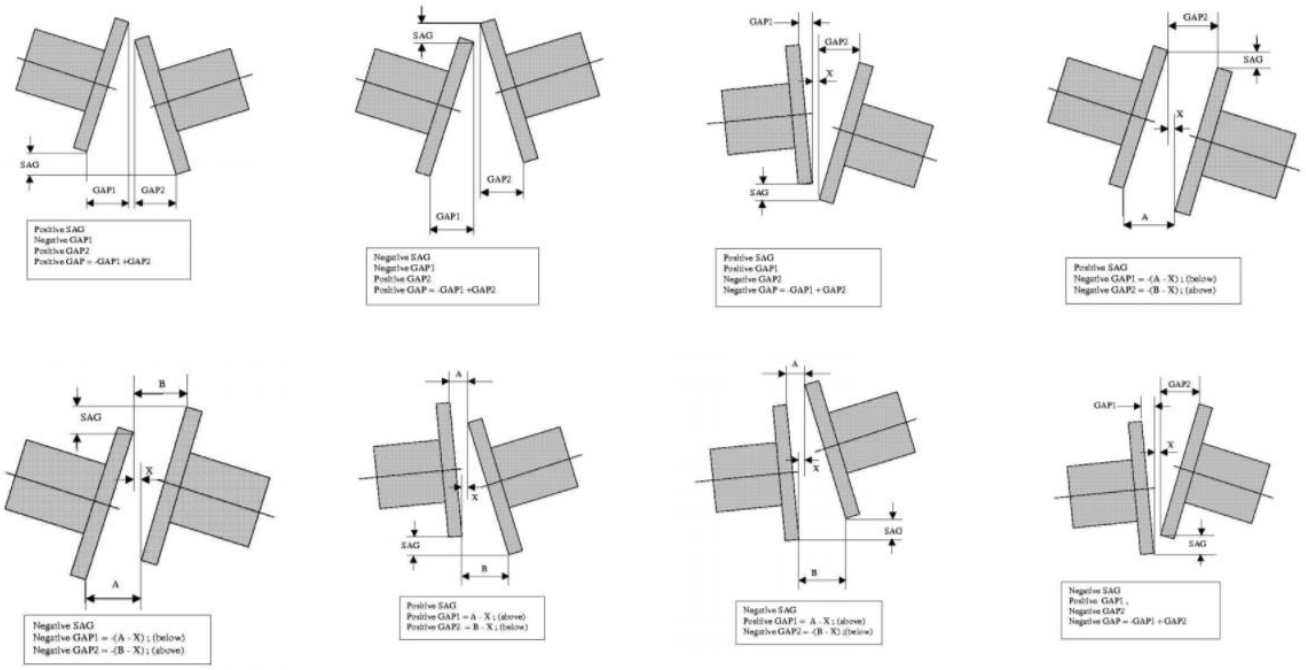

Figure 2-6: SAG AND GAP MEASUREMENT TYPES [7]

Sag and Gap measurements should be conducted after all the following steps are completed:

- Main engine and gear (if applicable) are installed
- Temporary supports are installed
- Shafts are placed and hanging freely and propeller is mounted
- The propeller shaft is in contact with the bottom shell at the foremost stern tube
  (It is possible for this step to add a weight in the foremost end of the propeller shaft to balance the propeller weight and maintain contact with all bearings)

2.4.2 Sighting Through

One of the most important stages of the alignment application is the vertical position of the support point offsets according to a predefined reference line. There are several ways to accurately define this reference line and establish it in the physical world. The process of establishing a reference line is often called sighting through or bore sighting and is commonly conducted by piano wire method, optical instruments or laser. Additionally it is essential to define a credible method to measure distances from the reference line.

The sighting through procedure is generally conducted as follows:

1. Piano wire or optical method machinery are installed
2. Reference line is defined to match the center line of the aft stern tube bearing
3. Target points are defined at the location of the bearings
4. Target points are offset to match the prescribed offsets for dry dock condition
5. Bearings, gear box and main engine are positioned into place
6. Slope boring angles are marked or inclination angle is applied to the stern tube bearing

Piano Wire Application

In this method a thin metal string/wire is bound at the aft position of the engine, above the shaft and connect a weight at the other side of the string in order to keep the wire tense and as straight as possible. The method is presented in the following figure:

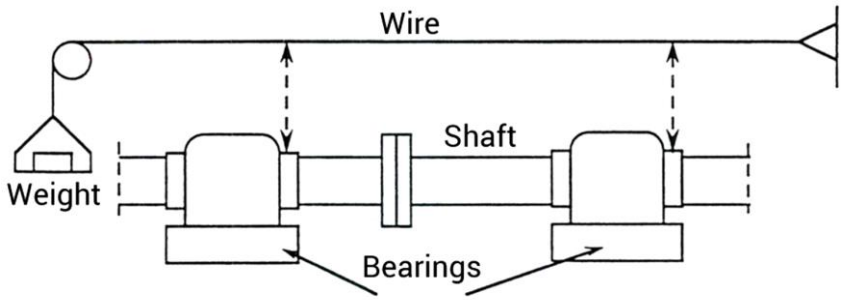

Figure 2-7: THE PIANO WIRE METHOD [29]

The prescribed vertical offset is measured as a distance between the wire and the location of the particular support point. The vertical offset and longitudinal position of the bearings are defined using piano wire as reference but must be corrected for piano wire sagging.

Although this is a very simple method, it is not very accurate due to the following apparent reasons:

- It is very hard to measure from the wire accurately without touching it and thus altering slightly the vertical position/ measurement.
- It is very difficult to make the wire rest perfectly
- Any weight movement (e.g. installation of shafts) my affect the wire sag
- It is very hard to make corrections for the continuous small amplitude vibrations of the piano wire

Optical Methods

The most accurate methods for alignment implementation are the optical methods: optical telescope and laser. The optical means equipped are very accurate and therefore the outcome is high quality. In the first step of the application, the telescope/ laser is positioned on the aft end of the shafting system. A reference target is positioned on the other end and several targets are positioned at the exact vertical offsets and longitudinal positions. These targets have a narrow hole in the middle in order to allow laser beam to pass through. Once the reference line is established between telescope/laser and the fore target, the offsets of support points can be measured by simply adjusting the telescopes dials. The targets are adjusted starting from the fore one and moving aft end of the shafting system.

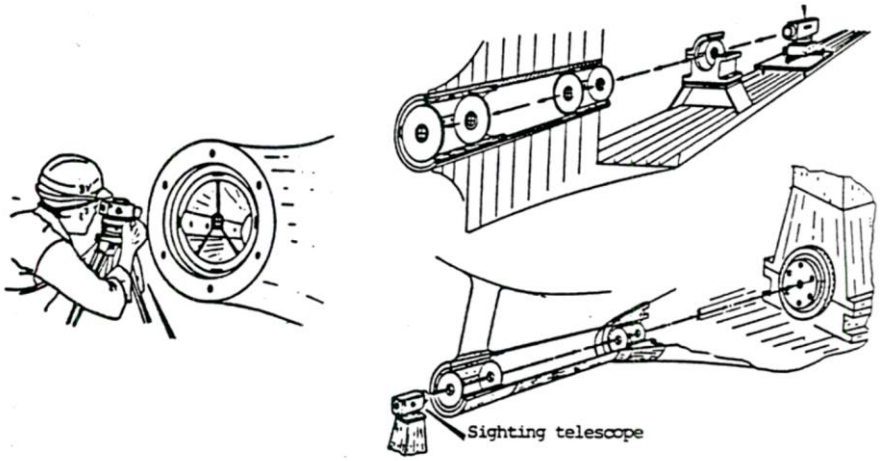

Figure 2-8: ALIGNMENT WITH OPTICAL METHODS [29]

The targets are usually inscribed with concentric circles of various diameters in order to provide improved resolution, additionally to the scale on the graded dials. This method has the advantage of improved accuracy and additionally provides the benefit of being able to place objects/ targets at any pre-defined position simply by adjusting the telescope dials at a specific focus, distance and offset and matching the object's position with the selected target. Another advantage that is important for sloped stern tube bearings, is that laser can set a reference line at any desired angle. In the case of single or double slope boring/ inclination of the stern tube bearing, the reference line is defined by the main slope of the stern tube bearing, therefore the optic methods are the only eligible method for accurate shaft alignment.

2.4.3 Bearing Reaction Forces

Once the alignment process is completed, the shafts are coupled and the temporary support points have been removed, it is essential to measure the actual reason forces of the remaining support points. The most common techniques to measure bearing reaction forces are utilizing:

- Hydraulic jacks
- Strain gauges

2.4.3.1 Hydraulic Jack Test

This is the most widely applied method to measure bearing reactions in cold condition. It is a very simple and easy to use method that takes a direct measurement and requires no special skills or expensive equipment. A hydraulic jack is placed below the shaft and along the centerline, as close as possible to the bearing. The jack should be placed at a steady and sufficiently stiff foundation throughout the process. A micrometer or a digital dial gauge is placed on top of the shaft and a load shell is placed between the jack and the shaft. It is recommended to jack-up the shaft for at least 0.5 mm before the test starts, in order to ensure accurate measurements. Then the shaft is jacked up until it reaches the upper shell of the bearing bush and then return to the initial position. This should be done a few times in order to minimize the systematic measurement errors. During the process simultaneous measurements of the jack reaction force and the shaft vertical displacement are taken. The following figure illustrates the curve of these measurements.

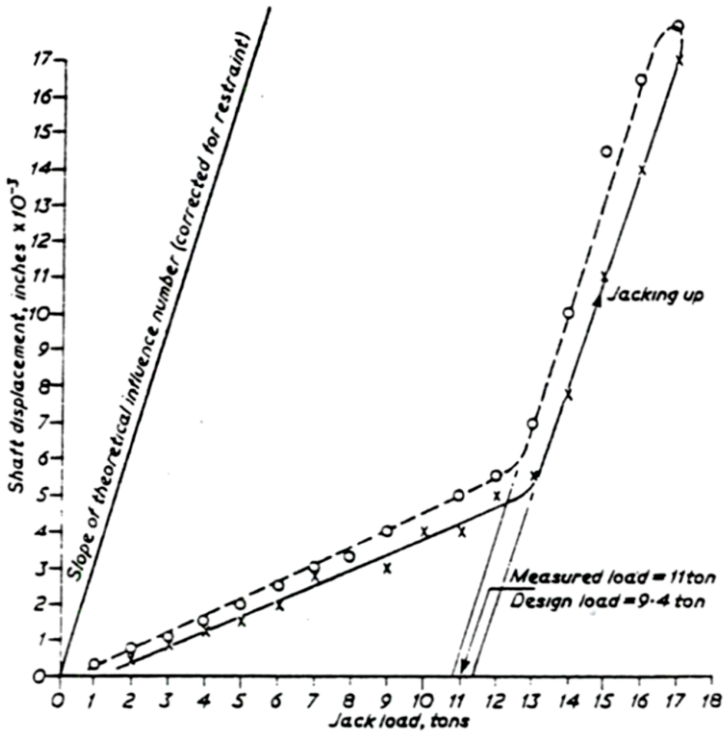

Figure 2-9: JACK-UP TEST MEASUREMENT CURVES [7]

In the first part of the curve, the mild slope demonstrates that the shaft load is still supported by the bearing. This effect happens due to the elastic deformations of the bearing and shaft under heavy loads. The second part of the diagram with the steep slope demonstrated full loading of the jack and the slope corresponds to the influence factor of the support point (jack). This influence factor is very similar to the

bearing's influence factor, since the jack is placed close to the bearing, therefore correction factors may be used. The difference is actually very small since the longitudinal shift of the support point is very small compared to the length of the entire shafting system. The last part of the graph depicts measurements taken while the jack is on the way down. The slight difference between values is attributed to friction. The actual value of the bearing reaction can be derived by simply extending the average between the lifting and lowering curve (steep part) of the diagram towards zero shaft displacement.

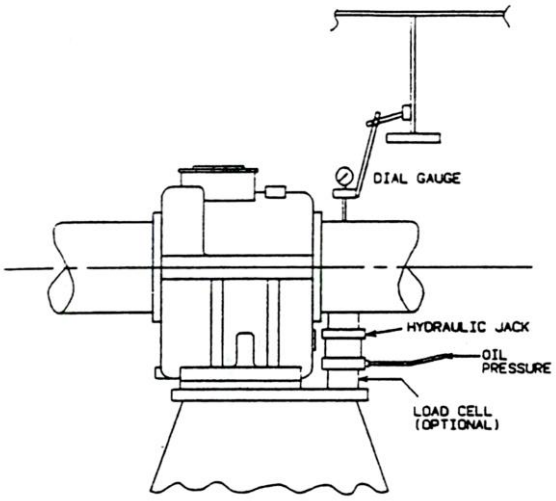

Figure 2-10: HYDRAULIC JACK INSTALLATION [7]

The jack up method can additionally be used to measure permanent bending deformations of the shaft, by taking four measurements and rotating the shaft 90 degrees after each one. Comparing these results we can conclude if the shaft is skewed.

2.4.3.2 Strain Gauge Test

This method utilizes strain gauges to measure stress at any point of the shaft and therefrom calculate the reaction forces. It is a very accurate method and enables measurements at the exact position of the contact point, where jacks can't be mounted. It provides both vertical and horizontal loads and has the potential to provide simultaneous information on more than one bearing loads. To improve the accuracy of measurements, more than one gauge can be installed at the same longitudinal position, usually four gauges are installed in pairs, 180° apart from each other, forming a Wheatstone bridge. Additionally it is easily repeatable after the initial strain gauge installation. Another advantage of this method, is that data provided (strains and bending moments) may easily be utilized to calculate the exact shaft bending curvature and thereof the actual bearing position. On the contrary, the long installation time is one of the main disadvantages of the method, as well as the expensive and sophisticated equipment needed for the measurement. Furthermore, specialized personnel is required to conduct this measurement, which takes approximately one hour per strain gauge, due to high complexity and the required accuracy of the installation. In comparison to the hydraulic jack testing, data accuracy in the strain gauge test depends a lot on a detailed and accurate shafting system modeling.

Telemetric strain gauges can be used as monitoring devices in running condition too and provide very useful information during vessel operation.

3 Journal Bearings

3.1 Introduction

Journal bearings, according to [2] are the most common and simple type of radial bearings. They are used in a variety of applications and are extensively used for the support of the propulsion shaft of a vessel, for supporting radial loads and guide a smooth transmission of torque from the engine to the propeller. A journal bearing consists of two parts. The stator or bushing, which is a stationary sleeve, usually with a complete 360° arc and the rotor, which in our case is the propulsion shaft. In advanced designs, the bushing may consist of various arrangements, partial arcs or arcs in a housing structure. The stator is typically lined with soft metals, such as lead, tin, Babbitt or bronze. The shaft rotates inside the bushing and, in between, a thin film of lubricant fills the gap. Lubricant is supplied to the system from arrangements such as inlet holes or more sophisticated systems for improved lubricant distribution, such as axial, circumferential and helical grooves.

As the shaft is rotating, it drags lubricant which is forced to fill the converging (wedge- shaped) geometry between the shaft and the stator. The incompressible lubricant develops the desired pressure to preserve the hard metal shaft separated from the soft metal bushing. This is essential in order to avoid “dry friction” which is disastrous for the lifespan of the bearing. At the initiation of a rotary motion the shaft is forced, due to friction, to roll at the opposite direction within the bearing sleeve. This motion, accompanied with adequate lubricant supply, helps to immediately form a lubricant film and lift the shaft into steady state position. Lubrication starts taking effect at any relative rotational velocity greater than zero and is also very steady in sudden impulses or vibrations. A common instability that journal bearings face over the years, also known as self-excited oil whirl, is constrained using tilting- pads, elliptical, pressure dam and offset split bearings.

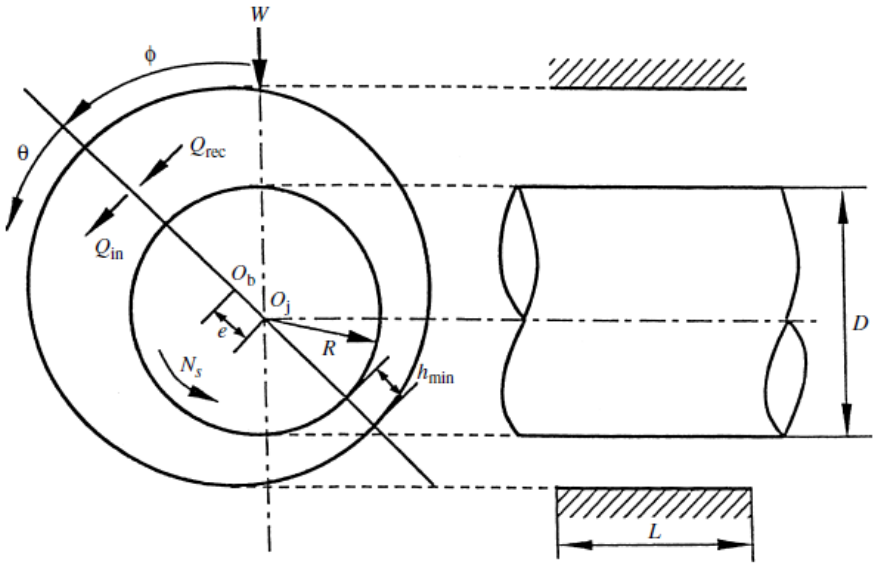

Figure 3-1: CROSS SECTION OF A JOURNAL BEARING [1]

Once the shaft is in steady state, it is in a position within the bearing clearance and at some point along the circumference. This position can be defined by the eccentricity e and the attitude angle ϕ as shown in Figure 3-1. Attitude angle is the angle between the centers of the bore and the shaft and eccentricity is the distance of between these points. Vigorous oil-film pumping at higher speeds and increased viscosity will result to decrease of the eccentricity and increase of the attitude angle.

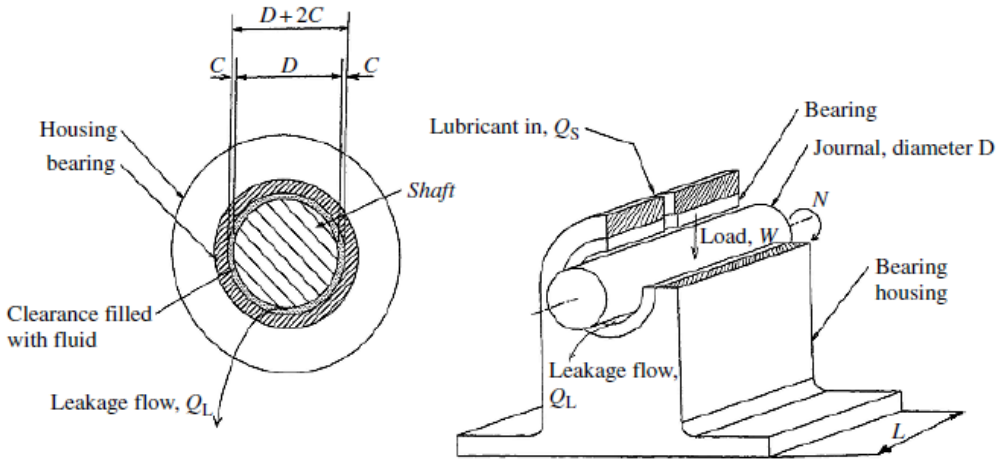

Figure 3-2: JOURNAL BEARING GEOMETRY AND NOMENCLATURE [2]

Journal bearings can be constructed quite simply and with very small tolerances, therefore they are used for high precision projects that also demand minimum wear and increased lifespan. Such bearings are quite economical, especially when they are produced massively. Additionally they have high capacity in sense of absorbing and damping vibrations, impulses or sudden force variation. On the other hand, journal bearings require frequent maintenance and special care against dust in the lubricant area. Additionally they require a significant amount of lubricant and the friction coefficient during startup process is inevitably high. In applications where the startup process in under an applied load, the hydrodynamic lubrication film is developed above a value of rotation speed and may become turbulent above a certain speed limit. A turbulent lubrication film is thinner and is also stressing the bore due to high temperature. A tangential rotational shaft speed of 75 mm/s is considered high enough, but in certain applications rotational speed around 150 mm/s has also been achieved.

There are five different lubrication types of journal bearing according to [2]:

Hydrodynamic Lubrication: When the relative rotation speed surpasses a certain margin, a hydrodynamic pressure film is developed separating the two surfaces. A constant supply of lubricant is necessary, but there is no requirement for a certain inlet pressure.

Hydrostatic Lubrication: High pressure lubricant is fed to the system in order to separate the facing edges. There is no need for relative motion.

Elasto- hydrodynamic Lubrication: This is an extension of hydrodynamic lubrication, taking into account the elastic deformations of the shaft and the bore during operation.

Boundary Lubrication: This type takes place when the lubricant thickness is inadequate, due to small bearing surface, low rotational speed, inadequate amount of lubricant or high applied load. The transition between boundary and hydrodynamic lubrication occurs gradually and the intermediate condition is called mixed lubrication.

Solid- film Lubrication: A solid type of lubricant is used in applications where mineral oils cannot be used, or in cases of excessive heating of the interacting components.

In the present Thesis, only hydrodynamic lubrication of journal bearings will be researched. Fundamentals of hydrodynamic lubrication will be further analyzed in a following section.

3.1.1 Bearing Material

Based on [5], [21], [31]

Bearings must be able to withstand several loading conditions without altering the overall performance and additionally to that should resist to wear and fatigue. In case of improper alignment, bearings must offer a margin for safe operation and occasionally withstand contradictory requirements. The materials used must generally be rigid enough to avoid any distortion but in many case they must offer enough flexibility in order to temporarily conform imperfect alignment.

Journal bearings are meant to include sleeve, plain, shell and Babbitt bearings. The term Babbitt actually refers to the layers of softer metals (lead, tin and copper) which form the metal contact surface of the bearing shell. These softer metals overlay a stronger steel support shell and are needed to cushion the shell from the harder rotating shaft. Simple shell-type journal bearings accept only radial loading, perpendicular to the shaft, generally due to the downward weight or load of the shaft. Thrust or axial loads, along the axis of the shaft, can also be accommodated by journal bearings designed for this purpose.

Designers often use a steel-backed “tri-metal” designs. For highly loaded bearings, such as the crankshaft and stern tube ones, bearings are steel-backed with high-strength leaded bronze lining materials. For lightly loaded ones, steel-backed aluminum materials are used. The overlay selection process depends on application requirements. Harder overlays offer better resistance to fatigue. At a higher cost, sputtered aluminum-tin overlays for improved resistance in wear and fatigue can be applied to bronze and aluminum linings. Most commonly, electroplated lead-tin-copper and lead-indium overlays are used. For intermediate levels of performance and cost, electroplated overlays with ceramic hard-phase particles have recently been introduced. An alternative bearing design that improves resistance to wear, while maintaining at the same time a degree of conformability, is called “Rillenlager”. The design forms inlaid bands of overlay material in the lining surface.

3.1.2 Bearing Lubricants

According to: [1], [3] and [21]

The purpose of lubrication is to reduce friction, wear and heating of machine parts moving relative to each other. In the case of journal bearings, the shaft is the rotating part and the bearing bushing is the stationary part. During normal operation, the shaft rotates at sufficient speed to force oil between the conforming curved surfaces of the shaft and shell, thus creating an oil wedge and a hydrodynamic oil film. This full hydrodynamic fluid film allows journal bearings to support extremely heavy loads and operate at high rotational speeds. The rotational speed, load and oil temperature determine the viscosity grade of the lubricant. Proper use of a lubricant implies that under normal operating conditions there is no contact between the bearing and the shaft and therefore no heat is released. Typical lubricants are either oil lubricants or greases, in limited cases with low RPM, shock loading and frequent start and stop.

Oil lubricants are commonly used in journal bearings when cooling is required or contaminants or debris need to be flushed away from the bearing. High-speed journal bearings are always lubricated with oil rather than a grease. Oil is supplied to the bearing by either a pressurized oil pump system, an oil ring or collar or a wick. Grooves in the bearing shell are used to distribute the oil throughout the bearings’ surfaces. If the oil viscosity selected is too low, heat will be generated due to insufficient film thickness and metal-to-metal contact will occur. If the oil viscosity is too high, heat will again be generated, due to the internal fluid friction created within the oil. Selecting an oil which is too high in viscosity can also increase the likelihood of cavitation. The high- and low-pressure zones, which are created within the oil on each side of the area of minimum film thickness, can cause oil cavitation in these bearings.

It is common to use additives in varying quantities, in order to improve certain properties of the oil lubricant. The most common lubricant additives can be divided in the following categories:

- Wear and friction improvers
  - Absorption or boundary additives
  - Anti-wear additives
  - Extreme pressure additives
- Anti-Oxidants
  - Metal deactivators
  - Radical inhibitors
  - Peroxide decomposers
- Corrosion control additives
  - Corrosion inhibitors
  - Rust inhibitors
- Contamination control additives
  - Mild dispersants
  - Over-based dispersants
- Viscosity improvers
- Pour point depressants
- Foam inhibitors

3.1.3 Common Bearing Damages

Typical bearing damages are caused from various reasons [31], usually inter-related ones. The most common journal bearing damages can be divided into the following general categories:

Bearing Damage Types	Comments
Abrasion	Very common type, caused by debris rotating along with oil in the lubricant film or insufficient lubrication.
Fatigue	Can be avoided by using stronger bearing linings and cautious design.
Corrosion	Different bearing alloys suffer corrosion under different conditions.
Wiping	Occurs in any kind of lining material if insufficient lubrication or cooling of the oil takes place.
Cavitation	The risk of cavitation increases with rising of bearing speeds and loads.
Fretting	Occurs due to insufficient contact pressure, local welding and tearing having taken place between the bearing back and housing bore.
Design faults	Can be avoided had pre-production testing taken place.
Incorrect assembly	Typical cases are: incorrect positioning of oil feed connections or incorrect tension of the housing bolts
Static fretting	This can be caused during assembly of the shafting system.
Misalignment	Causes can be taper-shaped in the housing or journal surface and debris may be trapped between shell and housing.
Geometric factors	Geometric inaccuracies may cause damages in regions of the bush.

Table 3-1: COMMON BEARING DAMAGE TYPES

According to classification societies, bearing, or shaft alignment related damages are being reported, mostly for offshore supply vessels and special purpose vessels but lately an increasing number of such failures are reported for bulk, oil and container carriers as well.

3.2 Hydrodynamic Lubrication

3.2.1 Hydrodynamic Lubrication Theory

According to [1] Hydrodynamic lubrication is the phenomenon in which two relatively moving non-parallel surfaces are separated by a pressurized thin lubricating fluid film Figure 3-3. The upper surface is the stator and is misaligned to the bottom surface (runner). Between the two, lubricating oil is also moving at a certain speed. The condition of relative motion and misalignment of the two surfaces is essential for the generation of this hydrodynamic film. During this motion, a pressure field is generated in the fluid and the pressure gradient causes the fluid velocity profile to bend inwards at the entrance of the wedge and outwards at the exit. The generated pressure field has the ability to support a certain load applied to the slider. It was found by Reynolds and many later researchers that most of the lubricating effect of oil could be explained in terms of its relatively high viscosity. Stachowiak in [1] mentions: "All hydrodynamic lubrication can be expressed mathematically in the form of an equation which was originally derived by Reynolds and is commonly known throughout the literature as the 'Reynolds equation'. There are several ways of deriving this equation. Since it is a simplification of the Navier-Stokes momentum and continuity equation it can be derived from this basis. It is, however, more often derived by considering the equilibrium of an element of liquid subjected to viscous shear and applying the continuity-of-flow principle." Reynolds equation also expresses the conditions that need to be valid in order to achieve hydrodynamic lubrication, meaning the non-zero relative rotation and misalignment of runner and stator to drag lubricant into the wedge. Additionally it clearly describes the influence of the geometry, on the spatial rate of pressure change.

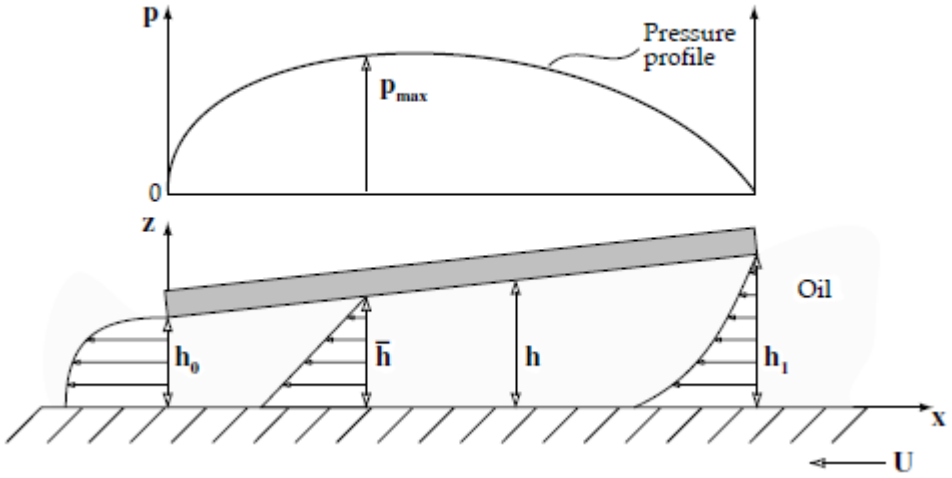

Figure 3-3: HYDRODYNAMIC PRESSURE GENERATION BETWEEN NON- PARALLEL SURFACES [4]

To sum up, in order to use the Reynolds equation to mathematically express the principles of hydrodynamic lubrication of journal bearings, the basic assumptions that need to be true are:

- The lubricant is a Newtonian, viscous fluid,
- Lubricant inertia induced forces are negligible compared to viscous forces,
- Gravitational forces can be neglected,
- The lubricant is an incompressible fluid,
- Lubricant viscosity remains spatially constant (Isoviscous condition),
- Lubricant flow is steady (temporal effects are neglected, steady-state condition is assumed),
- Bearing inner diameter to bearing clearance ratio is close to infinity,

3.2.2 Journal Bearing Geometry

The geometry of a cylindrical bearing is shown in Figure 3-4, with its circumferential coordinate θ measured directly from the line of centers, i.e. the maximum film thickness. The journal bearing radius is R_1 and the shaft radius is R_2. O_B is the center of the bearing and O_S is the center of the shaft, eccentricity e is the distance between these centers and attitude angle ϕ is the angle between the y- axis and the line defined by O_B and O_S, at which the minimum and maximum film thickness is derived.

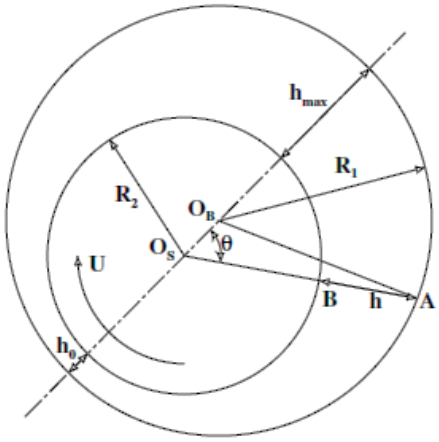

Figure 3-4: BEARING CROSS SECTION [1]

Film thickness h is described by the following approximation, which is used in almost all analyses:

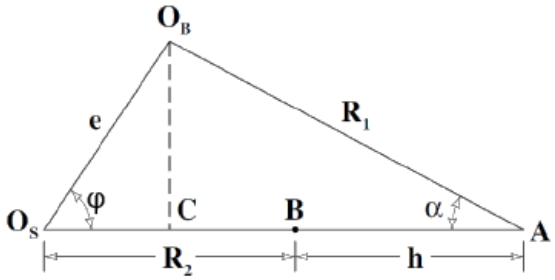

Figure 3-5: GEOMETRY DETAILS FOR THE EVALUATION OF FILM SHAPE [1]

According to Figure 3-5 the mathematical modeling of film thickness h derives from the following expressions:

$$\mathbf{O_SA = O_SC + CA = O_SB + BA}$$

$$O_SA = e \cdot \cos\theta + R_1 \cdot \cos\alpha = R_2 + h$$

Thus: $$h = e \cdot \cos\theta + R_1 \cdot \cos\alpha - R_2 \quad (1)$$

Applying the sine rule: $$\sin\alpha = e/R_1 \cdot \sin\theta \quad (2)$$

Since $e/R_1 << 1$ and $\sin^2\alpha + \cos^2\alpha = 1$ $$\cos\alpha = \sqrt{1 - (e/R_1)^2 \sin^2\theta} \approx 1 \quad (3)$$

Substituting, $c = R_1 - R_2$, $$\mathbf{h = c + e \cdot \cos\theta = c \cdot (1 + \varepsilon \cdot \cos\theta)} \quad (4)$$

Where: the eccentricity ratio $\varepsilon = e / c$

The equation above describes the film geometry with an accuracy of 0.1%.

3.2.3 Mathematical Approach – Reynolds Approximation

The assumptions that need to be introduced, in order to derive the Reynolds equation are:

Basic assumptions	Comments
Body forces are neglected	This assumption is always valid, since there are no extra outside fields of forces acting on the fluid with an exception of magneto-hydrodynamic fluids and their applications.
Constant pressure through the film thickness	Usually valid, since hydrodynamic film thickness is in the range of several micrometers, exception are elastic films.
No slip is assumed at the fluid-solid edges	Always valid, since the velocity of the oil layer adjacent to the boundary is considered equal to the velocity of the boundary.
Lubricant is or behaves as a Newtonian fluid	Depends on the fluid used, usually is valid
Flow is laminar	Valid for relatively small bearings, exception are large bearings of turbines
Fluid inertia is neglected	Valid for low rotational speeds or high loads. Inertia effects can be included with additional modifications for exact analyses.
Fluid density is constant	Usually valid for fluids without or with low thermal expansion, not valid for gases.
Viscosity is constant throughout fluid domain	Very crude assumption to simplify calculations, since viscosity depends on temperature and therefore is not constant throughout the generated film.

Table 3-2: ASSUMPTIONS TO DERIVE THE REYNOLDS EQUATION

Force equilibrium and continuity of flow

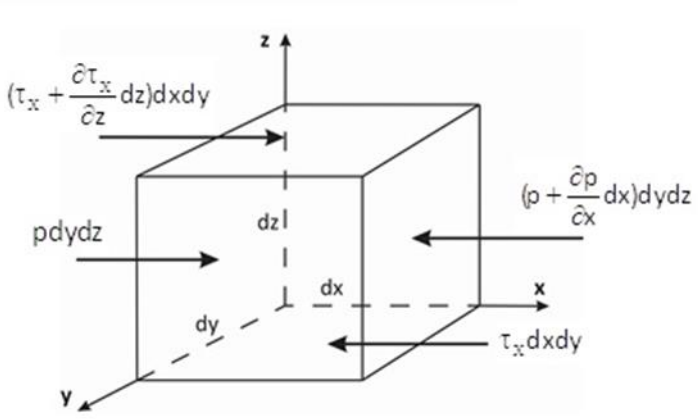

Figure 3-6: FORCE EQUILIBRIUM AT FLUID ELEMENT

In Figure 3-6, the forces equilibrium on an infinitesimal fluid element of a hydrodynamic film are depicted. For simplicity it is assumed that the forces act only in the 'x' direction. The element is in equilibrium which means that the forces acting to the left must balance the forces acting to the right, so:

$$pdydz + (\tau_X + \frac{\partial \tau_X}{\partial z} dz)dxdy = (p + \frac{\partial p}{\partial x} dx)dydz + \tau_X dxdy \quad (1)$$

After simplifying Eq. (1) we get:

$$\frac{\partial \tau_X}{\partial z} dxdydz = \frac{\partial p}{\partial x} dxdydz \quad (2)$$

Since the infinitesimal volume (dx·dy·dz) is non-zero, both sides of the Eq. (2) can be divided by (dx·dy·dz), which yields:

$$\frac{\partial \tau_X}{\partial z} = \frac{\partial p}{\partial x} \quad (3)$$

Following the same methodology for the forces acting on the 'y' direction (shear stress values are different from those acting on the 'x' direction), then the following equation can be derived:

$$\frac{\partial \tau_Y}{\partial z} = \frac{\partial p}{\partial y} \quad (4)$$

Since pressure is assumed constant throughout the film thickness, the pressure gradient in the 'z' direction is equal to zero, thus:

$$\frac{\partial p}{\partial z} = 0 \quad (5)$$

If 'u' and 'v' are the velocities in the direction of 'x' and 'y', respectively, the corresponding values of shear stress can be written as:

$$\tau_X = \eta \frac{\partial u}{\partial z} \quad (6)$$

$$\tau_Y = \eta \frac{\partial v}{\partial z} \quad (7)$$

Substituting Eq. (6) and Eq. (7) in Eq. (3) and Eq. (4), respectively, results in the following equations for the 'x' and 'y' directions:

$$\frac{\partial p}{\partial x} = \frac{\partial}{\partial z}\left(\eta \frac{\partial u}{\partial z}\right) \quad (8)$$

$$\frac{\partial p}{\partial y} = \frac{\partial}{\partial z}\left(\eta \frac{\partial v}{\partial z}\right) \quad (9)$$

Eq. (12), Eq. (13) can be integrated. The viscosity of the fluid is assumed constant throughout the film. Separating the variables gives:

$$\frac{\partial p}{\partial x} \partial z = \partial\left(\eta \frac{\partial u}{\partial z}\right) \quad (10)$$

$$\frac{\partial p}{\partial y} \partial z = \partial\left(\eta \frac{\partial z}{\partial z}\right) \quad (11)$$

Integrating gives:

$$\frac{\partial p}{\partial x} z + C_1 = \eta \frac{\partial u}{\partial z} \quad (12)$$

$$\frac{\partial p}{\partial y}z + C_2 = \eta\frac{\partial v}{\partial z} \tag{13}$$

Separating variables again gives,

$$\left(\frac{\partial p}{\partial x}z + C_1\right)\partial z = \eta\partial u \tag{14}$$

$$\left(\frac{\partial p}{\partial y}z + C_2\right)\partial z = \eta\partial v \tag{15}$$

Integrating yields:

$$\frac{\partial p}{\partial x}\frac{z^2}{2} + C_1 z + C_3 = \eta u \tag{16}$$

$$\frac{\partial p}{\partial y}\frac{z^2}{2} + C_2 z + C_4 = \eta v \tag{17}$$

At the boundaries of the wedge, the boundary conditions are:

$$u\big|_{z=0} = U_2,\ u\big|_{z=h} = U_1,\ v\big|_{z=0} = V_2,\ v\big|_{z=h} = V_1$$

By substituting the boundary conditions, at Eq. (16) and Eq. (17) the constants C_1 to C_4 are calculated:

$$C_3 = \eta U_2$$

$$C_1 = \frac{\eta}{h}(U_1 - U_2) - \frac{\partial p}{\partial x}\frac{h}{2}$$

$$C_4 = \eta V_2$$

$$C_2 = \frac{\eta}{h}(V_1 - V_2) - \frac{\partial p}{\partial y}\frac{h}{2}$$

Substituting those constants into Eq. (16) and Eq. (17) yields:

$$\frac{\partial p}{\partial x}\frac{z^2}{2} + \left(\frac{\eta}{h}(U_1 - U_2) - \frac{\partial p}{\partial x}\frac{h}{2}\right)z + \eta U_2 = \eta u$$

$$\frac{\partial p}{\partial y}\frac{z^2}{2} + \left(\frac{\eta}{h}(V_1 - V_2) - \frac{\partial p}{\partial y}\frac{h}{2}\right)z + \eta V_2 = \eta v$$

Dividing and simplifying gives the expressions for fluid velocity in ‘x’ and ‘y’ directions:

$$u = \left(\frac{z^2 - zh}{2\eta}\right)\frac{\partial p}{\partial x} + (U_1 - U_2)\frac{z}{h} + U_2 \tag{18}$$

$$v=\left(\frac{z^2-zh}{2\eta}\right)\frac{\partial p}{\partial y}+\left(V_1-V_2\right)\frac{z}{h}+V_2 \tag{19}$$

The three terms of each velocity profile represent the different velocity components, presented in the following Figure 3-7.

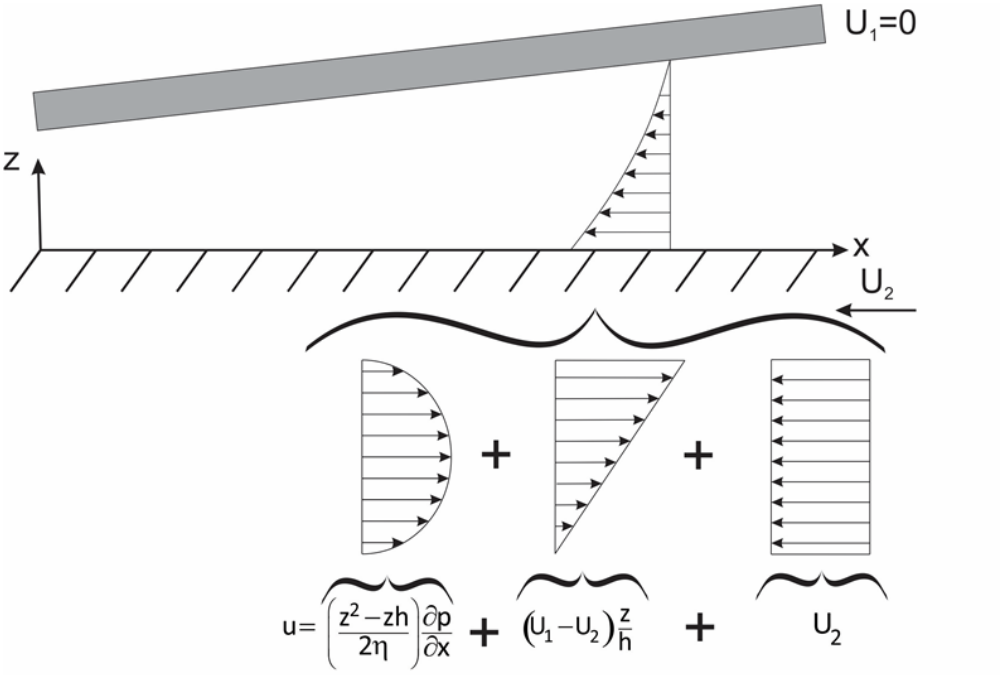

Figure 3-7: VELOCITY PROFILES AT THE INFLOW REGION OF A SIMPLE SLIDER [1]

Considering a lubricant element as shown in the following figure (3-8), the lubricant mass flows into the element at rates of 'ρ·u·dy·dz', 'ρ·v·dx·dz', 'ρ·w·dx·dy', and out of the column at rates of $\left(\rho u+\frac{\partial(\rho u)}{\partial x}dx\right)dydz$, $\left(\rho v+\frac{\partial(\rho v)}{\partial y}dy\right)dxdz$, $\left(\rho w+\frac{\partial(\rho w)}{\partial z}dz\right)dxdy$,in the direction of 'x' axis, 'y' axis and 'z' axis, respectively. The lubricant mass accumulation rate in the element is $\frac{\partial\rho}{\partial t}dxdydz$. The principle of continuity of flow requires that the lubricant mass accumulation rate is equal to the difference between the influx and efflux rate of the control volume thus:

$$\begin{aligned}\frac{\partial\rho}{\partial t}dxdydz=\rho udydz+\rho vdxdz+\rho wdxdy-\left(\rho u+\frac{\partial(\rho u)}{\partial x}dx\right)dydz\\ -\left(\rho v+\frac{\partial(\rho v)}{\partial y}dy\right)dxdz-\left(\rho w+\frac{\partial(\rho w)}{\partial z}dz\right)dxdy\end{aligned} \tag{20}$$

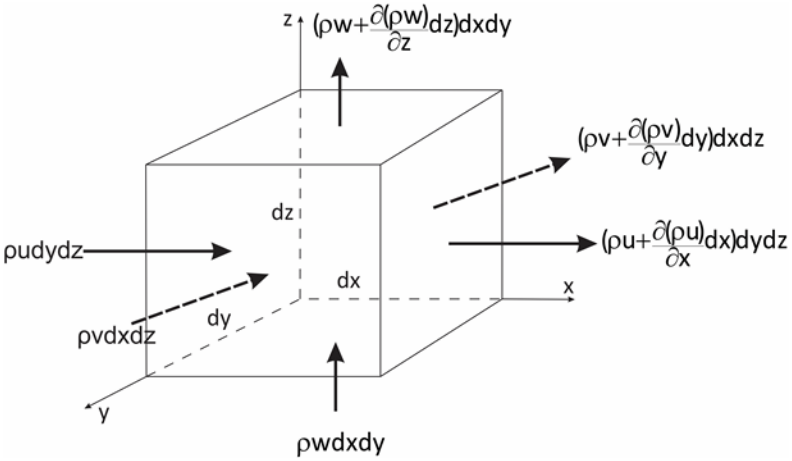

Figure 3-8: CONTINUITY OF FLOW IN A FLUID ELEMENT

After simplifying Eq.(20), it yields:

$$\frac{\partial \rho}{\partial t}dxdydz+\frac{\partial(\rho u)}{\partial x}dxdydz+\frac{\partial(\rho v)}{\partial y}dydxdz+\frac{\partial(\rho w)}{\partial z}dzdxdy=0 \tag{21}$$

Since (dx·dy·dz) ≠ 0, Eq. (21) can be rewritten as:

$$\frac{\partial \rho}{\partial t}+\frac{\partial(\rho u)}{\partial x}+\frac{\partial(\rho v)}{\partial y}+\frac{\partial(\rho w)}{\partial z}=0 \tag{22}$$

The next step is to integrate the terms of Eq. (22) over the film thickness h. The Leibnitz rule for differentiation of integrals is used for the integration of the first, second and third term. Fluid density is considered constant through the film thickness and, thus the first term yields:

$$\int_0^h \frac{\partial \rho}{\partial t}\,dz=\frac{\partial}{\partial t}\int_0^h \rho dz-\rho\frac{\partial h}{\partial t}=\frac{\partial(\rho h)}{\partial t}-\rho\frac{\partial h}{\partial t} \tag{23}$$

Integrating the second term of Eq. (22) gives:

$$\begin{aligned}\int_0^h \frac{\partial(\rho u)}{\partial x}\,dz&=\frac{\partial}{\partial x}\int_0^h \rho u\,dz-\rho u\big|_{z=h}\frac{\partial h}{\partial x}=\frac{\partial}{\partial x}\left(\int_0^h \rho\left(\frac{z^2-zh}{2\eta}\right)\frac{\partial p}{\partial x}+\rho(U_1-U_2)\frac{z}{h}+\rho U_2\,dz\right)-\rho U_1\frac{\partial h}{\partial x}=\\&=\frac{\partial}{\partial x}\left(\rho\left(\frac{z^3}{3}-\frac{z^2h}{2}\right)\frac{1}{2\eta}\frac{\partial p}{\partial x}+\rho(U_1-U_2)\frac{z^2}{2h}+\rho U_2 z\Big|_0^h\right)-\rho U_1\frac{\partial h}{\partial x}=\\&=\frac{\partial}{\partial x}\left(-\rho\frac{h^3}{12\eta}\frac{\partial p}{\partial x}+\rho(U_1-U_2)\frac{h}{2}+\rho U_2 h\right)-\rho U_1\frac{\partial h}{\partial x}=\\&=\frac{\partial}{\partial x}\left(-\rho\frac{h^3}{12\eta}\frac{\partial p}{\partial x}+\rho h\frac{U_1+U_2}{2}\right)-\rho U_1\frac{\partial h}{\partial x}\end{aligned} \tag{24}$$

Integrating the third term of Eq. (22) gives:

$$\int_0^h \frac{\partial(\rho v)}{\partial y}\,dz = \frac{\partial}{\partial y}\int_0^h \rho v\,dz - \rho v\big|_{z=h}\frac{\partial h}{\partial y} = \frac{\partial}{\partial y}\left(\int_0^h \rho\left(\frac{z^2 - zh}{2\eta}\right)\frac{\partial p}{\partial y} + \rho\left(V_1 - V_2\right)\frac{z}{h} + \rho V_2 dz\right) - \rho V_1\frac{\partial h}{\partial y} =$$

$$= \frac{\partial}{\partial y}\left(\rho\left(\frac{z^3}{3} - \frac{z^2 h}{2}\right)\frac{1}{2\eta}\frac{\partial p}{\partial y} + \rho\left(V_1 - V_2\right)\frac{z^2}{2h} + \rho V_2 z\Big|_0^h\right) - \rho V_1\frac{\partial h}{\partial y} =$$

$$= \frac{\partial}{\partial y}\left(-\rho\frac{h^3}{12\eta}\frac{\partial p}{\partial y} + \rho\left(V_1 - V_2\right)\frac{h}{2} + \rho V_2 h\right) - \rho V_1\frac{\partial h}{\partial y} = \tag{25}$$

$$= \frac{\partial}{\partial y}\left(-\rho\frac{h^3}{12\eta}\frac{\partial p}{\partial y} + \rho h\frac{V_1 + V_2}{2}\right) - \rho V_1\frac{\partial h}{\partial y}$$

Integrating the last term of Eq. (22) with the same assumption yields:

$$\int_0^h \frac{\partial(\rho w)}{\partial z}\,dz = \rho w\big|_{z=h} - \rho w\big|_{z=0} \tag{26}$$

Substituting the above integrated terms into Eq. (22) yields:

$$\frac{\partial(\rho h)}{\partial t} - \rho\frac{\partial h}{\partial t} + \frac{\partial}{\partial x}\left(-\rho\frac{h^3}{12\eta}\frac{\partial p}{\partial x} + \rho h\frac{U_1 + U_2}{2}\right) - \rho U_1\frac{\partial h}{\partial x} + \frac{\partial}{\partial y}\left(-\rho\frac{h^3}{12\eta}\frac{\partial p}{\partial y} + \rho h\frac{V_1 + V_2}{2}\right)$$
$$-\rho V_1\frac{\partial h}{\partial y} + \rho w\big|_{z=h} - \rho w\big|_{z=0} = 0 \tag{27}$$

Assuming that there is no local variation in surface speed in the direction of ‘x’ and ‘y’ axis, Eq. (27) gives:

$$\frac{\partial(\rho h)}{\partial t} - \rho\frac{\partial h}{\partial t} + \frac{\partial}{\partial x}\left(-\rho\frac{h^3}{12\eta}\frac{\partial p}{\partial x}\right) + \frac{U_1 + U_2}{2}\frac{\partial(\rho h)}{\partial x} - \rho U_1\frac{\partial h}{\partial x} + \frac{\partial}{\partial y}\left(-\rho\frac{h^3}{12\eta}\frac{\partial p}{\partial y}\right)$$
$$+\frac{V_1 + V_2}{2}\frac{\partial(\rho h)}{\partial y} - \rho V_1\frac{\partial h}{\partial y} + \rho w\big|_{z=h} - \rho w\big|_{z=0} = 0 \tag{28}$$

Finally, after simplifications, the full Reynolds equation in three dimensions can be derived:

$$\frac{\partial}{\partial x}\left(\frac{h^3}{\eta}\frac{\partial p}{\partial x}\right) + \frac{\partial}{\partial y}\left(\frac{h^3}{\eta}\frac{\partial p}{\partial y}\right) = 6\left(U\frac{\partial \rho h}{\partial x} + V\frac{\partial \rho h}{\partial y}\right) + 12(w_h - w_0) \tag{29}$$

3.2.4 Reynolds Equation Simplifications for Journal Bearings

There are some additional simplifications that can be implemented to the Reynolds equation in order to use it to study journal bearings. These are the following:

- Unidirectional velocity approximation

In journal bearings the hydrodynamic film is generated by the angular rotation of the shaft without any axial motion. Choosing an axis in such a way that some velocities from Eq. (29) are equal to zero, assuming that $V_1=V_2=0$, Eq. (29) can be rewritten as:

$$\frac{\partial}{\partial x}\left(\frac{h^3}{\eta}\frac{\partial p}{\partial x}\right)+\frac{\partial}{\partial y}\left(\frac{h^3}{\eta}\frac{\partial p}{\partial y}\right)=6U\frac{\partial \rho h}{\partial x}+12(w_h-w_0) \quad (30)$$

- Steady or Variable Film thickness approximation

During operation of a bearing, the outer part of the bearing (stator) is held stationary and only the inner part (shaft) rotates. The lubricant film geometry is defined as the space between the bearing and the shaft. For the formulation of the journal bearing problem, it is equivalent to assume that the bearing rotor has a horizontal velocity $U_2=U$, while the shaft is stationary. In the vertical direction, the bearing stator is fixed ($w|_{z=0}=0$), while the shaft can undergo small vertical motion (squeeze film motion). The vertical velocity of the shaft ' $w|_{z=h}$ ' is equal to the film thickness variation in time:

$$w|_{z=h}=\frac{\partial h}{\partial t}$$

The distance between the operating surfaces 'h' may periodically vary due to dynamic loading conditions but in this work $w|_{z=h}$ = 0. Taking this into account, Eq. (30) can be written as:

$$\frac{\partial}{\partial x}\left(\frac{h^3}{\eta}\frac{\partial p}{\partial x}\right)+\frac{\partial}{\partial y}\left(\frac{h^3}{\eta}\frac{\partial p}{\partial y}\right)=6U\frac{\partial \rho h}{\partial x} \quad (31)$$

- Isoviscous approximation

Viscosity 'η' is assumed to be constant over the lubricant film (thermal effects which affect the viscosity are neglected). This approach is known in the literature as the 'isoviscous' modeling approach. Assuming that η=constant, Eq. (31) can be further simplified:

$$\frac{\partial}{\partial x}\left(h^3\frac{\partial p}{\partial x}\right)+\frac{\partial}{\partial y}\left(h^3\frac{\partial p}{\partial y}\right)=6U\eta\frac{\partial \rho h}{\partial x} \quad (32)$$

In the present work, the form of Reynolds equation that will be used for the study of plain journal bearings is that of Eq. (32).

- Constant fluid density

In the region of the bearing where positive pressures exist (active zones), lubricant density can be assumed constant (ρ=constant), as the lubricant is a non-compressible fluid. Reynolds Eq.(32) can be further simplified to the following form:

$$\left[\frac{\partial}{\partial x}\left(h^3\frac{\partial p}{\partial x}\right)+\frac{\partial}{\partial y}\left(h^3\frac{\partial p}{\partial y}\right)\right]\frac{1}{\eta}=6U\frac{\partial h}{\partial x} \quad (37)$$

To sum up, the final form of the Reynolds Equation that describes the journal bearing and will be used in the following steps of the present work is:

$$\left[\frac{\partial}{\partial x}\left(h^3\frac{\partial p}{\partial x}\right)+\frac{\partial}{\partial y}\left(h^3\frac{\partial p}{\partial y}\right)\right]\frac{1}{\eta}=6U\frac{\partial h}{\partial x} \tag{37}$$

Where:

- U is the tangential velocity of the shaft,
- η, is the lubricant dynamic viscosity,
- h is a function that describes lubricant film thickness in 3D space and,
- p, is the pressure distribution in 3D space.

For the analysis of the journal bearing that will be described in the next sections, it is important to present here the concept of unwrapped bearing geometry as presented in the following picture.

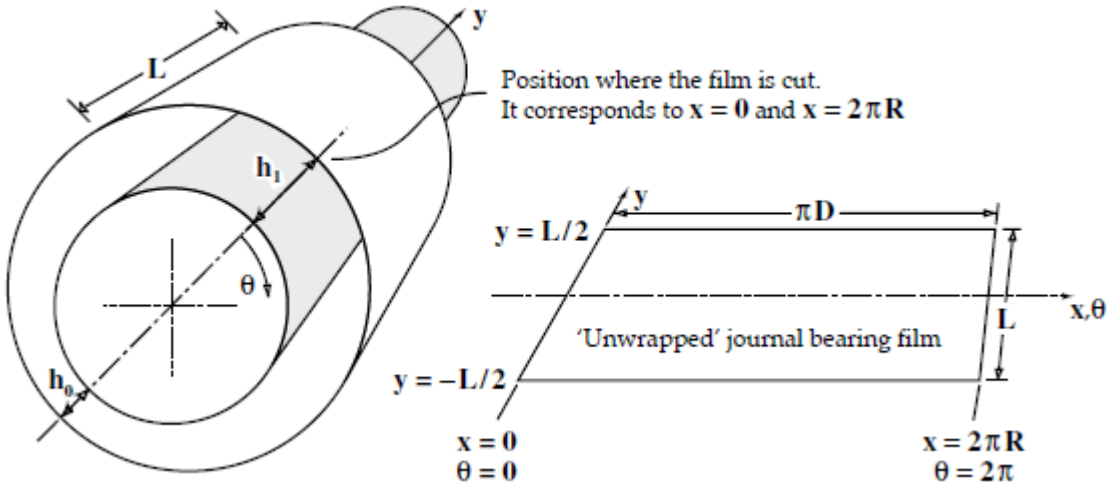

Figure 3-9: UNWRAPPED BEARING GEOMETRY [31]

In an unwrapped journal bearing <u>without misalignment</u>, the geometry is symmetric around the axis that passes through the minimum film thickness 'h_{min}', as it is illustrated in the following figure:

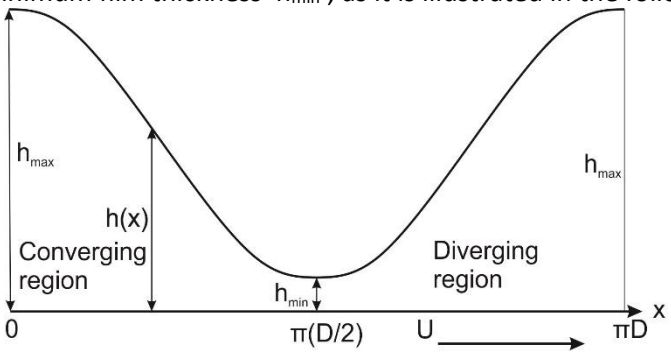

Figure 3-10: FILM THICKNESS GEOMETRY IN AN UNWRAPPED JOURNAL BEARING [31]

3.2.5 Boundary Conditions

To solve the Reynolds equation, appropriate boundary conditions for the pressure distribution must be set. Of all the boundary conditions proposed, the most notable according to [1] are:

- The Full-Sommerfeld condition: which assumes that pressure is equal to zero at the edges of the wedge. Consequentially a negative bearing pressure of similar distribution and magnitude is developed at the diverging section of the geometry, which makes total pressure and therefore load capacity equal to zero. Thus this condition is unrealistic and is rarely used.
- The Half Sommerfeld condition: which assumes that the positive pressure distribution at the converging section is identical to the full Sommerfeld condition, whereas negative pressure values at the diverging region are equal to zero. The method is quite simple but its physical basis is erroneous since it leads to discontinuity of flow between the two regions.
- The Reynolds condition: This boundary condition suggests that negative pressure values should be set to zero and that at the boundary pressure gradient should also be: **p = dp / dx = 0**. The Reynolds boundary condition gives more accurate results in comparison to the Full and Half Sommerfeld conditions, and it is used for the pressure calculations of the present work. In the following Figure, the pressure distribution in Reynolds boundary condition is presented.

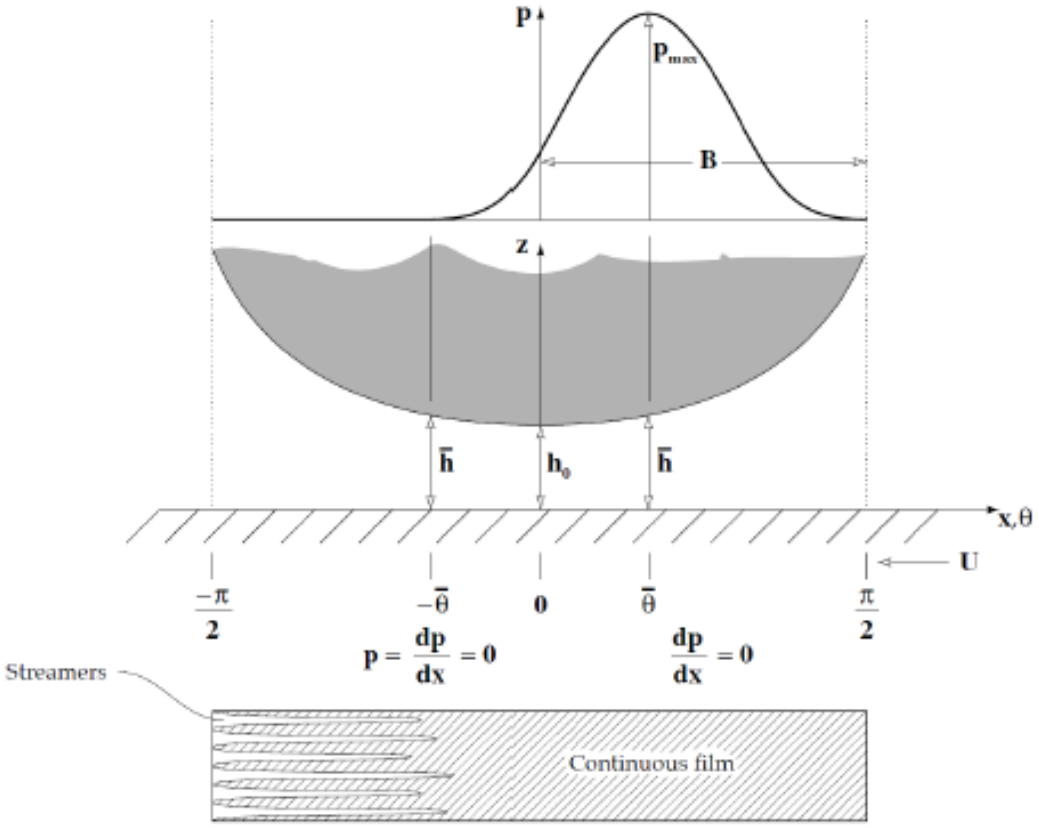

Figure 3-11: REYNOLDS BOUNDARY CONDITION [1]

3.3 Design and Performance Parameters

3.3.1 Load Capacity

In journal bearings, the total load that can be supported with hydrodynamic lubrication can be derived from integration of the pressure at the circumference of the shaft. This load will be resolved into two perpendicular loads. The first one is acting along the line of the shaft and bush centers and the second is a perpendicular load vector. The sum of these vectors yields the total load and the angle between the total load and the first component is the attitude angle, which defines the line at which minimum and maximum film thickness occur at the side of converging and diverging section of the shaft respectively.

The expressions of the load components "Wx" , "Wz", as demonstrated in figure 3.12, derive from assumption of a lubricant film area as: R·dy·dθ where the hydrodynamic load is p·R·dy·dθ. The two force components are:

dWx= p·cos(ϕ+θ-π/2)·R·dy·dθ yielding a load of: $W_X = \int_0^{2\pi} \int_0^L p \cdot \cos\left(\varphi + \theta - \frac{\pi}{2}\right) \cdot R \cdot dy \cdot d\theta$ (38)

dWz= p·sin(ϕ+θ-π/2)·R·dy·dθ yielding a load of: $W_Z = \int_0^{2\pi} \int_0^L p \cdot sin\left(\varphi + \theta - \frac{\pi}{2}\right) \cdot R \cdot dy \cdot d\theta$ (39)

The total load-carrying capacity is: $W = \sqrt{{W_X}^2 + {W_Z}^2}$ (40)

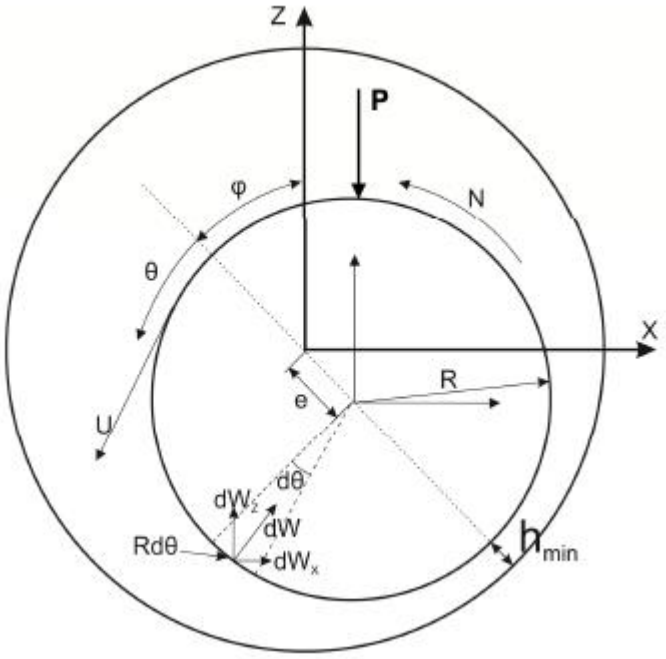

Figure 3-12: HYDRODYNAMIC LOAD COMPONENTS IN A JOURNAL BEARING

3.3.2 Sommerfeld Number

The Sommerfeld number is a non-dimensional parameter that comprises of both design and operation elements. It characterizes the performance of the bearing and is used to compare similar bearings in deferent operational conditions or different bearing designs for a precise operation.

Sommerfeld number can be calculated according to the following formula:

$$S = \frac{\eta N_s DL}{W}(\frac{R}{c})^2 \tag{41}$$

Where:

- η is the lubricant viscosity (Pa· s)
- N_s is the rotor angular velocity (RPS)
- *D* is the bearing diameter (m)
- *L* is the bearing length (m)
- *W* is the applied load (N)
- *R* is the bearing radius (m)
- *c* is the bearing clearance (m)

3.3.3 Friction Force and Friction Coefficient

Integration of the x-component of shear stress, 'τ_x', over the bearing area yield the total amount of Friction force:

$$F = \int_0^L \int_0^{\pi D} \tau_x dxdy = \int_0^L \int_0^{\pi D} \eta \frac{du}{dz} dxdy \tag{33}$$

For journal bearings, Eq. (18) can be written as:

$$u = \left(\frac{z^2 - zh}{2\eta} \right) \frac{\partial p}{\partial x} + U\frac{z}{h} \tag{34}$$

Differentiating with respect to 'z' gives:

$$\frac{du}{dz} = \left(\frac{2z - h}{2\eta} \right) \frac{\partial p}{\partial x} + \frac{U}{h} \tag{35}$$

Using Eq. (35), Eq. (33) yields:

$$F = \int_0^L \int_0^{\pi D} \left(\frac{2z - h}{2} \frac{\partial p}{\partial x} + \frac{U}{h} \right) dxdy \tag{36}$$

Friction coefficient

The friction coefficient 'μ' can be calculated from the following formula, where F stands for the friction forces and W refers to the total load:

$$\mu = \frac{F}{W} \tag{37}$$

3.3.4 Inlet and Outlet flow rates

The inlet flow rate per unit length can be calculated as:

$$q_x = \int_0^h u\,dz = \left| \left(\frac{z^3}{3} - \frac{z^2 h}{2} \right) \frac{\partial p}{2\eta \partial x} - U_2 \frac{z^2}{2h} + U_2 z \right|_0^h = \left(\frac{h^3}{3} - \frac{h^3}{2} \right) \frac{\partial p}{2\eta \partial x} - U\frac{h}{2} + Uh = -\frac{h^3}{12\eta}\frac{\partial p}{\partial x} + U\frac{h}{2} \quad (38)$$

Thus lubricant inflow can be calculated at the bearing entrance by integrating Eq. (38) over the entire bearing length:

$$Q_I = \int_0^L q_x\big|_{x=0}\,dy = \int_0^L \left(-\frac{h^3}{12\eta}\frac{\partial p}{\partial x} + U\frac{h}{2} \right)\Bigg|_{x=0} dy \quad (39)$$

The lubricant outflow rate per unit width can be calculated as:

$$q_y = \int_0^h v\,dz = \left| \left(\frac{z^3}{3} - \frac{z^2 h}{2} \right) \frac{\partial p}{2\eta \partial y} \right|_0^h = -\frac{h^3}{12\eta}\frac{\partial p}{\partial y} \quad (40)$$

Thus, the lubricant side leakage can be calculated by integrating Eq. (40) over the bearing sides:

$$Q_L = \int_0^{\pi D} q_y\big|_{y=0}\,dx + \int_0^{\pi D} q_y\big|_{y=L}\,dx = \int_0^{\pi D} \left(-\frac{h^3}{12\eta}\frac{\partial p}{\partial y} \right)\Bigg|_{y=0} dx + \int_0^{\pi D} \left(-\frac{h^3}{12\eta}\frac{\partial p}{\partial y} \right)\Bigg|_{y=L} dx \quad (41)$$

For normal bearing operation, lubricant must be supplied to the bearing at the same rate as that of the lubricant leakage; otherwise lubricant starvation will occur, which will generally lead to smaller values of minimum film thickness and higher values of oil temperature.

3.3.5 Power Loss

The power loss derives from the friction losses and can be calculated as follows:

$$P_{loss} = F \cdot U = W \cdot \mu \cdot \omega \cdot R \quad (51)$$

Where:

- μ, is the friction coefficient
- W, is the total bearing load
- F, is the total friction force
- ω, is the angular speed of the shaft
- R, is the bearing radius

3.3.6 Advanced Film Thickness Geometry

The area between the rotating shaft and the bearing housing, filled with lubricant, will be geometrically modeled based on several parameters. These parameters are either constant parameters of the system (L, R, and c) or they represent variables of the system (θ, e, and ϕ). It is evident that film thickness geometry 'h' is variable and must be recalculated at every time step of the solution, before solving the Reynolds equation. As it will be analyzed in the next section, an iterative process will be followed to calculate the final equilibrium. Assuming that inertia effects in the film are neglected, the flow is laminar, the fluid is incompressible and Newtonian, the density, specific heat and thermal conductivity are constant, the film thickness for a journal bearing is given by:

$$\mathrm{h}(\theta) = \mathrm{h}_0(\theta) + \mathrm{h}_\mathrm{e}(\theta) + \mathrm{h}_\mathrm{t}(\theta) \tag{52}$$

Where:

- $h_o(\theta)$ is the nominal film thickness, for a rigid bearing according to (5): $h_0(\theta) = c + e_0\cos(\theta)$
- $h_e(\theta)$ is the elastic deformation of the bearing housing due to hydrodynamic pressures,
- $h_t(\theta)$ is the thermal deformation due to thermal expansion of the shaft and the bearing housing

The elastic component in the film thickness equation occurs due to the hydrodynamic pressures applied on the housing of the bearing, assuming the shaft is rigid. Since bearings are highly compliant, radial displacement at a given point depends on all forces acting on the housing. In the current optimization work only cases with an optimum hydrodynamic pressure profile will be analyzed, therefore no shaft to housing connection will occur resulting to minimum elastic deformations. As a compromise between time and accuracy, elastic deformations will not be included in the present thesis.

The modification of the film thickness due to thermal deformations has two origins. The first one is the thermal expansion of the shaft and the second is the deformation due to the bearing housing dilatation. The aft stern tube bearing that is analyzed in this thesis, does not suffer much from thermal variations (in comparison to crankshaft bearings), if operating at proper conditions, therefore thermal deformation should be minimum at design conditions and thus will not be included in the analysis of the present work.

Under ideal shaft alignment conditions, the shaft and bearing centerlines are parallel. In that case bearing-shaft misalignment is zero and bearing misalignment can be defined as the angle between the centerlines of these two parts. Usually though, misalignment values are not zero due to improper shaft alignment, excessive loading or other operational purposes. Misalignment angle can be resolved into two perpendicular angles, similar to the external load angles, one about each axis of the coordinate system. Thus, lateral misalignment angles describe shaft rotations about the vertical y axis, and vertical misalignment angles describe rotations about the horizontal z axis.

Eq. (5) will then be modified to:

$$h_{hydro}(\theta, z) = c + e_0\cos(\theta) + z\left[\psi_y\cos(\theta + \varphi_0) + \psi_x\sin(\theta + \varphi_0)\right] \tag{53}$$

Bearing-shaft misalignment has a negative impact on the lubrication characteristics of the bearing. For a given pair of eccentricity and attitude angle values, the misaligned shaft is brought closer to the bearing surface (in comparison to non-misaligned design), minimum film thickness decreases and the hydrodynamic lubrication film becomes less able to support the weight of the shaft.

Another consequence of bearing-shaft misalignment is the alteration of the pressure distribution of the lubricant. At a no-misalignment design lubricant pressure is lengthwise symmetrical, with a maximum value located at the center of the bearing surface. On the contrary, under misalignment, pressure will form a more discreet peak, with maximum pressure being located closer to the edge of the bearing and the longitudinal position of minimum film thickness. This should is the main reason why single or double slope bearing designs are proposed.

Under some conditions, the shaft might start grinding against the inner bearing surface until portion of the bearing's lower part has been removed by the shaft. This kind of adaptation is expected to happen during the first years of a system's operation and is considered to improve bearing performance as it reduces the effect of misalignment. The wear is then modeled and Eq. (53) is modified as:

$$h_{hydro}(\theta, z) = c + e_0 \cos(\theta) + z\left[\psi_y \cos(\theta + \varphi_0) + \psi_x \sin(\theta + \varphi_0)\right] + \delta_h(\theta) \quad (54)$$

In the present work, single and double slope designs of the stern tube bearing are proposed and therefore no wear is estimated.

In order to take into account the slope of the bearing housing, Eq. (53) is modified as follows:

$$h_{hydro}(\theta, z) = c + e_0 \cos(\theta) + z\left[\psi_y \cos(\theta + \varphi_0) + \psi_x \sin(\theta + \varphi_0)\right] - z \cdot slope \cos(\theta + \varphi_0) \quad (55)$$

This is the final form of the geometrical modeling of the journal bearing film thickness and will be used in the analysis of the bearing. Double slope design is proposed for stern tube bearings in order to maximize the contact area between the shaft and the bearing bush and thereof yield to minimum pressure through the length of the bearing. In comparison to other bearings of the shafting system, the aft stern tube bearing, due to the large L/D ratio is more likely to require double slope instead of single slope inclination. The main reason for this, is that the shaft within the bearing might actually be elastically bent which will be further discussed in the next sections of this thesis. In the following figure, an example of a double slope design is presented in Figure 3-13.

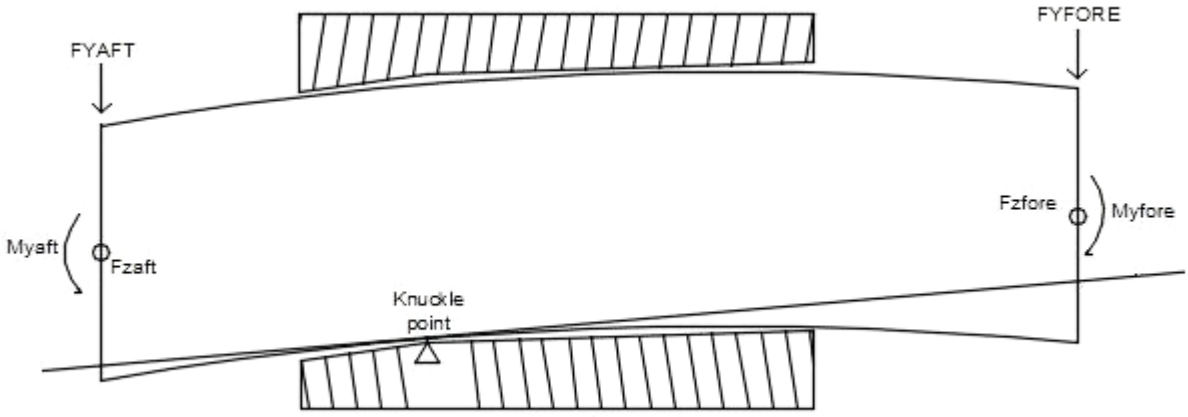

Figure 3-13: DOUBLE SLOPE BEARING DESIGN WITH BENT SHAFT

4 Coupled Optimization Problem

4.1 Problem Identification

The goal of the present thesis, is to optimize the performance of double slope designs for the stern tube bearing. To achieve this goal, a coupled problem of shaft alignment and bearing performance must be defined, solved and optimized. The solution part, mainly concerns the hydrodynamic lubrication of the stern tube bearing, which is highly dependent on the predefined shaft alignment plan. The elementary optimization problem is the performance optimization of a specific bearing design, operating at a given condition. An initial design is optimized following a specific optimization algorithm and the "best" results are proposed as optimum. It is evident that more than one designs may be optimum and the choice between these has to be done by the user. In this work the several optimum designs will be tested for extreme conditions in order to eliminate the less "rigid" solutions. The double slope solution is a very complex solution, in terms of manufacturing and by any means not a panacea. In most cases it can be used to increase safety factors in cases of poor shaft alignment, or extreme bearing misalignment.

To solve such a complex problem, several preexisting tools were utilized and a few new ones were developed. For the design of the double slope geometry, a new add-on tool was developed, namely CalcGeom. This tool will be called as a function in the main program that solves the Reynolds equation in order to create an unwrapped model of lubricant film for a given double slope bearing design. The output of this program is an h (i,j) matrix. The solution of the Reynolds equation is completed, using an existing code developed at NTUA that is described in [31]. The alteration of the h(i,j) matrix, does not influence the remaining solution process. For better understanding of this, an algorithm for the solution of Reynolds equation is presented. Detailed study of the Reynolds equation process yields a unique optimum solution, had the shaft been modeled with sole inclination. The solution for bearing slope would be such an inclination as the one of the shaft. Since the L/D ratio of a stern tube bearing is approximately 2, the inclination of the shaft is expected to alter considerably as the shaft is bent due to the propeller bending loads. This actually makes the problem much more complex as the shaft model must be redesigned within the CalcGeom tool. To correct the shaft inclination, the local elastic line of the shaft must be calculated and a correct inclination must be proposed. The inclination of the shaft when modeled as a linear non-bent shaft is represented by ψ_y, ψ_x parameters in Eq. (55). In the case of bent shaft these are replaced with matrices of different inclination along the bearing length. To calculate the local elastic line, the existing ShaftAlign tool is used and two add-on applications are developed in order to create the input file for ShaftAlign (named: Shaft_Align_Input) and to edit the results and create the correct inclination matrices for the case of bent shaft (named: Correct_Shaft_Inclination). The programming language used for the development of the programs described above is object-oriented C++. Finally, a built in Matlab optimizer will be used for optimization and a new Matlab script will be developed to serve as two objective function. The post-processing of the results is done using Matlab software to plot various results, and with Microsoft Office Excel to compare results and sort the optimum solutions.

In the following sections, an algorithm is proposed for the solution of the coupled problem and the Reynolds equation for hydrodynamically lubricated journal bearings. Then, the finite difference method that is used to solve at the unwrapped journal bearing domain is quickly demonstrated. Subsequently, the shaft alignment tool will be presented and the aspects of its use will be determined. For this purpose, a necessary analysis concerning the number of longitudinal divisions of the shaft is presented. Finally the selected optimization algorithm will be presented and analyzed.

4.2 The Coupled Problem - Solution Algorithm

The solution of a multilevel and complex problem must be disintegrated into smaller and simpler sub-problem solutions. In the present work, a complex design optimization problem is identified and in this section, the solution algorithm for a "coupled" problem is presented. The three sections that describe and affect the entire optimization problem are: Shaft Alignment Optimization, Bearing Design Optimization and Bearing Operational Optimization.

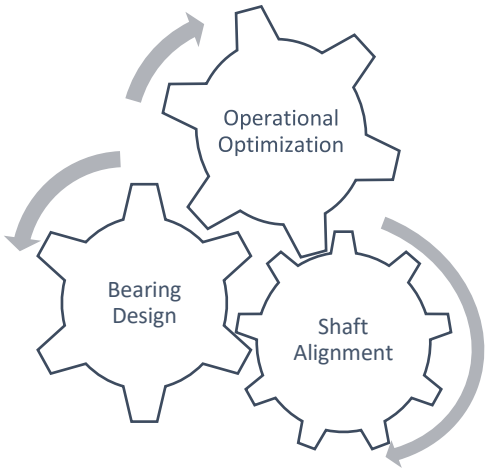

Figure 4-1: A COUPLED SYSTEM

Figure 4-1 demonstrates how the problem is reduced into three parts. These sub-problems are evidently connected, since the parameters of each one also affect the remaining two. According to this, a final solution is the outcome of an iterative process.

The most common sequence followed to converge a final solution according to literature is to initially conduct the Shaft Alignment and then decide which existing bearing design is more efficient. The operational optimization takes place at a later stage. All three sections have to meet several acceptance criteria and safety margins in order to result to an acceptable "optimal" design.

In the present work, an iterative process is followed, starting from an assumption of a simplified initial bearing geometry, followed by shaft alignment calculations that yield the initial bearing loading. Then the Reynolds equation is solved and the pressure field is calculated for the initial condition. After this stage, a new loading condition is described by means of new contact area and contact point location. At the second step of the process, shaft alignment calculations are repeated, using the new loading condition as input. These results are fed to the system and the Reynolds equation is solved again. A new loading condition is derived and several iterations of this step might take place to converge in a final pressure field and load equilibrium. Then the geometry is fed to the optimizer to conclude the optimization process. In the following Figure 4-2 the main steps of this process are illustrated.

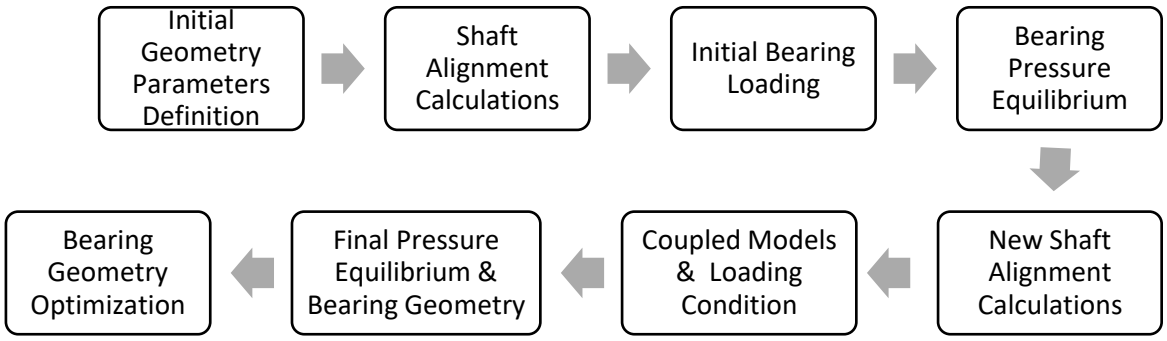

Figure 4-2: GEOMETRY OPTIMIZATION PROCESS

Going into further detail of this process a much more complex algorithm is reviled, as it is illustrated in Figure 4-3. This is the algorithm followed in this work, and it represents how various programs were linked together to solve the coupled optimization problem. In the Chapter 5 each program that we used will be presented and analyzed separately. Three main programs are utilized, namely, a Reynolds equation

solver (JournalBearing), a shaft alignment tool (ShaftAlign) and a genetic algorithm optimizer (NSGA-II). Four add-on tools were developed to link them and perform advanced calculations:

	Tool / Add-on Name	Tool purpose
1.	**CalcGeom**	Calculates externally the double slope geometry
2.	**ShaftAlignInput**	Creates the desired input file for ShaftAlign program
3.	**CorrectShaftInclination (within CalcGeom)**	Reads the output of ShaftAlign and makes appropriate corrections at the inclination (ψ_x)of the elastically bent shaft
4.	**2ObjFunction**	Describes the two objective function used by the optimizer

Table 4-1:ADD-ON TOOLS DEVELOPED AND THEIR PURPOSE

Additionally to the above mentioned programs, a Matlab script was developed in order to run the various components of the algorithm, save design and operational data the optimized geometries and plot critical information such as the film thickness (h) and pressure distribution profiles at the unwrapped journal bearing domain.

In the following flowchart, the coupled problem solution algorithm is presented.

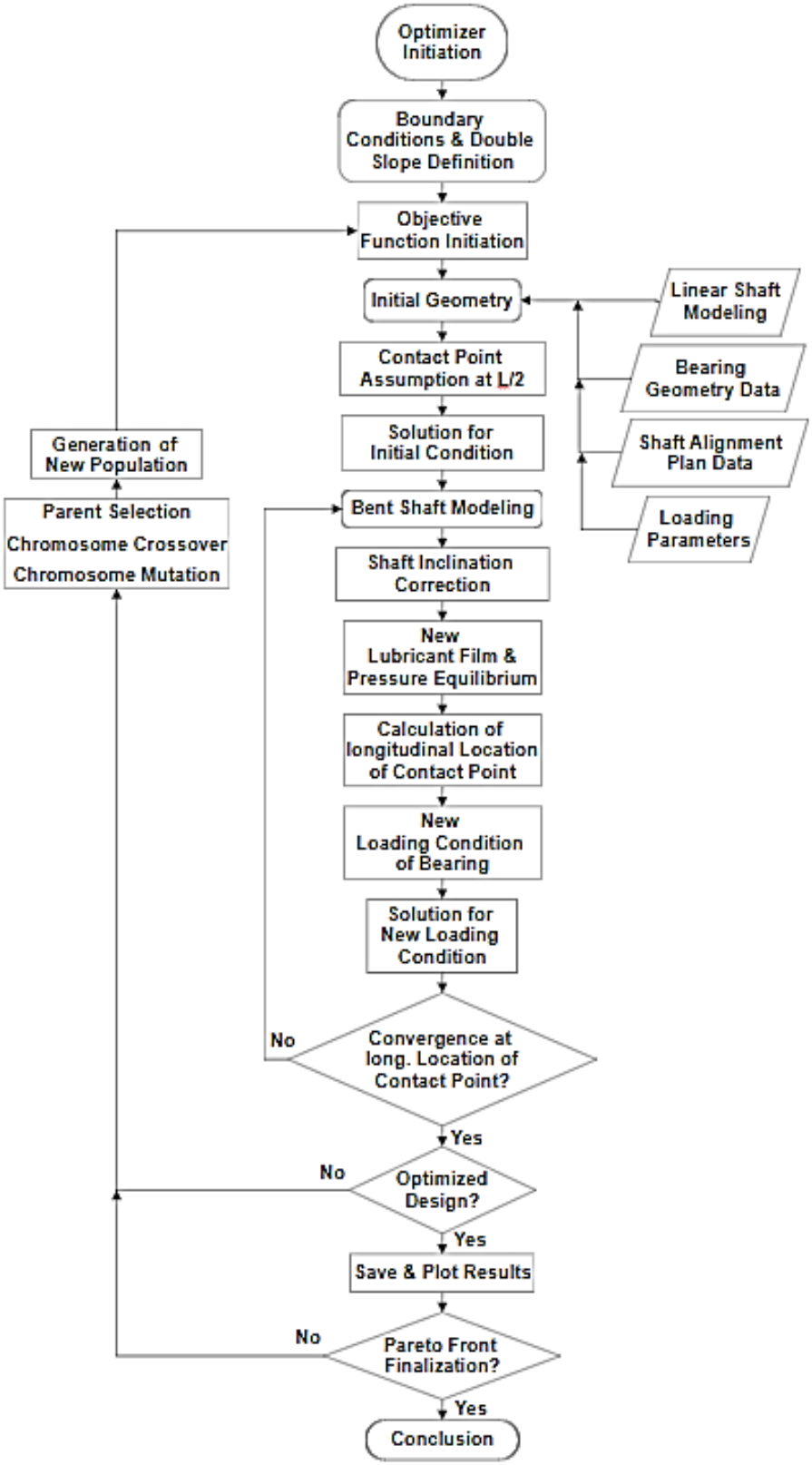

Figure 4-3: THE COUPLED PROBLEM ALGORITHM

4.3 Reynolds Equation in Journal Bearings - Solution Algorithm

Several algorithms have been proposed to solve problems of hydrodynamic lubrication. The most accurate method would be to solve the Navier Stokes momentum and continuity equation. In this case an enormous amount of calculating power would be required. In order to improve the cost-efficiency of this "expensive" solution, several simplifications are made and the Reynolds equation is derived from this basis, as mentioned extensively in Chapter 3. To solve this equation the following algorithm will be followed, introduced by Raptis [31]. The in-house solver for the Reynolds equation that we used in the present work had been developed in the section of Marine Engineering of NTUA and will be shortly presented here for the sake of completeness. Only minor modifications were made in order to include the add-on tool (CalcGeom) that was developed in the present work.

At the start of this algorithm, all the necessary geometric details of the journal bearing (L, D, c, operating speed etc.), the solver parameters (grid details, solver selection, convergence criteria, points per cycle, etc.), and the applied bearing loads in the x-and y-directions are read from an input file. At this point, the CalcGeom add-on tool is involved, to read the additional parameters of the geometry from a separate input file and calculate the complex double slope geometry.

After reading the input parameters, the program discretizes the unwrapped journal bearing into small divisions. At first, an initial assumption is made for eccentricity 'e_0' and attitude angle 'ϕ_0', and, by using Eq. (55), the film thickness geometry 'h_0' is calculated. Then, the Reynolds equation is solved numerically according to the Gauss-Seidel iterative method, and the pressure field is calculated. The hydrodynamic force components in axis z, x are derived by integration of the pressure field on the bearing surface. If the initial assumptions for eccentricity 'e_0' and attitude angle 'ϕ_0' are correct, force equilibrium is attained. Usually, proper values of the 'e_0' and 'ϕ_0' need to be re-estimated by means of a Newton-Raphson method for two variables, until force equilibrium is reached. At the end, all the bearing operational parameters of interest are calculated (friction force 'F', maximum pressure 'p_{max}', mean pressure 'p_{mean}', etc.) and printed to an output file for further processing.

This solution process is repeated several times in the optimization problem that we are trying to solve, for different Design conditions and Operational conditions. The correlation between lubricant film performance, different operational conditions and the design optimization forms a complex, multiscale coupling problem put in order in Table 4-2, where the connection between the parameters is visible. At this point it is important to mention that no algorithm can provide a single optimum solution for the entire coupled problem, therefore the user is responsible to take the final decision.

Design Optimization	• Improved Design for extreme loading • Improved safety margin
Bearing Operational Conditions	• Good pressure distribution • Low power loss
Lubricant Film Performance	• Minimization of p_{max} • Maximization of h_{min}

Table 4-2: COUPLED PROBLEM OPTIMIZATION PROCESS

In Figure 4-4 the algorithm followed to solve the Reynolds equation is presented:

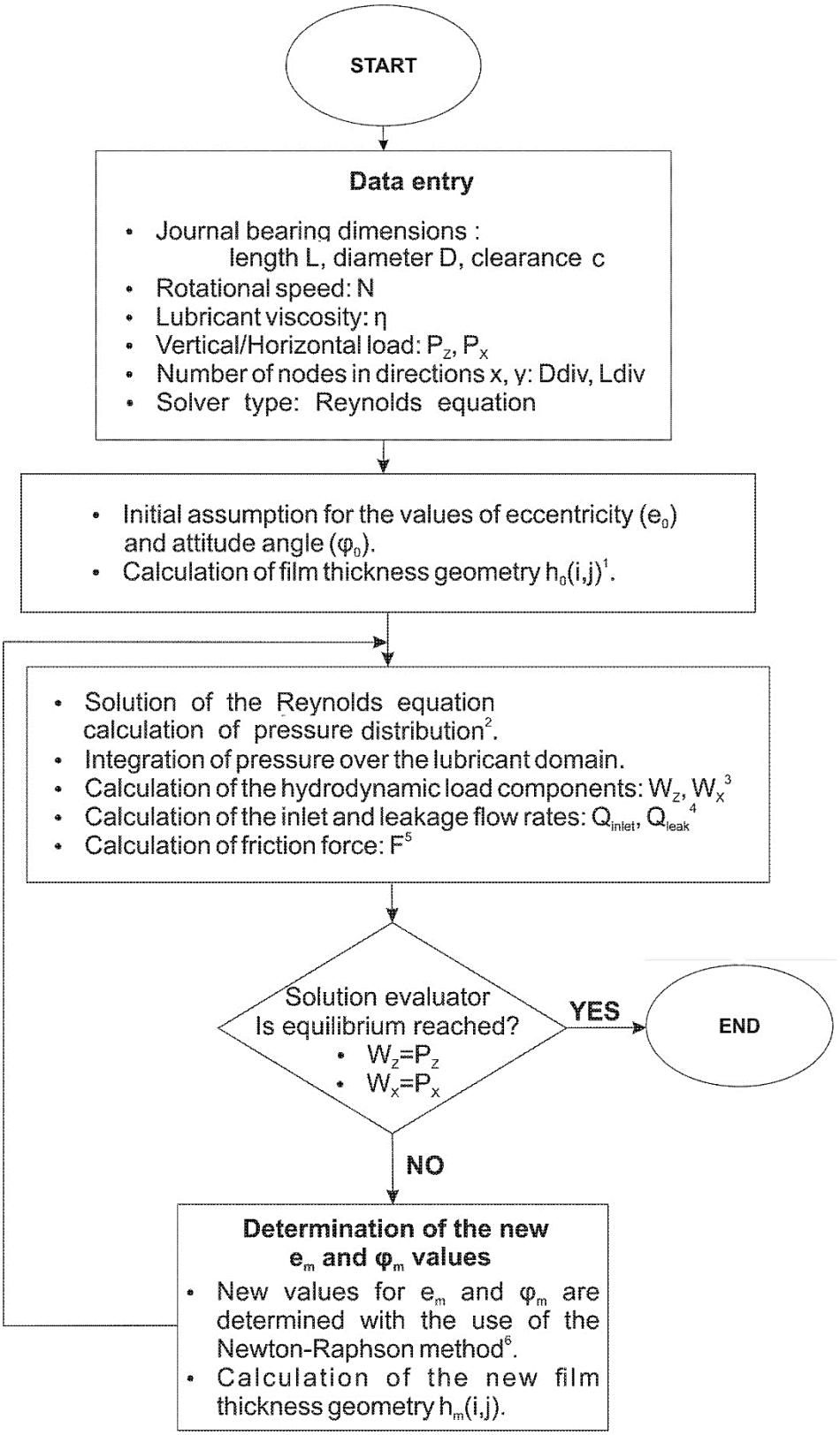

Figure 4-4:REYNOLDS EQUATION - SOLUTION ALGORITHM

Notes:

1. The film thickness geometry is calculated by Eq. (55)
2. Solution of Reynolds equation is performed using the Gauss-Seidel numerical method.
3. The hydrodynamic load components are calculated by integration of the pressure field over the lubricant domain, using Eq. (38) and Eq. (39). Integration is performed according to the Simpson's rule.
4. The inlet and leakage flow rates of the lubricant are calculated by Eq. (48), (50). Integrations are performed using the Simpson's rule.
5. Friction force is calculated from Eq. (45), integration is performed using Simpson's rule.
6. The load equilibrium equations solved using the Newton-Raphson method are:

$$f_1(e,\phi) = W_Z - F_Z$$

$$f_2(e,\phi) = W_X - F_X$$

A brief description of the Newton-Raphson method is given hereinafter.

Firstly, the following quantities are defined:

The array with the initial guess of the solution, x = [e,ϕ]T.

The array with the equations to be solved f(x) = [f_1(x) f_2(x)] T = [f_1(e,ϕ) f_2(e,ϕ)]T

The Jacobian of the two dimensional system:

$$J_f = \begin{bmatrix} \partial f_1 / \partial e & \partial f_1 / \partial \phi; \\ \partial f_2 / \partial e & \partial f_2 / \partial \phi \end{bmatrix}$$

A new solution approximation can be calculated by the following equation:

$$x_{NEW} = \left[e_{NEW}, \phi_{NEW} \right]^T = x - J_f^{-1}(x) \cdot f(x)$$

This procedure is repeated until the method converges to the solution of the equations.

4.3.1 Finite Difference Method

According to section 3.2.4 the Journal Bearing geometry is studied in the unwrapped domain and as mentioned in 4.3 the solution of Reynold's equation calculates a pressure distribution at the same domain. This unwrapped bearing domain is discretized by a finite element grid of 'Ldiv' points at the y-axis and 'Ddiv' points at the x-axis. In this work a uniform spacing in the x- and y- direction is assumed, therefore 'Ldiv' represent the number of divisions along the length of the bearing and 'Ddiv' represent the number of divisions along the circumference of the bearing. Each point is identified by i, j indices and has four neighboring nodes (except for the boundary nodes). The unwrapped journal bearing grid is presented in Figure 4-5.

The coordinates x (i) and y (j) of each point are calculated according to Eq. (56), (57).

$x(i) = i \cdot dx$, where: dx = π·D/ (Ddiv-1) (56)

$y(j) = j \cdot dy$, where: dy = L/ (Ldiv-1) (57)

To solve the Reynolds equation with the finite difference method, for a given set of eccentricity 'e' and attitude angle 'ϕ' values the film thickness h(i, j) can be calculated according to Eq.(55), replacing:

θ = θ(i, j), z = y(j), $\psi_x = \psi_x$ (j), $\psi_y = \psi_y$(j), slope(j)

Where: θ (i, j) = x (i) · 2·π/ x (Ddiv-1) , (58)

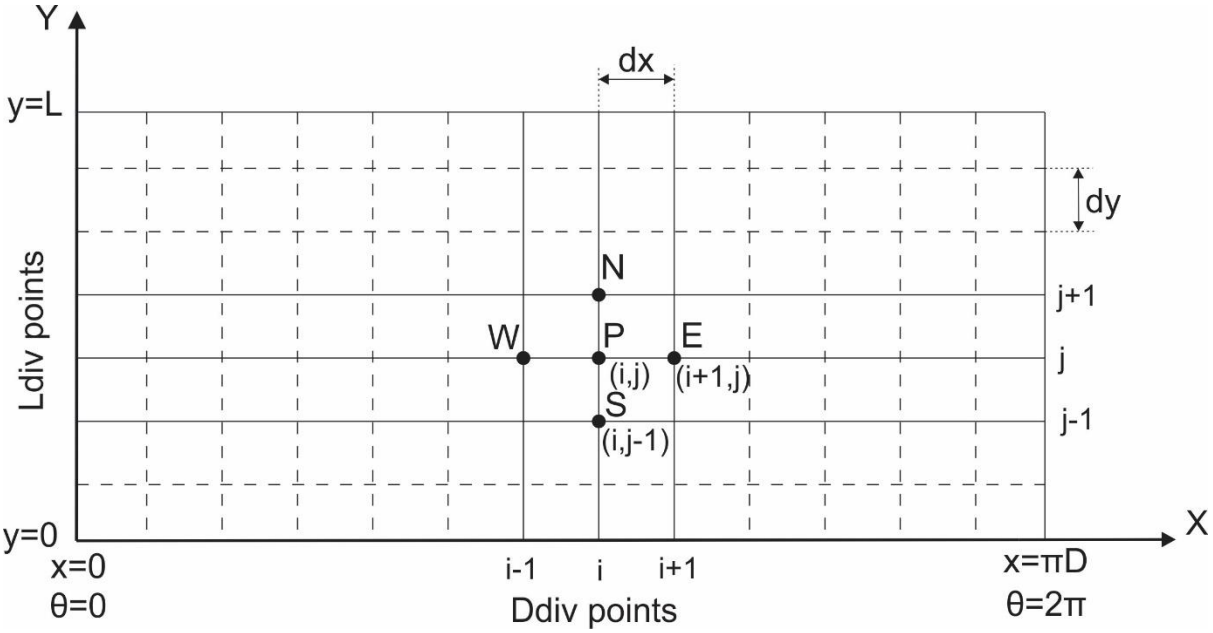

Figure 4-5: UNWRAPPED JOURNAL BEARING GRID

The Reynolds equation in the form of Eq. (37), can be numerically solved over the lubricant domain using the Finite Difference Method (FDM).According to this, the derivatives of the Reynolds equation are replaced with algebraic difference quotients which come from the Taylor series expansion.

$$f(\mathrm{i}+1,\mathrm{j}) = f(\mathrm{i},\mathrm{j}) + \left.\frac{\partial f}{\partial x}\right|_{i,j} \cdot \Delta x + \left.\frac{\partial^2 f}{\partial x^2}\right|_{i,j} \cdot \frac{\Delta x^2}{2!} + \left.\frac{\partial^3 f}{\partial x^3}\right|_{i,j} \cdot \frac{\Delta x^3}{3!} + \ldots$$

$$f(\mathrm{i}-1,\mathrm{j}) = f(\mathrm{i},\mathrm{j}) - \left.\frac{\partial f}{\partial x}\right|_{i,j} \cdot \Delta x + \left.\frac{\partial^2 f}{\partial x^2}\right|_{i,j} \cdot \frac{\Delta x^2}{2!} - \left.\frac{\partial^3 f}{\partial x^3}\right|_{i,j} \cdot \frac{\Delta x^3}{3!} + \ldots$$

For small Δx, the higher order terms can be neglected and therefore the finite central difference quotient for the first derivative can be written as:

$$\left.\frac{\partial f}{\partial x}\right|_{i,j} = \frac{f(\mathrm{i}+1,\mathrm{j}) - f(\mathrm{i}-1,\mathrm{j})}{2 \cdot \Delta x}$$

Using the same assumption, the finite central difference quotient for the second derivative is:

$$\left.\frac{\partial^2 f}{\partial x^2}\right|_{i,j} = \frac{f(\mathrm{i}+1,\mathrm{j}) - 2 \cdot f(\mathrm{i},\mathrm{j}) + f(\mathrm{i}-1,\mathrm{j})}{\Delta x^2}$$

The extended Finite Difference Method used for the solution of the simplified Reynolds can be found in existing literature [31]. What is important to mention though at this point, is that the alteration due to the double slope geometry only affects the calculation of h (i, j) and the remaining solution is completely identical.

4.4 Multi-Objective Optimization and Pareto Front

Optimization is "the action of making the best or most effective use of a situation or resource" according to the oxford dictionary. Modern science has put a lot of resources into finding optimization mechanisms and find a more effective approach in order to deal with various and very complex problems arising in areas such as engineering, machine design and finance. Mathematical models have been introduced and developed as well as complex algorithms. One of the most difficult part of an optimization analysis is the quantification of results in order to compare optimization techniques. The introduction of computer science into optimization process has brought major advantages such as quick and automatic solution and comparison of multiple cases, new optimization algorithms and the capability to conduct multi objective optimization with minimum human resources. In the present thesis, one of the most popularly used genetic algorithm will be used, namely a genetic algorithm seeking Pareto optimal solution. Firstly several optimization definitions will be presented, then the genetic algorithm concept will be analyzed and finally an example of the algorithm that will be used in the present work will be given.

4.4.1 Definitions

The solution algorithms can be separated into two categories, based on the optimization objectives. Single objective optimization problems have a unique solution, when in the contrary non-trivial multi objective problems (MOPs) do not have a unique solution. In that case, the objectives are called conflicting and there are more than one optimal solutions. As a result, when solving multi-objective problems, the final solution is obtained by choosing one of the optimum ones, based on other constraints of the problem. In this thesis, a multi objective optimization problem will be analyzed, therefore the focus will be on corresponding algorithms. In the following table, several definitions according to [26] will be presented in order to understand and analyze the optimization concept. All definitions are presented in terms of minimization, without any loss of generality.

Definition 1:	**Single-objective optimization problem**
A general single-objective optimization problem is defined as minimizing f(x) subject to $g_i(x) \leq 0$, i= {1, 2, 3…m} and $h_j(x) = 0$, j= {1, 2, 3 … p} $x \in \Omega$.	
Definition 2:	**Multi-objective optimization problem**
A general multi-objective optimization problem is defined as minimizing f(x) subject to $g_i(x) \leq 0$, i= {1, 2, 3…m} and $h_j(x) = 0$, j= {1, 2, 3 … p} $x \in \Omega$.	
Definition 3:	**Convex Function**
A function f(x) is called convex over the domain of $\mathbb{R}$ if for any two vectors $x_1, x_2 \in \mathbb{R}$, $f(kx_1 + (1-k)x_2) \leq kf(x_1) + (1-k)f(x_2)$ where k is a scalar in the range $0 \leq k \leq 1$	
Definition 4:	**Pareto Optimality**
A solution $x \in \Omega$ is said to be Pareto Optimal with respect to Ω if and only if the is no $x' \in \Omega$ for which v=F(x') dominates u=F(x)	
Definition 5:	**Pareto Dominance**
A vector u is said to dominate another vector v if and only if u is partially less than v	
Definition 6:	**Pareto Optimal Set**
For a given MOP, f(x), the Pareto Optimal Set, P* is defined as: $P^* := \{ x \in \Omega \mid -\exists\, x' \in \Omega$ f(x') dominates f(x)$\}$	
Definition 7:	**Pareto Front**
For a given MOP, f(x) and Pareto Optimal Set, P*, the Pareto Front is defined as: $PF^* = \{u = f(x) \mid x \in P^*\}$	

Table 4-3: OPTIMIZATION DEFINITIONS ACCORDING TO COELLO [26]

Note: In def. 1 & 2, g_i, h_j represent constraints of the problem that must be fulfilled during the minimization of f(x).

4.4.2 Genetic Algorithms

Genetic algorithms are numerical optimization tools, inspired by the biology. According to Mayr 1988 one genetic biologist once said: “Evolution is an optimization process”. The concepts of evolution, natural selection, mutation and gene diversification have inspired computer scientists to mimic these processes, in order to solve multi-objective optimization problems. These adaptive search algorithms are called evolutionary algorithms and have been proven very successful when used for optimization purposes. The primary reason for using such algorithms is their ability to find a high number of Pareto optimal solutions in one simulation run. On the other hand, complex engineering problems with chaotic components and many non-linearities are very difficult to be approached, which sets a limit for these algorithms.

Genetic algorithms use binary digits, meaning 0 and 1 or strings, to represent different chromosomes. A set of chromosomes forms a vector of specified length which represents a proposed solution for the problem. At the beginning a specific amount of individual solutions are created randomly, representing the initial population. These “individuals” are the parent population which after certain genetic operations, meaning selection, crossover and random mutation will produce the individuals of the next population. Most often the population is specified, meaning that the amount of offspring matches the quantity of parents. Some parents may be moved to the next generation intact. The optimization idea, is included in the process since every new population has probably a better mean fitness value than the parent generation. The algorithm continues until a termination criteria is reached, meaning convergence to an optimum solution. In order to better understand the concept of natural selection and mating, the following fundamental operators of must be explained.

The selection operator mimics the natural process of mating. Individuals are selected based on a “fitness function”, which maps them with their respective fitness values. Parents of higher fitness value are more likely to be reproduced, passing their genes to the next population. Reproduction is the process of mating, thus binding the chromosomes of the parents to produce children.

Crossover is the operator responsible to exchange genes between the chromosomes of the two parents. The process is pseudo random, meaning that the crossover point(s) are chosen randomly. There are two types of crossover, the single and the two point crossover. The latter is presented in the following figure.

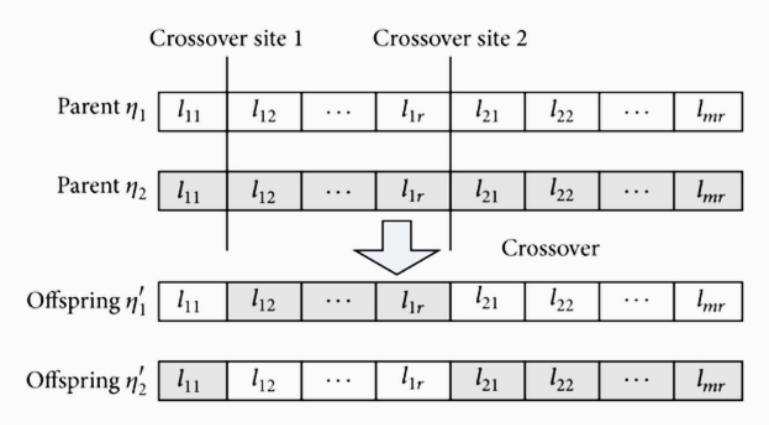

Figure 4-6: TWO POINT CROSSOVER OPERATION

Replacement or random mutation is an operator that randomly changes the gene of a parent in order to maintain genetic diversity between the two generations. The mutation is achieved by introducing a mutation probability at each gene. The mutation is a process that takes place after crossover and is very important for genetic algorithms in order to introduce diversity and avoid reaching a local minima which would result to very similar solutions and termination of the evolution and the optimization process. On

the other hand, mutation probability must not be very high, in order to preserve evolution according to the fitness function and avoid random offspring creation, which will transform the algorithm into a random search algorithm. In the following figure, the mutation operation is illustrated.

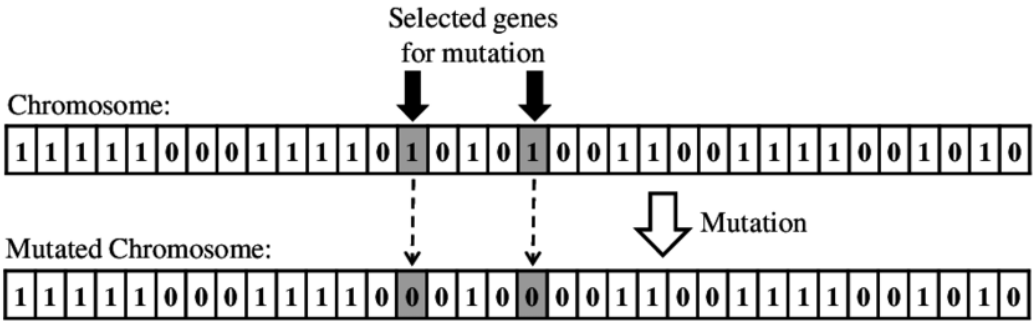

Figure 4-7: MUTATION OPERATION

As mentioned previously, genetic algorithms are mainly used due to their ability to find a high number of Pareto optimal solutions in one simulation run. Apart from that, they offer a series of advantages in comparison to traditional optimization methods. One of the most important ones, is that they do not use directly the initial parameters of the problem, rather they use coded versions.

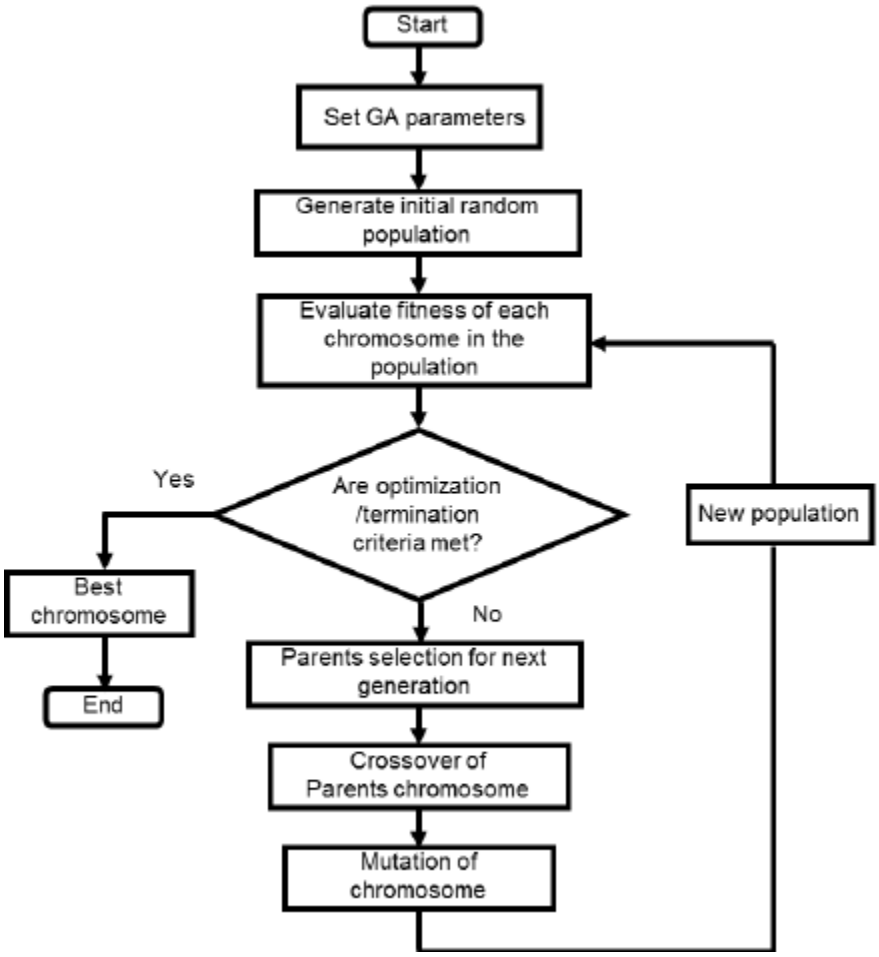

Figure 4-8: GENETIC ALGORITHM FOR OPTIMIZATION

A second advantage is that while other methods use a single parameter to search, genetic algorithms always search the whole population. This technique minimizes the risk, for the algorithm, to be trapped in a local optimum point, improving the chance to find a global optimum solution.

A third advantage is that genetic algorithms can be used to solve almost every optimization problem.

Genetic algorithms do especially thrive when a multi objective solution is desired, meaning complex problems such as the one we are presenting in this thesis, where more than one solutions are possible to match the requirements /constraints of the design optimization problem.

4.4.3 Optimization Algorithm Example

Based on the definitions presented it can be concluded that a multi-objective optimization problem solution can be found by solving the equivalent optimal Pareto front approximation problem. Thereof any optimization algorithm has two individual goals: to minimize the distance to the Pareto front, yielding an optimum solution and to maximize the diversity of these solutions. These two objectives can be met and converge utilizing genetic algorithms. Decisive parameters for quick convergence are the number of generations and the population size that will be decided.

A vector of design variables $\vec{x}$ is defined, containing all the involving design parameters of the problem. For example, in the case study that will be presented later on this work, such parameters are the non-dimensional slopes angles and the position of the knuckle point. Then *m* constraints will be included in the constraints vector, $\vec{g}$ and *k* objective functions will form the vector $\vec{f}$, which is going to be minimized.

The optimization problem can be formulated as:

$$\begin{Bmatrix} \min \vec{f}(\vec{x}) = (\vec{f_1}(\vec{x}), \vec{f_2}(\vec{x}), \dots, \vec{f_k}(\vec{x}))^T \\ \vec{x} \in X = \{\vec{x} \in \Re^n\} \\ \vec{g}_j(\vec{x}) \leq 0, j = 1, \dots, m \end{Bmatrix}$$

The design variables refer to both the constraints and objective functions:

$$\begin{Bmatrix} \vec{f}_i(\vec{x}) = \vec{f}_i(x_1, x_2, \dots, x_n), i = 1, \dots, k \\ \vec{g}_j(\vec{x}) = \vec{g}_j(x_1, x_2, \dots, x_n), j = 1, \dots, m \end{Bmatrix}$$

In multi-objective minimization methodologies, it is common practice to seek Pareto optimal (or dominant) solutions. A solution $\vec{x}_1$ is defined as dominant over $\vec{x}_2$ when:

$$\vec{f}_i(\vec{x}_1) \leq \vec{f}_i(\vec{x}_2)\ \forall i = 1, \dots, k\ and$$
$$\vec{f}_i(\vec{x}_1) < \vec{f}_i(\vec{x}_2)\ \exists i = 1, \dots, k$$

The collection of all Pareto Dominant Solutions is called “Pareto Front”. An example for the case of two objective functions (k=2) is shown in Figure 4-4.

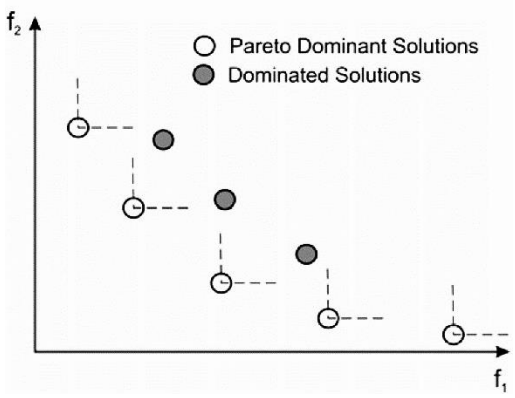

Figure 4-9: PARETO FRONT FOR A CASE WITH TWO OBJECTIVE FUNCTIONS

4.5 Numerical Modeling – Software Development

In the course of the present thesis, several programs were developed serving diverse purposes. The goal is to create a software that is capable of solving the coupled problem algorithm as it was previously demonstrated. This study has been a continuation of previous work done in the laboratory of marine engineering of NTUA in the field of shaft alignment and tribology.

The first milestone concerned the modeling of the lubricant film geometry. Based on existing literature, the simplified geometry is expressed by Eq. (4), which is converted into Eq. (54) taking into account the inclination of the shaft and a wear deformation [37]. Although the optimization problem, does not include wear deformation calculations, these modifications were significant conceptual tools utilized to derive Eq. (55), which describes a sloped bearing geometry. This source code is compiled into a library file, namely CalcGeom.dll, utilized when calculating the Reynolds equation.

Solving the Reynolds equation, assuming a linear shaft model, yields the following critical conclusion:

"The optimum geometry is the one, at which shaft and bearing slopes are parallel."

Stern tube bearings are frequently inclined at steep slopes since the propeller load is very close to the stern tube, resulting to large bending moment. Additionally to this, the relatively large length of these bearings indicates that the shaft itself should be modeled as elastically bent within the bearing bushing in order to account for actual loading condition. Therefore, an extensive study was done in order to calculate the actual inclination of the shaft along the length of the stern tube bearing. Making use of an existing code that calculates the elastic line of the shafting system, namely ShaftAlign, the inclination of the particular section is calculated and corrections at the CalcGeom code are included accordingly. To use the existing code though, several add on tools were developed, one for the purpose of creating an input file for ShaftAlign that represents only the shaft section of interest and another one to make the appropriate corrections at the shaft inclination parameter expressed within the CalcGeom tool.

Lastly, an existing Matlab optimizer based on genetic algorithms was used. The fitness function of this was developed using Matlab as well. For convenience and adaptability the source code representing the solution of the coupled problem algorithm, post processing and plotting of the results was also developed in Matlab environment. In this section, the developed source codes will be presented.

All the above mentioned software is collected and grouped in the following Table 5-1:

SOFTWARE DEVELOPMENT
Lubricant Film Geometry Modeling - C++
•Double Slope bearing modeling
Bent Shaft Modeling - C++
•Automatic creation of Input File for shaftAlign •Post processing of shaftAlign results & •Correction of shaft inclination (within calcGeom tool)
Journal Bearing Solver - C++ (Raptis - [31])
•Equilibrium of pressure distribution •Calculation of the longitudinal position of contact point •Calculation of bearing's operational parameters
Numerical Simulation & Optimization - Matlab
•Script for process initiation •Two-objective fitness function •Plotting of results

Table 4-4: SOFTWARE DEVELOPMENT

4.5.1 Lubricant Film Thickness Modeling Tool

This tool is basically a function named as: CalcGeom that is called by the Reynolds equation solver in order to calculate externally the lubricant film thickness, given a specific set of eccentricity and attitude angle values (e_0, ϕ). The solver creates additionally a file containing essential geometric parameters of the system, such as: L, D, c, ψ_X and ψ_Y. It defines also the meshing that will be used for the unwrapped journal bearing lubricant film, through the Ldiv and Ddiv parameters, which impose the divisions in the length and circumference of the bearing. For our convenience the slope parameters (non-dimensional main & secondary slope, number of slopes, length of each segment as % of L), are read from a separate file, which is created either manually or automatically during the optimization process.

After reading all the essential parameters, the x[i], y[j] coordinates are calculated according to Eq.(56) & Eq.(57) and their values are stored in the corresponding matrices. Then the θ[i] angle is calculated by Eq.(58). After this step the code should read some data from an automatically created file, which will dictate if the shaft will be modeled linear or elastically bent. In the first case only ψ_x and ψ_Y values are required and no further changes are done, on the second case, the variable inclination at several longitudinal locations - x, is read from a separate file created by the ShaftAlign tool which is programmed to run before this function is called. Specifics concerning the creation of this are analyzed in the next section. If the number of longitudinal divisions of the bent shaft model and the Ldiv number do not match, then the correct inclination at every longitudinal location – x[i] is calculated, by linear interpolation between the given longitudinal position values and the required ones. At the end of this process, a matrix of variable ψ_X[j] or ψ_Y[j] is created.

Lastly, all the non-dimensional parameters are converted into dimensions. After this all the required information are gathered and the lubricant film thickness can be calculated by Eq.55 as:

$$h_{lub}(\theta[i], y[j]) = c + e_0 \cos(\theta[i]) + y[j]\left[\psi_y \cos(\theta[i] + \varphi_0) + \psi_x \sin(\theta[i] + \varphi_0)\right] - \\ - y[j] \cdot slope[j] \cos(\theta[i] + \varphi_0) \quad (55a)$$

Or in the case of bent shaft model:

$$h_{lub}(\theta[i], y[j]) = c + e_0 \cos(\theta[i]) + y[j]\left[\psi_y[j] \cos(\theta[i] + \varphi_0) + \psi_x\,[j] \sin(\theta[i] + \varphi_0)\right] - \\ - y[j] \cdot slope[j] \cos(\theta[i] + \varphi_0) \quad (55b)$$

At the end of the process, the h_{lub} matrix is exported and read by the solver to continue the Reynolds equation solution.

To sum up, CalcGeom:

1. Is called within the Reynold's equation solver.
2. Reads geometric parameters of the system and a set of eccentricity and attitude angle.
3. Reads the slope geometry parameters.
4. Reads (if applicable) the variable inclination matrix for bent shaft models.
5. Calculates the x[i], y[j] and θ[i] values for the unwrapped journal bearing mesh.
6. Converts all non-dimensional parameters into dimensions.
7. Utilizes Eq.55 (a) or (b) to calculate the lubricant film thickness at every point of the mesh.
8. Exports the lubricant film thickness matrix.

4.5.2 Bent Shaft Modeling

In order to model the shaft as an elastically bent beam, the elastic line or curve of the shaft must be calculated for a given loading condition. On the contrary, the loading condition of the shaft changes constantly during operation. During the design stage and after the shaft alignment process is completed, several parameters such as the longitudinal and vertical position of each bearing, the total bearing reaction and the local shaft inclination are calculated. From the entire elastic line though, only the section of the shaft that is "near" the aft stern tube bearing is required for the bearing operation calculations. Initial coupling of the shaft alignment calculations with bearing calculations already exists in literature ref. [29], [47] but for the context of this work utilizing such a complex system within the numerus runs required by the optimizer would require a disproportionately large amount of time and calculating power.

Therefore a "smart" tool must be developed to reduce the complexity of the problem. To this objective it is of outmost importance to recognize which are the parameters of the problem, when and how are they calculated and what is the effect on other parameters. For example the length of the bearing is calculated based on the load carrying capacity required by the shafting system and several external constraints such as the availability of space in the installation area. The loading capacity of the bearing is measured in terms of mean pressure, or in other words P=F/A where F is the reaction force and A is the area of contact (usually calculated as L*Pi*D). This bearing length is also closely connected to the bearing diameter and clearance according to manufacturers. The bearing length is decided during shaft alignment and should be a constant for the system linking diameter (D) and clearance (c) also as constants. On the other hand the single contact point's longitudinal location is constrained by the bearing length but it is calculated after the shaft alignment by solving the Reynolds equation and calculating the exact pressure distribution. So the bearing length affects the pressure distribution and therefore the longitudinal position of the contact point (single point contact). In the aftermath, the length should remain a constant to the system at any stage after the shaft alignment.

Studying the stern tube bearing an optimization process is proposed to yield the optimum geometry of the bearing. It is evident that parameters such L, D, c must remain constant during optimization and Slope parameters will diversify. Ultimately, the Sommerfeld number must remain the same during the optimization process, which means that the absolute viscosity of the lubricant, the speed of the rotating shaft and the load per unit of projected bearing area are the constant parameters of the optimization. On the other hand the longitudinal and vertical position of the contact point are restrained by the above mentioned constants but may vary during optimization of the bearing geometry.

Coming back to the initial problem, which is the coupling of shaft alignment and optimization process one very important assumption is concluded to avoid complex and numerus numerical simulations:

"**The Sommerfeld number must not change during optimization**."

After the conclusion of shaft alignment calculations, a specific reaction force is calculated for each bearing, as well as a longitudinal and vertical position for the contact point. The value of the shaft misalignment angle ψ_X is also calculated for the designed shaft line locally at the contact point. Shaft misalignment angle can be defined for a linear shaft model as: $(U_{y\_fore}-U_{y\_aft})/L$, where U_y is the vertical location of the shaft and L is the bearing length. This angle is an outcome of the shaft alignment process and it highly affects the geometry of the bearing in terms of bearing misalignment angle or double slope angles, when in the contrary the vertical and longitudinal offset of the contact point do not affect the bearing geometry at all. This is narrowing down the non-constant, non-optimizing parameters to only one, the ψ_X which should vary longitudinally, modeling the shaft as a bending beam instead of single contact point. This is after all the reason why it is essential to model the shaft as an elastically bent beam.

In order to simplify the coupling problem and effectively model only a section of the shaft, without loss of generality, the following conditions are set:

"Modeling the elastic line of the shaft locally, requires the total force imposed to be equal to the reaction force of the bearing, maintain constant Sommerfeld number and additionally the shaft misalignment angle between the fore and aft edge of the bearing should match the corresponding angle of the integrated shaft model."

To calculate the elastic line and rotation angle of the shaft an existing program developed in NTUA will be utilized, namely **ShaftAlign**. In order to use this automatically, a tool was developed, to create the corresponding input file. A general solution requires introduction of the following parameters:

- F_r, M_r are the force and moment reactions from the contact point. The reaction moment M_r is basically an equivalent of a set of forces, applied to the area of contact (which can't be modeled), times their lever arm.
- "l_{aft}" = the shaft protruding distance from the aft end of the bearing and aft-wards
- "l_{fore}"= the shaft protruding distance from the forward end of the bearing and forwards
- "$R_{otxfore}$"= the fore shaft inclination, imposed to preserve continuity with the full shaft system
- "l_{cp}", "V_{cp}" = is the longitudinal and vertical distance of the contact point from the aft end of the bearing, which can be evaluated only after the Reynolds equation is solved.

The loading model studied is illustrated in the following Figure 4-10:

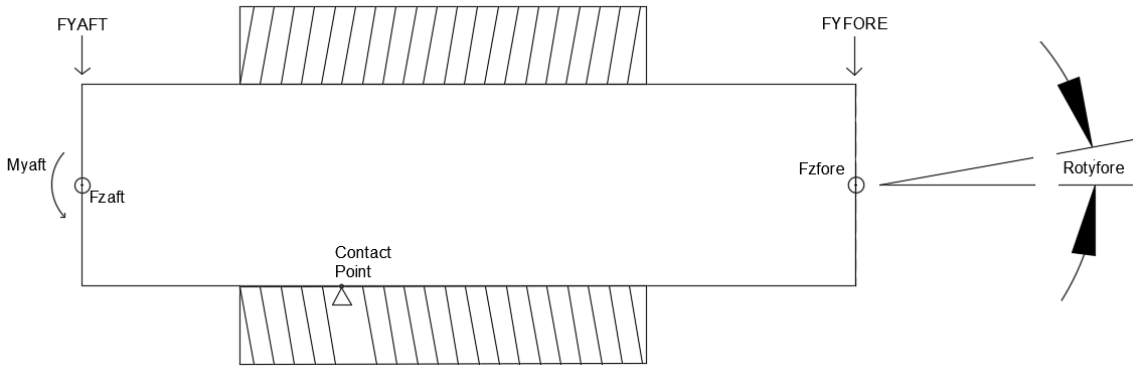

Figure 4-10: EQUIVALENT LOADING MODEL

The fore end must be constrained and sometimes inclined when the aft end is unconstrained by definition, since only the propeller is aft-wards. The model is an equivalent to a beam fixed at one end (fore) and simply supported at some location near the other end (contact point) and has an additional overhang. The loading parameters are known from shaft alignment calculations and the only unknown parameter of the system is the "l_{cp}" and "V_{cp}".

The analytical solution for elastic line and angle calculation that describes the system above is:

$$EIw'' = -M_y = -M_{yaft} + F_{YAFT}(x + l_{aft}) + F_r(x - lcp) - M_r = -A + Bx$$

Where: $A = M_{yaft} + M_r - F_{YAFT}l_{aft} + F_r lcp$ and $B = F_{YAFT} + F_r$

$$EIw' = -Ax + \frac{Bx^2}{2} + C_1$$

$$EIw = -\frac{Ax^2}{2} + \frac{Bx^3}{6} + C_1x + C_2$$

The C1, C2 values can easily be calculated from the boundary conditions of the problem.

At this point there is a critical "causality dilemma" for the modeling process. The exact "l_{cp}" and "V_{cp}" values are an aftermath of the Reynolds equation solver on top of the shaft alignment calculations since the values assumed during the shaft alignment process are $l_{cp}= L_{bearing}/2$ and the V_{cp} is usually included only during bearing installation. Modeling the shaft as a bent beam, should cause alteration of the film thickness geometry which will result to new l_{cp}, V_{cp} and this will keep happening for several iterations.

Examining this in detail, the problem can be separated into two sub-problems. The first one is the coupling of a shaft align tool with the bearing solver [29] and a second one to model the bent shaft, utilizing the shaft align tool to make corrections for inclination (variable ψ_x). The reason why these problems can't be solved together is that their parameters are correlated e.g. the L_{cp} and contact area affect the shaft loading condition, which in return affects vertical shaft offset).

In order to minimize the running time of the optimizer the following bypass methods are proposed and tested:

1. Model the contact point as two nodes closely located and impose a vertical offset according to the shaft misalignment angle.
2. Model the contact point as two nodes closely located and impose a vertical offset according to the local slope of the shaft.
3. Model the system with a node at each edge of the bearing and impose a vertical offset according to the shaft misalignment angle.

From the above mentioned methods, the third one seems to be more efficient and yields results closest to the analytical solution as presented in Figure 4-11. The first to methods have quite controversial assumptions but they can be a good starting point for the study. Unfortunately the non-equal division of the bearing length that is required in these cases, creates a very unstable discrepancy of the shaft angle near the contact point, therefore a new approach was required, resulting to the third equivalent model. The major advantage against the first two methods is that the final solution should be modeled as single contact model (according to regulations) so the program must yield one value for vertical and horizontal offset (not an area) and most importantly one inclination. Inclination definition is a key factor, since it can be calculated as $(h_{fore}-h_{aft})/L$ or as inclination (tangent) at the contact point. Modeling the system according to the second definition the inclination changes if the vertical or longitudinal position of the contact point is altered (the loading system is different), which is beneficial only in order to solve the shaft alignment problem. Following the first definition shaft misalignment angle can be a valuable <u>constant</u> parameter that we need to calculate the vertical position between two points (fore & aft end of the bearing) and then make corrections for local inclination within the bearing. These corrections will yield a new long position of the contact point, when the Reynolds equation is solved, due to the altered shaft modeling and not the loading itself. Then the system will solve the bearing-bent shaft system coupled. A few iterations between the 2 problems should be sufficient to solve the system. This method basically exploits the fact that the inclination correction required is not affected by vertical offsets.

A great benefit of this "problem bisection" method is that it can be utilized to connect the shaft alignment with the bearing performance analysis using only the parameters that actually affect every separate problem. Then each one can be thoroughly studied separately, time efficiently and more effectively after all. Important conclusions can be produced from the study of each part of the problem. At the end of the study, the respective solutions can be coupled yielding the final equilibrium.

Numerical calculations and test results for a “test case” geometry model are presented below:

Model Parameters		
L	1.05	m
D	0.52	m
c (diametrical)	0.0009	m
L_{aft}	0.407	m
L_{fore}	0.5412	m
M_{aft}	409948.0	Nm
F_{Yaft}	-202598.2	N
F_{Yfore}	-107261.7	N
F_{Zaft}, F_{Zfore}, M_{fore}	0	N
$R_{otyfore}$	0.000465	rad

Table 4-5: SHAFT MODEL PARAMETERS

In the graph presented in Figure 4-11 the resulting curves for the three model types for Ψz = 0.8 are illustrated. The analysis was implemented for 10 divisions at the bearing length. Also a reference line at the shaft misalignment angle is drawn to show the difference between linear and bent shaft design. Note that the diametrical clearance within the bearing is at the range of 10 mm, which means that especially for shaft misalignment angles larger than 0.4% of 2c/L the effect of the shaft curvature is substantial. The deviation from the analytical results of the first model is at a range of 10-70 μm and 5-30 μm for the second model when in the third model deviates only 2-15 μm. Further study of the relation between shaft misalignment angle (between aft and fore bearing edge) and local shaft angle at the contact point (or contact area) might result to very interesting findings but will not be included within the present work.

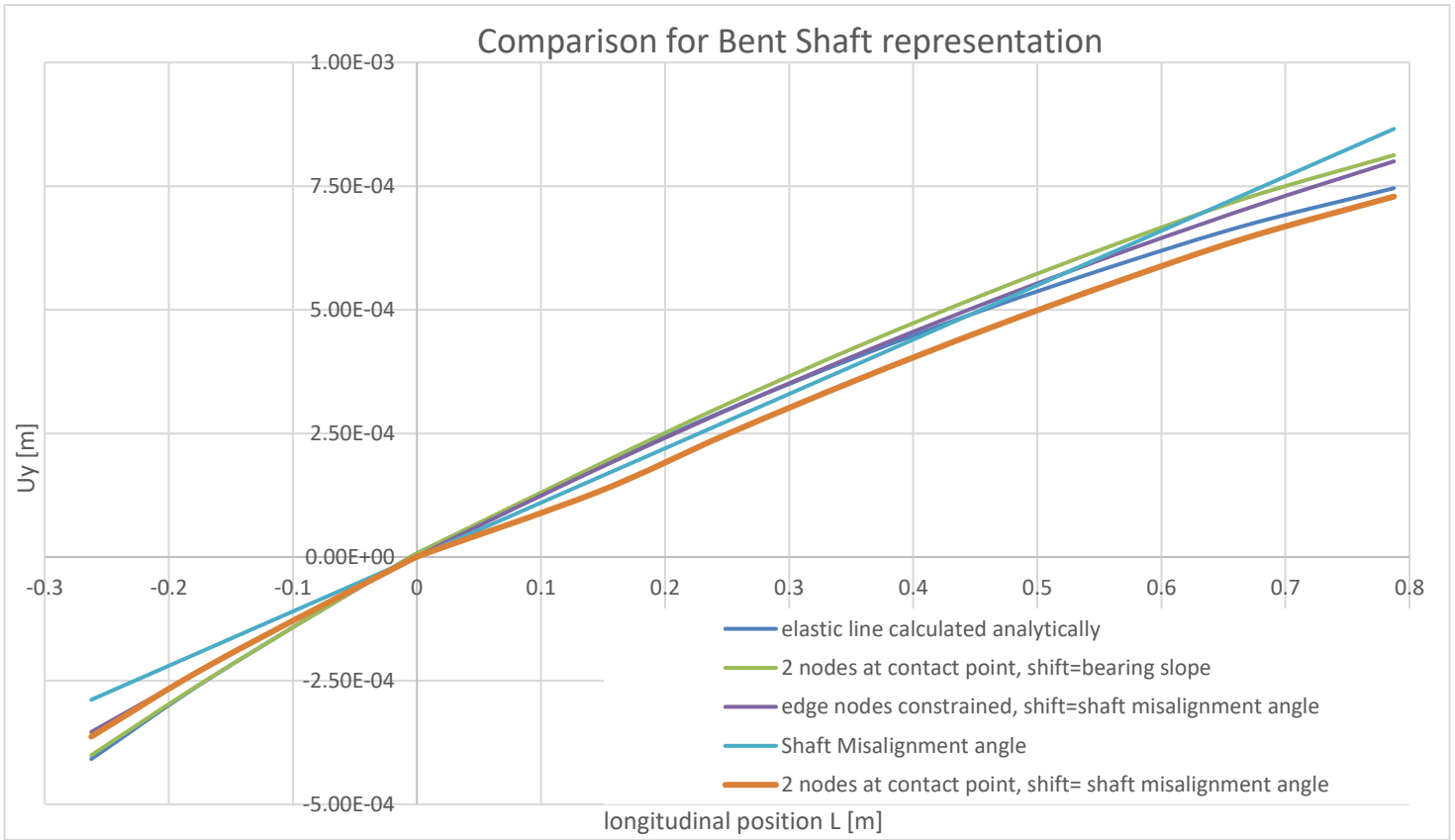

Figure 4-11:COMPARISON FOR BENT SHAFT REPRESENTATION

4.5.3 ShaftAlign Tool

The ShaftAlign tool is able to calculate the vertical offset and rotation angle at nodes located in the sides of a beam element. The beam may be modeled as a single beam or more often as multiple beam elements connected with nodes. The support and loading locations can be set at any node. The number of beam elements depends on the complexity of the shaft geometry. An elastically bent shaft model looks like the one presented in Figure 4-12.

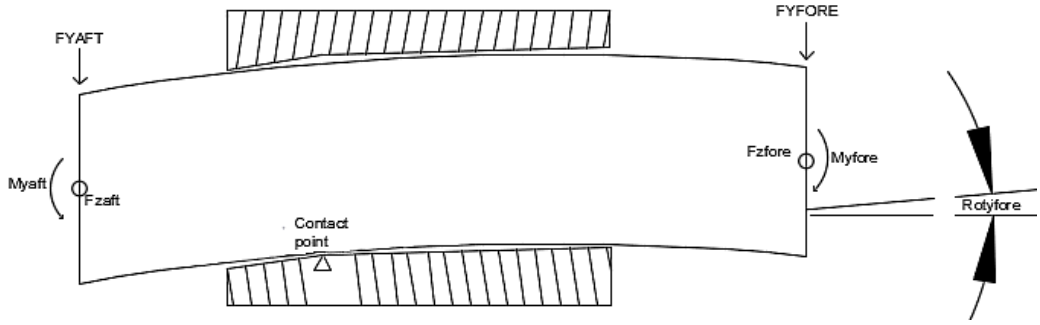

Figure 4-12:BENT SHAFT MODEL

From this model it is evident that the protruding sections of the element will be modeled as two beams with length L_{aft} and L_{fore} respectively. The length of the bearing will be evenly divided into segments. The number of segments depends on the number of nodes required to describe accurately the shaft geometry. The longitudinal divisions at the unwrapped journal bearing mesh are usually in the order of 50-100 but it is estimated that less nodes are required to calculate the vertical offset and angle and the intermediate values can be calculated with linear interpolation. For the purposes of this study, a sensitivity analysis is performed for the shaft model, seeking the number of nodes required for accurate representation of the elastically bent shaft. In this case, several tests are done considering 10, 20, 50, 100 divisions of the shaft along the bearing length. The analysis showed that 10 divisions provide excellent accuracy, in the range of micrometers. Although the 20 and 50 divisions provide about ten times better accuracy, a mesh of 10 divisions of the shaft length will be created in order to slightly minimize the runtime of the coupled solution system and ultimately the optimizer. For the purposes of this study, without loss of generality a reference loading case for the above presented "test case" geometry is modeled and studied. The numerical results for a value of L_{div} =100 are studied and the deviation due to linear interpolation is calculated for each node and compared with the 100 nodes reference case. The only variable parameter is basically the shaft misalignment angle ψ_x, which is set "as per case" by the user.

In the following Figure 4-13 the visual representation of the model in ShaftAlign program is displayed:

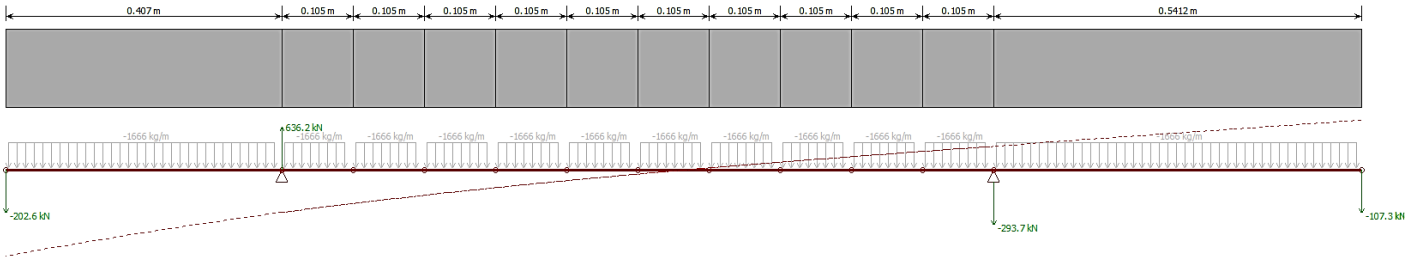

Figure 4-13: SHAFT ALIGN MODEL REPRESENTATION

Note that in the model above, the negative force at the fore end of the bearing is **not** the actual bearing reaction force, rather a reaction force of the equivalent model, which has similar shaft misalignment angle and boundary loading with the initial shaft model.

4.5.4 Input File Creator

In order to use the ShaftAlign program it is essential to automatically create an input file containing the "local" shaft model parameters. Therefore a simple Input File Creator is developed. The input file for ShaftAlign program requires a specific structure and set of parameters. The model parameters are read from an external file that can be edited either by the user or automatically and then they are processed accordingly. Some derivative sizes such as: the beam Inertia, the distributed weight of the shaft and the vertical offset of constrained nodes due to the imposed shaft misalignment are calculated. Lastly, all parameters required by the ShaftAlign tool are exported in a .sft file with a pre-specified architecture.

In the following tables, the Input and Output parameters are grouped and presented.

Read Parameters		
General	Number of constrained nodes	e.g. 2 nodes
	Number of segments	e.g. 10 segments
	Young modulus of shaft	Y_{mod}
	Constrained node(s) - ID	e.g. 2^{nd}, 10^{th}, 100^{th} etc.
Shaft Geometry	Length of shaft	L
	Diameter of shaft	D
	Aft protruding distance	L_{aft}
	Fore protruding distance	L_{fore}
Shaft Loading	Moment at aft protruding edge	M_{aft}
	Moment at fore protruding edge	M_{fore}
	Force at aft protruding edge	F_{Yaft}
	Force at fore protruding edge	F_{Yfore}
	Loading axis	Y - axis
System Constraints	Fore inclination of shaft	$R_{otyfore}$
	Shat misalignment angle	ψ_X

Table 4-6:READ PARAMETERS FOR SHAFT MODEL

File Creator Output – Input File structure	
Number_of_segments	
Number_of_constrained_nodes	
Angle	
Segment:	Lengths
	Loads
	Inertias
	Young Moduli
Nodal:	Shifts
	Forces_Y
	Forces_Z
	Bending_Moments_Y
	Bending_Moments_Z
	Slopes
Constrained Nodes	

Table 4-7:SHAFTALIGN INPUT FILE STRUCTURE

4.5.5 Numerical Simulation and Optimization Tool

According to: [22], [23], [24], [27], [28]

The bearing solver described in Section 5.1 was coupled with a two-objective optimization code using the Matlab built-in optimizer.

In this thesis, the design of double slope bearing is examined. The optimization process includes the following three (3) dimensionless design parameters:

1. *Secondary_slope_angle* is the non-dimensional slope at the aft section of the bearing
2. *Primary_slope_angle* is the non-dimensional slope at the fore section of the bearing
3. *Knuckle_point_position* is the non-dimensional position of the knuckle point along the length of the bearing

All parameters are dimensionless, since the slope angles are defined as a percentage of 2c/L and knuckle point position is defined as a percentage of the bearing length.

A 4th parameter is indirectly included, meaning the remaining length between the knuckle point and the fore end of the bearing.

The optimization aims at maximizing lubricant film thickness and minimizing the maximum pressure, with the first being equivalent to minimizing dimensionless eccentricity ratio. The objectives for minimum film thickness and maximum pressure are:

- Maximization of h_{min}
- Minimization of p_{max}

To this end, a main Matlab script is used to initiate the optimization procedure, and a separate Matlab function, was developed for the two objective optimization.

A built-in Matlab function will be used to find the minima using a genetic algorithm. The name of the function is: *gamultiobj* function, and the format used to call this function is the following:

[x,fval] = gamultiobj(FitnessFunction,numberOfVariables,[],[],[],[],LB,UB,options);

Specifically this function finds the Pareto front of the objective function `FITNESSFCN`. The fitness function that is used for slope boring is: *bearing_2Obj_Fun_Slope*. The number of variables is set as 3. Linear equalities and linear inequalities have not been used in our case, so a symbol of *[]* has been used. Boundary constraints for both cases are shown in Table 5-1:

Table 4-8: UPPER AND LOWER BOUNDARY CONSTRAINTS

Parameters for double slope design optimization	Lower boundary	Upper boundary
Primary slope	0	0.3
Secondary slope	0	0.6
Knuckle Point Position	0	0.5

Specific options for the genetic algorithm can be created with the *gaoptimset* function, an example of which is shown just below:

options='gaoptimset('PlotFcns',{@gaplotpareto,@gaplotscorediversity},'Generations',40,'PopulationSize',40)'.

Parameter *'PlotFcns'* is used to plot several quantities during simulation. In our case it plots two quantities: *@gaplotpareto and @gaplotscorediversity. The* gaplotpareto command plots a Pareto front for the two objectives, and *gaplotscorediversity* plots a histogram of the scores of the current generation. The other two parameters of the genetic algorithm options are the *generations* and *populationsize,* which state the maximum number of generations allowed and the number of individuals each generation contains, respectively. In our case both parameters are set to be 40, which means a maximum size of 40 generations, with 40 individuals in each generation. This means that, in total, each optimization problem required 1600 different solutions. In our case the optimization process was stopped when the Pareto front was stabilized around certain values. Each solution is saved in a text file, so after each different case is solved, it can be accessed and processed, accordingly. Then the "dominant" optimum solutions were sorted out using an excel spreadsheet, since there was no available built in tool from Matlab.

The above solving process using Matlab is depicted in Figure 5-1

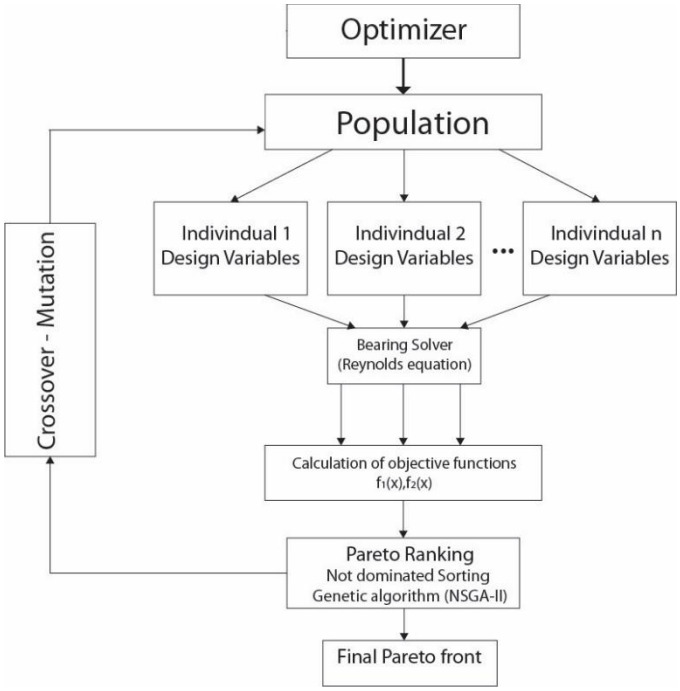

Figure 4-14:OPTIMIZATION ALGORITHM IN MATLAB

Finally, another Matlab script was used for post processing of the results in order to visualize the fluid film geometry (film thickness, *h*), and to plot the resulting pressure distribution, of several bearing designs selected by the user.

5 Numerical Simulations - Case Studies

In this section two case studies will be presented. Utilizing the tools introduced in Chapter 4 to study the Stern tube bearing operation and design. In the first case study, the effects of single and double slope will be tested and compared for both linear and bent shaft models. These designs, are basically the outcome of optimizing processes and a set among the most interesting cases will be subjected to a robustness test to demonstrate their performance in "worse" or overloaded conditions. The second case study concerns exclusively the double slope designs and will examine the effect of different shaft misalignment angles to the parameters of the double slope optimization. For both cases the same test geometry will be used. All the initial parameters are presented below in Table 5-1. For the meshing of the unwrapped journal bearing, a mesh of $\mathbf{L_{div} \times D_{div} = 100 \times 60}$ divisions was chosen, based on similar case studies existing in literature.

"Test –case" Model - Input Parameters			
Bearing length	L	1.05	m
Bearing diameter	D	0.52	m
Diametrical clearance	c	0.0009	m
Unwrapped Journal Bearing mesh longitudinal divisions	L_{div}	100	-
Unwrapped Journal Bearing mesh circumferential divisions	D_{div}	60	-
Nominal RPM	RPM	90	RPM
Lubricant temperature	T	40	°C
Lubricant Type		SAE 30	
Absolute viscosity	v	0.07	mPa·s
Young modulus of shaft	Y_{mod}	206	GPa
Distributed shaft weight load	W_{shaft}	-16343	N
Longitudinal divisions of the shaft model	L_{bear_div}	10	-
Aft protruding edge	L_{aft}	0.407	m
Fore protruding edge	L_{fore}	0.5412	m
Moment at the aft end	M_{aft}	409948	Nm
Force at the aft end	F_{Yaft}	-202598	N
Force at the fore end	F_{Yfore}	-107261	N
Loading at the Z - axis	F_{Zaft} F_{Zfore} M_{fore}	0 0 0	N N N
Shaft angle at the fore protruding edge	$R_{otyfore}$	0. 465	m·rad
Non-dimensional shaft misalignment angle (At the X - axis)	Ψ_X	**variable**	-
Non-dimensional shaft misalignment angle (At the Y – axis)	Ψ_Y	0	-
Sommerfeld Number	S	0.061764	-
Solution type		**Steady**	
Thermal analysis		**Isothermal**	

Table 5-1: "TEST CASE" MODEL - INPUT PARAMETERS

5.1 Performance Optimization Case Study

The purpose of this case study is to compare the bearing performance analysis results for several model types, aiming to demonstrate the effect of single and double slope geometry on bearing performance. The process to evaluate the journal bearing performance parameters for both linear and bent shaft model is also included and compared. In order to highlight the impact of the double slope geometry, two cases with different Ψx values are presented, for 0.3 and 0.6 non-dimensional shaft misalignment angles respectively.

In the following table the six model types that will be analyzed in the case study are illustrated:

Reference Case	•No slope model and linear shaft approximation •No slope model and bent shaft approximation
Single Slope Case	•Single slope model and linear shaft approximation •Single slope model and bent shaft approximation
Double Slope Case	•Double slope model and linear shaft approximation •Double slope model and bent shaft approximation

Table 5-2: CASE STUDIES

The most characteristic operational parameters will be grouped and compared, aiming to highlight the impact of bent shaft modeling to the bearing study. Initially, two reference models are presented for linear and bent shaft model respectively, without any slope. Thereafter, single and double sloped bearing geometry models are introduced and compared for both linear and bent shaft models.

The second phase of this case study concerns the performance of the stern tube bearing in several "extreme" conditions. The most accurate modeling methods for both single and double sloped bearing will be tested in the following scenarios:

1. 20% RPM Increase
2. 30% RPM Decrease
3. 50% Extra Load
4. 50% Less Load
5. 20˚ C Oil Temperature Increase

Concerning cases 3, 4 the load is added or removed uniformly from the shaft, without any impact on the shaft misalignment angle. This assumption might not be very accurate for real time performance but is a good method to demonstrate the unique attributes of the double slope modeling against the single slope design. In cases 1, 4 an improved performance is expected, since the stern tube bearing is more often heavily loaded, rather than in danger to be unloaded. The reason behind these test is again the comparison between the response of single and double slope design respectively.

Although major conclusions can be extracted from the case of 0.3 misalignment angle, a case for 0.6 non-dimensional shaft misalignment angle will also be presented. Thereof the scaling of the added value that the double slope geometry provides in angles larger than c/L will be highlighted.

5.1.1 Initial Case For: Ψx = 0.3

Linear Shaft Model

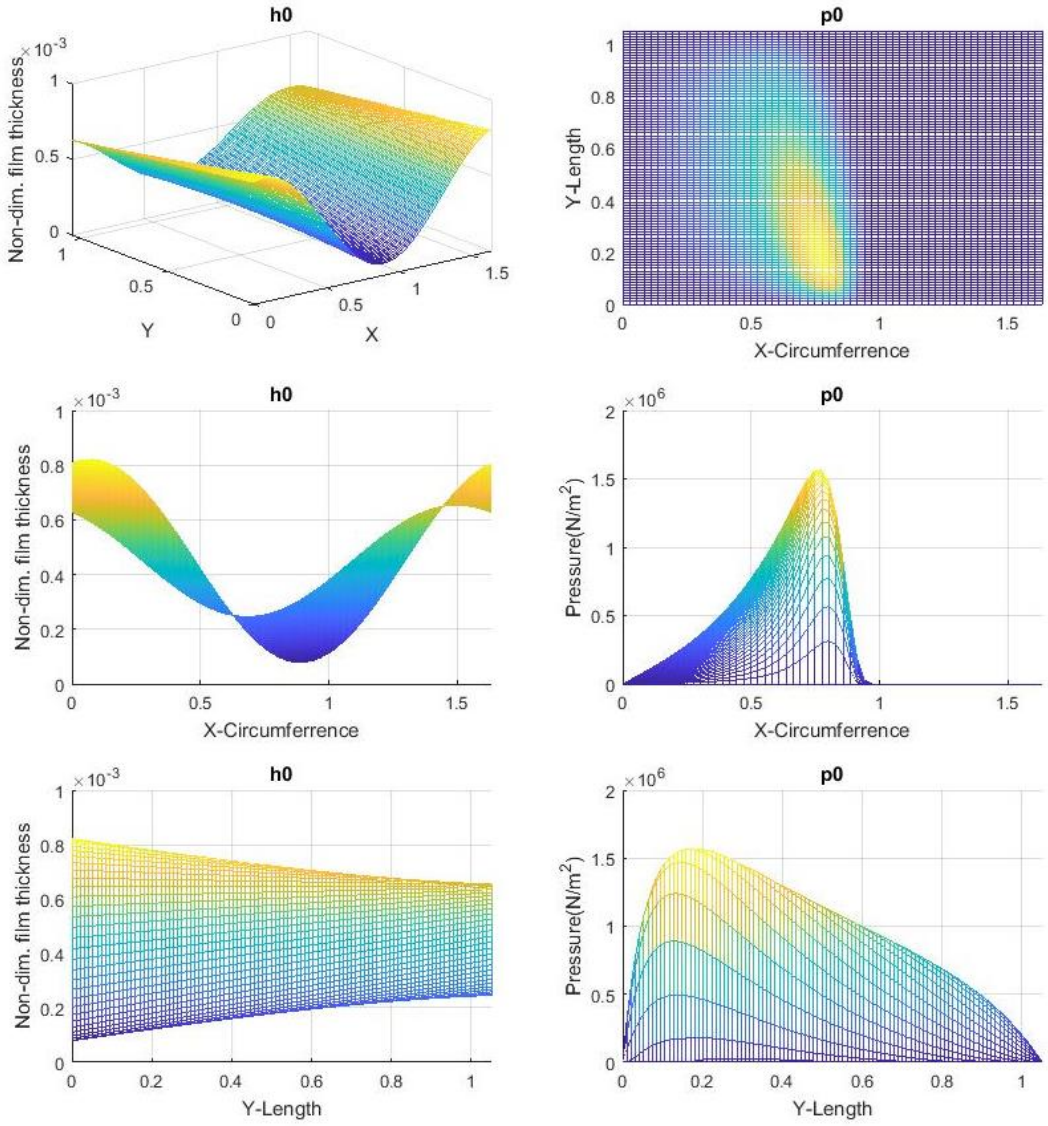

Figure 5-1:INITIAL MODEL FOR Ψx=0.3, LINEAR SHAFT

In the figure above, the distribution of lubricant film thickness 'h' (on the left) and pressure (on the right) in three major planes, over the unwrapped journal bearing geometry is presented

Comments:

This is the initial condition of the stern tube bearing with Ψx=0.3. The shaft model is linear and such a model is very common especially for bearings such as the intermediate bearings, with small L/D ratios. For the stern tube bearing design this model does not accurately describe the actual condition. This can be further justified in comparison to the following cases. This model will be used as a comparison reference for the cases with single and double slope design with linear shaft model, as well as the reference case. Such a model can be very useful for fairly accurate and quick calculations on cases with very small misalignment angles. This will be further examined in the second case study.

Bent Shaft Model

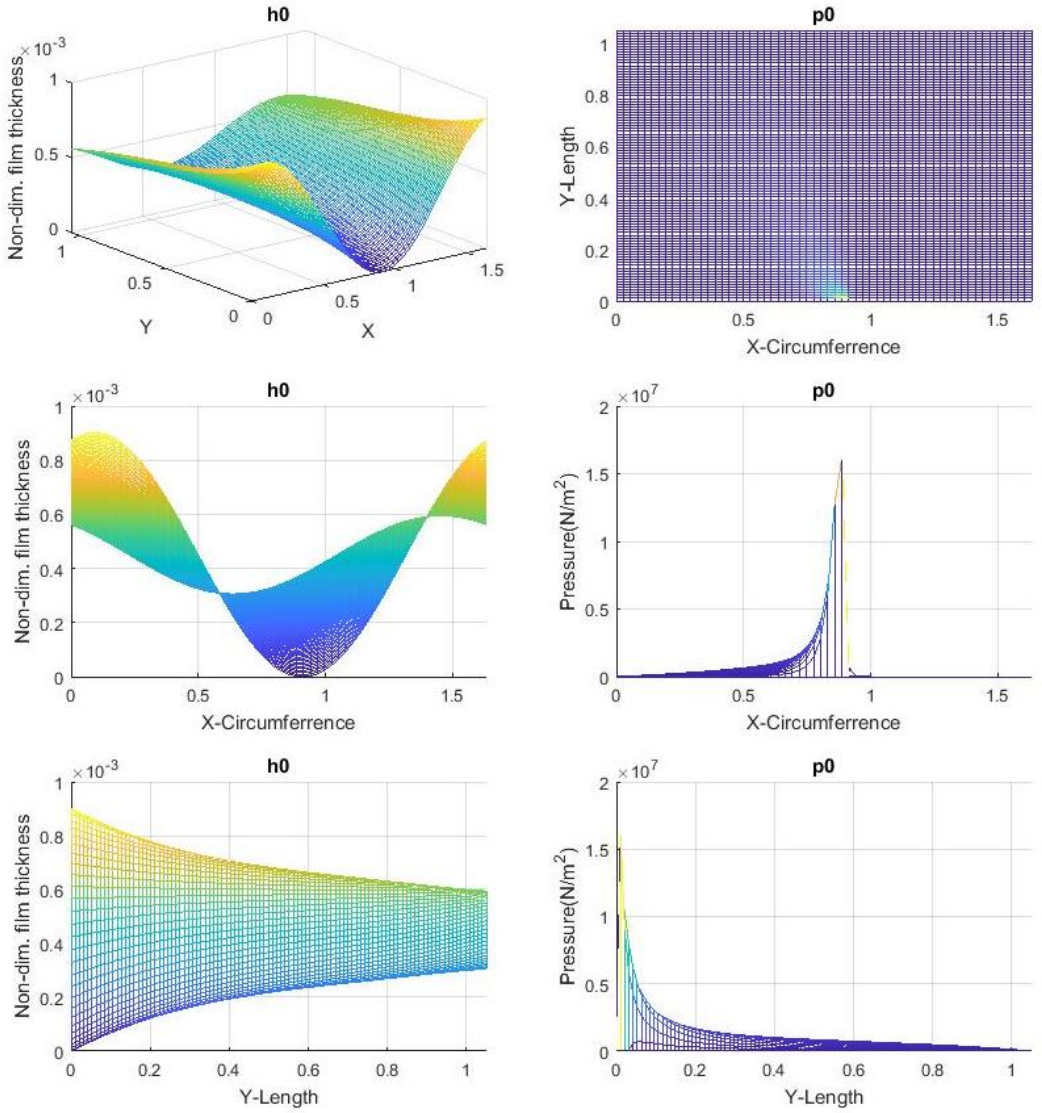

Figure 5-2: INITIAL MODEL FOR Ψx=0.3, BENT SHAFT

In the figure above, the distribution of lubricant film thickness 'h' (on the left) and pressure (on the right) in three major planes, over the unwrapped journal bearing geometry is presented

Comments:

From this example, it becomes obvious that bent shaft modeling is critical for accurate representation of the lubricant film thickness. In this case, the linear shaft model could not detect that the shaft is in contact to the bearing surface in the aft end of the bearing length. This could potentially cause erroneous sense of safety for the designer. Bent shaft modeling is rather complex on the other side, since it requires coupling of the shaft alignment output and the bearing performance calculations. Furthermore, the bearing should be able to perform acceptably in various and often transient conditions concerning both load and shaft misalignment. This introduces a new level of complexity to the study of the stern tube bearing and journal bearings in general.

5.1.2 Single Slope Case For: Ψx = 0.3

Linear Shaft Model

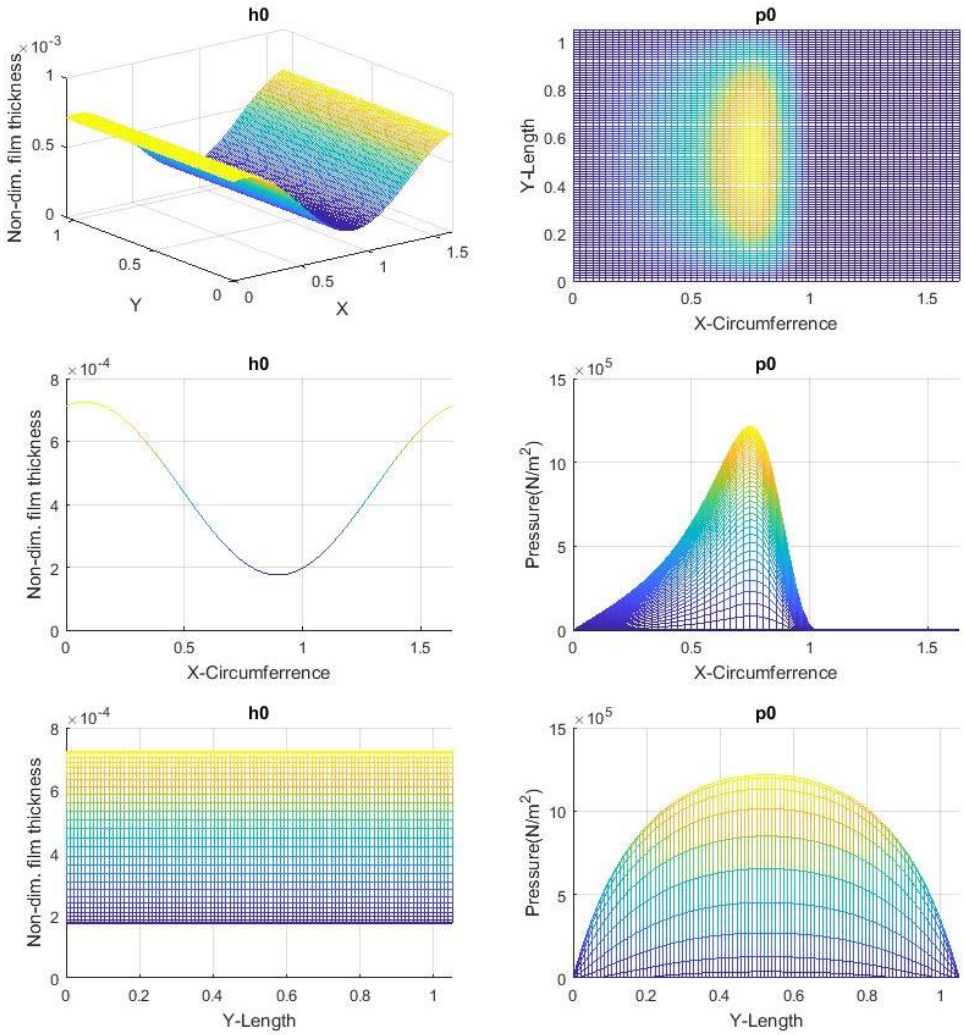

Figure 5-3: SINGLE SLOPE MODEL FOR Ψx=0.3, LINEAR SHAFT

In the figure above, the distribution of lubricant film thickness 'h' (on the left) and pressure (on the right) in three major planes, over the unwrapped journal bearing geometry is presented

Comments:

This case is basically a theoretical model, where the shaft and the slope are inclined identically. In actual condition examples this can't take place since non linearities exist on both surfaces. In terms of optimization, the Reynolds equation solution for single slope optimization yields (by definition) as single optimum solution, the geometry presented above. This single slope geometry is usually the best solution when the shaft inclination within the bearing is limited or close to 10%·c/L rad. Important factor is also the L/D ratio of the bearing. Stern tube bearings though, due to the proximity of the bearing to the propeller and the excessive loading, rarely come under this scenario.

Bent Shaft Model

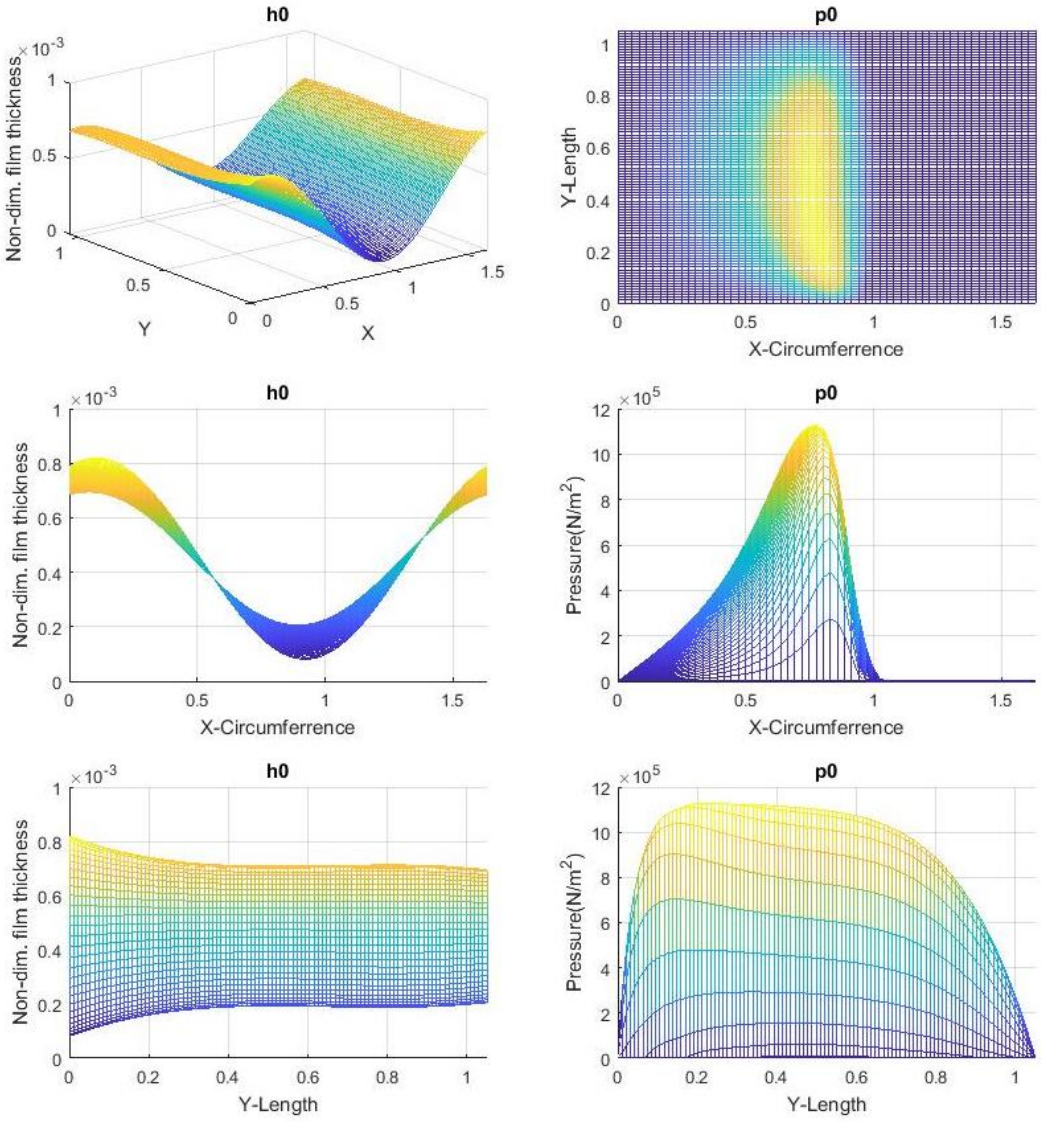

Figure 5-4: SINGLE SLOPE MODEL FOR Ψx=0.3, BENT SHAFT

In the figure above, the distribution of lubricant film thickness 'h' (on the left) and pressure (on the right) in three major planes, over the unwrapped journal bearing geometry is presented

Comments:

In this case, the shaft is modeled bent under the assumption of a constant shaft misalignment angle between the fore and aft edge of the bearing. The single slope is the same as in the previous example, defined by a 0.3 non dimensional angle. This model has a very accurate representation of the lubricant film and yields interesting results concerning the actual benefit from single slope modeling. Two important observations extracted from the figure above, are the following:

1. The non-dimensional lubricant film thickness is almost constant after the first 30% of the length. This coincides, as expected, with the correction for bent shaft model.
2. The pressure profile is very smooth and p_{max} is applied for a larger length within the bearing than in the case of single slope, linear shaft, causing p_{max} to be significantly lower (about 0.10 GPa).

5.1.3 Double Slope Case For: Ψx = 0.3

Linear shaft Model

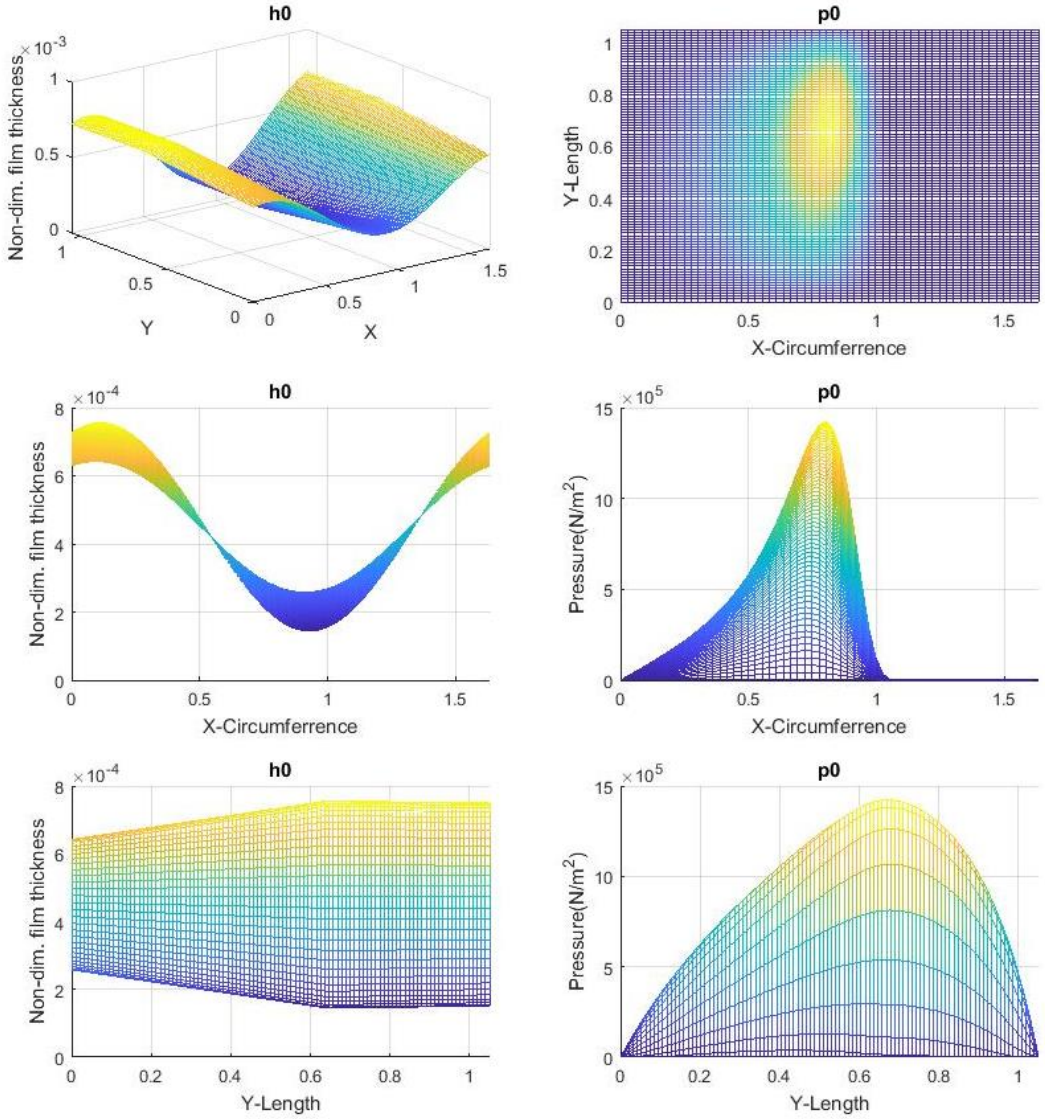

Figure 5-5: DOUBLE SLOPE MODEL FOR Ψx=0.3, LINEAR SHAFT

In the figure above, the distribution of lubricant film thickness 'h' (on the left) and pressure (on the right) in three major planes, over the unwrapped journal bearing geometry is presented

Comments:

The slope non-dimensional parameters were extracted through an optimization process as presented in Chapter 4 and are:

$Slope_{Aft}$= 0.31 $Length_{Aft}$= 0.61 $Slope_{Fore}$= 0.11 $LengthF_{ore}$= 0.39

The most important observation extracted from the figure above, is that the non-dimensional film thickness has a knuckle point at the location where the slopes coincide, which was expected theoretically. The interesting feature is that the optimizer yielded a solution at which the minimum film thickness and therefore the maximum pressure is "split" into two linear segments both in terms of film thickness and pressure derivative.

Bent Shaft Model

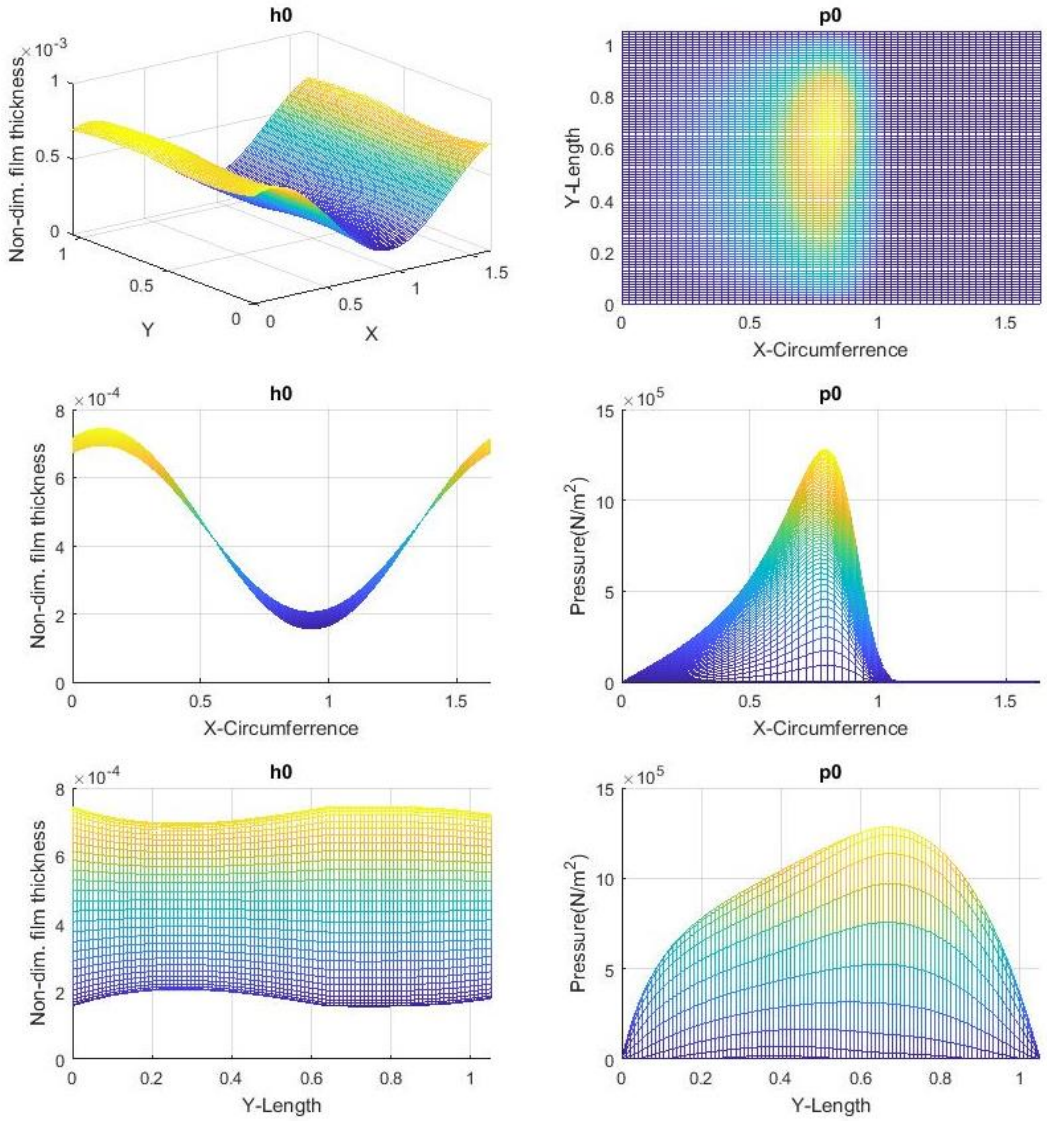

Figure 5-6: DOUBLE SLOPE MODEL FOR Ψx=0.3, BENT SHAFT

In the figure above, the distribution of lubricant film thickness 'h' (on the left) and pressure (on the right) in three major planes, over the unwrapped journal bearing geometry is presented

Comments:

The slope non-dimensional parameters are as in the previous case:

$Slope_{Aft}$= 0.31 $Length_{Aft}$= 0.61 $Slope_{Fore}$= 0.11 $LengthF_{ore}$= 0.39

In this case the film thickness curve resembles much more to the actual condition within the bearing, without any tips and edges. The importance of the bent shaft effect on the aft end of the bearing can also be observed here, in comparison to Figure 5-5. The pressure distribution is not as uniform as in the case of single slope model (Figure 5-4) and it can be circumscribed by three pressure derivatives. The location of p_{max} appears closer to the fore end of the bearing, in comparison to the single slope model where it appeared closer to the aft end.

5.1.4 Comparison of Results for Various Model Types for Ψx=0.3

In the following table the most important parameters of the model types presented are collected:

Shaft Misalignment Angle = 0.3						
Slope Modeling	**No Slope**	**No Slope**	**Single Slope**	**Single Slope**	**Double Slope**	**Double Slope**
Shaft Modeling	**Linear**	**Bent**	**Linear**	**Bent**	**Linear**	**Bent**
h_{min} *[μm]*	79.1	2.25	175	**80.8**	145	**156**
p_{max} *[GPa]*	1.56	16.1	1.22	**1.13**	1.42	**1.28**
Angle of p_{max}	39.1566	53.7014	22.0853	**26.2591**	27.8491	**27.2431**
Ploss [kW]	2.395	2.564	2.342	**2.349**	2.352	**2.334**
Distance of Support Point from L/2 [m]	0.074414	0.170052	-4.62E-05	**0.031465**	-0.041679	**-0.016205**
Ecc ratio	0.593616	0.505511	0.345666	**0.301117**	0.141203	**0.106152**
Att angle	48.3091	38.4472	37.3396	**35.4116**	30.8999	**30.294**
S	0.0617644	0.0617644	0.0617644	**0.0617644**	0.0617644	**0.0617644**

Table 5-3: PERFORMANCE PARAMETERS COMPARISON FOR Ψx=0.3

In the following chart the major performance parameters of Table 5-3 are compared:

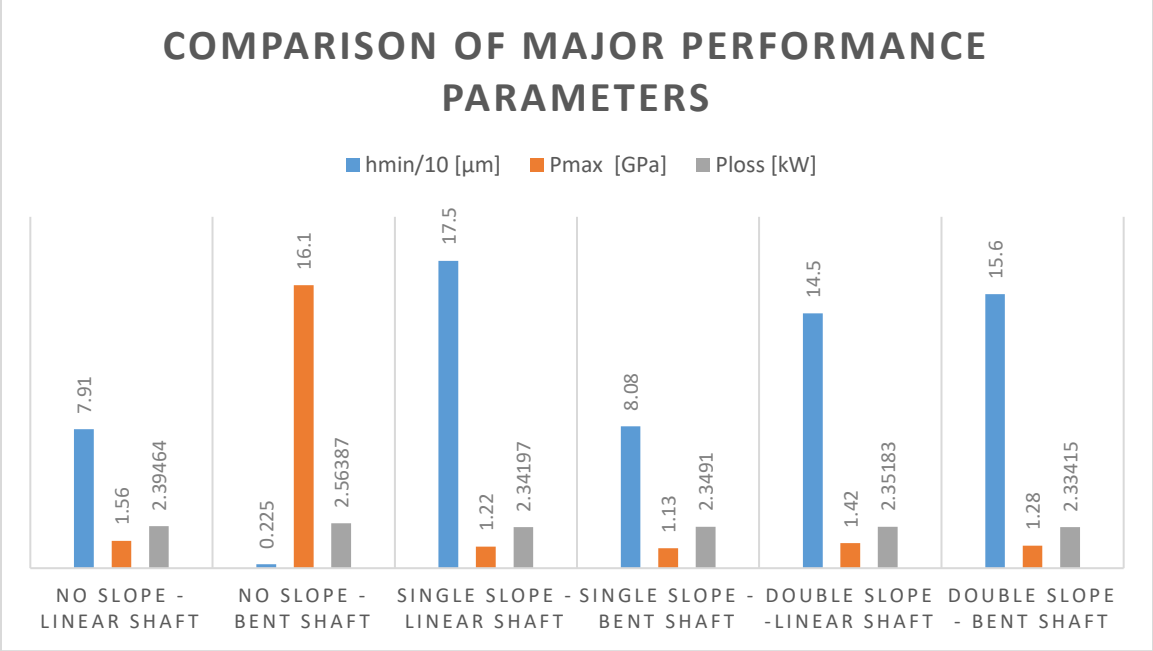

Figure 5-7: PERFORMANCE PARAMETERS COMPARISON FOR Ψx=0.3

Although both the single and double slope models provide improved performance in comparison to the reference case, it is visible that the double slope model provides significant improvement especially concerning the h_{min} for bent shaft models. The major advantage that the double slope geometry is providing, is that it can "follow" the bent shaft geometry much more accurately than the single slope, resulting to improved film thickness and pressure distribution. Another important outcome is that bent shaft modeling is very critical since it may significantly alter the perspective of the problem. To further analyze the capabilities of double and single slope designs, several test will be run for extreme conditions, aiming to conclude to the design that improves to the maximum the survivability and performance of the stern tube bearing. The bent shaft - double and single slope models are the reference cases respectively.

5.1.5 Optimum Solution Robustness Test For: Ψx = 0.3 – 20%RPM Increase

Single Slope Model

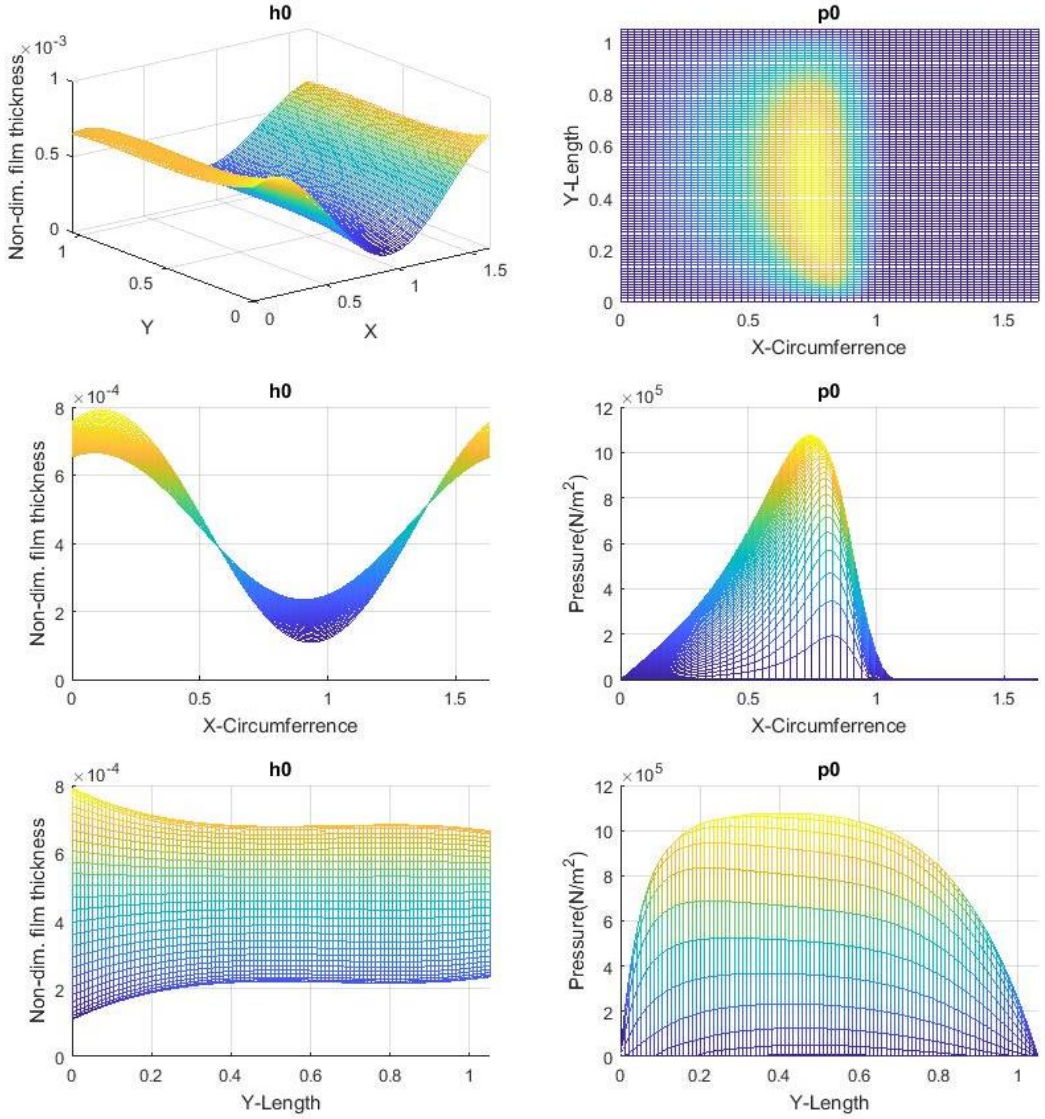

Figure 5-8: SINGLE SLOPE MODEL WITH BENT SHAFT, FOR 20% INCREASED RPM

In the figure above, the distribution of lubricant film thickness 'h' (on the left) and pressure (on the right) in three major planes, over the unwrapped journal bearing geometry is presented

In the following table the test results are presented and compared to the reference model:

Test:	**20% Increased RPM**		**Test Result**	**Deviation from Ref. %**
Shaft Model:	**Bent**	h_{min} =	109 µm	34.86
Slope Type:	**Single**	p_{max} =	1.08 GPa	-4.68
S =	**0.0754898**	P_{loss} =	3.222 kW	37.19
Distance of Support Point from L/2 =			0.264272 m	-16.01

Table 5-4: SINGLE SLOPE MODEL WITH BENT SHAFT, FOR 20% INCREASED RPM

Comments: Steady design, the performance is slightly improved as expected, both curves are very smooth and especially the pressure curve demonstrates a wide and homogenous loading along the bearing length.

Double Slope Model

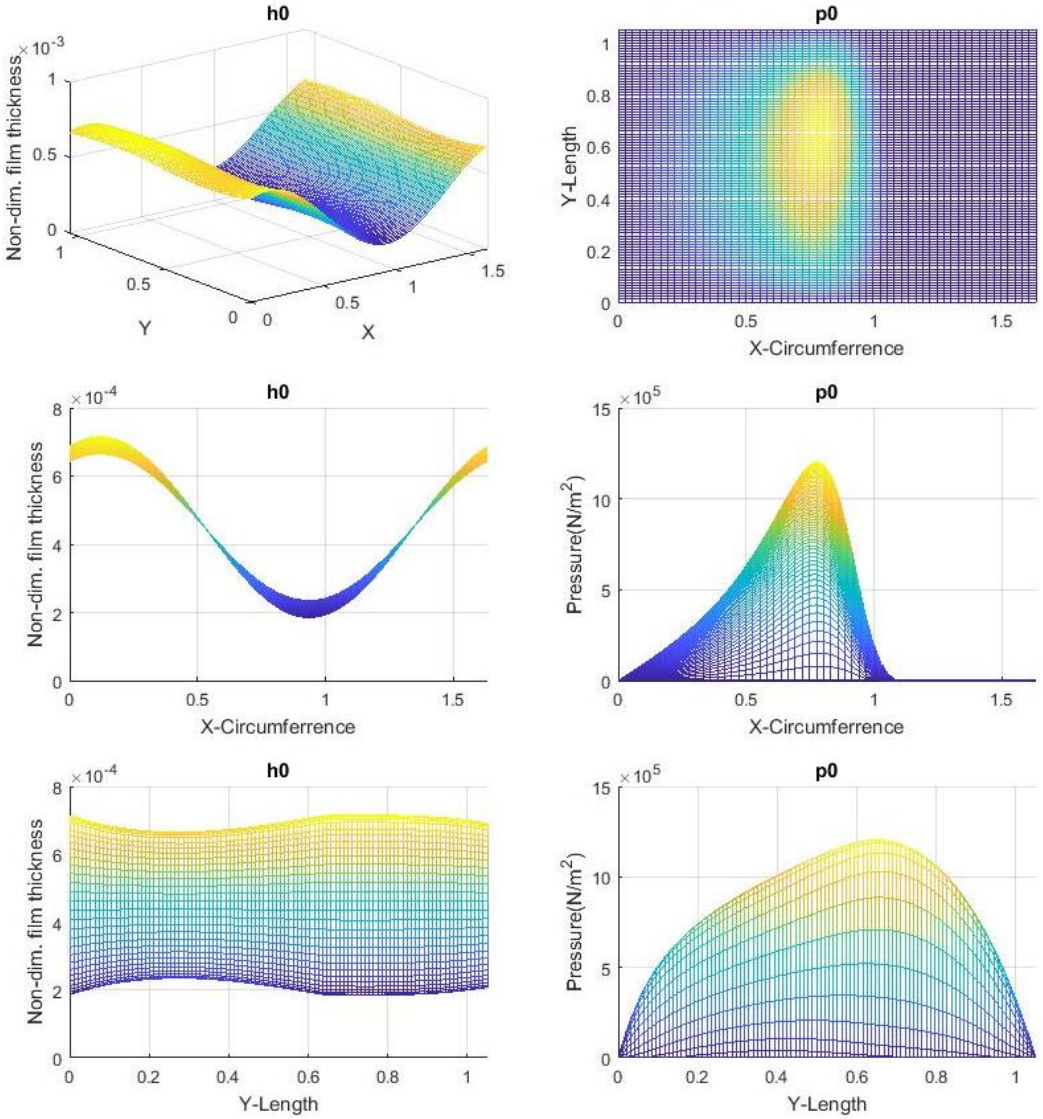

Figure 5-9: DOUBLE SLOPE MODEL WITH BENT SHAFT, FOR 20% INCREASED RPM

In the figure above, the distribution of lubricant film thickness 'h' (on the left) and pressure (on the right) in three major planes, over the unwrapped journal bearing geometry is presented

In the following table the test results are presented and compared to the reference model:

Test:	**20% Increased RPM**		**Test Result**	**Deviation from Ref. %**
Shaft Model:	**Bent**	h_{min} =	185 µm	18.80
Slope Type:	**Double**	p_{max} =	1.20 GPa	-6.14
S =	**0.0754898**	P_{loss} =	3.205 kW	37.33
Distance of Support Point from L/2 =			-0.0146336 m	-9.70

Table 5-5: DOUBLE SLOPE MODEL WITH BENT SHAFT, FOR 20% INCREASED RPM

Comments: Comparable results to the single slope design and steady operation. Note that the reference case is the initial double slope model, which provided already improved performance.

5.1.6 Optimum Solution Robustness Test For: Ψx = 0.3 – 30% RPM Decrease

Single Slope Model

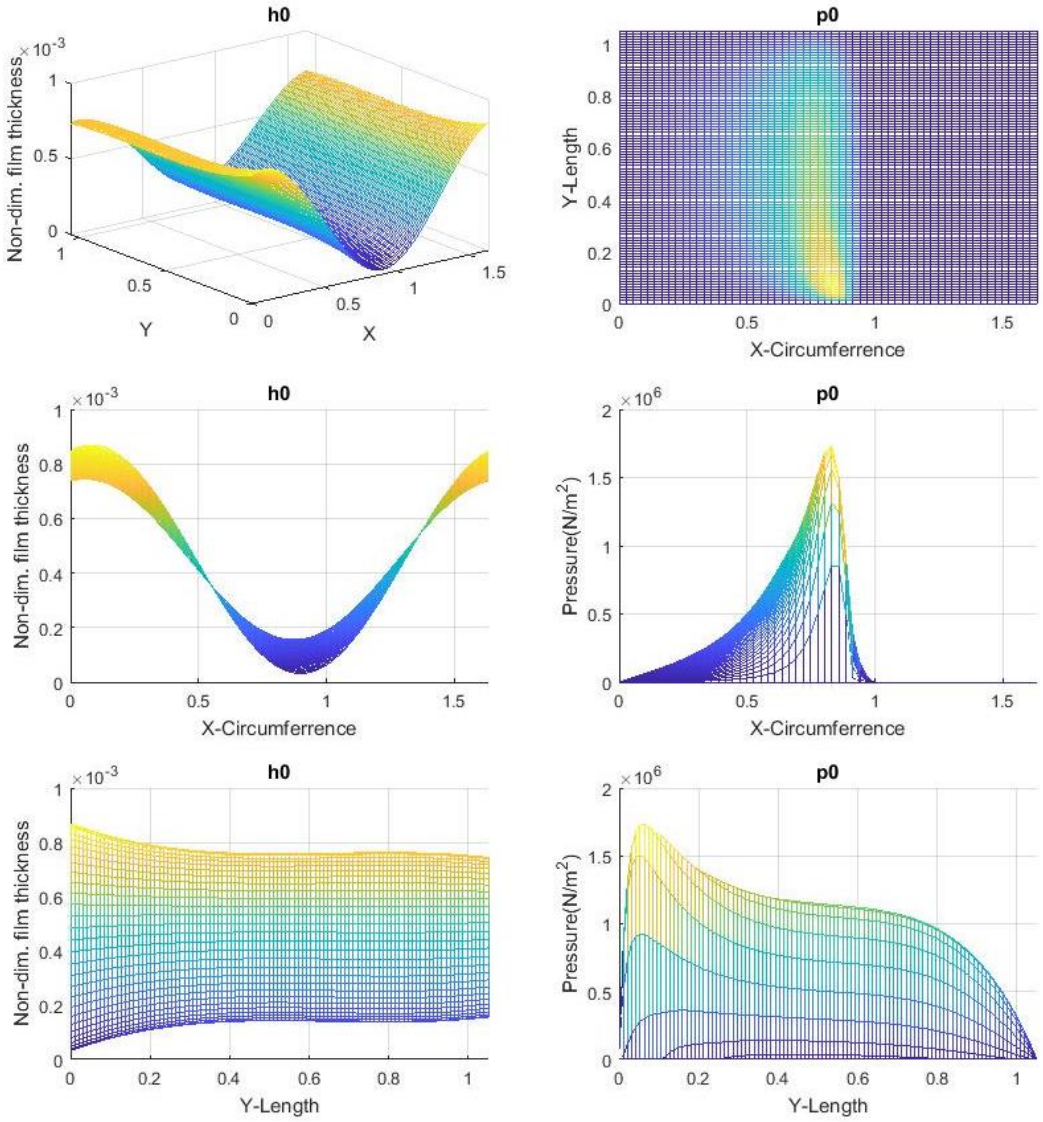

Figure 5-10: SINGLE SLOPE MODEL WITH BENT SHAFT, FOR 30% DECREASED RPM

In the figure above, the distribution of lubricant film thickness 'h' (on the left) and pressure (on the right) in three major planes, over the unwrapped journal bearing geometry is presented

In the following table the test results are presented and compared to the reference model:

Test:	**30% Decreased RPM**		**Test Results**	**Deviation from Ref. %**
Shaft Model:	**Bent**	h_{min} =	31.9 μm	-60.57
Slope Type:	**Single**	p_{max} =	1.73 GPa	53.23
S =	**0.0411763**	P_{loss} =	1.273 kW	-45.81
Distance of Support Point from L/2 =			0.0520628 m	65.46

Table 5-6: SINGLE SLOPE MODEL WITH BENT SHAFT, FOR 30% DECREASED RPM

Comments: The system is overloaded, the P_{max} has shifted towards the aft edge, where the minimum film thickness is expected. The effect of the bent shaft is critical and the shaft is going to touch the bushing, being provided with some additional external load.

Double Slope Model

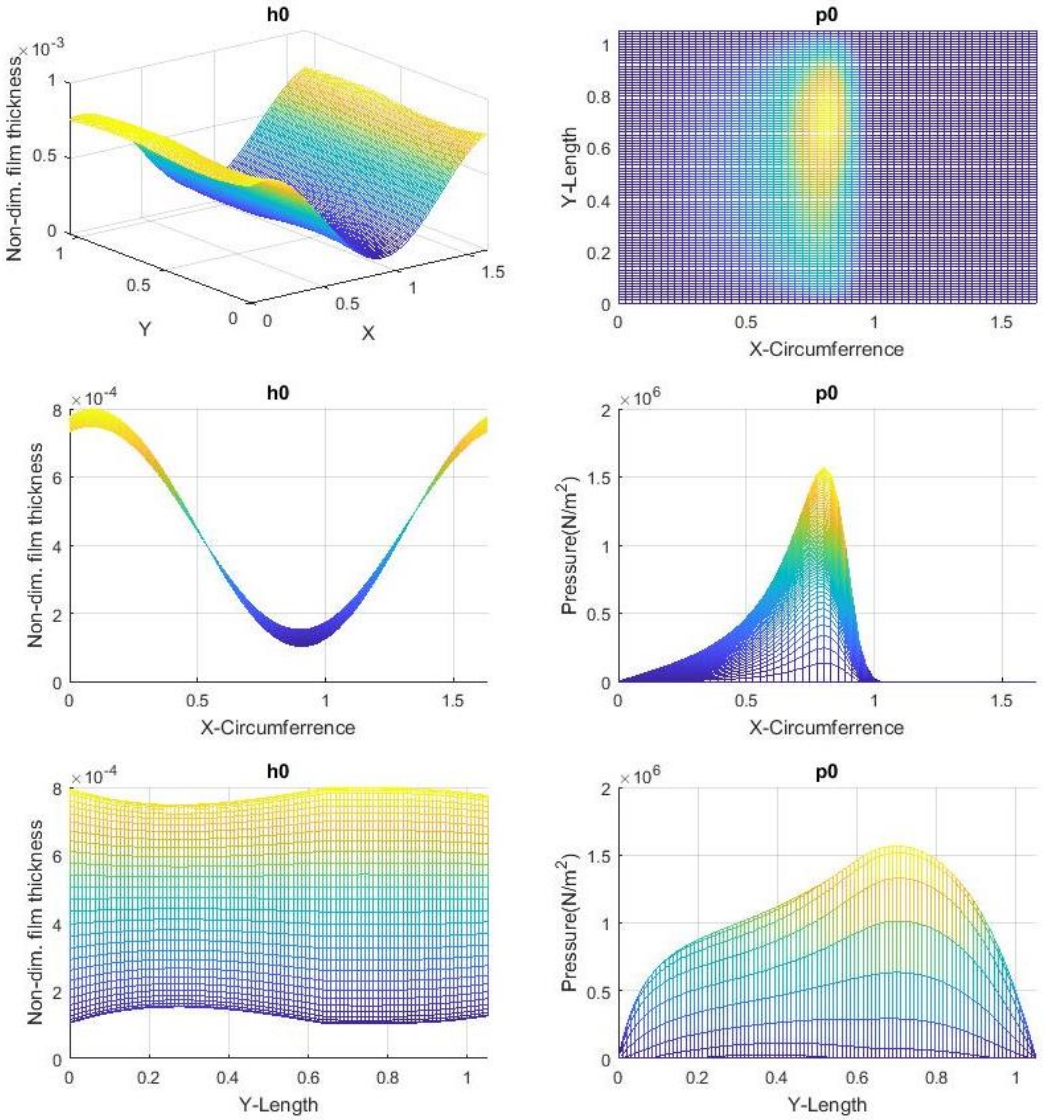

Figure 5-11 : DOUBLE SLOPE MODEL WITH BENT SHAFT, FOR 30% DECREASED RPM

In the figure above, the distribution of lubricant film thickness 'h' (on the left) and pressure (on the right) in three major planes, over the unwrapped journal bearing geometry is presented

In the following table the test results are presented and compared to the reference model:

Test:	**30% Decreased RPM**		**Test Results**	**Deviation from Ref. %**
Shaft Model:	**Bent**	h_{min} =	102 μm	-34.15
Slope Type:	**Double**	p_{max} =	1.57 GPa	22.10
S =	**0.0411763**	P_{loss} =	1.266 kW	-45.78
Distance of Support Point from L/2 =			-0.02344 m	44.64

Table 5-7: DOUBLE SLOPE MODEL WITH BENT SHAFT, FOR 30% DECREASED RPM

Comments: The system seems to be much more robust in comparison to the single slope design. The lubricant film remains steady and it is shifted vertically almost homogenously. Furthermore, the pressure distribution peak is also homogenously increased but it hasn't shifted to a new longitudinal position as in the single slope case. The system seems adequate for further RPM reduction.

5.1.7 Optimum Solution Robustness Test For: Ψx = 0.3 – 50% Overload

Single Slope Model

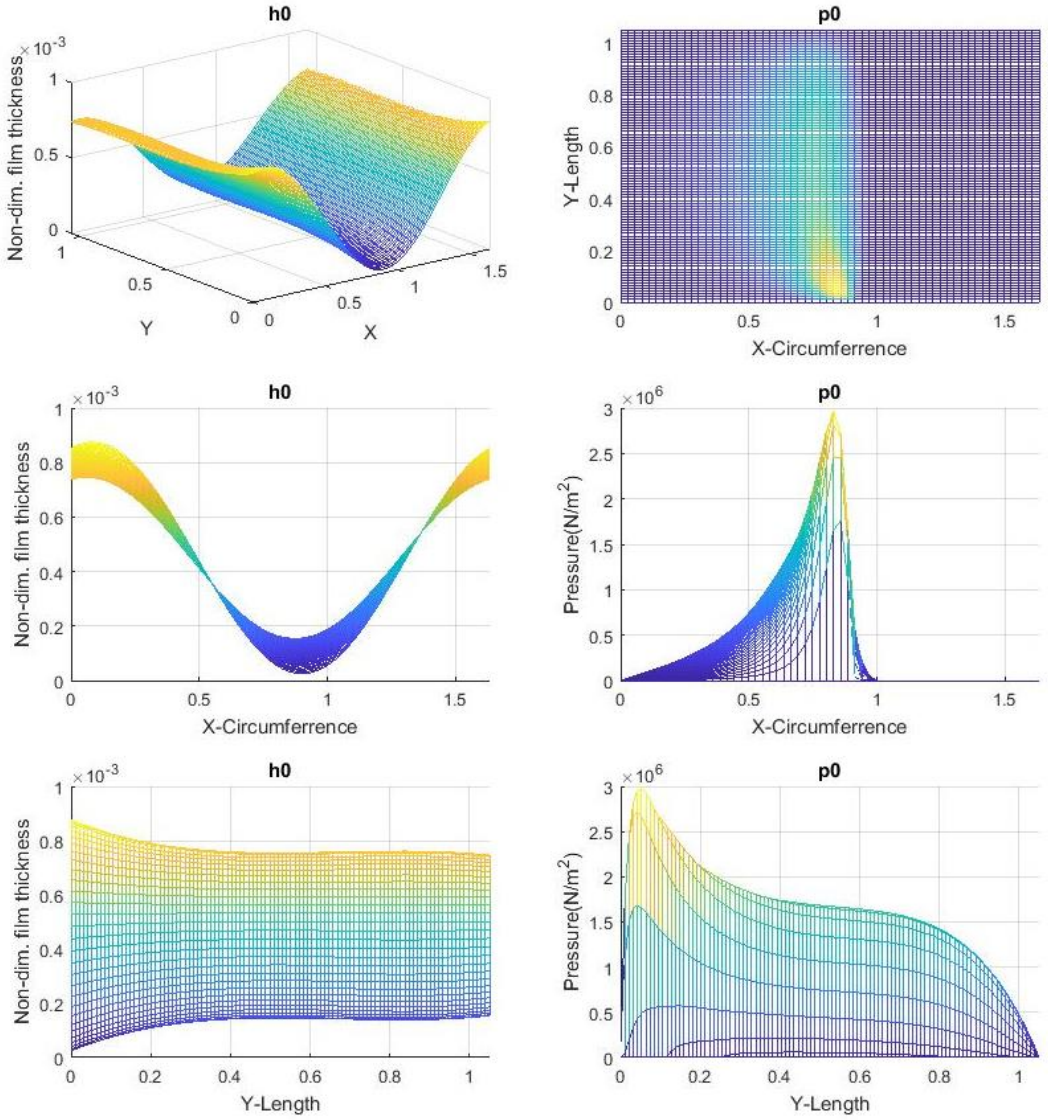

Figure 5-12: SINGLE SLOPE MODEL WITH BENT SHAFT, FOR 50% ADDITIONAL LOAD

In the figure above, the distribution of lubricant film thickness 'h' (on the left) and pressure (on the right) in three major planes, over the unwrapped journal bearing geometry is presented

In the following table the test results are presented and compared to the reference model:

Test:	**50% Additional Load**		**Test Results**	**Deviation from Ref. %**
Shaft Model:	**Bent**	h_{min} =	25.5 μm	-68.44
Slope Type:	**Single**	p_{max} =	2.97 GPa	162.99
S =	**0.0411763**	P_{loss} =	2.873 kW	22.28
Distance of Support Point from L/2 =			0.0570636 m	81.36

Table 5-8: SINGLE SLOPE MODEL WITH BENT SHAFT, FOR 50% ADDITIONAL LOAD

Comments: Similar concerns as in the previous test, the pressure is increased aftwards and the system has almost reached its limits. The fore part of the bearing seems unable to receive and support the additional load.

Double Slope Model

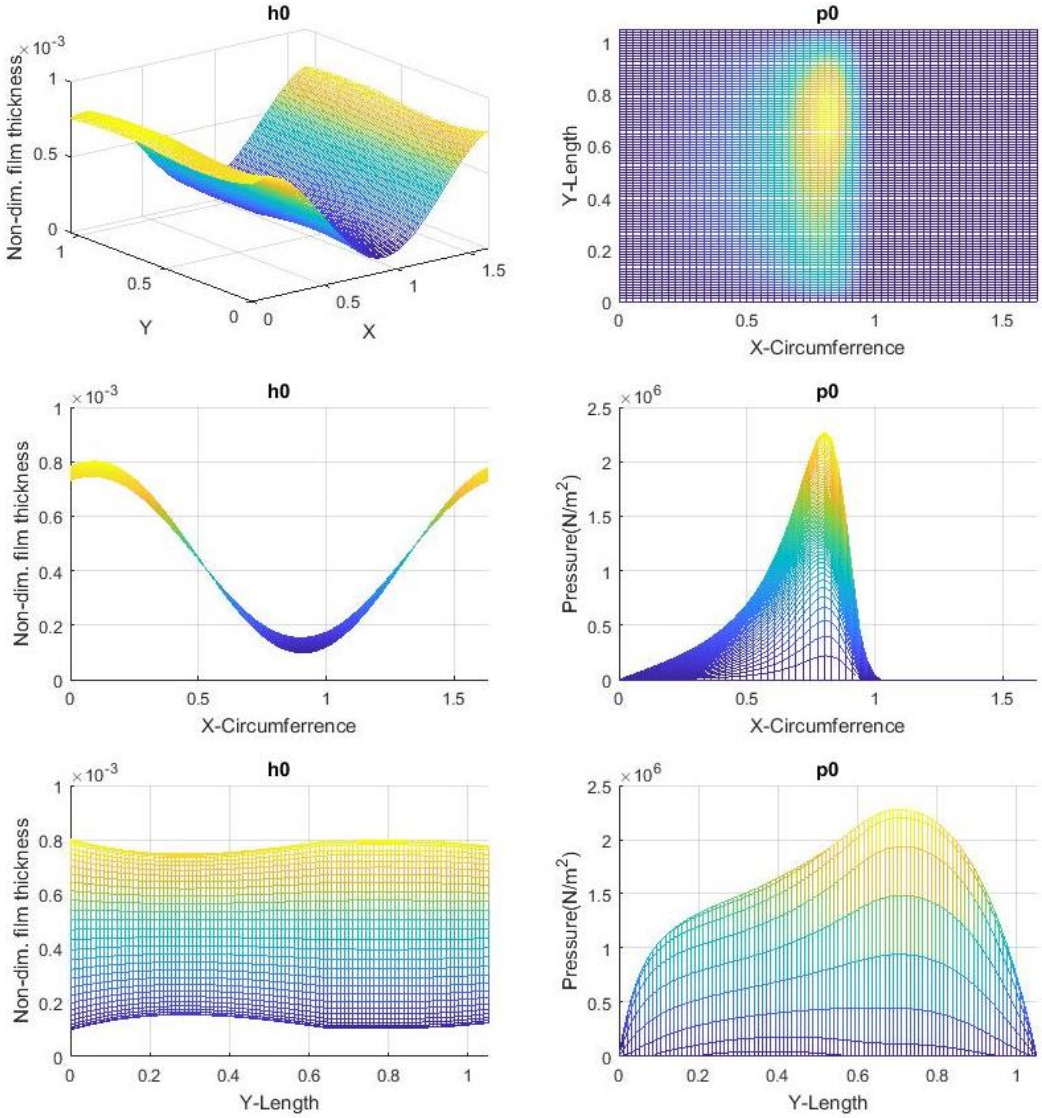

Figure 5-13: DOUBLE SLOPE MODEL WITH BENT SHAFT, FOR 50% ADDITIONAL LOAD

In the figure above, the distribution of lubricant film thickness 'h' (on the left) and pressure (on the right) in three major planes, over the unwrapped journal bearing geometry is presented

In the following table the test results are presented and compared to the reference model:

Test:	**50% Additional Load**		**Test Results**	**Deviation from Ref. %**
Shaft Model:	**Bent**	h_{min} =	98.1 μm	-36.95
Slope Type:	**Double**	p_{max} =	2.28 GPa	77.70
S =	**0.0411763**	P_{loss} =	2.835 kW	21.44
Distance of Support Point from L/2 =			-0.02187 m	34.94

Table 5-9: DOUBLE SLOPE MODEL WITH BENT SHAFT, FOR 50% ADDITIONAL LOAD

Comments: The bearing has responded much better to the extreme condition and the additional load seems to be supported from both the fore and the aft side of the bearing. Characteristically, the support point location has slightly shifted aftwards and the pressure peak is still at the fore length of the bearing.

5.1.8 Optimum Solution Robustness Test For: Ψx = 0.3 – 50% Unload

Single Slope Model

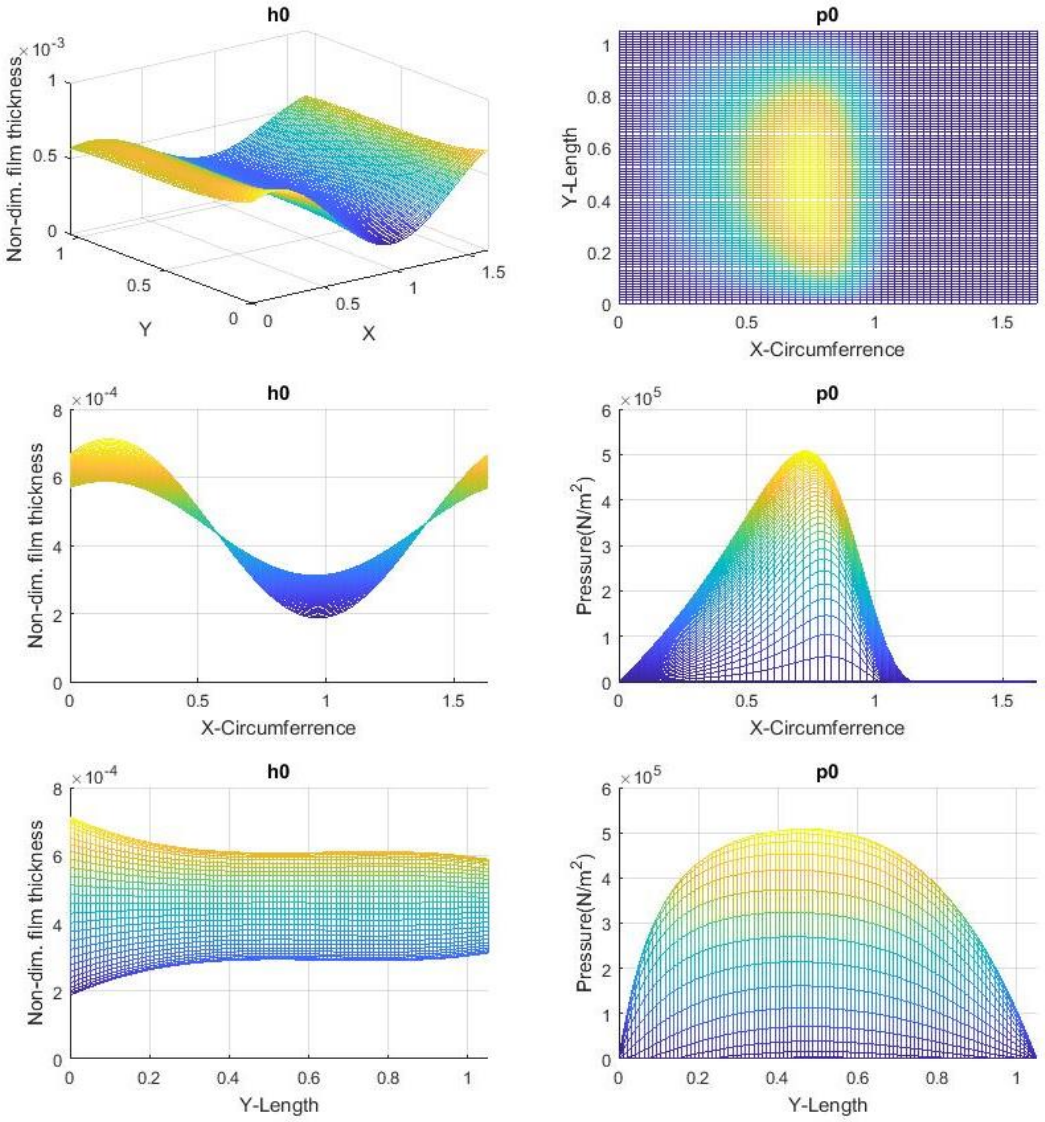

Figure 5-14: SINGLE SLOPE MODEL WITH BENT SHAFT, FOR 50% REDUCED LOAD

In the figure above, the distribution of lubricant film thickness 'h' (on the left) and pressure (on the right) in three major planes, over the unwrapped journal bearing geometry is presented

In the following table the test results are presented and compared to the reference model:

Test:	**50% Reduced Load**		**Test Results**	**Deviation from Ref. %**
Shaft Model:	**Bent**	h_{min} =	187 μm	131.63
Slope Type:	**Single**	p_{max} =	0.508 GPa	-55.04
S =	**0.123529**	P_{loss} =	1.840 kW	-21.66
Distance of Support Point from L/2 =			0.02073 m	-34.11

Table 5-10: SINGLE SLOPE MODEL WITH BENT SHAFT, FOR 50% REDUCED LOAD

Comments: The system is responding very well, all the parameters have improved significantly from the reference case and no sign of bearing unloading is visible. Of course the stern tube bearing is rarely confronted with unloading scenario.

Double Slope Model

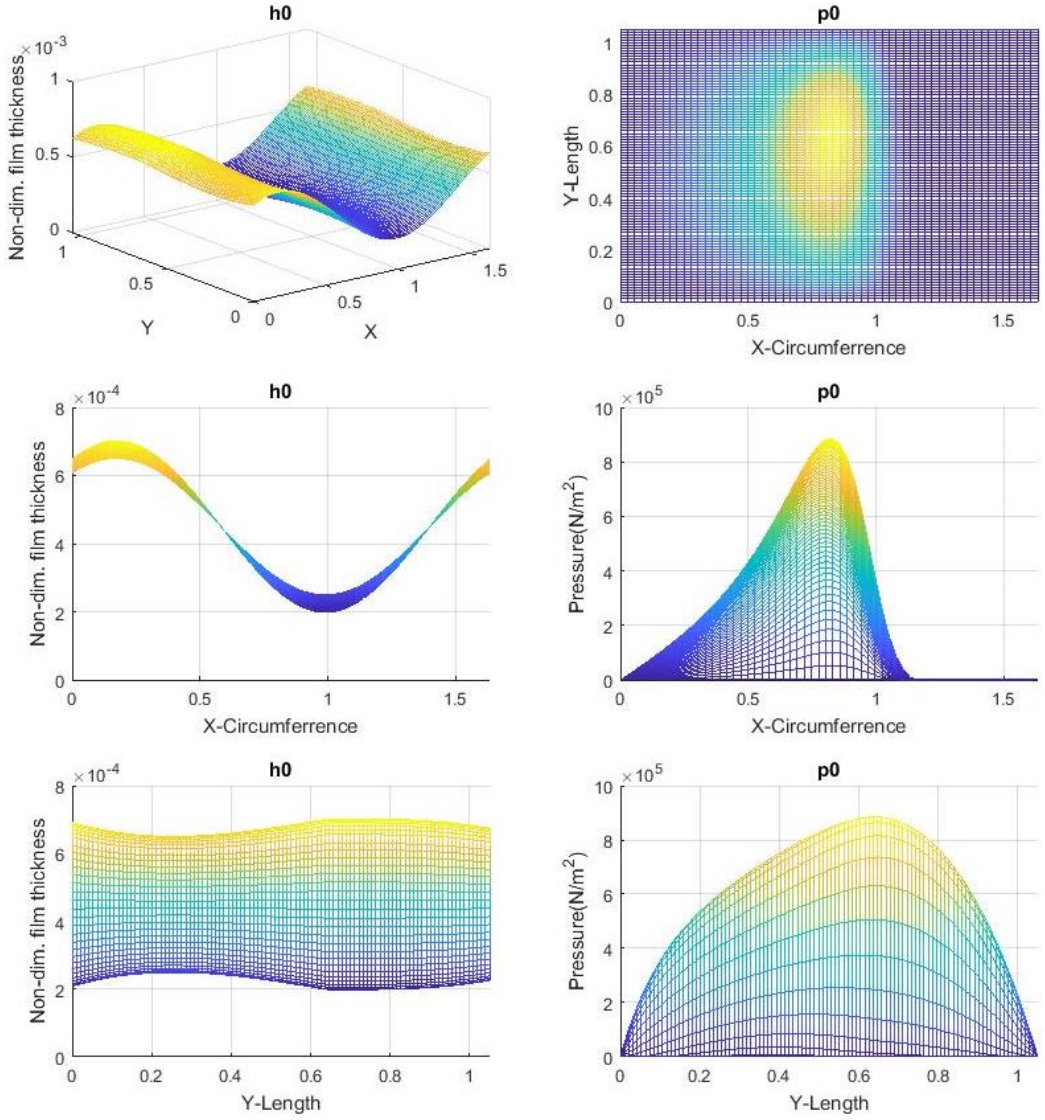

Figure 5-15: DOUBLE SLOPE MODEL WITH BENT SHAFT, FOR 50% REDUCED LOAD

In the figure above, the distribution of lubricant film thickness 'h' (on the left) and pressure (on the right) in three major planes, over the unwrapped journal bearing geometry is presented

In the following table the test results are presented and compared to the reference model:

Test:	**50% Reduced Load**		**Test Results**	**Deviation from Ref. %**
Shaft Model:	**Bent**	h_{min} =	198 μm	27.52
Slope Type:	**Double**	p_{max} =	0.885 GPa	-31.00
S =	**0.123529**	P_{loss} =	2.072 kW	-11.24
Distance of Support Point from L/2 =			-0.013277 m	-18.07

Table 5-11: DOUBLE SLOPE MODEL WITH BENT SHAFT, FOR 50% REDUCED LOAD

Comments: The design does not show any unwanted characteristics, the load is still supported by the fore section mainly and the pressure has been developed almost uniformly along the circumference, on a similar way to the single slope design. A minor increase of the lubricant film thickness at the fore end of the bearing might be crucial in case of further load reduction, which is very uncommon though.

5.1.9 Optimum Solution Robustness Test For: Ψx = 0.3 – 20°C Temperature Increase

Single Slope Model

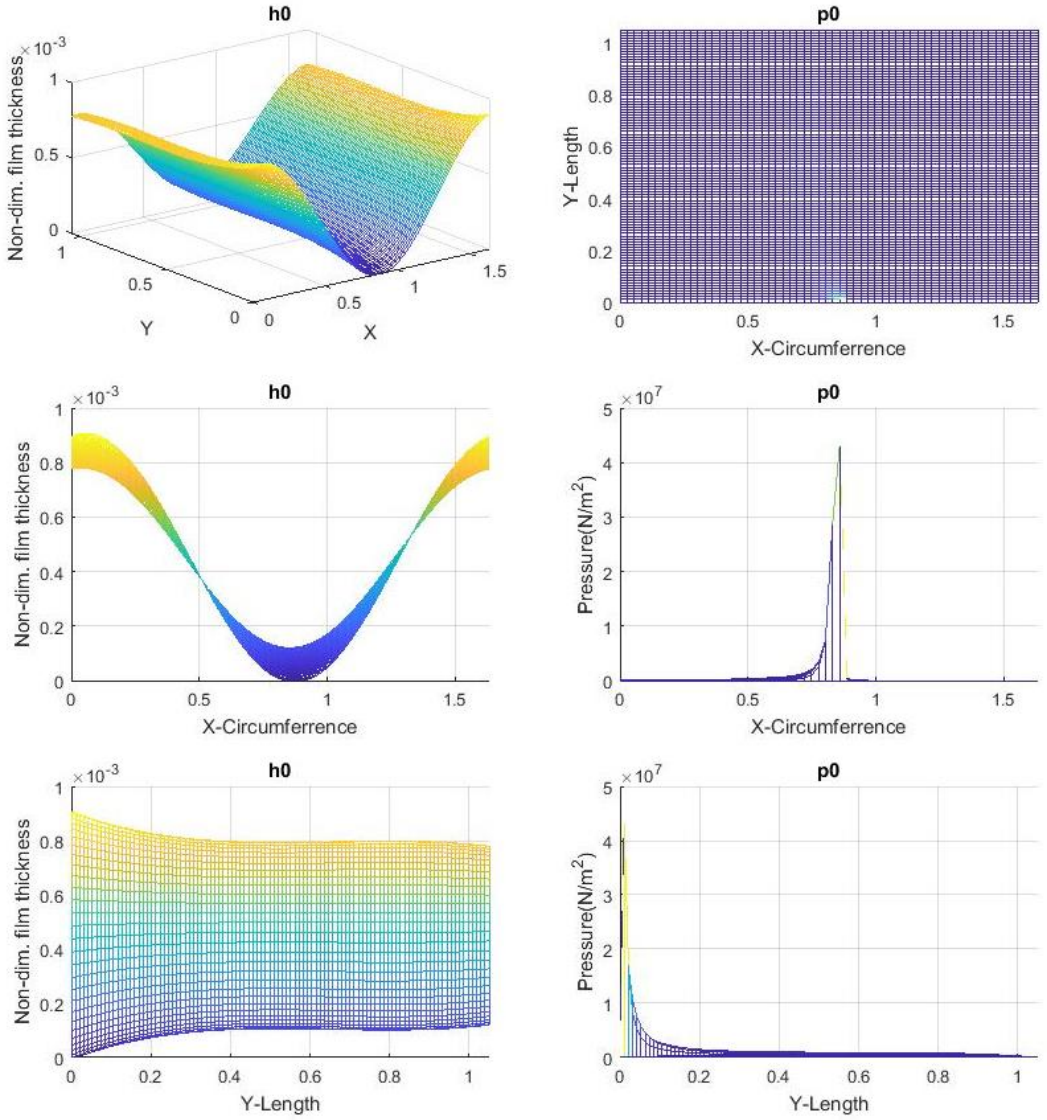

Figure 5-16: SINGLE SLOPE MODEL WITH BENT SHAFT, FOR 20°C TEMPERATURE INCREASE

In the figure above, the distribution of lubricant film thickness 'h' (on the left) and pressure (on the right) in three major planes, over the unwrapped journal bearing geometry is presented

In the following table the test results are presented and compared to the reference model:

Test:	**20°C Temperature Increase**		**Test Results**	**Deviation from Ref. %**
Shaft Model:	**Bent**	h_{min} =	2.25 μm	-97.22
Slope Type:	**Single**	p_{max} =	43.1 GPa	3714.54
S =	**0.0229411**	P_{loss} =	1.464 kW	-37.70
Distance of Support Point from L/2 =			0.145489 m	362.39

Table 5-12: SINGLE SLOPE MODEL WITH BENT SHAFT, FOR 20°C TEMPERATURE INCREASE

Comments: This condition is **fatal** for the bearing, the support point has shifted dramatically aftwards and due to the reduced power loss it seems that only a portion of the bearing length is supporting the load.

Double Slope Model

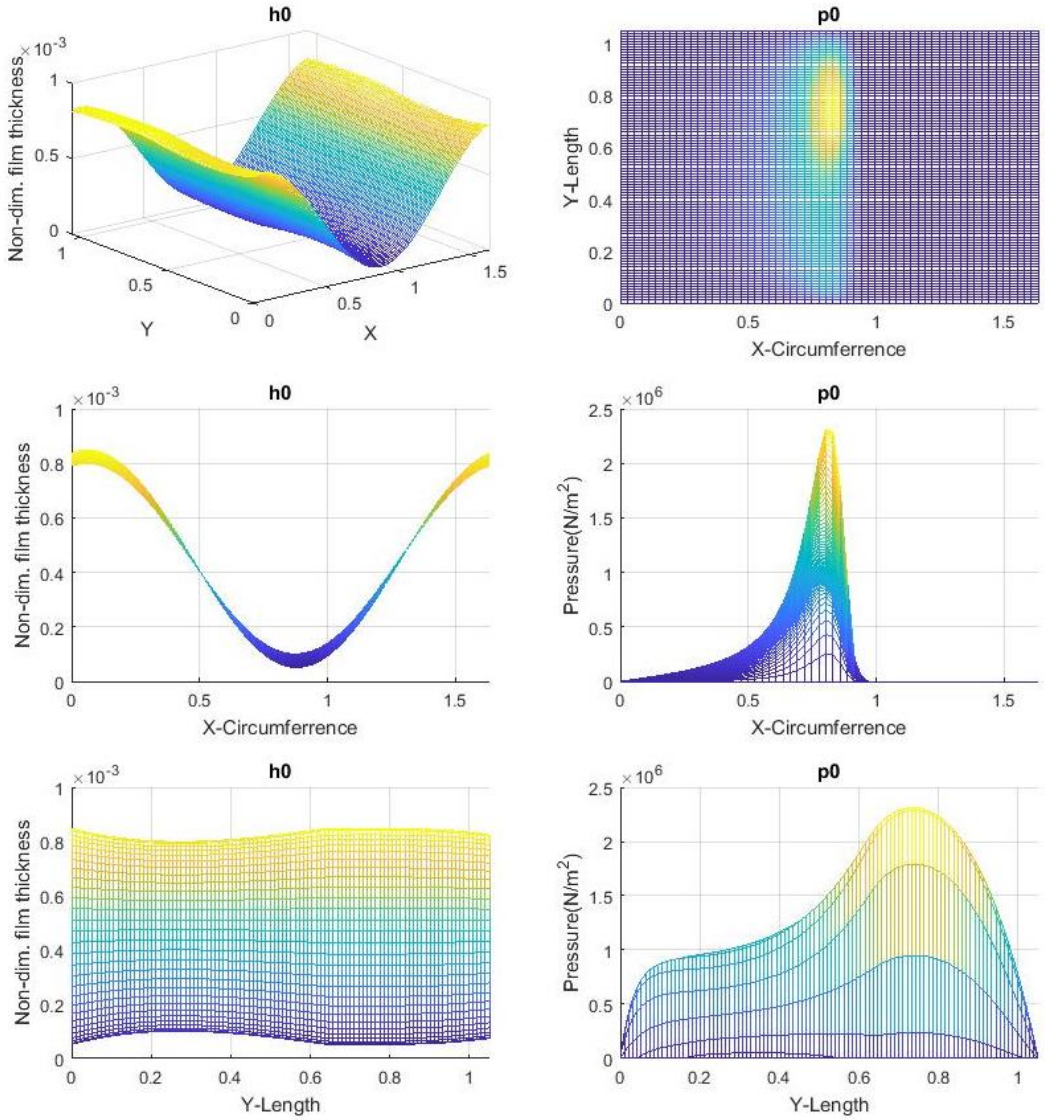

Figure 5-17: DOUBLE SLOPE MODEL WITH BENT SHAFT, FOR 20°C TEMPERATURE INCREASE

In the figure above, the distribution of lubricant film thickness 'h' (on the left) and pressure (on the right) in three major planes, over the unwrapped journal bearing geometry is presented

In the following table the test results are presented and compared to the reference model:

Test:	**20°C Temperature Increase**		**Test Results**	**Deviation from Ref. %**
Shaft Model:	**Bent**	h_{min} =	51.3 μm	-67.06
Slope Type:	**Double**	p_{max} =	2.31 GPa	80.29
S =	**0.0229411**	P_{loss} =	1.434 kW	-38.56
Distance of Support Point from L/2 =			-0.04373m	169.85

Table 5-13: DOUBLE SLOPE MODEL WITH BENT SHAFT, FOR 20°C TEMPERATURE INCREASE

Comments: Unlike the single slope model the double slope design is much more robust and can withstand worse conditions. The film thickness is still more than 50 microns and the location of the support point is shifted forwards. Further temperature increase will inevitably be fatal but the double slope design provides an additional "safe operation" margin, vital to the shafting system.

5.1.10 Comparison of Robustness Test Results for: Ψx = 0.3

In the following tables and figures, the results of all the robustness tests presented above are grouped for comparison. Reference models for each test are the double slope and single slope design with a bent shaft model presented in sections: 5.1.2 and 5.1.3 respectively.

Test Type	20% RPM Increase	30% RPM Decrease	50% Load Increase	50% Load Decrease	20°C Temp. Increase	Reference Case
h_{min} [µm]	109	31.9	25.5	187	2.25	80.8
p_{max} [GPa]	1.08	1.73	2.97	0.508	43.1	1.13
Angle of p_{max}	21.3385	34.473	34.1716	15.7901	31.8096	26.2591
P_{loss} [kW]	3.223	1.273	2.873	1.840	1.464	2.349
Distance of Support Point from L/2 [m]	0.0264272	0.0520628	0.0570636	0.0207331	0.145489	0.0314646
Ecc ratio	0.234672	0.40895	0.401569	0.059418	0.477106	0.301117
Att angle	36.5927	31.4222	31.1208	37.146	22.6571	35.4116
S. Number	0.0754898	0.0411763	0.0411763	0.123529	0.0229411	0.0617644
Deviation From Reference Case						
h_{min} %	34.86	-60.57	-68.44	131.63	-97.22	-
p_{max} %	-4.68	53.23	162.99	-55.04	3,714.54	-
P_{loss} %	37.19	-45.81	22.28	-21.66	-37.70	-
Distance of Support Point from L/2 [m]	-16.01	65.46	81.36	-34.11	362.39	-

Table 5-14: ROBUSTNESS TEST RESULTS OF SINGLE SLOPE BEARING, FOR Ψx=0.3

Test Type	20% RPM Increase	30% RPM Decrease	50% Load Increase	50% Load Decrease	20°C Temp. Increase	Reference Case
h_{min} [µm]	185	102	98.1	198	51.3	156
p_{max} [GPa]	1.20	1.57	2.28	0.885	2.31	1.28
Angle of p_{max}	18.6989	24.5769	24.5075	41.3924	19.3716	27.2431
P_{loss} [kW]	3.205	1.266	2.835	2.072	1.434	2.334
Distance of Support Point from L/2 [m]	-0.0146336	-0.0234399	-0.0218665	-0.0132768	-0.0437304	-0.016205
Ecc ratio	0.0321562	0.230777	0.222988	0.001	0.341771	0.106152
Att angle	27.8515	27.6277	27.5583	38.3415	22.4225	30.294
S. Number	0.075489	0.041176	0.041176	0.12352	0.022941	0.0617644
Deviation From Reference Case						
h_{min} %	18.80	-34.15	-36.95	27.52	-67.06	-
p_{max} %	-6.14	22.10	77.70	-31.00	80.29	-
P_{loss} %	37.33	-45.78	21.44	-11.24	-38.56	-
Distance of Support Point from L/2 [m]	-9.70	44.64	34.94	-18.07	169.85	-

Table 5-15: ROBUSTNESS TEST RESULTS OF DOUBLE SLOPE BEARING, FOR Ψx=0.3

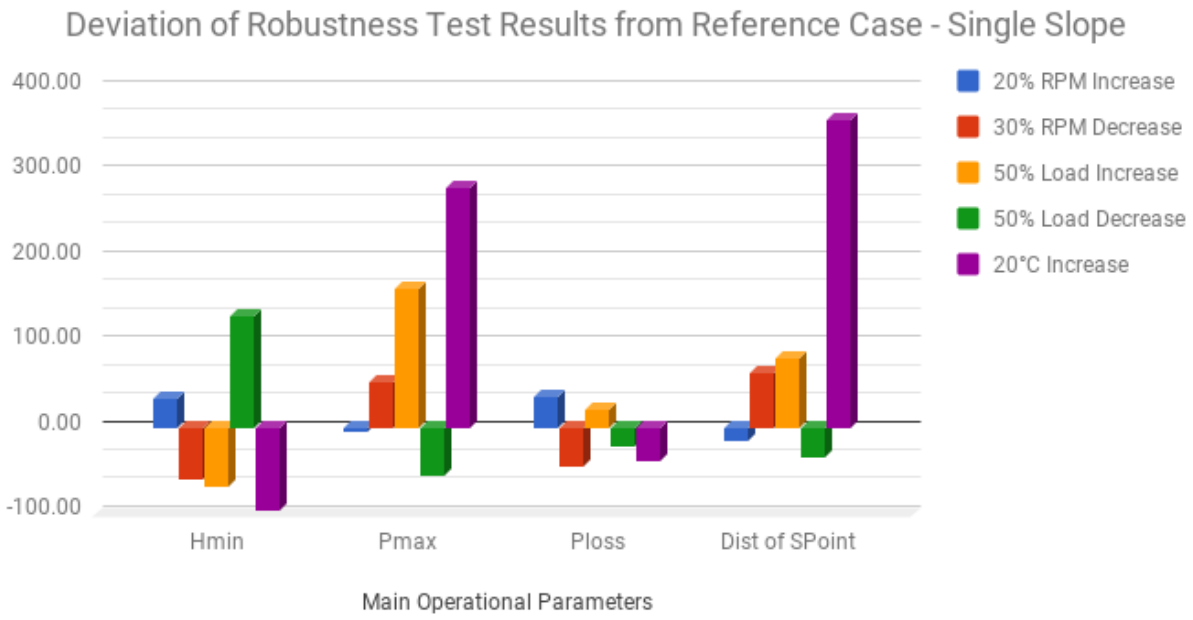

Figure 5-18: ROBUSTNESS TEST RESULTS OF SINGLE SLOPE BEARING, FOR Ψx=0.3

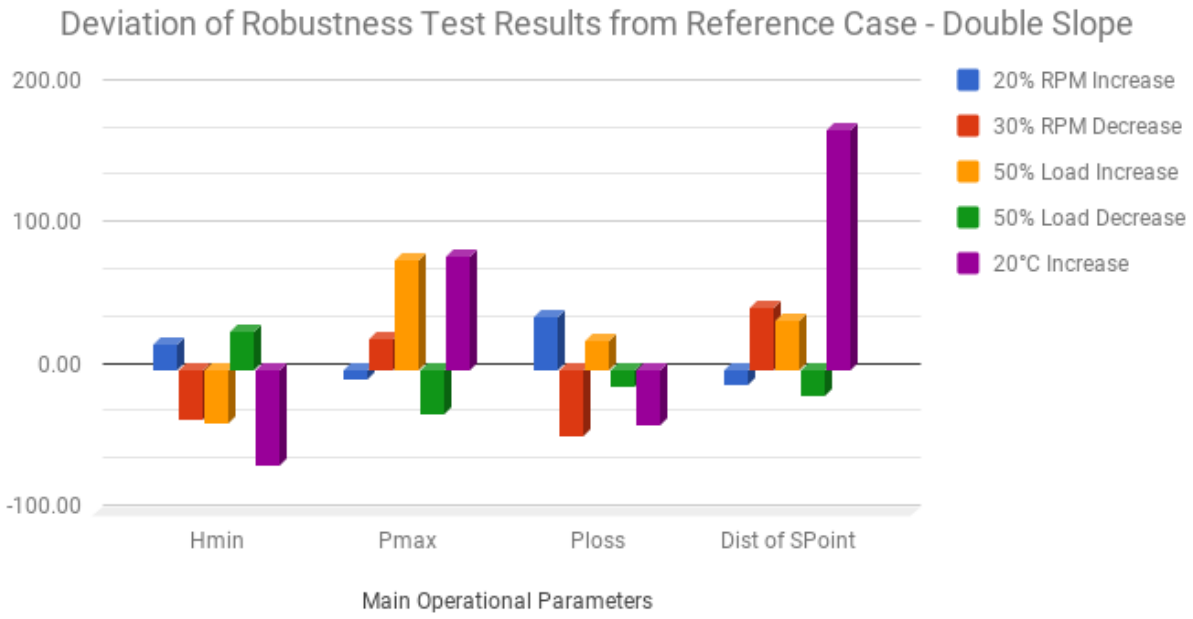

Figure 5-19: ROBUSTNESS TEST RESULTS OF DOUBLE SLOPE BEARING, FOR Ψx=0.3

Overall, the double slope design is a significantly more robust design. Especially in the scenarios with temperature or load increase and RPM decrease, where the bearing is overloaded, the double slope design is mostly affected in terms of longitudinal displacement of the theoretical contact point and additional power losses, rather than vertical offset of the bearing and minimization of lubricant film thickness. This is vital for the survivability of the vessel in extreme loading conditions which may take place due to bad weather or due to failure (or malfunction) of another component of the shafting system.

5.1.11 Reference Case For: Ψx = 0.6

Linear shaft Model

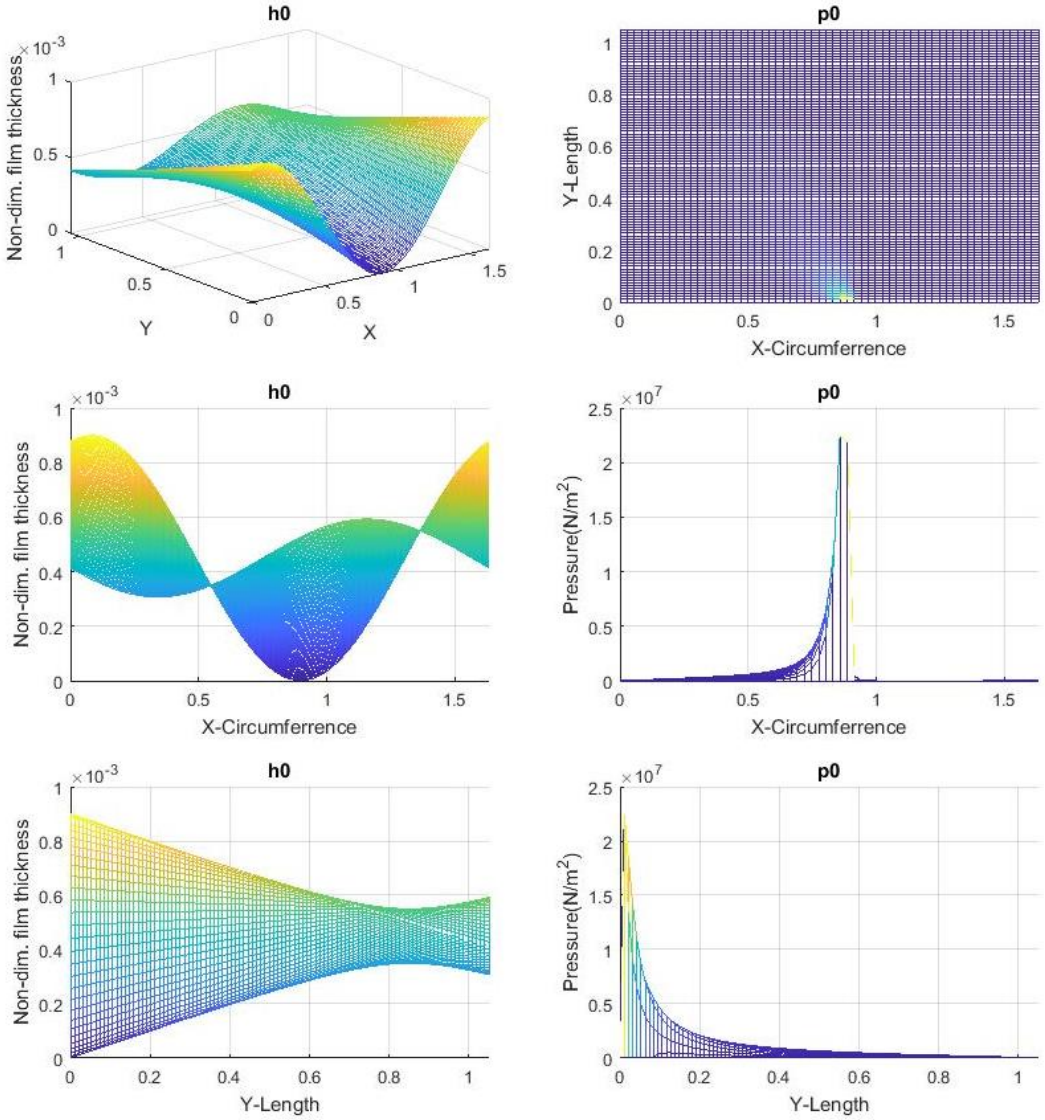

Figure 5-20:INITIAL MODEL FOR Ψx=0.6, LINEAR SHAFT

In the figure above, the distribution of lubricant film thickness 'h' (on the left) and pressure (on the right) in three major planes, over the unwrapped journal bearing geometry is presented

Comments:

This is the initial condition of the stern tube bearing with Ψx=0.6. In this case, the bearing already from this condition is in contact to the shaft. Such a design is unacceptable and the case is only presented, in order to accentuate the necessity of bearing geometry modifications in certain designs, where such extreme shaft misalignment angles are present and inevitable. Note that in the fore end of the bearing the curve that is visible at the bottom and left graph is not due to the bent shaft but due to the wrinkled unwrapped film thickness geometry. This model can only be used as a reference for the cases with single and double slope design with linear shaft model, as well as the bent shaft modeled reference case.

Bent Shaft Model

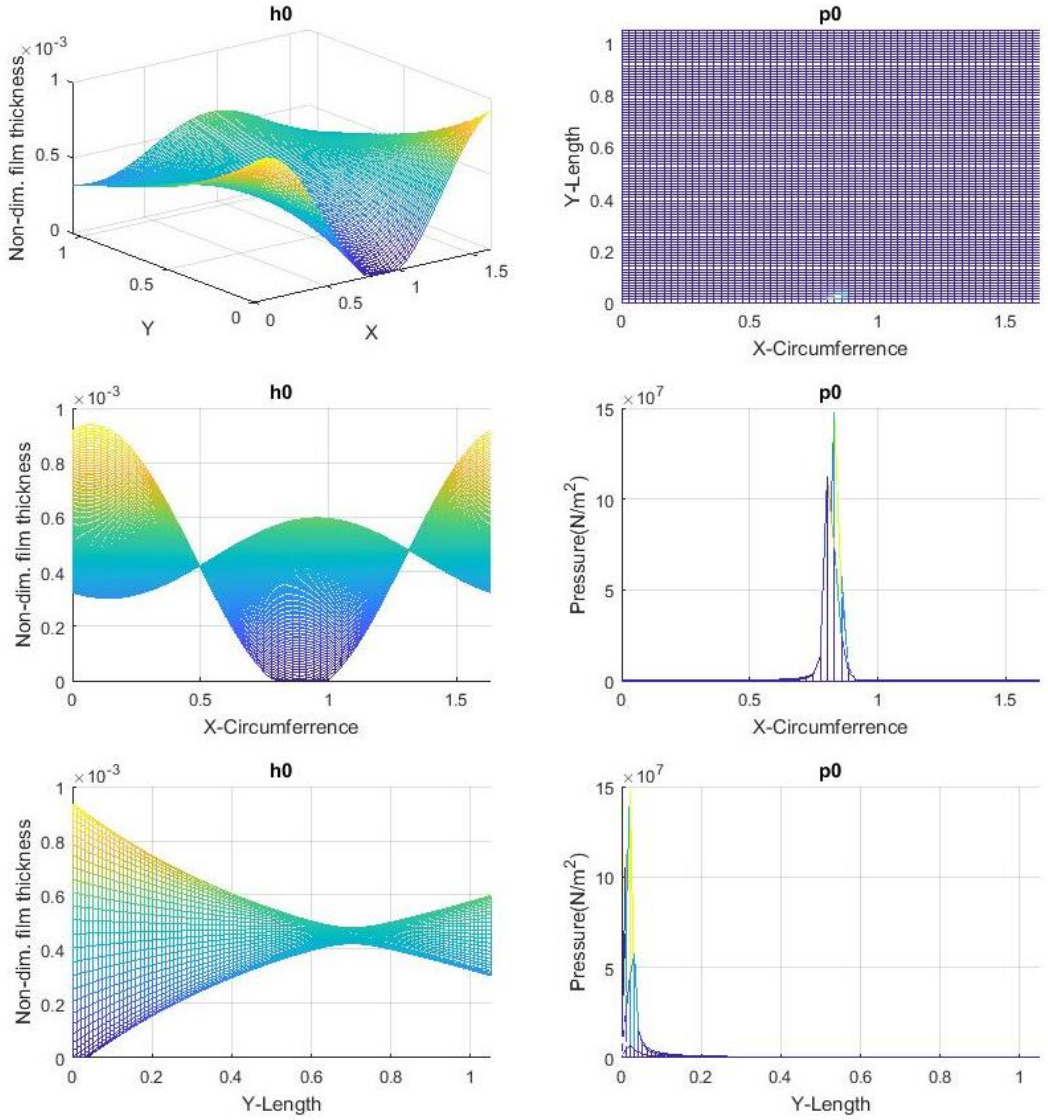

Figure 5-21:INITIAL MODEL FOR Ψx=0.6, BENT SHAFT

In the figure above, the distribution of lubricant film thickness 'h' (on the left) and pressure (on the right) in three major planes, over the unwrapped journal bearing geometry is presented

Comments:

In this case, the effect of the bent shaft is heavily affecting the aft edge of the bearing. Modeling the shaft properly should provide the most accurate shaft geometry, which is essential in order to design the bearing properly. It becomes obvious that bent shaft modeling is critical for accurate representation of the lubricant film thickness. In this case, the linear shaft model would severely underestimate the contact area length, resulting to poor decision making during bearing design. This case will be the reference for every design/case with bent shaft that will be presented in the following analysis. Note that any proposed design should be able to perform acceptably in in various and often transient conditions concerning both load and shaft misalignment. Thereof a robustness test will follow for the optimum single and double slope solutions.

5.1.12 Single Slope Case For: Ψx = 0.6

Linear shaft Model

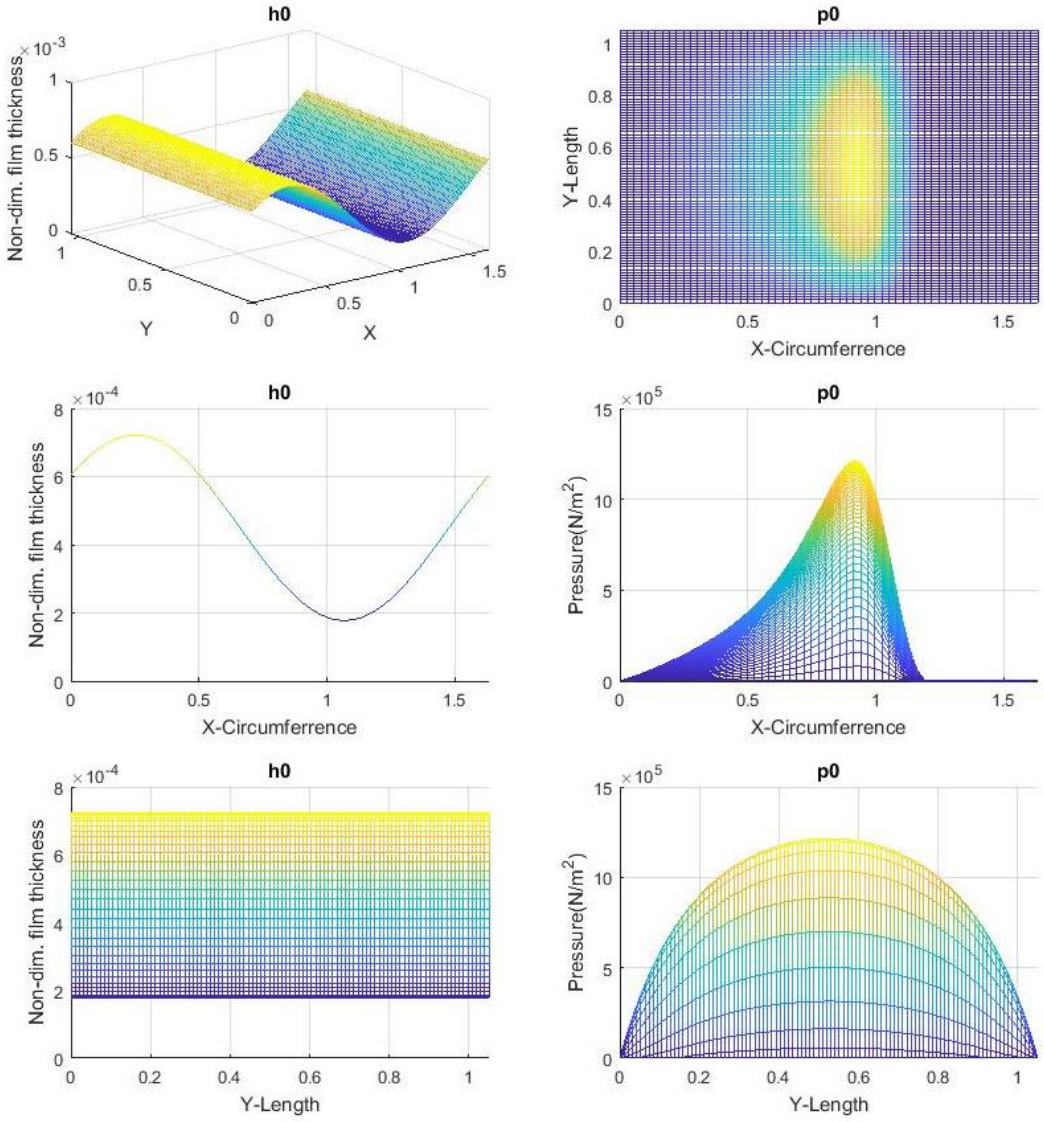

Figure 5-22: SINGLE SLOPE MODEL FOR Ψx=0.6, LINEAR SHAFT

In the figure above, the distribution of lubricant film thickness 'h' (on the left) and pressure (on the right) in three major planes, over the unwrapped journal bearing geometry is presented

Comments:

The optimum single slope inclination according to the Reynolds equation solution is equal to the shaft misalignment angle. Therefore in this case study, the optimum single slope has a non-dimensional angle of 0.6. This is a theoretical case, nonexistent in actual operation conditions and it is only presented for completeness and consistency of the present work. Note that only in cases of cold condition or during the shaft alignment process such a model can actually be adequately accurate for study of several static phenomena.

Bent Shaft Model

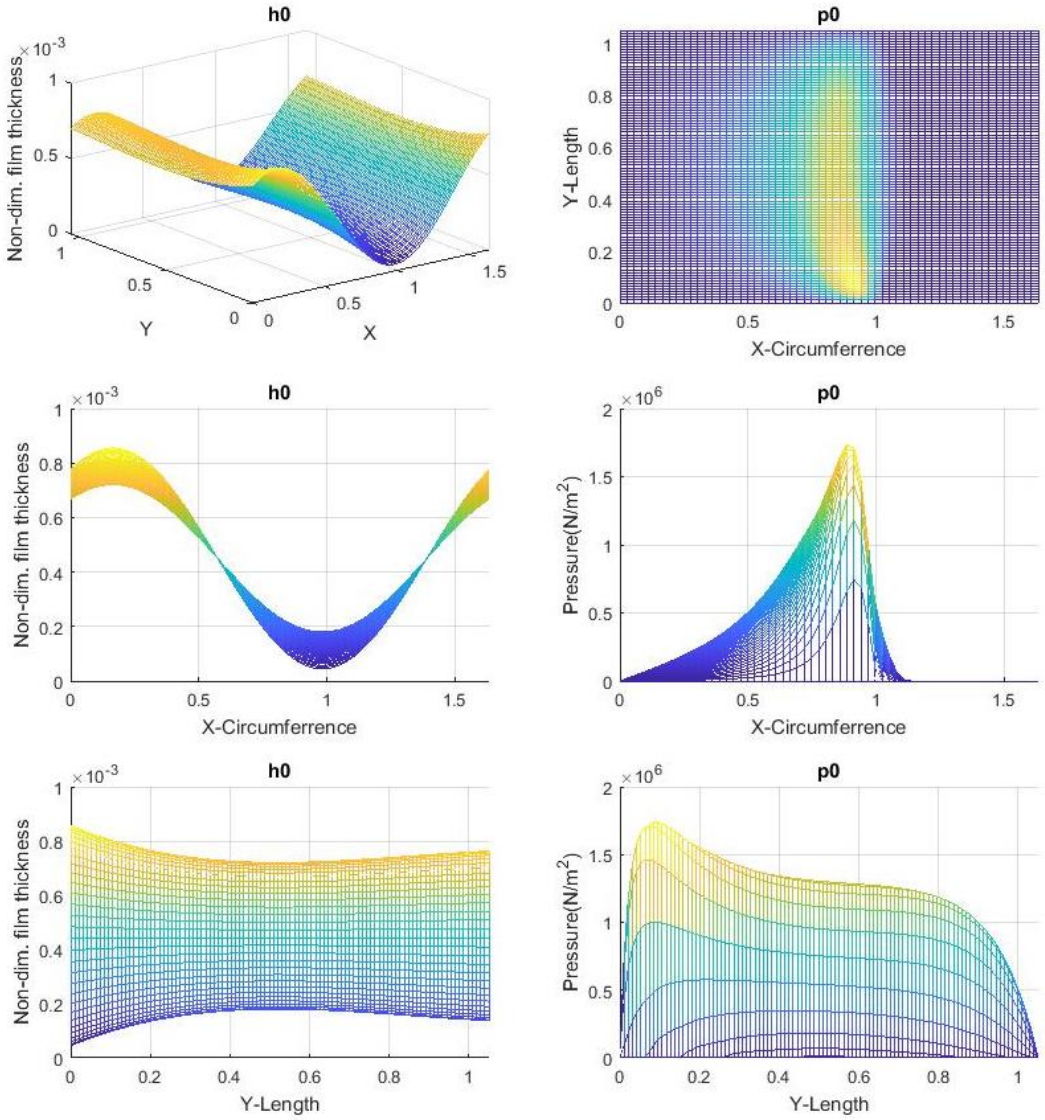

Figure 5-23: SINGLE SLOPE MODEL FOR Ψx=0.6, BENT SHAFT

In the figure above, the distribution of lubricant film thickness 'h' (on the left) and pressure (on the right) in three major planes, over the unwrapped journal bearing geometry is presented

Comments:

In this case, the shaft is modeled bent under the assumption of a constant shaft misalignment angle between the fore and aft edge of the bearing. The single slope is the same as in the previous example, defined by a 0.6 non dimensional angle. This model has a very accurate representation of the lubricant film and yields interesting results concerning the actual benefit from single slope modeling. Two important observations extracted from the figure above, are the following:

1. The non-dimensional lubricant film thickness doesn't have any knuckle points and it is smooth throughout the length of the bearing. The geometric place of all film thickness minima for every segment of the length gives an idea of the shaft inclination within the bearing.
2. The pressure profile is very smooth forwards and has a peak aftwards, where P_{max} is applied on a narrow area within the bearing length this is a warning of poor design.

5.1.13 Double Slope Case For: Ψx = 0.6

Linear shaft Model

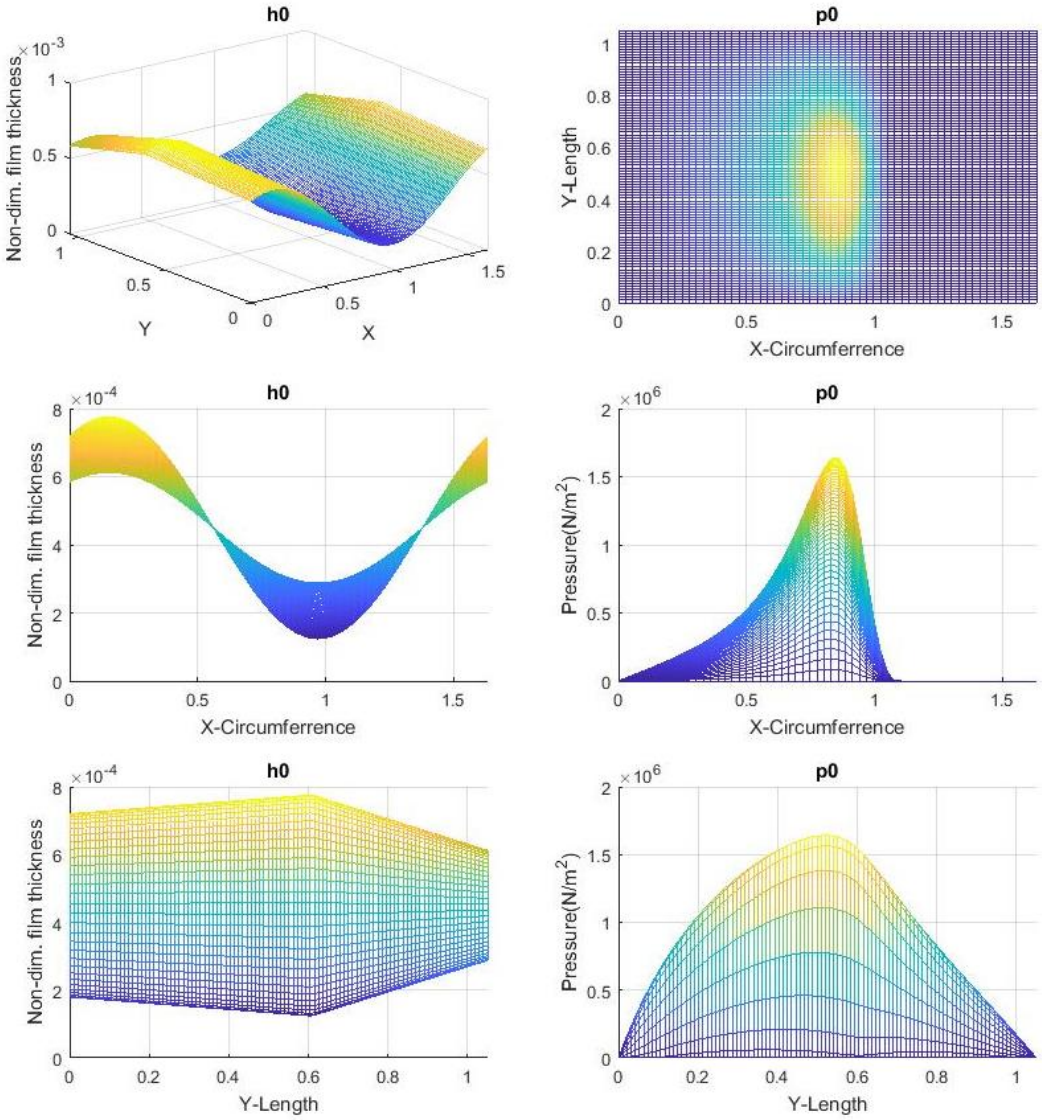

Figure 5-24: DOUBLE SLOPE MODEL FOR Ψx=0.6, LINEAR SHAFT

In the figure above, the distribution of lubricant film thickness 'h' (on the left) and pressure (on the right) in three major planes, over the unwrapped journal bearing geometry is presented

Comments:

The slope non-dimensional parameters were extracted through an optimization process as presented in Chapter 4 and are:

$Slope_{Aft}$= 0.41 $Length_{Aft}$= 0.58 $Slope_{Fore}$= 0.07 $LengthF_{ore}$= 0.42

The most important observation extracted from the figure above, is that the non-dimensional film thickness has a knuckle point at the location where the slopes coincide, which was expected theoretically. The interesting feature is that the optimizer yielded in this example as well a solution at which the minimum film thickness and therefore the maximum pressure is "split" into two almost linear segments both in terms of film thickness and pressure derivative. This conclusion was also the same in the case of Ψx=0.3 and gives an idea on how the optimizer is operating in order to minimize the maximum pressure.

Bent Shaft Model

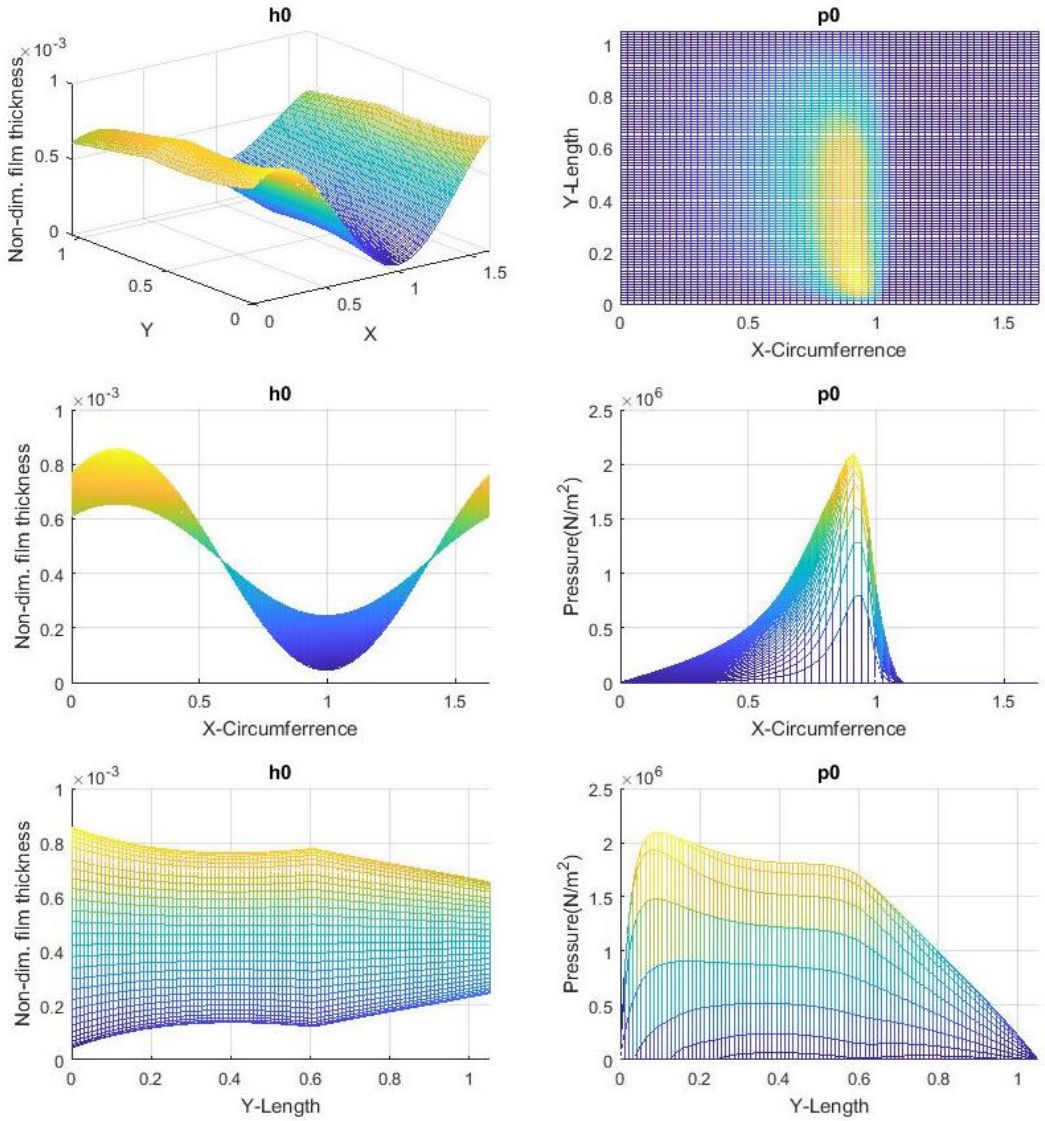

Figure 5-25: DOUBLE SLOPE MODEL FOR Ψx=0.6, BENT SHAFT

In the figure above, the distribution of lubricant film thickness 'h' (on the left) and pressure (on the right) in three major planes, over the unwrapped journal bearing geometry is presented

Comments:

The slope non-dimensional parameters are as in the previous case:

$Slope_{Aft}$= 0.41 $Length_{Aft}$= 0.58 $Slope_{Fore}$= 0.07 $LengthF_{ore}$= 0.42

In this case the film thickness curve presents a knuckle point around 0.58·L and the fore part is almost linear, meaning that the shaft has a constant inclination locally. Another interesting observation is that the pressure distribution from the knuckle point and forwards has a steep and steady decreasing rate. The importance of the bent shaft effect on the aft end of the bearing can also be observed here, in comparison to Figure 5-24. The pressure distribution is similar to the one in case of single slope model (5.1.12) but the peak, where P_{max} appears, is reaching at much higher pressures. The minimum film thickness is presented closer to the aft edge of the bearing and is identical to the one of the single slope model.

5.1.14 Comparison of Results for Various Model Types For: Ψx=0.6

In the following table the most important parameters of the model types presented are collected:

Shaft Misalignment Angle = 0.6						
Slope Modeling	**No Slope**	**No Slope**	**Single Slope**	**Single Slope**	**Double Slope**	**Double Slope**
Shaft Modeling	**Linear**	**Bent**	**Linear**	**Bent**	**Linear**	**Bent**
h_{min} [μm]	2.25	2.25	178	**45.1**	124	**44.6**
p_{max} [GPa]	22.4	148	1.21	**1.74**	1.64	**2.10**
Angle of p_{max}	39.912	22.4467	77.5747	**51.7351**	43.0209	**54.5821**
Ploss [kW]	2.598	3.360	2.334	**2.603**	2.425	**2.690**
Distance of Support Point from L/2 [m]	0.273123	0.403482	5.34E-05	**0.0300629**	0.0247799	**0.0509153**
Ecc ratio	0.434913	0.194695	0.00927588	**0.001**	0.001	**0.001**
Att angle	30.7595	19.3959	56.2188	**36.4809**	33.8683	**39.3279**
S	0.0617644	0.0617644	0.0617644	**0.0617644**	0.0617644	**0.0617644**

Table 5-16: PERFORMANCE PARAMETERS COMPARISON FOR Ψx=0.6

In the following chart the major performance parameters of Table 5-16 are compared:

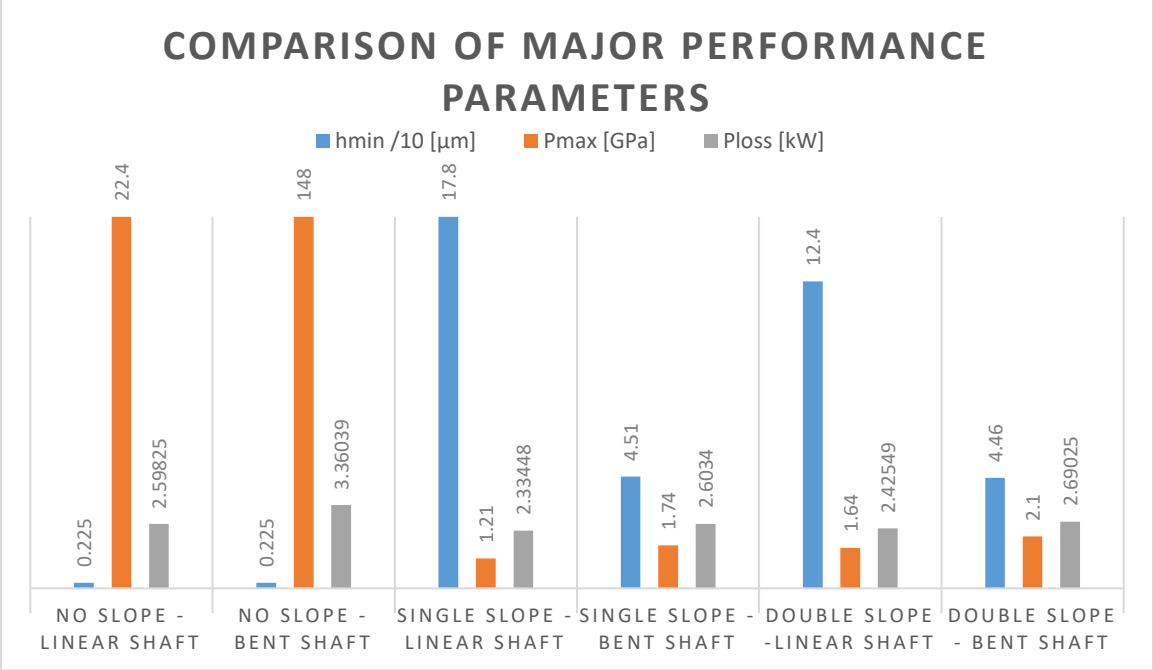

Figure 5-26: PERFORMANCE PARAMETERS COMPARISON FOR Ψx=0.6

The figure is scaled in order to demonstrate and easily compare the most important data.

Although both the single and double slope models provide improved performance in comparison to the reference case, it is visible that the **single slope** model provides significant improvement especially concerning the minimum film thickness. In this case study it is evident that bent shaft modeling is very critical since it may significantly alter the perspective of the problem. To further analyze the capabilities of double and single slope designs, several test will be run for extreme conditions, aiming to conclude to the design that improves to the maximum the survivability and performance of the stern tube bearing. The bent shaft - double and single slope models are the reference cases respectively.

5.1.15 Optimum Solution Robustness Test For: Ψx = 0.6 – 20%RPM Increase

Single Slope Model

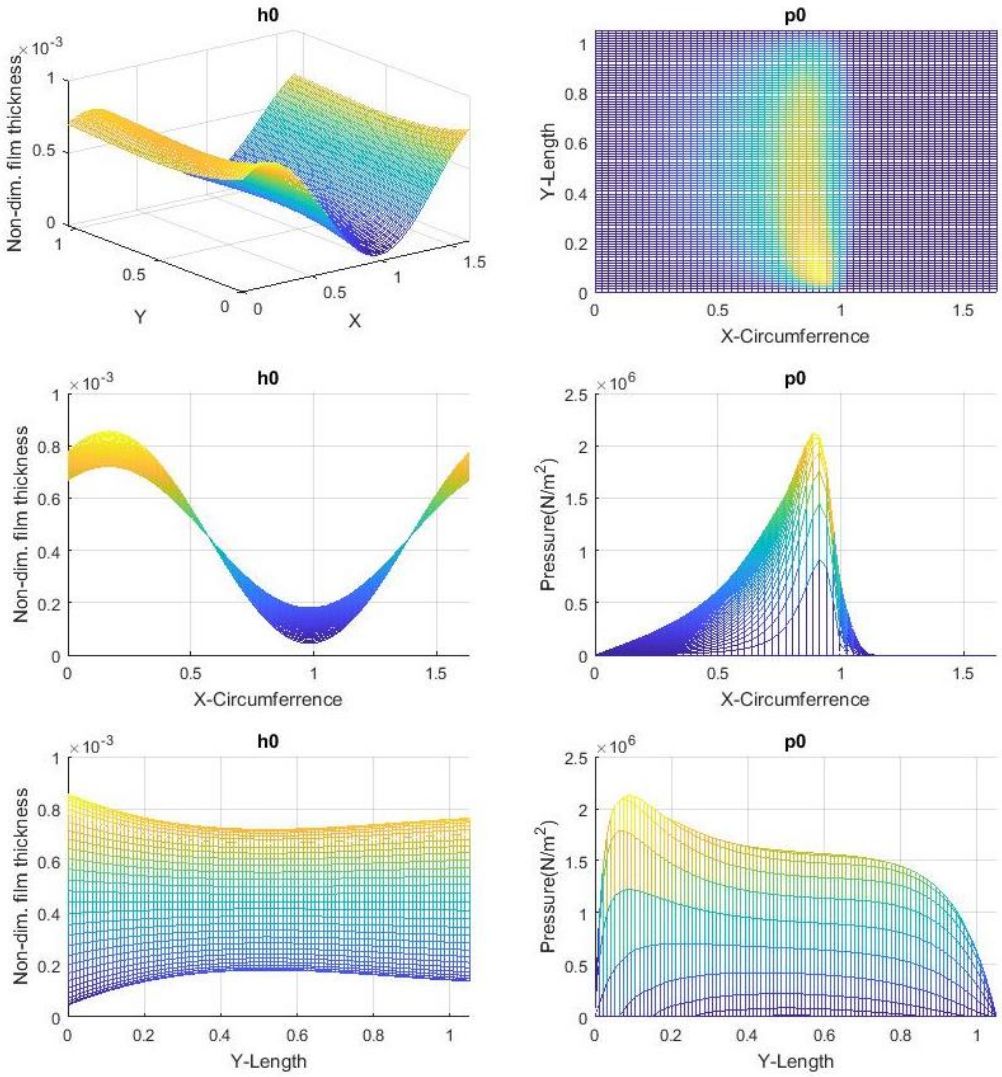

Figure 5-27: SINGLE SLOPE MODEL WITH BENT SHAFT, FOR 20% INCREASED RPM

In the figure above, the distribution of lubricant film thickness 'h' (on the left) and pressure (on the right) in three major planes, over the unwrapped journal bearing geometry is presented

Test:	20% RPM Increase		Test Results	Deviation from Ref. %
Shaft Model:	**Bent**	h_{min} =	45.1 µm	0.0
Slope Type:	**Single**	p_{max} =	2.12 GPa	22.22
S =	**0.0754898**	P_{loss} =	3.889 kW	49.38
Distance of Support Point from L/2 =			0.03 m	0.00

Table 5-17: SINGLE SLOPE MODEL WITH LINEAR SHAFT, FOR 20% INCREASED RPM

Comments: Steady design, the performance is slightly improved as expected, both curves are very smooth and especially the pressure curve demonstrates a wide and homogenous loading along the bearing length.

Double Slope Model

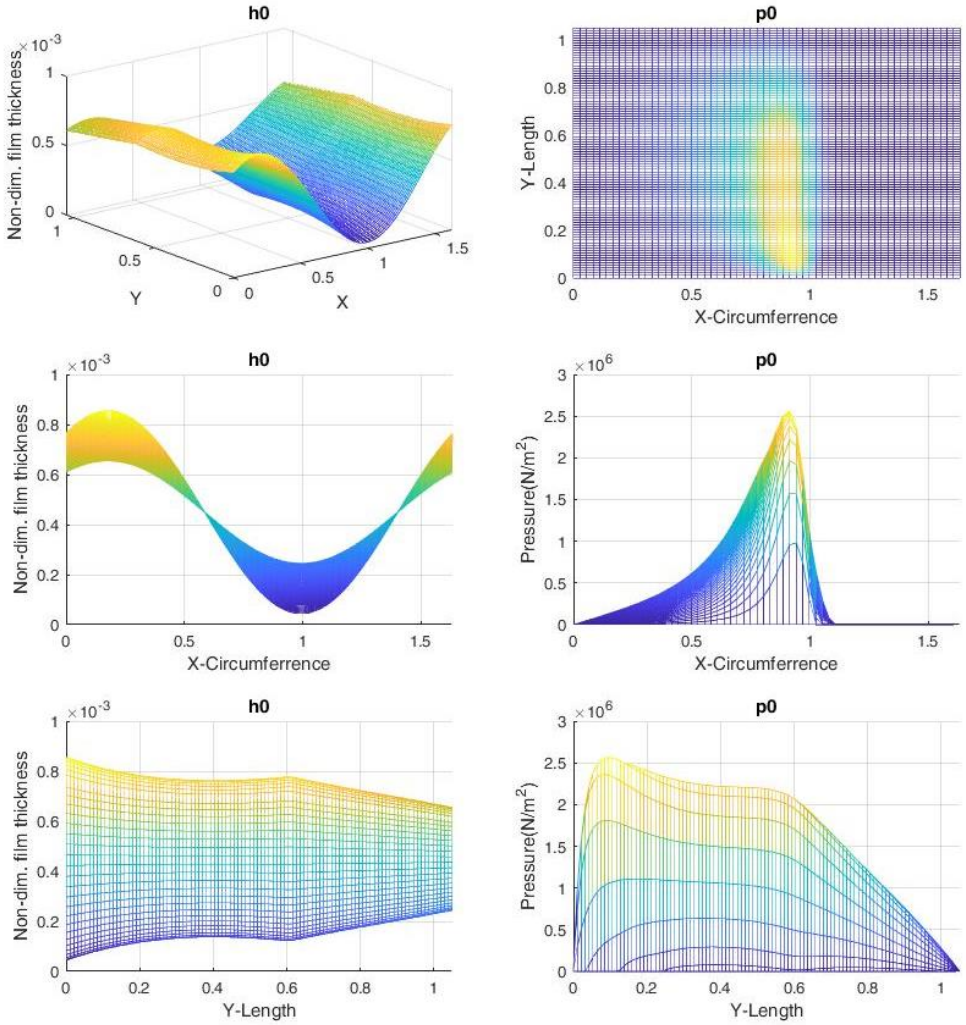

Figure 5-28: DOUBLE SLOPE MODEL WITH BENT SHAFT, FOR 20% INCREASED RPM

In the figure above, the distribution of lubricant film thickness 'h' (on the left) and pressure (on the right) in three major planes, over the unwrapped journal bearing geometry is presented

Test:	**20% RPM Increase**		**Test Results**	**Deviation from Ref. %**
Shaft Model:	**Bent**	h_{min} =	44.6 μm	0.0
Slope Type:	**Double**	p_{max} =	2.56 GPa	22.22
S =	**0.0754898**	P_{loss} =	4.076 kW	51.38
Distance of Support Point from L/2 =			0.05499 m	8.00

Table 5-18: DOUBLE SLOPE MODEL WITH LINEAR SHAFT, FOR 20% INCREASED RPM

Comments: Comparable results to the single slope design and steady operation. Note that the reference case is the initial double slope model, which provided already improved performance. From an energy consumption point of view this loading condition should be avoided in order to minimize the power losses and the single slope design would seem preferable. These losses are very small in comparison to the overall foc so the main focus should be on the minimization of the risk of failure, which typically leads to significant expenses for repair or reconstruction.

5.1.16 Optimum Solution Robustness Test For: Ψx = 0.6 – 30% RPM Decrease

Single Slope Model

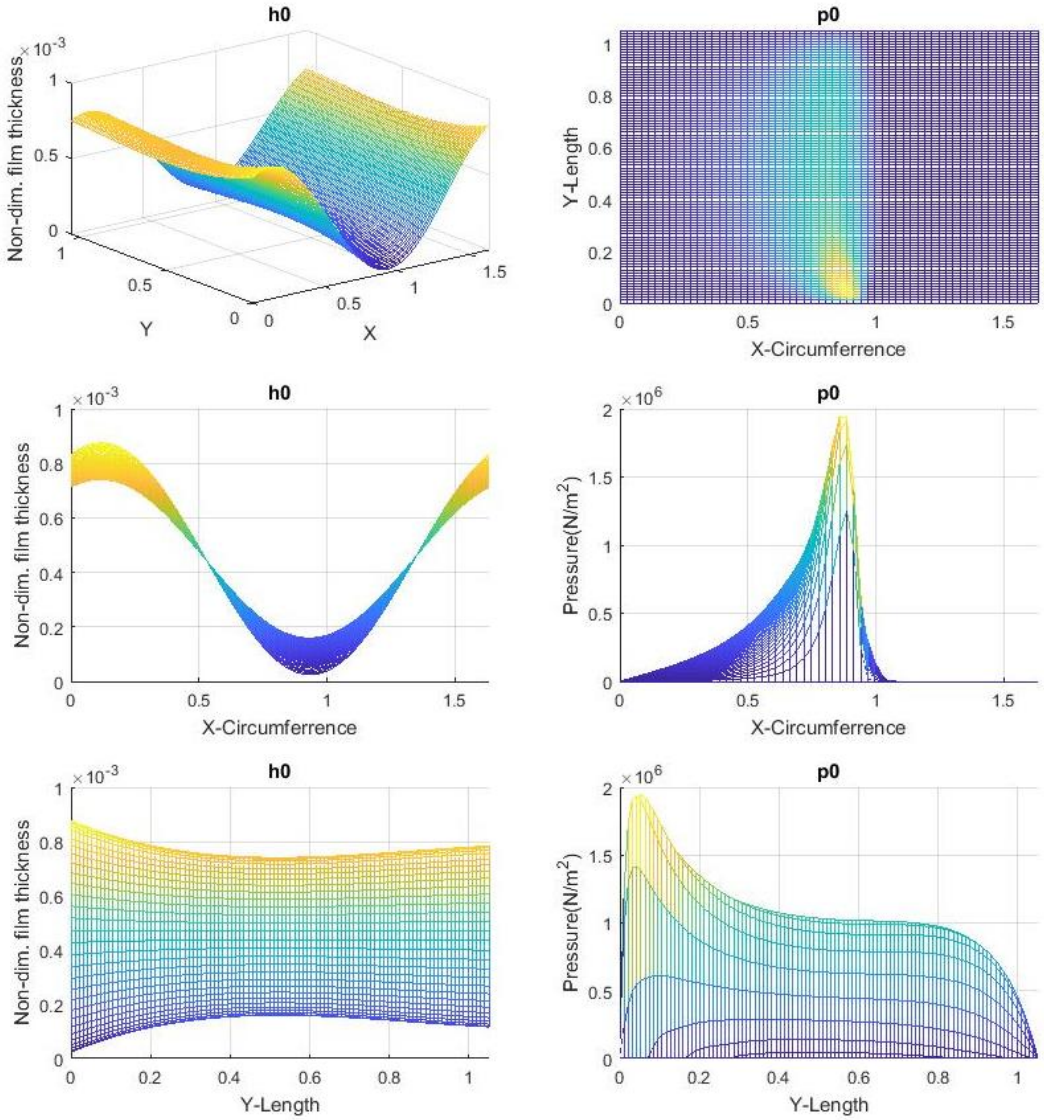

Figure 5-29: SINGLE SLOPE MODEL WITH BENT SHAFT, FOR 30% DECREASED RPM

In the figure above, the distribution of lubricant film thickness 'h' (on the left) and pressure (on the right) in three major planes, over the unwrapped journal bearing geometry is presented

Test:	30% Decreased RPM		Test Results	Deviation from Ref. %
Shaft Model:	**Bent**	h_{min} =	24.5 µm	-46.03
Slope Type:	**Single**	p_{max} =	1.95 GPa	12.17
S =	**0.0411763**	P_{loss} =	1.269 kW	-51.27
Distance of Support Point from L/2 =			0.046317 m	54.07

Table 5-19: SINGLE SLOPE MODEL WITH LINEAR SHAFT, FOR 30% DECREASED RPM

Comments: The system is overloaded, the P_{max} has shifted towards the aft edge, where the minimum film thickness is expected. A small area in the aft end of the bearing seems to support most of the total load. The effect of the bent shaft is critical and the shaft is going to "touch" the bushing, if loaded additionally. The circumferential distribution of the pressure is much steeper than in previous conditions.

Double Slope Model

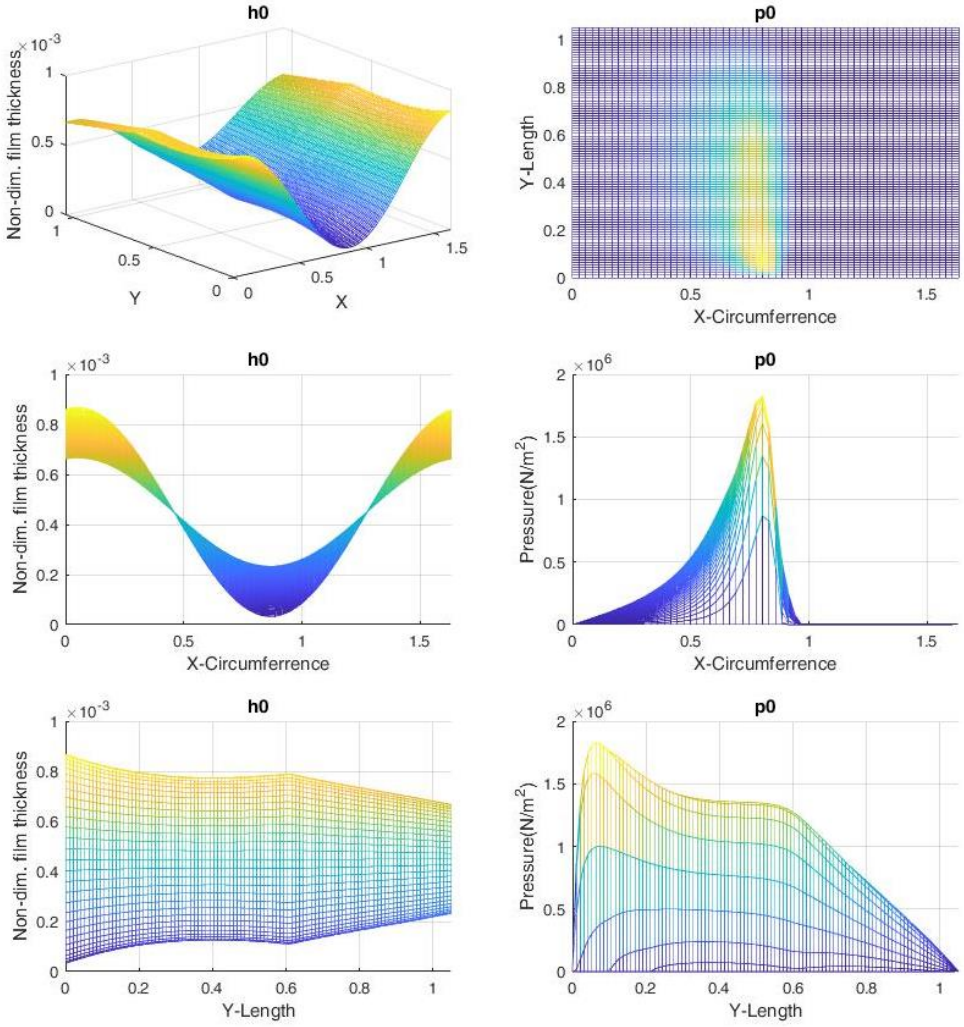

Figure 5-30: DOUBLE SLOPE MODEL WITH BENT SHAFT, FOR 30% DECREASED RPM

In the figure above, the distribution of lubricant film thickness 'h' (on the left) and pressure (on the right) in three major planes, over the unwrapped journal bearing geometry is presented

Test:	**30% Decreased RPM**		**Test Results**	**Deviation from Ref. %**
Shaft Model:	**Bent**	h_{min} =	33.1 μm	-25.85
Slope Type:	**Double**	p_{max} =	1.83 GPa	-12.88
S =	**0.0411763**	P_{loss} =	1.271 kW	-52.74
Distance of Support Point from L/2 =			0.0933095 m	83.26

Table 5-20: DOUBLE SLOPE MODEL WITH LINEAR SHAFT, FOR 30% DECREASED RPM

Comments: The system seems to be much more robust in comparison to the single slope design. The lubricant film remains steady and it is shifted vertically almost homogenously. Furthermore, the pressure distribution peak is also homogenously decreased although it hasn't shifted to a new longitudinal position as in the single slope case. The part within 0.3-0.5 of L has been the major receiver of the additional load. In comparison to the single slope design the pressure distribution as presented in the top and right figure is wider and much more excessive. This system seems to be adequate for further RPM reduction.

5.1.17 Optimum Solution Robustness Test For: Ψx = 0.6 – 20% Overload

Single Slope Model

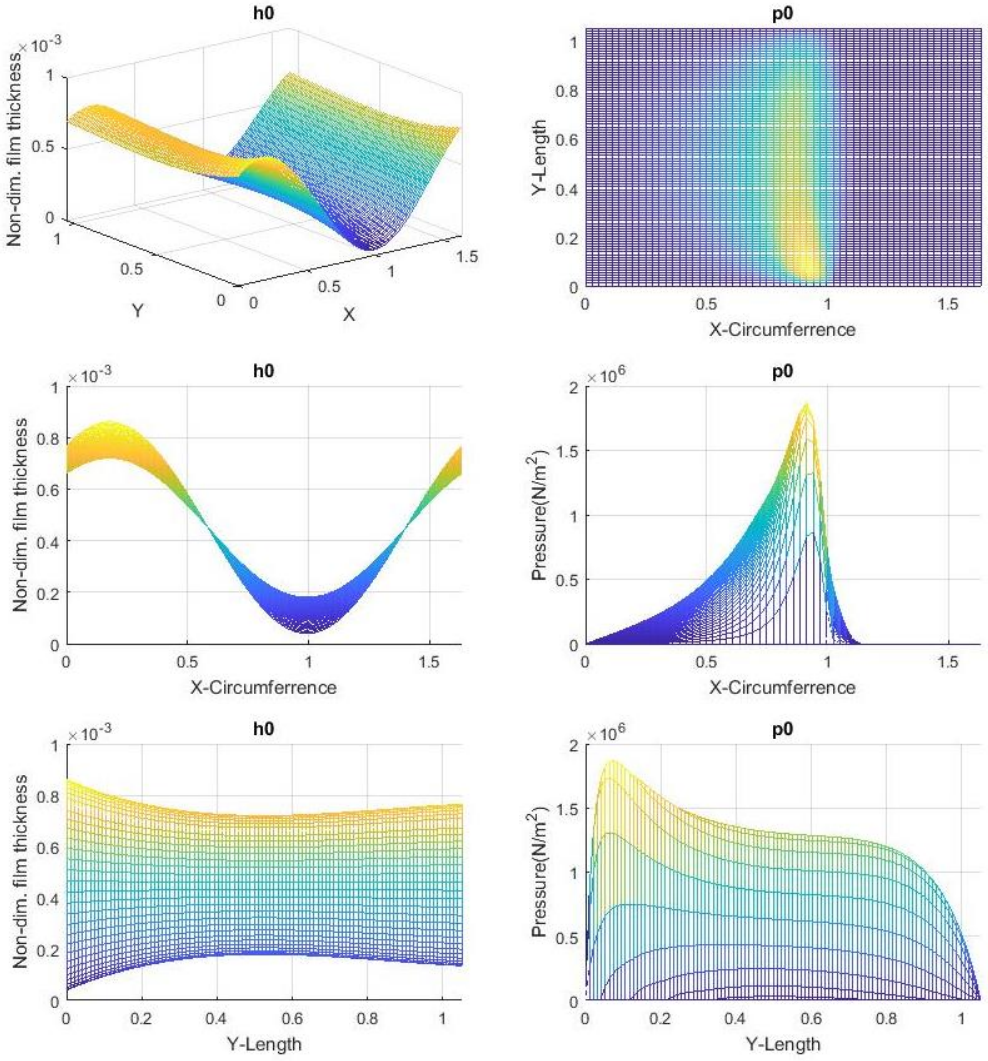

Figure 5-31: SINGLE SLOPE MODEL WITH BENT SHAFT, FOR 20% INCREASED LOAD

In the figure above, the distribution of lubricant film thickness 'h' (on the left) and pressure (on the right) in three major planes, over the unwrapped journal bearing geometry is presented

Test:	**20% Increased Load**		**Test Results**	**Deviation from Ref. %**
Shaft Model:	**Bent**	h_{min} =	40.0 μm	-11.38
Slope Type:	**Single**	p_{max} =	1.87 GPa	7.51
S =	**0.0514703**	P_{loss} =	2.622 kW	0.71
Distance of Support Point from L/2 =			0.029938 m	-0.42

Table 5-21: SINGLE SLOPE MODEL WITH BENT SHAFT, FOR 20% INCREASED LOAD

Comments: In this example a 50% Load increase would be catastrophic, therefore a 20% load increase test has been conducted for better comparison between the models. In this test, similar concerns as in the previous one are detected. The pressure is increased aftwards, in a narrow area and the system has almost reached its limits. The fore part of the bearing seems unable to receive and support any portion of the additional load. Therefore the load carrying capacity of the specific design is limited.

Double Slope Model

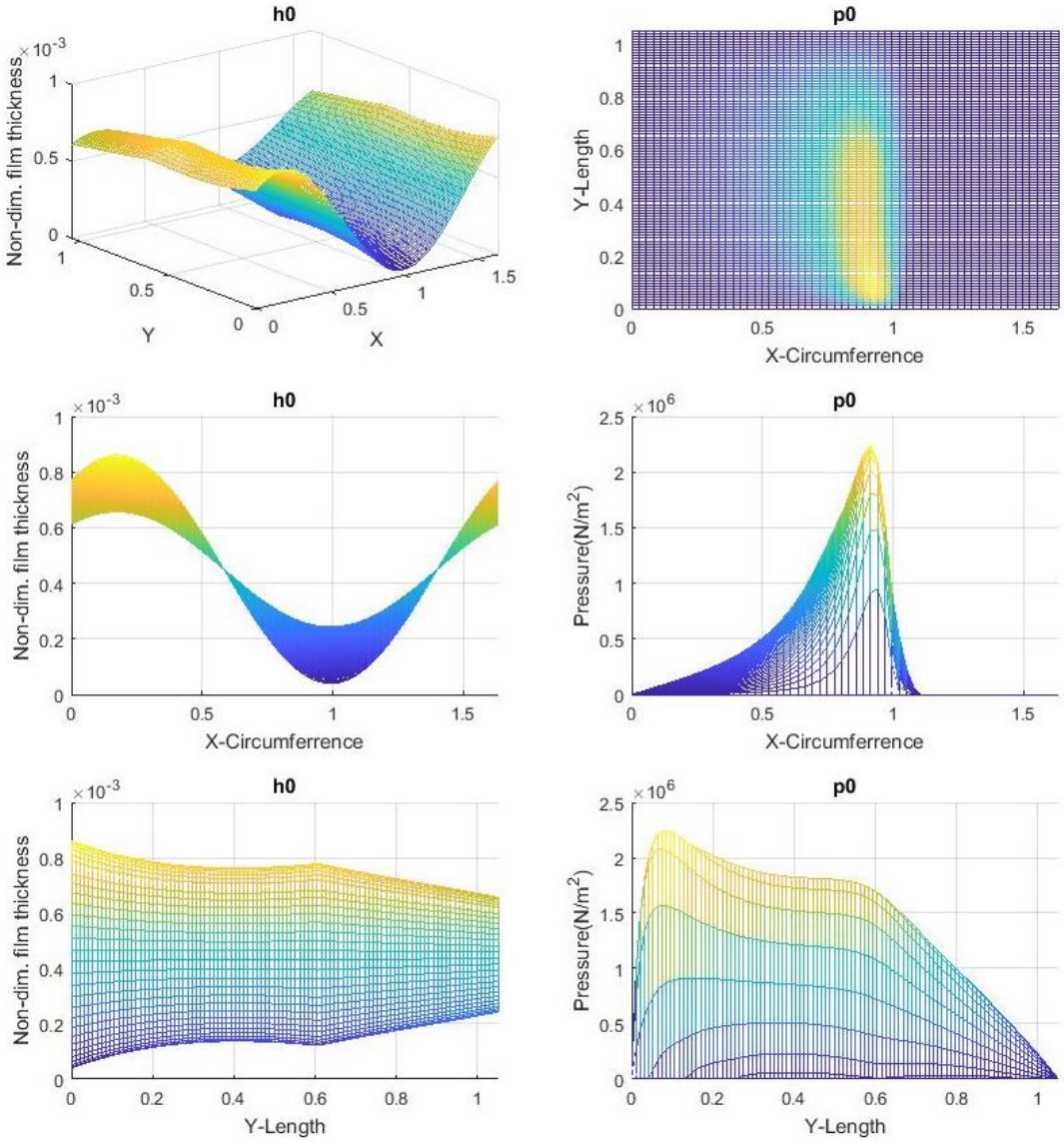

Figure 5-32: DOUBLE SLOPE MODEL WITH BENT SHAFT, FOR 20% INCREASED LOAD

In the figure above, the distribution of lubricant film thickness 'h' (on the left) and pressure (on the right) in three major planes, over the unwrapped journal bearing geometry is presented

Test:	20% Increased Load		Test Results	Deviation from Ref. %
Shaft Model:	**Bent**	h_{min} =	40.0 μm	-10.38
Slope Type:	**Double**	p_{max} =	2.24 GPa	6.79
S =	**0.0514703**	P_{loss} =	2.745 kW	2.03
Distance of Support Point from L/2 =			0.05748m	12.90

Table 5-22: DOUBLE SLOPE MODEL WITH BENT SHAFT, FOR 20% INCREASED LOAD

Comments: The bearing has responded much better to the extreme condition and the additional load seems to be supported from both the fore and the aft side of the bearing. Characteristically, the support point location has slightly shifted aftwards and although the pressure peak is still aftwards, high pressure distribution is visible at a wide area of the unwrapped journal bearing domain.

5.1.18 Optimum Solution Robustness Test For: Ψx = 0.6 – 50% Unload

Single Slope Model

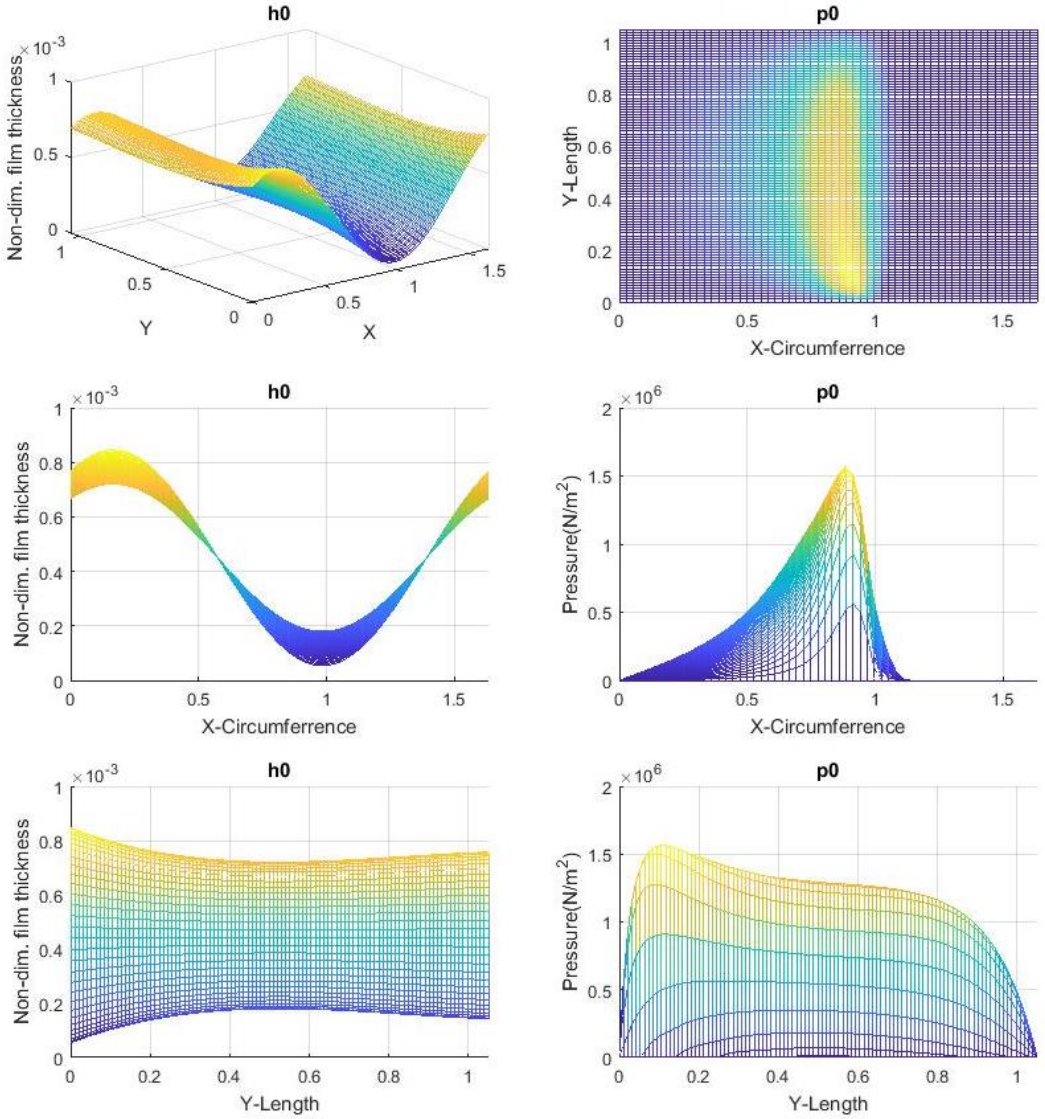

Figure 5-33: SINGLE SLOPE MODEL WITH BENT SHAFT, FOR 50% DECREASED LOAD

In the figure above, the distribution of lubricant film thickness 'h' (on the left) and pressure (on the right) in three major planes, over the unwrapped journal bearing geometry is presented

Test:	50% Decreased Load		Test Results	Deviation from Ref. %
Shaft Model:	**Bent**	h_{min} =	54.6 µm	21.05
Slope Type:	**Single**	p_{max} =	1.56 GPa	-9.98
S =	**0.123529**	P_{loss} =	2.569 kW	-1.34
Distance of Support Point from L/2 =			0.026748 m	-11.03

Table 5-23: SINGLE SLOPE MODEL WITH BENT SHAFT, FOR 50% DECREASED LOAD

Comments: The system is responding very well, all the parameters have improved significantly from the reference case and no sign of bearing unloading is visible. The pressure peak at the aft end has decreased significantly. Of course the stern tube bearing is rarely confronted with such unloading scenario.

Double Slope Model

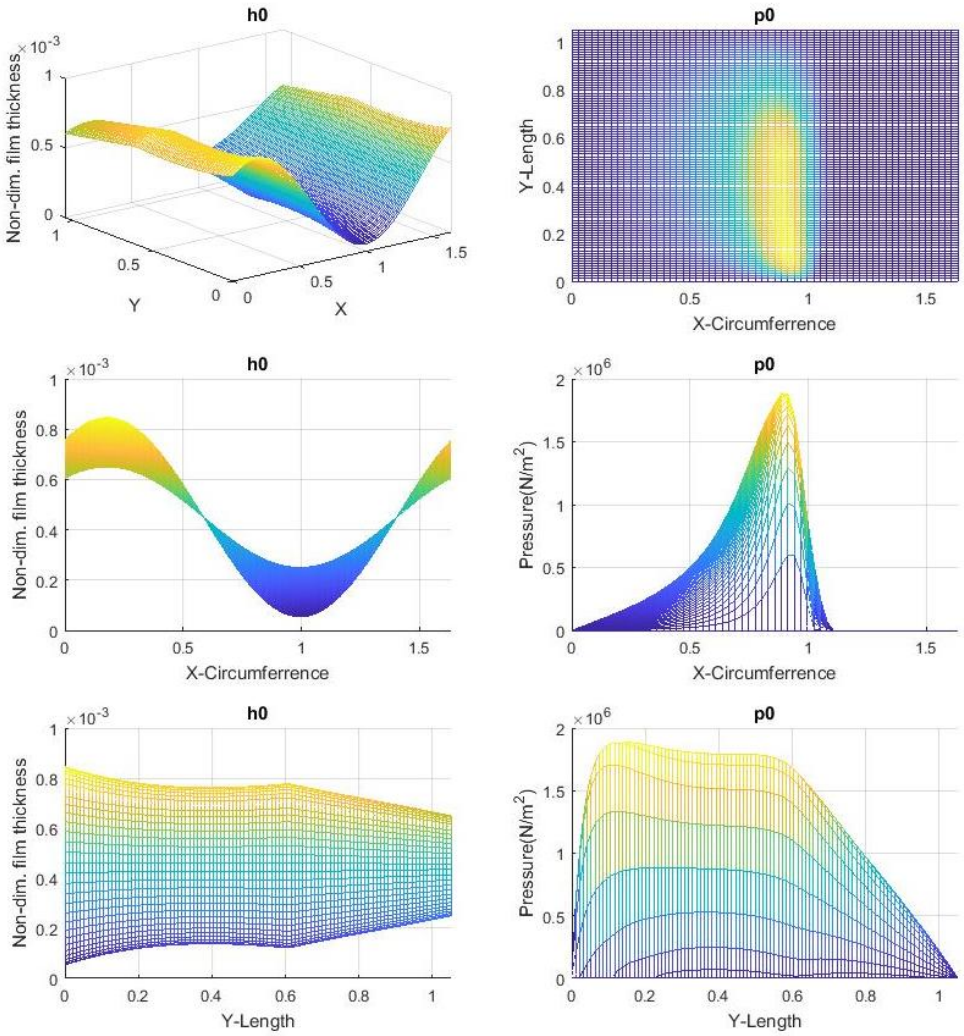

Figure 5-34: DOUBLE SLOPE MODEL WITH BENT SHAFT, FOR 50% DECREASED LOAD

In the figure above, the distribution of lubricant film thickness 'h' (on the left) and pressure (on the right) in three major planes, over the unwrapped journal bearing geometry is presented

Test:	**50% Decreased Load**		**Test Results**	**Deviation from Ref. %**
Shaft Model:	**Bent**	h_{min} =	54.1 μm	21.16
Slope Type:	**Double**	p_{max} =	1.88 GPa	-10.16
S =	**0.123529**	P_{loss} =	2.690 kW	0.0
Distance of Support Point from L/2 =			0.0509 m	0.0

Table 5-24: DOUBLE SLOPE MODEL WITH BENT SHAFT, FOR 50% DECREASED LOAD

Comments: The design does not show any unwanted characteristics, the load is still supported by a large area, the pressure peak has decreased and the pressure has been developed almost uniformly along the circumference, on a similar way to the single slope design. Further unloading of the bearing should cause a uniform pressure distribution along the bearing length.

5.1.19 Optimum Solution Robustness Test For: Ψx = 0.6 – 10°C Temperature Increase

Single Slope Model

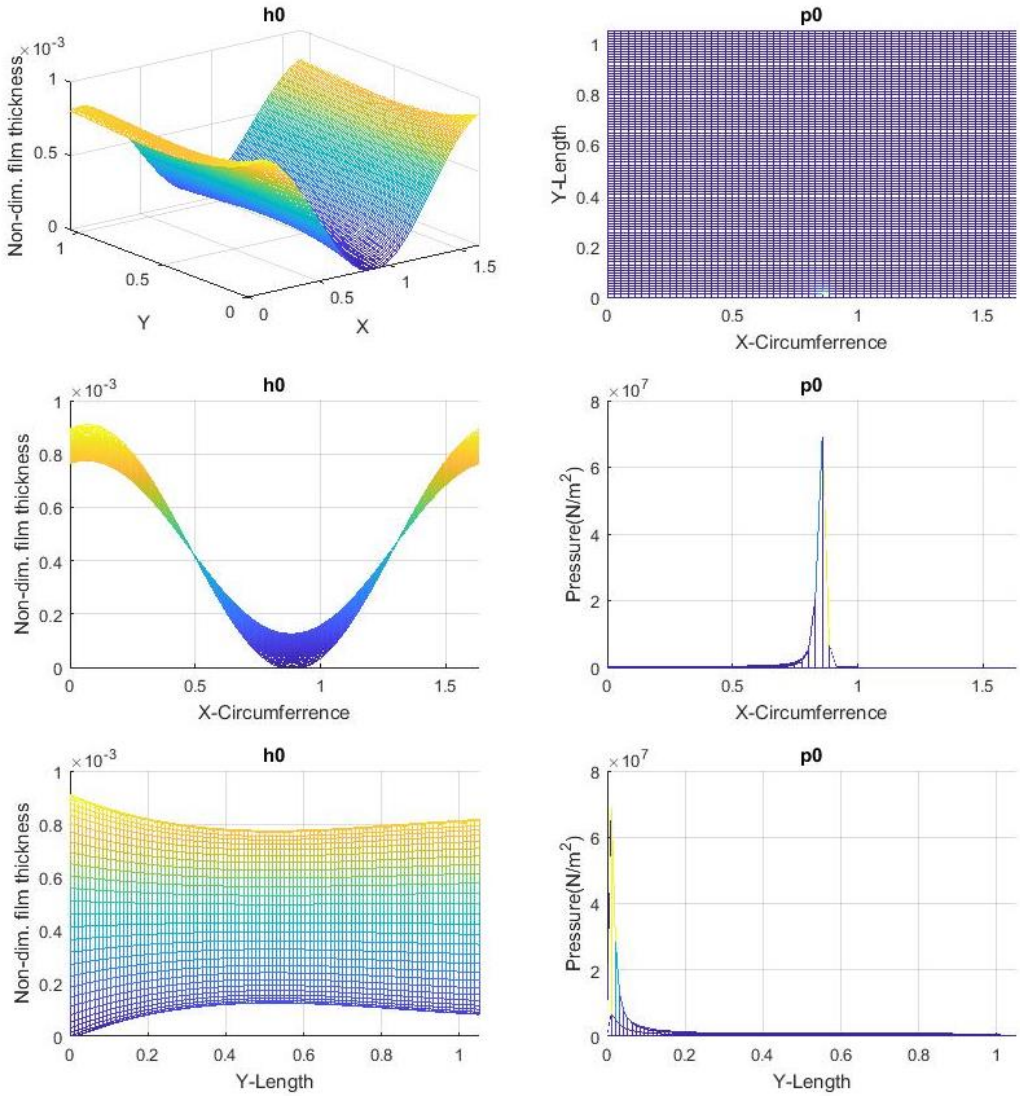

Figure 5-35: SINGLE SLOPE MODEL WITH BENT SHAFT, FOR 10°C TEMPERATURE INCREASE

In the figure above, the distribution of lubricant film thickness 'h' (on the left) and pressure (on the right) in three major planes, over the unwrapped journal bearing geometry is presented

Test:	**10°C Increased Temperature**		**Test Results**	**Deviation from Ref. %**
Shaft Model:	**Bent**	h_{min} =	21.2 μm	-52.91
Slope Type:	**Single**	p_{max} =	2.13 GPa	21.98
S =	**0.0397057**	P_{loss} =	1.867 kW	-28.29
Distance of Support Point from L/2 =			0.048914 m	62.70

Table 5-25: SINGLE SLOPE MODEL WITH BENT SHAFT, FOR 10°C TEMPERATURE INCREASE

Comments: This condition is **fatal** for the bearing, the support point has shifted dramatically aftwards and due to the reduced power loss it seems that only a limited area towards the aft end of the bearing is supporting the load. Mark that 10°C Temperature increase is actually not an extreme condition and can be caused by several reasons such as a minor malfunction or even wear.

Double Slope Model

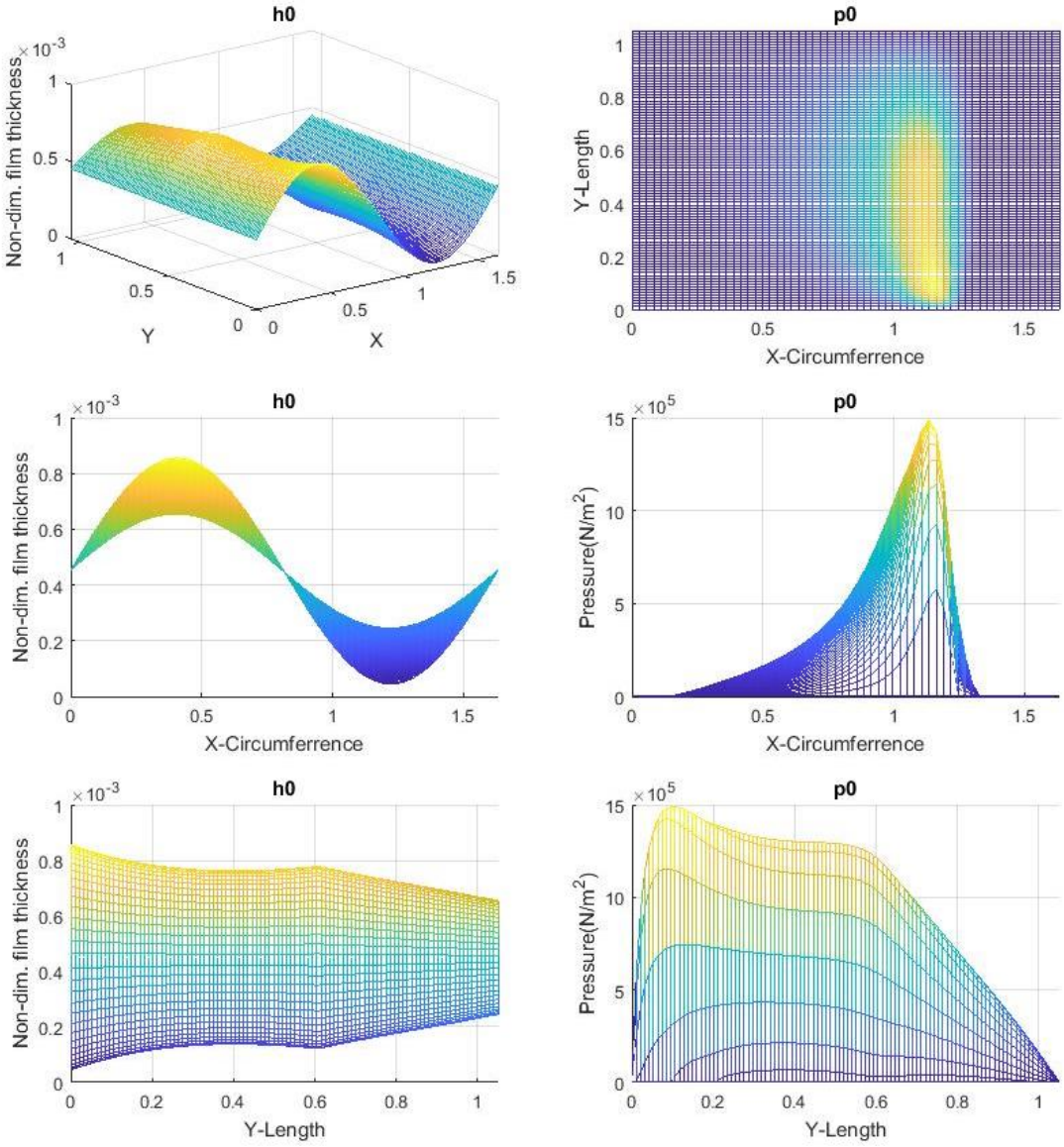

Figure 5-36: DOUBLE SLOPE MODEL WITH BENT SHAFT, FOR 10°C TEMPERATURE INCREASE

In the figure above, the distribution of lubricant film thickness 'h' (on the left) and pressure (on the right) in three major planes, over the unwrapped journal bearing geometry is presented

Test:	**10°C Increased Temperature**		**Test Results**	**Deviation from Ref. %**
Shaft Model:	**Bent**	h_{min} =	45.0 μm	0.81
Slope Type:	**Double**	p_{max} =	1.49 GPa	-28.92
S =	**0.0397057**	P_{loss} =	1.945 kW	-27.69
Distance of Support Point from L/2 =			0.112277 m	120.52

Table 5-26: DOUBLE SLOPE MODEL WITH BENT SHAFT, FOR 10°C TEMPERATURE INCREASE

Comments: Unlike the single slope model the double slope design is much more robust and can withstand worse conditions. The film thickness is still more than 40 microns and the location of the support point is shifted aftwards. Further temperature increase will inevitably be fatal but the double slope design provides an additional "safe operation" margin, vital to the shafting system

5.1.20 Comparison of Robustness Test Results for: Ψx = 0.6

In the following tables and figures, the results of all the robustness tests presented above are grouped for comparison. Reference models for each test are the double slope and single slope design with a bent shaft model presented in sections: 5.1.12 and 5.1.13 respectively.

Test Type	20% RPM Increase	30% RPM Decrease	20% Load Increase	50% Load Decrease	10° Temp. Increase	Reference Case
h_{min} [µm]	45.1	24.3	40.0	54.6	21.2	45.1
p_{max} [GPa]	2.12	1.95	1.87	1.56	2.12	1.74
Angle of p_{max}	51.735	36.5128	60.3229	51.9621	42.3228	51.7351
P_{loss} [kW]	3.889	1.269	2.622	2.569	1.867	2.603
Distance of Support Point from L/2 [m]	0.030	0.046317	0.029938	0.026748	0.048914	0.030063
Ecc ratio	0.001	0.0516289	0.001	0.001	0.059418	0.001
Att angle	36.481	27.360	38.967	36.708	27.0699	36.481
S. Number	0.0754898	0.0411763	0.0514703	0.123529	0.0397057	0.0617644
Deviation From Reference Case						
h_{min} %	0.00	-46.03	-11.38	21.05	-52.91	-
p_{max} %	22.22	12.17	7.51	-9.98	21.98	-
P_{loss} %	49.38	-51.27	0.71	-1.34	-28.29	-
Distance of Support Point from L/2 [m]	0.00	54.07	-0.42	-11.03	62.70	-

Table 5-27: ROBUSTNESS TEST RESULTS OF SINGLE SLOPE BEARING, FOR Ψx=0.6

Test Type	20% RPM Increase	30% RPM Decrease	20% Load Increase	50% Load Decrease	10° Temp. Increase	Reference Case
h_{min} [µm]	44.6	33.1	40.0	54.1	45.0	44.6
p_{max} [GPa]	2.56	1.83	2.24	1.88	1.49	2.10
Angle of p_{max}	60.3299	8.37333	60.0333	54.5821	160.321	54.5821
P_{loss} [kW]	4.073	1.271	2.745	2.690	1.945	2.690
Distance of Support Point from L/2 [m]	0.054989	0.093310	0.057484	0.050914	0.112277	0.050915
Ecc ratio	0.001	0.0274127	0.001	0.001	0.0107363	0.001
Att angle	38.974	11.424	38.677	39.328	90.151	39.328
S. Number	0.0754898	0.0411763	0.0514703	0.123529	0.0397057	0.0617644
Deviation From Reference Case						
h_{min} %	298.50	-46.03	-11.38	21.05	-52.91	-
p_{max} %	-16.69	12.17	7.51	-9.98	21.98	-
P_{loss} %	32.97	-51.27	0.71	-1.34	-28.29	-
Distance of Support Point from L/2 [m]	-100.06	54.07	-0.42	-11.03	62.70	-

Table 5-28: ROBUSTNESS TEST RESULTS OF DOUBLE SLOPE BEARING, FOR Ψx=0.6

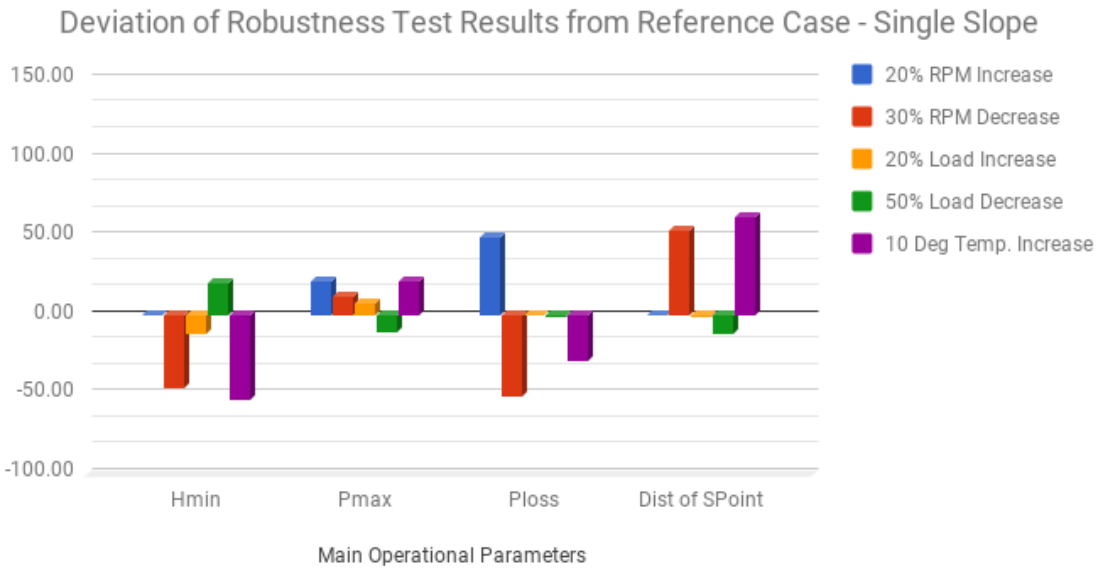

Figure 5-37: ROBUSTNESS TEST RESULTS OF SINGLE SLOPE BEARING, FOR Ψx=0.6

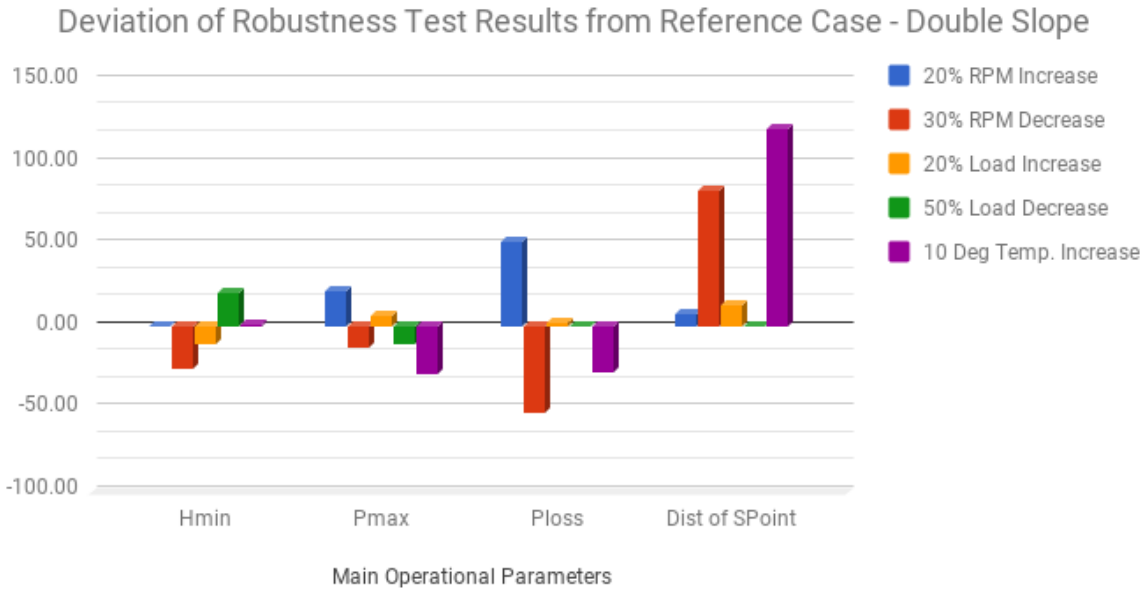

Figure 5-38: ROBUSTNESS TEST RESULTS OF DOUBLE SLOPE BEARING, FOR Ψx=0.6

Overall, **the double slope design is a significantly more robust design**. This is contradictory to the initial misbelief that the single slope model could offer a larger margin in terms of minimum film thickness. The robustness test brought to the spotlight an important inadequacy of the single slope design, in comparison to the double slope one, the limited adaptability to additional loading and alterations of the operational condition of the stern tube bearing. Especially in the scenarios with temperature or load increase and RPM decrease, where the bearing is overloaded, the double slope design is mostly affected in terms of longitudinal position of theoretical contact point and additional power losses, rather than vertical offset of the bearing and minimization of lubricant film thickness. This is vital for the survivability of the vessel in extreme loading conditions which may take place due to bad weather or due to failure (or overloading or malfunction) of another component of the shafting system.

5.2 Double Slope Optimization for Multiple Misalignment Angles

In this case study the double slope optimization results for several shaft misalignment angles are presented. The bearing input parameters are presented in Table 5-1. The purpose of this case study is to locate the optimum double slope parameters for several scenarios of shaft misalignment angle. It has been observed that the shaft angle is the most important parameter that defines the double slope geometry. Therefore the coupled optimizer algorithm presented in Chapter 4 is utilized in order to find the Pareto front and compare the performance parameters for each solution. In this case study, all the acceptable solutions provided by the optimizer will be presented, even if they are not included in the Pareto front (non- dominant solutions), in order to define the area or the margins of the two Slope angles and Lengths that describe an acceptable and optimum double slope design.

Elastic Line and Shaft Angle Calculations

In the following Table 5-29 and Figure 5-39 the calculations for shaft elastic line vertical offsets in the range of 0.0 - 1.0 are presented, for shaft length divided into 10 segments within the bearing length:

	Ux (aft=0)	Uy 0.0	Uy 0.1	Uy 0.2	Uy 0.3	Uy 0.4	Uy 0.5	Uy 0.6	Uy 0.7	Uy 0.8	Uy 0.9	Uy 1.0
1	0.000	-1.31E-04	-1.94E-04	-2.56E-04	-3.19E-04	-3.81E-04	-3.81E-04	-5.06E-04	-5.68E-04	-6.31E-04	-6.93E-04	-7.56E-04
2	0.407	0.00E+00	-2.25E-05	-4.50E-05	-6.75E-05	-9.00E-05	-9.00E-05	-1.35E-04	-1.58E-04	-1.80E-04	-2.02E-04	-2.25E-04
3	0.512	1.05E-05	-1.38E-06	-1.32E-05	-2.50E-05	-3.69E-05	-3.69E-05	-6.05E-05	-7.23E-05	-8.42E-05	-9.60E-05	-1.08E-04
4	0.617	1.49E-05	1.37E-05	1.24E-05	1.12E-05	9.91E-06	9.91E-06	7.40E-06	6.15E-06	4.89E-06	3.64E-06	2.39E-06
5	0.722	1.48E-05	2.39E-05	3.30E-05	4.21E-05	5.13E-05	5.13E-05	6.95E-05	7.86E-05	8.77E-05	9.68E-05	1.06E-04
6	0.827	1.14E-05	3.06E-05	4.98E-05	6.90E-05	8.82E-05	8.82E-05	1.27E-04	1.46E-04	1.65E-04	1.84E-04	2.03E-04
7	0.932	6.23E-06	3.51E-05	6.39E-05	9.27E-05	1.22E-04	1.22E-04	1.79E-04	2.08E-04	2.37E-04	2.66E-04	2.95E-04
8	1.037	5.27E-07	3.85E-05	7.65E-05	1.14E-04	1.53E-04	1.53E-04	2.28E-04	2.66E-04	3.04E-04	3.42E-04	3.80E-04
9	1.142	-4.31E-06	4.22E-05	8.87E-05	1.35E-04	1.82E-04	1.82E-04	2.75E-04	3.21E-04	3.68E-04	4.14E-04	4.61E-04
10	1.247	-6.91E-06	4.75E-05	1.02E-04	1.56E-04	2.11E-04	2.11E-04	3.19E-04	3.74E-04	4.28E-04	4.82E-04	5.37E-04
11	1.352	-5.93E-06	5.55E-05	1.17E-04	1.78E-04	2.40E-04	2.40E-04	3.62E-04	4.24E-04	4.85E-04	5.47E-04	6.08E-04
12	1.457	0.00E+00	6.75E-05	1.35E-04	2.02E-04	2.70E-04	2.70E-04	4.05E-04	4.73E-04	5.40E-04	6.07E-04	6.75E-04
13	1.998	1.57E-04	2.38E-04	3.19E-04	3.99E-04	4.81E-04	4.81E-04	6.42E-04	7.23E-04	8.04E-04	8.85E-04	9.66E-04

Table 5-29: VERTICAL OFFSET CORRECTION in [m] FOR MULTIPLE MISALIGNMENT ANGLES

Note that the 1st and 13th node is the aft and fore protruding edge respectively.

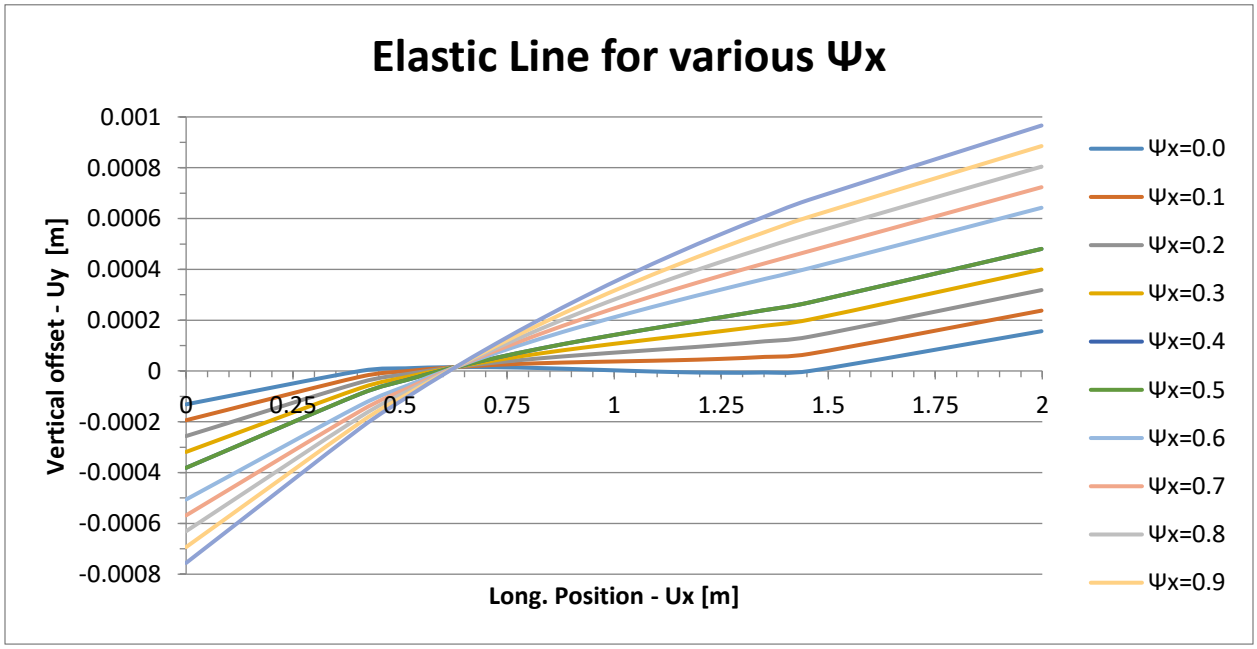

Figure 5-39: VERTICAL OFFSET CORRECTION FOR MULTIPLE MISALIGNMENT ANGLES

In the following Table 5-30 and Figure 5-40 the shaft angles in the range of 0.0 - 1.0 are presented, for shaft length divided into 10 segments within the bearing length:

	Ux (aft=0)	Rz 0.0	Rz 0.1	Rz 0.2	Rz 0.3	Rz 0.4	Rz 0.5	Rz 0.6	Rz 0.7	Rz 0.8	Rz 0.9	Rz 1.0
1	0.000	4.32E-04	5.30E-04	6.28E-04	7.26E-04	8.24E-04	8.24E-04	1.02E-03	1.12E-03	1.22E-03	1.31E-03	1.41E-03
2	0.407	1.83E-04	2.81E-04	3.79E-04	4.77E-04	5.75E-04	5.75E-04	7.71E-04	8.70E-04	9.68E-04	1.07E-03	1.16E-03
3	0.512	1.19E-04	2.17E-04	3.15E-04	4.12E-04	5.10E-04	5.10E-04	7.05E-04	8.03E-04	9.00E-04	9.98E-04	1.10E-03
4	0.617	6.89E-05	1.65E-04	2.61E-04	3.57E-04	4.54E-04	4.54E-04	6.46E-04	7.42E-04	8.38E-04	9.34E-04	1.03E-03
5	0.722	3.15E-05	1.25E-04	2.19E-04	3.13E-04	4.07E-04	4.07E-04	5.94E-04	6.88E-04	7.81E-04	8.75E-04	9.69E-04
6	0.827	7.20E-06	9.76E-05	1.88E-04	2.78E-04	3.69E-04	3.69E-04	5.49E-04	6.40E-04	7.30E-04	8.20E-04	9.11E-04
7	0.932	-4.10E-06	8.19E-05	1.68E-04	2.54E-04	3.40E-04	3.40E-04	5.12E-04	5.98E-04	6.84E-04	7.70E-04	8.56E-04
8	1.037	-2.40E-06	7.83E-05	1.59E-04	2.40E-04	3.20E-04	3.20E-04	4.82E-04	5.63E-04	6.43E-04	7.24E-04	8.05E-04
9	1.142	1.23E-05	8.67E-05	1.61E-04	2.36E-04	3.10E-04	3.10E-04	4.59E-04	5.33E-04	6.08E-04	6.82E-04	7.57E-04
10	1.247	3.99E-05	1.07E-04	1.74E-04	2.41E-04	3.09E-04	3.09E-04	4.43E-04	5.10E-04	5.77E-04	6.45E-04	7.12E-04
11	1.352	8.05E-05	1.39E-04	1.98E-04	2.57E-04	3.16E-04	3.16E-04	4.34E-04	4.93E-04	5.52E-04	6.11E-04	6.70E-04
12	1.457	1.34E-04	1.84E-04	2.33E-04	2.83E-04	3.33E-04	3.33E-04	4.33E-04	4.82E-04	5.32E-04	5.82E-04	6.32E-04
13	1.998	4.65E-04	4.65E-04	4.65E-04	4.65E-04	4.65E-04	4.65E-04	4.65E-04	4.65E-04	4.65E-04	4.65E-04	4.65E-04

Table 5-30: SHAFT ANGLE CORRECTION in [rad] FOR MULTIPLE MISALIGNMENT ANGLES

Note that the 1st and 13th node is the aft and fore protruding edge respectively.

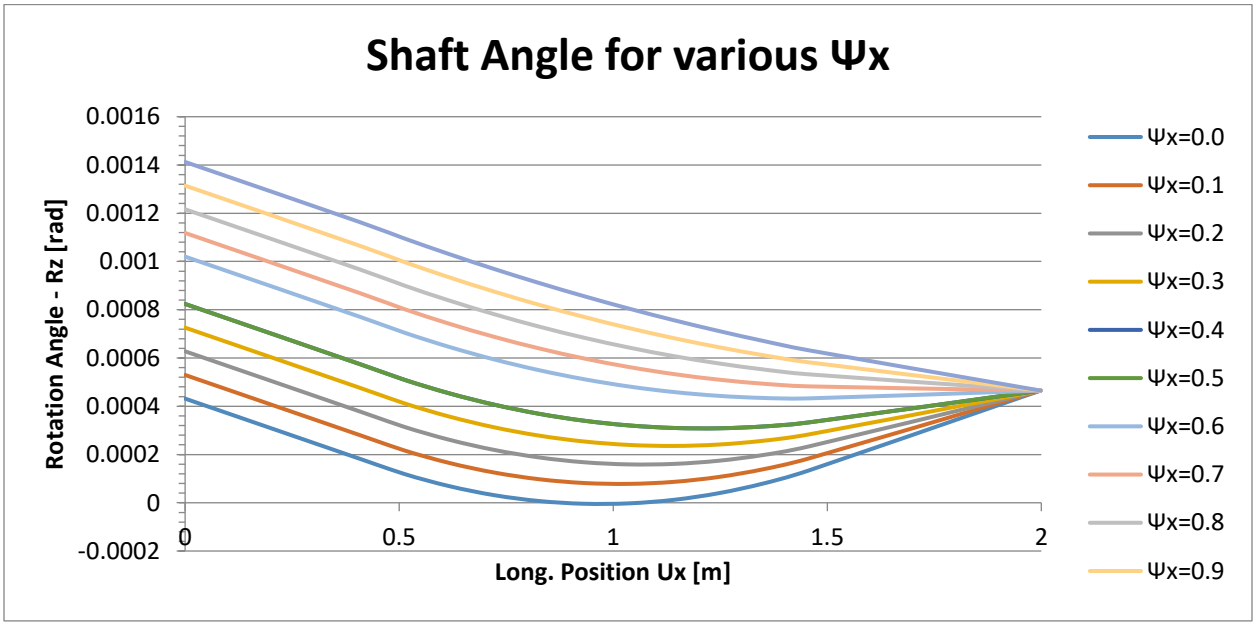

Figure 5-40: SHAFT ANGLE CORRECTION FOR MULTIPLE MISALIGNMENT ANGLES

Similar results and curves are used throughout the present work as per case. Such calculations can easily be executed with any beam modeling tool or had the shaft alignment plan been provided.

In the following subsections, the optimization results for shaft misalignment angles of 0.1/ 0.2/ 0.3/ 0.4/ 0.5/ 0.6 are presented. The Pareto optimization results are shown and the concluded double slope geometries are presented thereafter. Shaft misalignment larger than 0.6 have very scattered and limited solutions and it is advised not to design in such areas. Basically any design for shaft misalignment angles larger than 0.3 is an extreme and last measure solution since most cases obligingly require bearing treatment, either with single or double slope geometry.

5.2.1 Double Slope Optimization for Shaft Misalignment = 0.1

In the following figure, the optimization solutions are presented against minimum film thickness and maximum pressure. Variable parameters of the optimization are the two non-dimensional slope angles and lengths. In this optimization process, the minimum film thickness maximization and maximum pressure minimization are the objective functions. For every solution point, the power loss has been calculated additionally and is plotted via the colourbar. The Pareto front is developed and several solutions are considered Pareto dominant. An interesting observation is that the two objective functions are contradictory, therefore there is not a single Pareto dominant solution. On the other hand power loss minimization is observed to coincide with maximization of the film thickness and also maximum pressure.

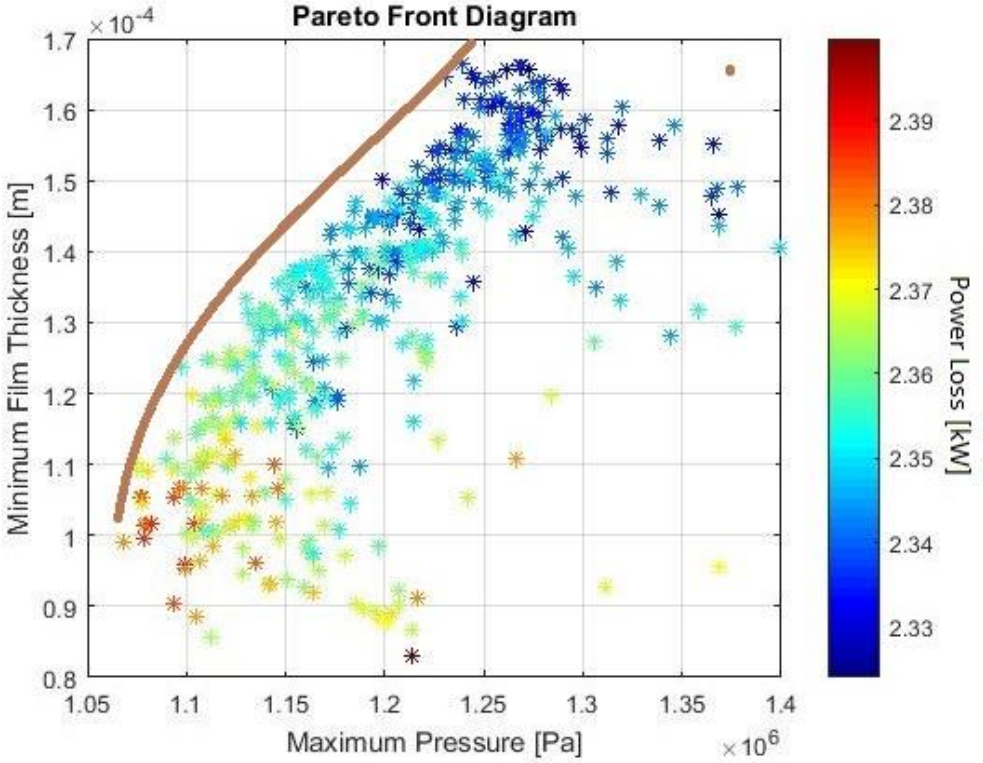

Figure 5-41: PARETO FRONT FOR Ψx=0.1

In the following table, four Pareto dominant solution parameters are presented for Ψx=0.1:

p_{max} [GPa]	h_{min} [μm]	$Slope_{Aft}$ (1)	$Length_{Aft}$ (1)	$Slope_{Fore}$ (2)	$Length_{Fore}$ (2)	P. Loss [kW]
1.24	167	0.12	0.2	0.12	0.8	2.35
1.27	166	0.15	0.37	0.07	0.63	2.32
1.21	150	0.09	0.44	0.13	0.56	2.35
1.10	119	0.07	0.67	0.17	0.33	2.37

Table 5-31: PARETO DOMINANT SOLUTIONS FOR Ψx=0.1

In the following figures, maps that include all the optimum geometries are presented. The solutions included are the ones that showed satisfactory improvement of the bearing performance compared to the plain bearing for double slope geometry. This map is narrowed to the area of most interest in terms of optimum solutions. The margins of areas with concentrated optimal solutions are very interesting since they can determine the area at which the double slope parameters should variate in order to yield the desired pressure or film thickness outcome.

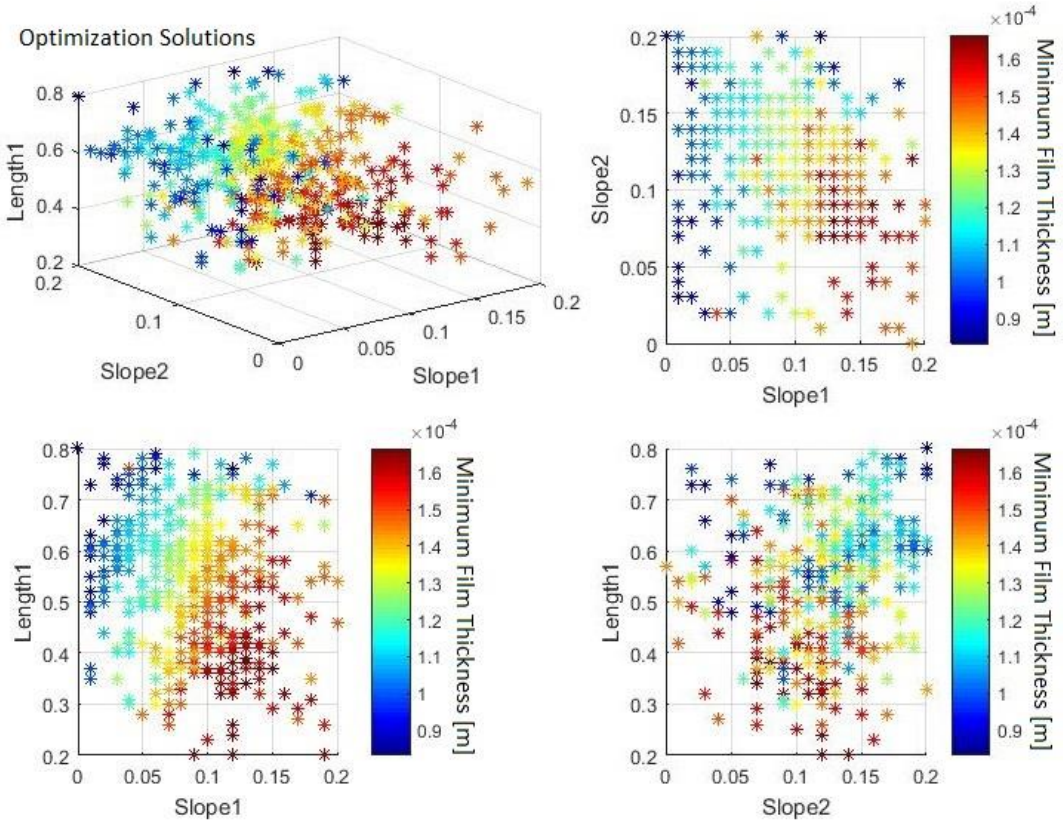

Figure 5-42: OPTIMIZATION SOLUTIONS OF Ψx=0.1, AGAINST MINIMUM FILM THICKNESS

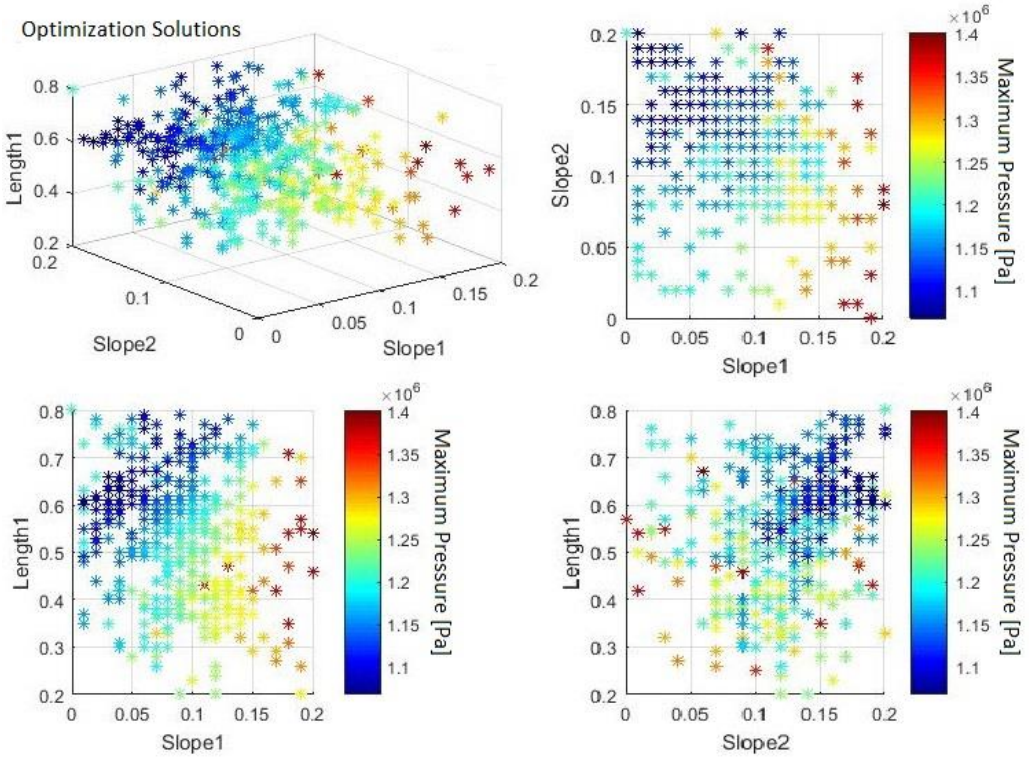

Figure 5-43: OPTIMIZATION SOLUTIONS OF Ψx=0.1, AGAINST MAXIMUM PRESSURE

5.2.2 Double Slope Optimization for Shaft Misalignment = 0.2

In the following figure, the optimization solutions for shaft misalignment angle = 0.2 are presented against minimum film thickness and maximum pressure. Variable parameters of the optimization are once again the two non-dimensional slope angles and lengths. In this optimization process, the pressure margin is limited in comparison to the case of Ψx=0.1. This gives the impression that maximization of the film thickness plays a more significant role. The minimum power loss coincides with maximum film thickness for this case as well. This conclusion is not expected to alter during the following optimization processes.

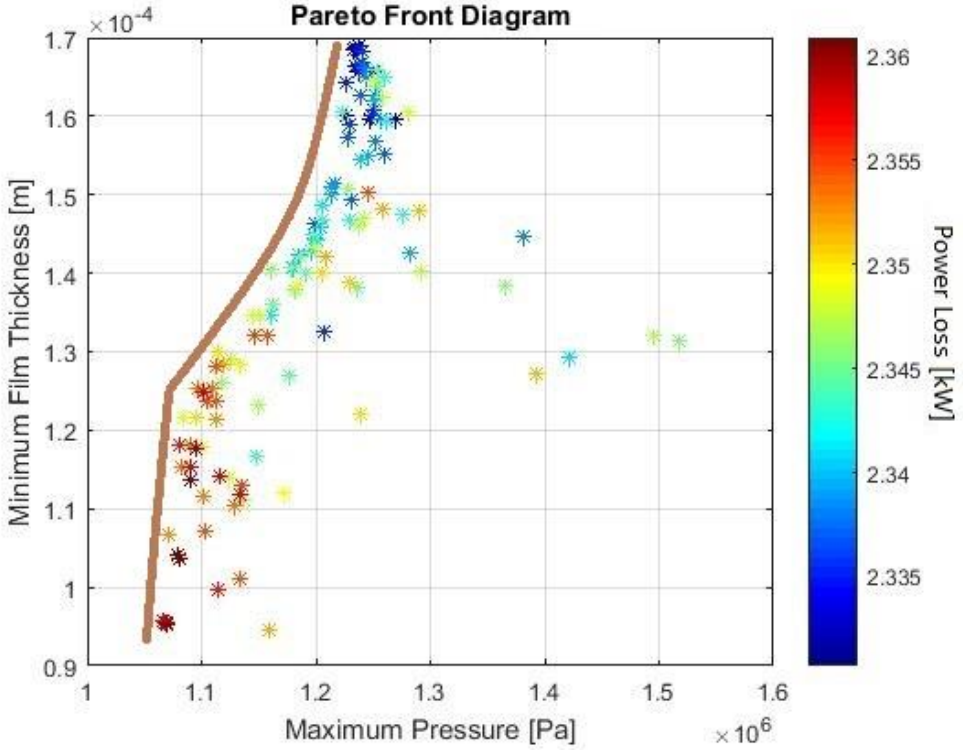

Figure 5-44: PARETO FRONT FOR Ψx=0.2

In the following table, four Pareto dominant solution parameters are presented for Ψx=0.2:

p_{max} [GPa]	h_{min} [μm]	$Slope_{Aft}$ (1)	$Length_{Aft}$ (1)	$Slope_{Fore}$ (2)	$Length_{Fore}$ (2)	Power Loss [kW]
1.23	169	0.16	0.3	0.15	0.7	2.33
1.25	160	0.18	0.44	0.15	0.56	2.32
1.23	150	0.16	0.48	0.18	0.52	2.34
1.08	121	0.17	0.74	0.17	0.26	2.35

Table 5-32: PARETO DOMINANT SOLUTIONS FOR Ψx=0.2

In the following figures, maps that include all the optimum geometries are presented. The solutions included are the ones that showed satisfactory improvement of the bearing performance compared to the plain bearing for double slope geometry. This map is narrowed to the area of most interest in terms of optimum solutions. The margins of areas with concentrated optimal solutions are very interesting since they can determine the area at which the double slope parameters should variate in order to yield the desired pressure or film thickness outcome. In this case mark that the slopes are narrowed into an area near 0.2, which is a significant indication for the area of optimum slope angles.

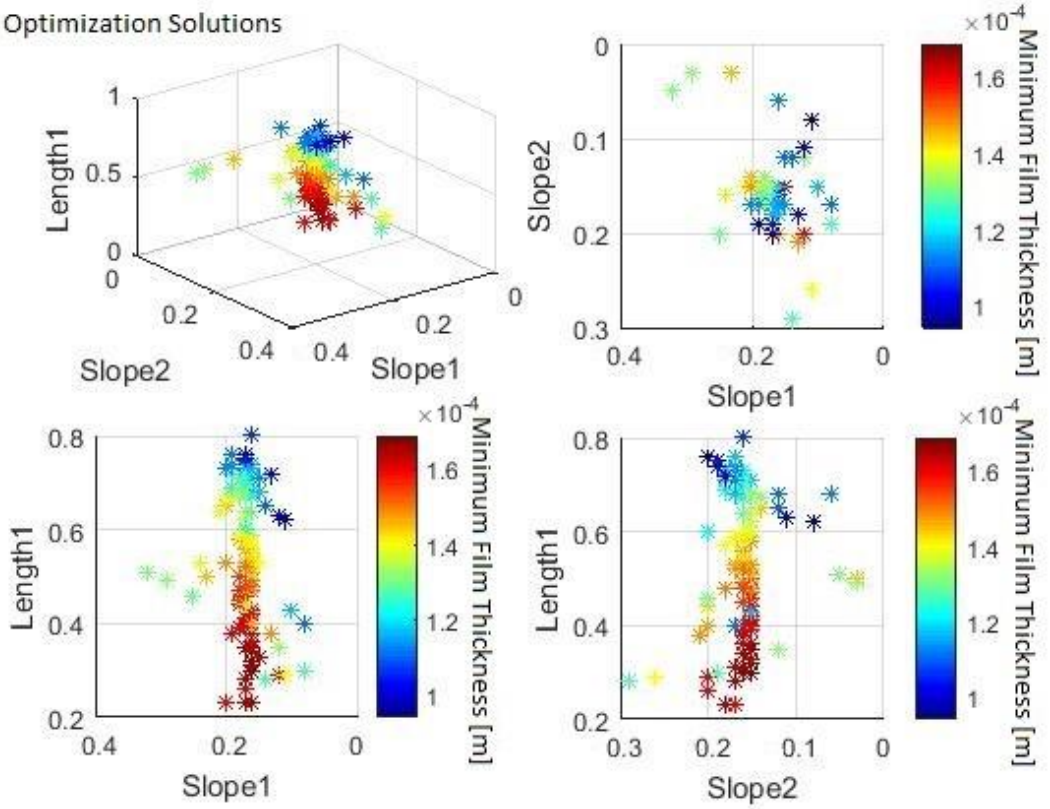

Figure 5-45: OPTIMIZATION SOLUTIONS OF Ψx=0.2, AGAINST MINIMUM FILM THICKNESS

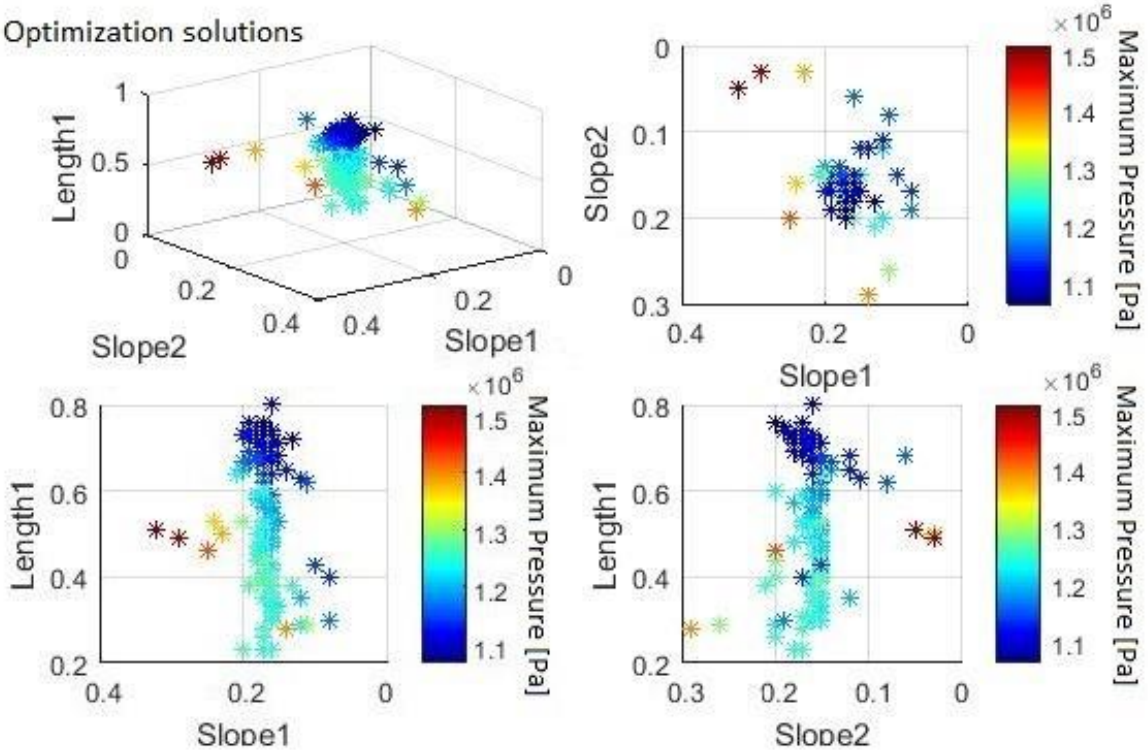

Figure 5-46: OPTIMIZATION SOLUTIONS OF Ψx=0.2, AGAINST MAXIMUM PRESSURE

5.2.3 Double Slope Optimization for Shaft Misalignment = 0.3

In the following figure, the optimization solutions for shaft misalignment angle = 0.3 are presented against minimum film thickness and maximum pressure. Variable parameters of the optimization are once again the two non-dimensional slope angles and lengths. In this optimization process, the Pareto front is similar to the one for Ψx=0.1.

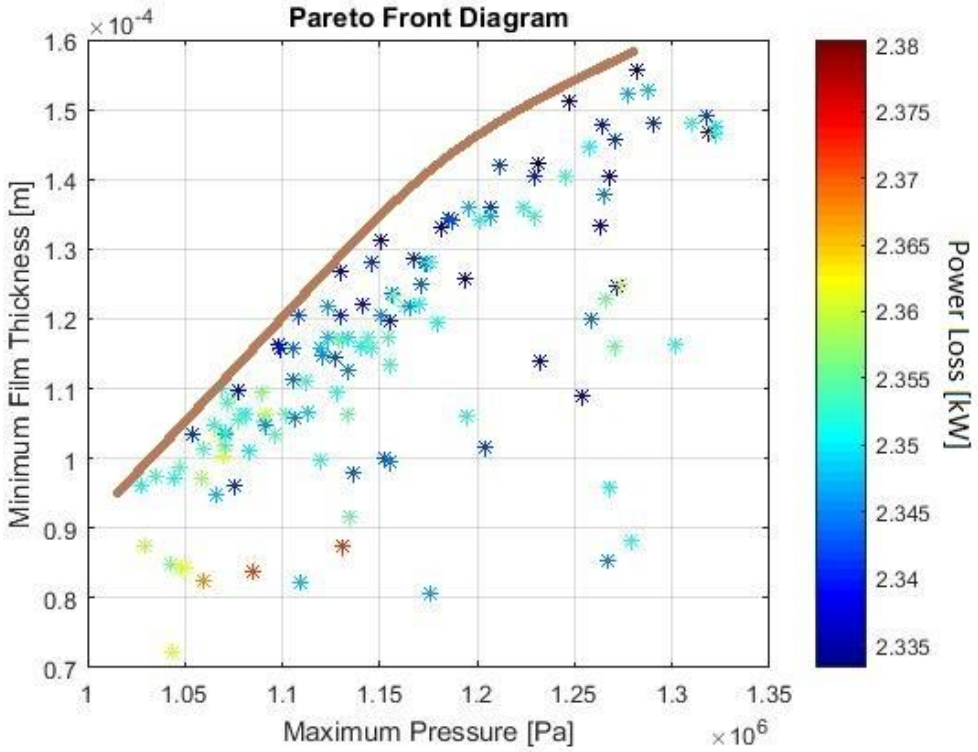

Figure 5-47: PARETO FRONT FOR Ψx=0.3

In the following table, four Pareto dominant solution parameters are presented for Ψx=0.3:

p_{max} [GPa]	h_{min} [μm]	$Slope_{Aft}$ (1)	$Length_{Aft}$ (1)	$Slope_{Fore}$ (2)	$Length_{Fore}$ (2)	Power Loss [kW]
1.28	156	0.31	0.61	0.11	0.39	2.33
1.25	151	0.31	0.65	0.12	0.35	2.33
1.15	131	0.29	0.71	0.15	0.29	2.34
1.06	101	0.25	0.74	0.2	0.26	2.35

Table 5-33: PARETO DOMINANT SOLUTIONS FOR Ψx=0.3

In the following figures, maps that include all the optimum geometries are presented. The solutions included are the ones that showed satisfactory improvement of the bearing performance compared to the plain bearing for double slope geometry. This map is narrowed to the area of most interest in terms of optimum solutions. The margins of areas with concentrated optimal solutions are very interesting since they can determine the area at which the double slope parameters should variate in order to yield the desired pressure or film thickness outcome. In this case mark that most solutions are grouped within a narrow area for Slope1= 0.2-0.3, Slpoe2= 0.1-0 and Length1=0.6-0.8. This is a good indication during the decision making of optimum double slope parameters.

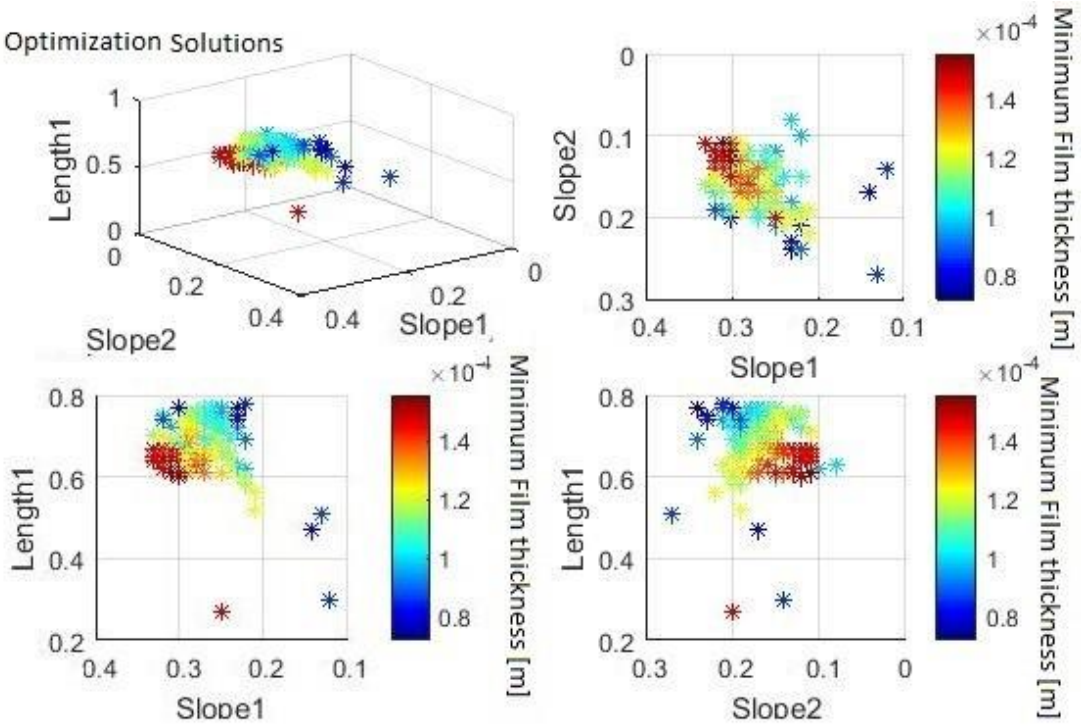

Figure 5-48: OPTIMIZATION SOLUTIONS OF Ψx=0.3, AGAINST MINIMUM FILM THICKNESS

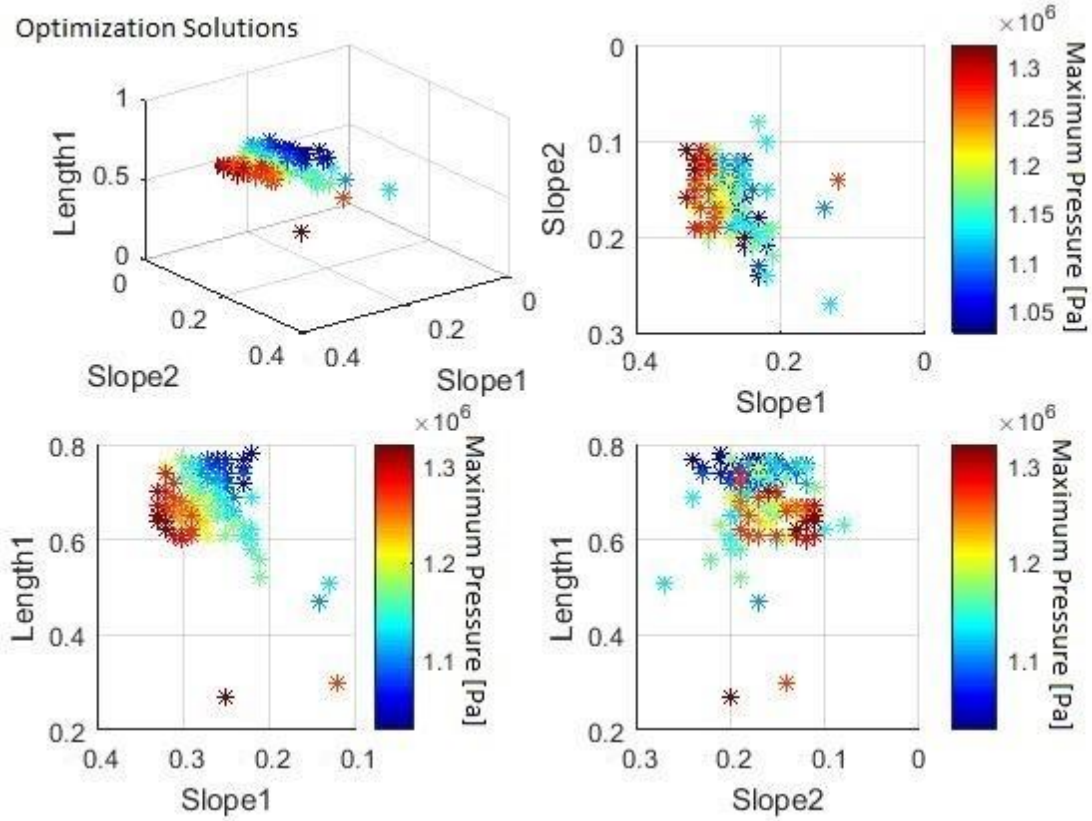

Figure 5-49: OPTIMIZATION SOLUTIONS OF Ψx=0.3, AGAINST MAXIMUM PRESSURE

5.2.4 Double Slope Optimization for Shaft Misalignment = 0.4

In the following figure, the optimization solutions for shaft misalignment angle = 0.2 are presented against minimum film thickness and maximum pressure. Variable parameters of the optimization are once again the two non-dimensional slope angles and lengths. In this optimization process, the pressure margin is limited in comparison to the previous cases. This gives the impression that maximization of the film thickness plays a more significant role. Also an unexpected non linearity of the Pareto front is observed. The power loss distribution plays a less significant role for the Pareto optimum solutions for Ψx=0.4.

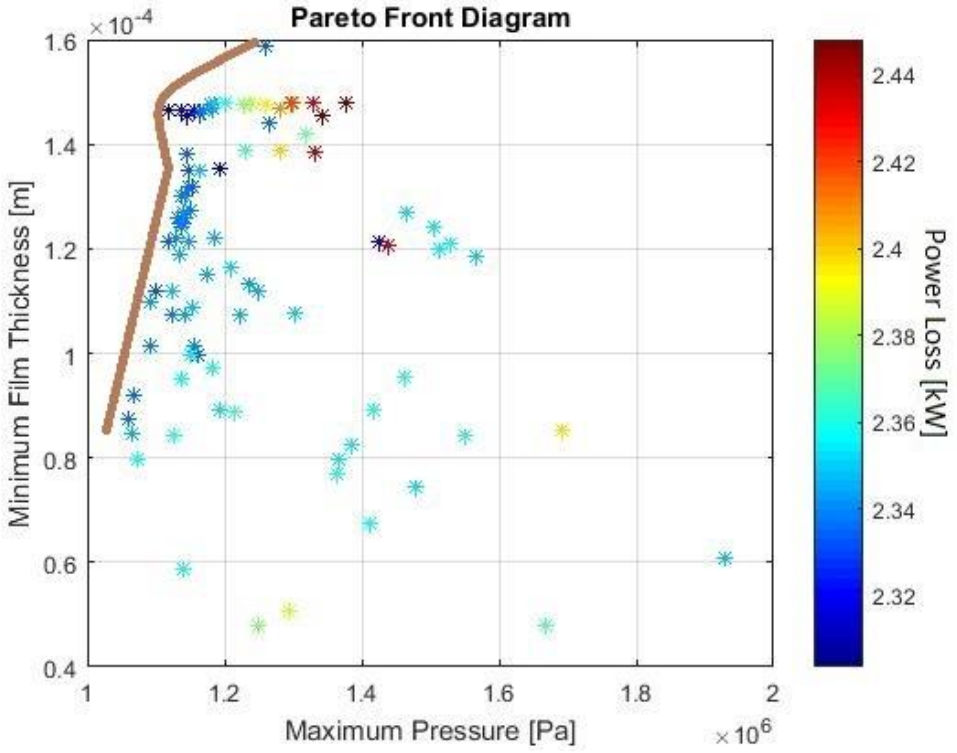

Figure 5-50: PARETO FRONT FOR Ψx=0.4

In the following table, four Pareto dominant solution parameters are presented for Ψx=0.4:

p_{max} [GPa]	h_{min} [μm]	$Slope_{Aft}$ (1)	$Length_{Aft}$ (1)	$Slope_{Fore}$ (2)	$Length_{Fore}$ (2)	Power Loss [kW]
1.26	159	0.24	0.34	0.17	0.66	2.33
1.12	147	0.2	0.32	0.31	0.68	2.30
1.09	110	0.24	0.67	0.16	0.33	2.34
1.06	86	0.14	0.34	0.29	0.66	2.34

Table 5-34: PARETO DOMINANT SOLUTIONS FOR Ψx=0.4

In the following figures, maps that include all the optimum geometries are presented. The solutions included are the ones that showed satisfactory improvement of the bearing performance compared to the plain bearing for double slope geometry. This map is narrowed to the area of most interest in terms of optimum solutions. The margins of areas with concentrated optimal solutions are very interesting since they can determine the area at which the double slope parameters should variate in order to yield the desired pressure or film thickness outcome. In this case mark that the slopes are narrowed into an area near 0.2-0.4, which is a significant indication for the area of optimum slope angles.

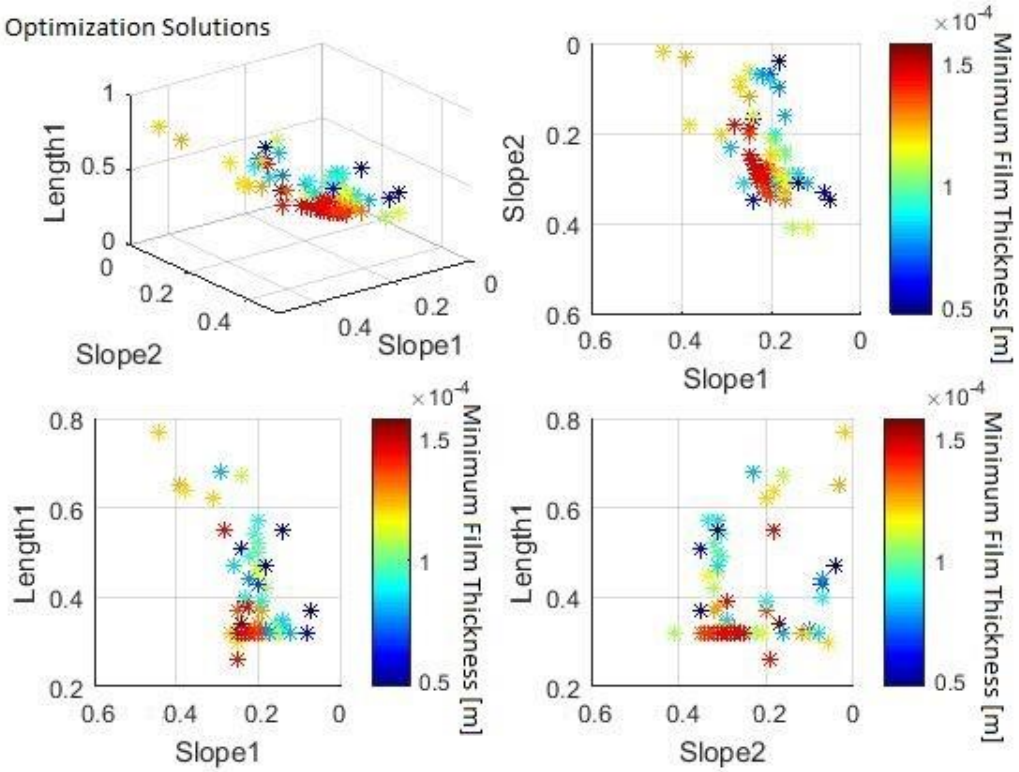

Figure 5-51: OPTIMIZATION SOLUTIONS OF Ψx=0.4, AGAINST MINIMUM FILM THICKNESS

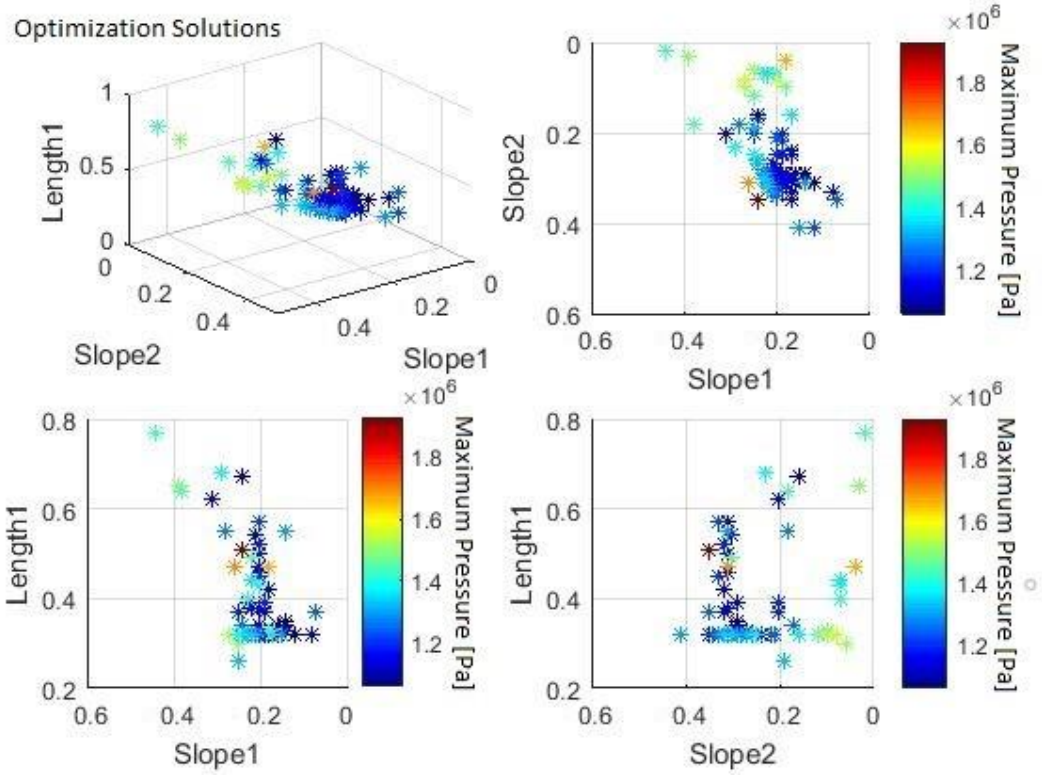

Figure 5-52: OPTIMIZATION SOLUTIONS OF Ψx=0.4, AGAINST MAXIMUM PRESSURE

5.2.5 Double Slope Optimization for Shaft Misalignment = 0.5

In the following figure, the optimization solutions for shaft misalignment angle = 0.2 are presented against minimum film thickness and maximum pressure. Variable parameters of the optimization are once again the two non-dimensional slope angles and lengths. In this optimization process, the pressure margin is wide but there seems to be a single Pareto dominant solution. The reason for this might be the limit on total runtime of the optimizer, which was a specific number of generations. Had the optimizer more flexible margins, more Pareto dominant solutions could have been provided. A mean power loss around 2.4 kW is observed, similar to most of the previously presented cases.

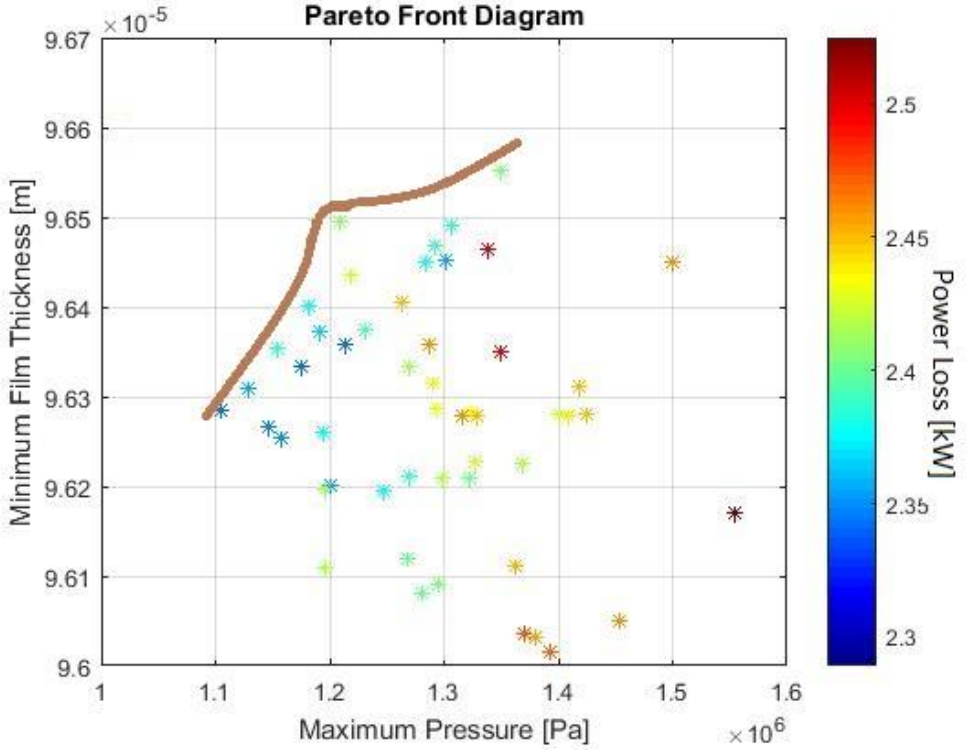

Figure 5-53: PARETO FRONT FOR Ψx=0.5

In the following table, three Pareto dominant solution parameters are presented for Ψx=0.5:

p_{max} [GPa]	h_{min} [μm]	$Slope_{Aft}$ (1)	$Length_{Aft}$ (1)	$Slope_{Fore}$ (2)	$Length_{Fore}$ (2)	Power Loss [kW]
1.21	96.5	0.3	0.5	0.24	0.5	2.41
1.35	96.55	0.33	0.5	0.13	0.5	2.40
1.10	96.3	0.28	0.49	0.25	0.51	2.34

Table 5-35: PARETO DOMINANT SOLUTIONS FOR Ψx=0.5

In the following figures, maps that include all the optimum geometries are presented. The solutions included are the ones that showed satisfactory improvement of the bearing performance compared to the plain bearing for double slope geometry. This map is narrowed to the area of most interest in terms of optimum solutions. The margins of areas with concentrated optimal solutions are very interesting since they can determine the area at which the double slope parameters should variate in order to yield the desired pressure or film thickness outcome. In this case mark that the slopes are narrowed into an area around Slope1=0.3 and Slope2=0.15-0.35. The total number of satisfactory solutions is limited in comparison to previous cases.

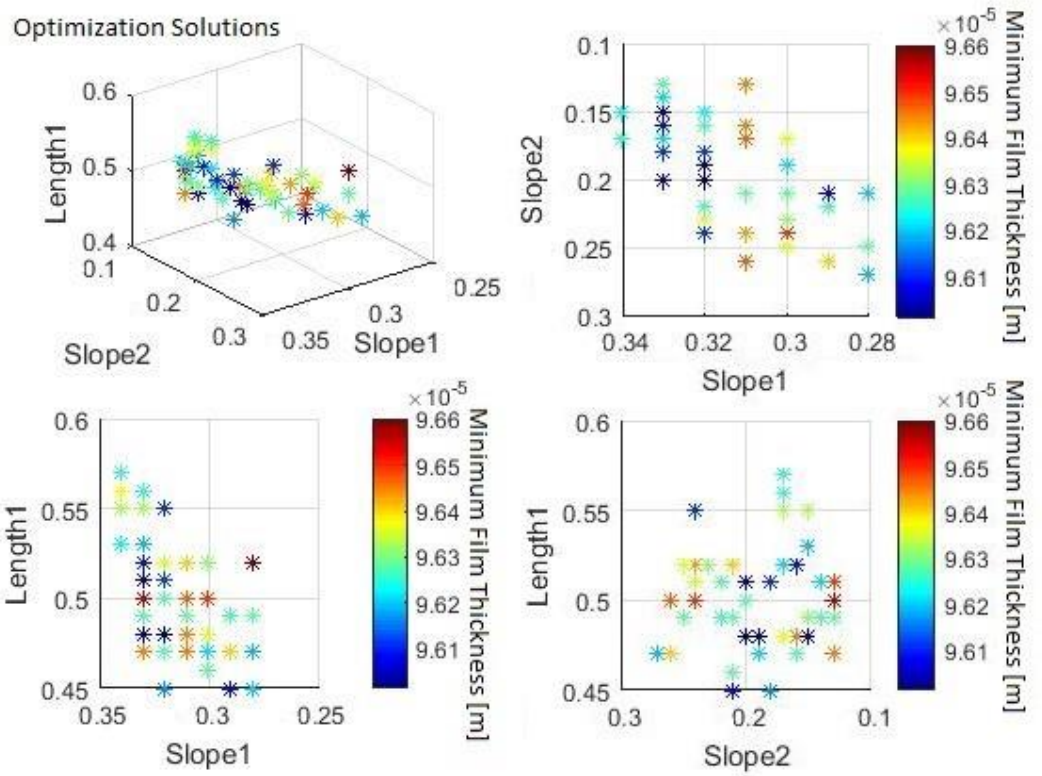

Figure 5-54: OPTIMIZATION SOLUTIONS OF Ψx=0.5, AGAINST MINIMUM FILM THICKNESS

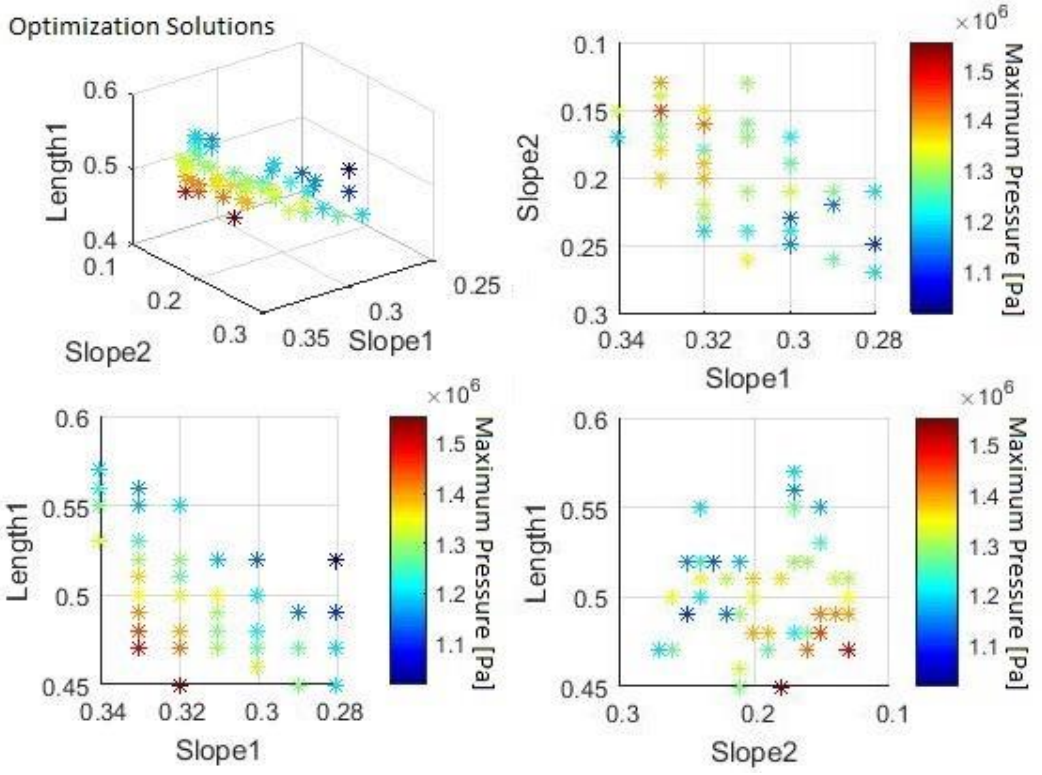

Figure 5-55: OPTIMIZATION SOLUTIONS OF Ψx=0.5, AGAINST MAXIMUM PRESSURE

5.2.6 Double Slope Optimization for Shaft Misalignment = 0.6

In the following figure, the optimization solutions for shaft misalignment angle = 0.6 are presented against minimum film thickness and maximum pressure. Variable parameters of the optimization are once again the two non-dimensional slope angles and lengths. In this optimization process, the maximum pressure limit is increase to approximately 1.6-1.8 x10^6 Pa. The minimum film thickness has also decreases dramatically around 45 microns. This indicates that further increase of the shaft misalignment angle will render the hydrodynamic lubrication capabilities of the bearing obsolete, in terms of supporting a required H_{min} (H_{min}> 30 microns according to regulations). The non-linearity of the Pareto front observed is a result of the limitation on optimizer generations, which is inevitable for a limited time research project.

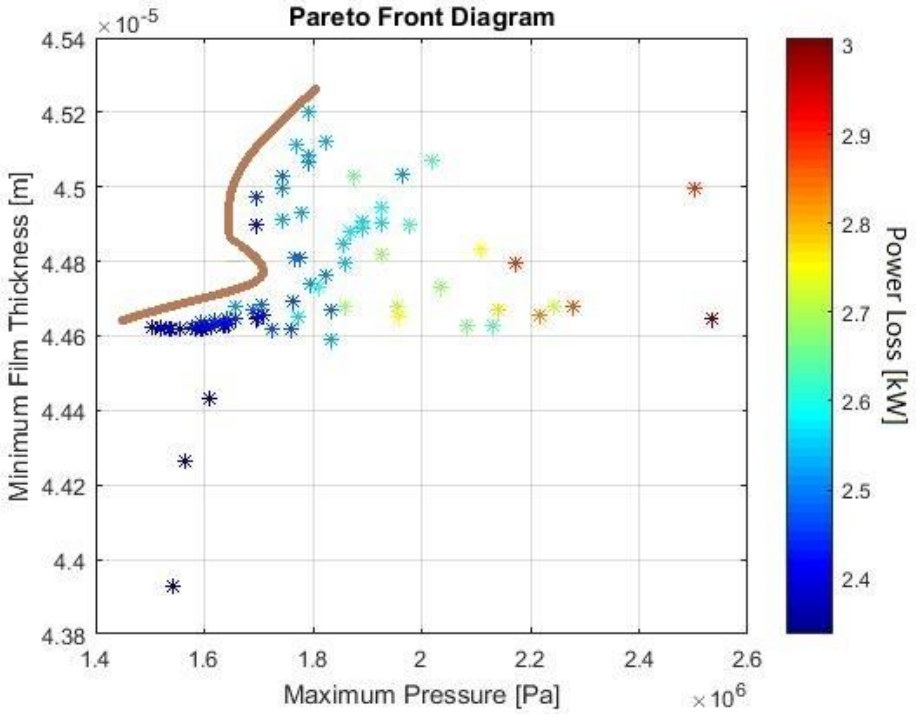

Figure 5-56: PARETO FRONT FOR Ψx=0.6

In the following table, four Pareto dominant solution parameters are presented for Ψx=0.6:

p_{max} [GPa]	h_{min} [μm]	$Slope_{Aft}$ (1)	$Length_{Aft}$ (1)	$Slope_{Fore}$ (2)	$Length_{Fore}$ (2)	Power Loss [kW]
1.79	45.2	0.36	0.58	0.15	0.42	2.54
1.69	44.95	0.36	0.61	0.12	0.39	2.45
1.594	44.6	0.35	0.66	0.24	0.34	2.47

Table 5-36: PARETO DOMINANT SOLUTIONS FOR Ψx=0.6

In the following figures, maps that include all the optimum geometries are presented. The solutions included are the ones that showed satisfactory improvement of the bearing performance compared to the plain bearing for double slope geometry. This map is narrowed to the area of most interest in terms of optimum solutions. The margins of areas with concentrated optimal solutions are very interesting since they can determine the area at which the double slope parameters should variate in order to yield the desired pressure or film thickness outcome. The limited film thickness for Ψx=0.6 indicates that the decision making process for optimum double slope geometry parameters should include a robustness test, similar to the ones conducted in Section 5.1 .

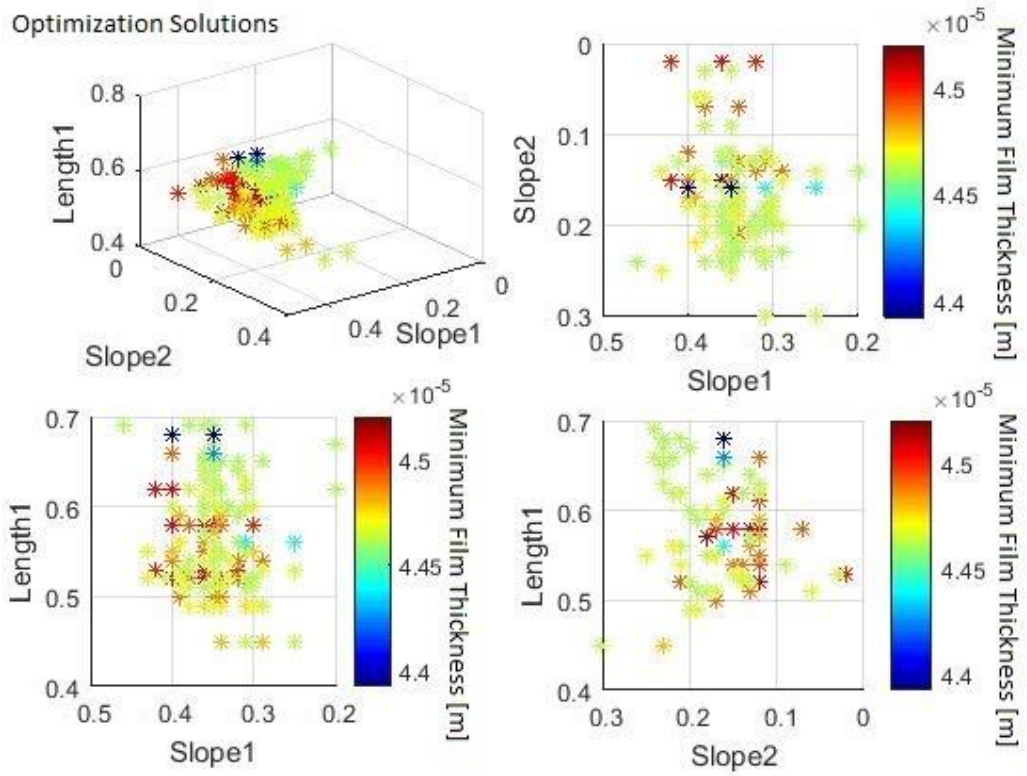

Figure 5-57: OPTIMIZATION SOLUTIONS OF Ψx=0.6, AGAINST MINIMUM FILM THICKNESS

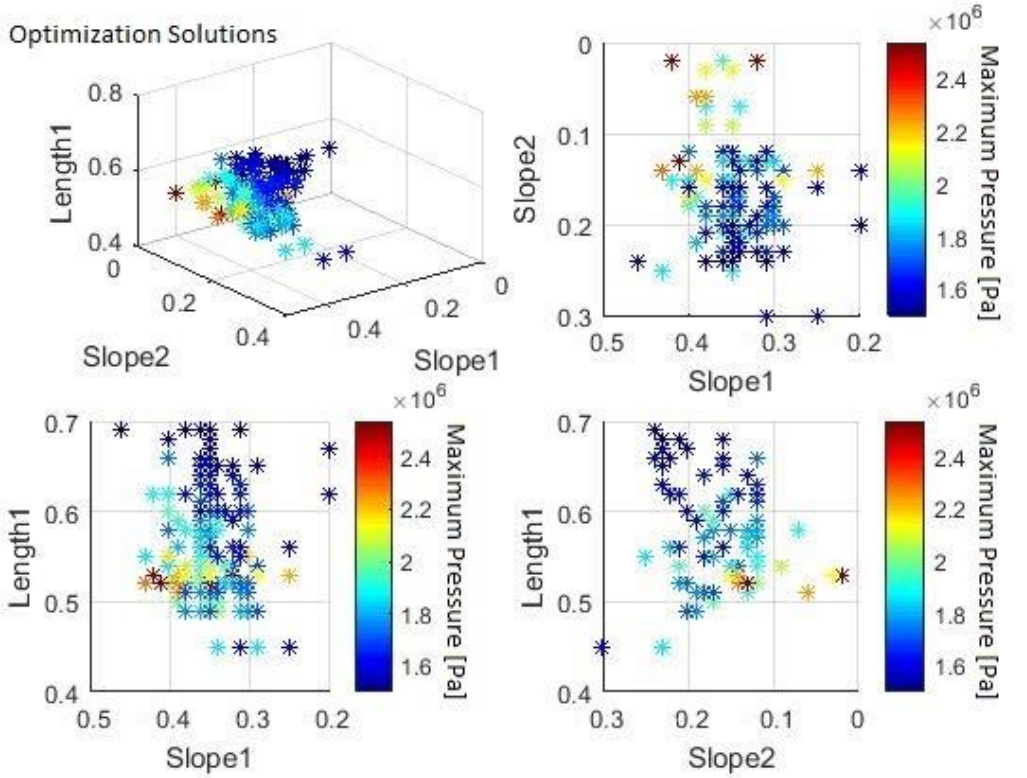

Figure 5-58: OPTIMIZATION SOLUTIONS OF Ψx=0.6, AGAINST MAXIMUM PRESSURE

6 Results and Discussion

Summarizing, in the present work, the stern tube bearing of marine vessels has been studied. Tribological analysis of the performance of the bearing was conducted and two innovative designs were compared, in particular bearings with single and double slope modifications. During the course of this thesis, several tools were developed in order to model the shaft and the bearing geometry as accurately as possible. Both geometries have a significant effect on the lubricant film thickness between the shaft and the bearing bushing. Proper modifications were done in order to accurately describe the single and double slope inclination of the bearing; additionally, an extensive study was conducted in order to model the shaft as a bent beam within the bearing length. The latter required coupling of the shaft alignment tool with the performance calculation algorithm. The equilibrium of pressure distribution was calculated on the unwrapped journal bearing geometry solving the Reynolds equation, having applied the Reynolds boundary conditions. The loading of the bearing was constant at every test case studied. The differential equation was solved using the finite difference method (FDM).

Aiming at demonstrating the optimum geometry modification for minimization of the maximum lubricant pressure and maximization of the minimum lubricant film thickness, several tools were developed and coupled with a genetic algorithm optimizer. The tools that required coupling with the solver of the Reynolds equation, which was a preexisting software developed at NTUA, were developed using object oriented C++, in order to be consistent to the existing code. The optimizer utilized was a preexisting Matlab function, and therefore the fitness function required was also developed using Matlab. The post-processing of the results was done using both Matlab and Microsoft Excel.

The developed tools were applied to compute the performance characteristics of a “test-case” stern tube bearing. Two case studies were conducted to study the effects of single and double slope parameters to the bearing performance and map the optimum double slope geometry parameters, respectively. In the first case study, two similar geometries with different non-dimensional shaft misalignment angles (Ψx= 0.3 and Ψx= 0.6) have been presented. Initially, the different modeling types for the shaft and slope types have been compared with a reference case. In both cases, the optimum single and double slope design has been applied and a robustness test has been conducted. In both cases the double slope geometry was concluded to be the most robust solution even though in the case of Ψx= 0.6, the initial slope implementation proved that the single slope design was the preferable solution. The most important conclusion was that the double slope design is less susceptible to film thickness and pressure distribution variation, due to its ability to “follow closely” the actual bent shaft geometry within the length of the bearing. The second case study included performance calculations and optimization for variable double slope parameters. This was conducted for non-dimensional shaft misalignment angles between 0.1 and 0.6. The results of the optimization process yielded a Pareto front for each case and several Pareto dominant solutions. The solutions that showed satisfactory improvement of the bearing performance compared to the plain bearing for double slope geometry were included to the maps presented for variable double slope parameters against minimum film thickness and maximum pressure limitations. As this technology is still developing, there hardly relevant literature to compare the findings of this work.

In summary, the present work concluded that double slope geometry modification to the stern tube bearing of marine vessels is an interesting and quite promising design, worth of further study and implementation. The most important benefit from the introduction of double slope stern tube bearing geometry is the operational margin increase, which might consequently be proven vital for the survivability of the vessel on extreme loading operational conditions.

7 Future Work

Future work, in continuation of the present, could include the following topics:

- Perform optimization analyses based on genetic algorithms for several initial geometric parameters of the system (L/D, c, RPM, μ, Load, Shaft Inclination) and create a map for optimum slope geometries.
- Perform operational based optimization analyses based on genetic algorithms, for identifying optimal slope parameters that maximize the bearing load capacity and the safe operation margin, or minimize the corresponding power losses.
- Create and couple a FEM model of the shaft to compare the elastic deformations of the shaft due to elastic bending.
- Create a FEM model of the Journal Bearing and the shaft to calculate the pressure distribution on the bearing and compare with the numerical results of this work.
- Extension of the present models to account for thermal effects in the lubricant domain and for elastic deformations of the bearing structure (thermo-elasto-hydrodynamic simulations).
- Extension of the current models to perform multi-slope optimization.
- Extension of the present models to account for transient loading of the bearing.
- Extension of the present models to account for dynamic biaxial loading of the bearing.
- Study the vibration characteristics and friction induced vibration for double slope stern tube bearing.
- Perform experiments with an experimental test-rig for journal bearings modified properly with double slope geometry to validate (a) the measurements of the developed pressure and temperature in the lubricating domain, (b) the measurements of eccentricity and attitude angle, and (c) the measurements of the shaft/bearing misalignment angle.
- Experiments on sloped journal bearings made of different materials, and comparison of their performance, under different combinations of applied loads and RPM.
- Evaluate the manufacturing techniques of slope boring and shaft inclination and propose the techno economically optimal one.
- Create an adaptive monitoring system that utilizes the coupled system algorithm to evaluate operational condition and control the offset or the inclination of the journal bearing (applies only to intermediate bearings).

Literature

[1] Stachowiak G. W. and Bathelor A. W., "Engineering Tribology", University of Western Australia, Department of Mechanical and Materials Engineering, Australia, Butterworth Heinemann, pp. 81-96, pp. 101-110, pp. 146-148, pp. 149-150, p. 154, p. 163, 2005.

[2] Khonsari M. M. and Booser R. E., "Applied Tribology," Bearing Design and Lubrication, Second Edition, John Wiley & Sons, Ltd, 2008, p. chapter 8: Journal Bearings, 2008.

[3] Cameron A., "Basic lubrication theory", Imperial College of Science and Technology London, Ellis Horwood Ltd, p. chapter 3: Reynolds equation, chapter 7: Journal bearings, 1983

[4] Szeri A.Z., "Fluid Film Lubrication", New York: Cambridge University Press, 2011.

[5] Piotrowski J., "Shaft alignment handbook", Taylor & Francis Group, 2007

[6] Harrington, R.L., "Marine Engineering", SNAME, Jersey City, N.J., 1992.

[7] American Bureau of Shipping, "Guidance Notes on Propulsion Shafting Alignment", April 2004.

[8] American Bureau of Shipping, Guide for Enhanced Shaft Alignment", October 2015

[9] Bureau Veritas, "Elastic Shaft Alignment (ESA)", April 2015

[10] NKK, Guidelines on Shafting Alignment, Nippon Kaiji Kyokai, 2006

[11] Murawski L., "Shaft Line Alignment Analysis Taking Ship Construction Flexibility and Deformations into Consideration", Marine Structures 18, pp. 62–84, 2005.

[12] Devanney J., Kennedy M., "The Down Ratchet and the Deterioration of Tanker Newbuilding Standards", Center for Tankship Excellence, 2003.

[13] Det Norske Veritas, "Damage to stern tube bearing and seals", Casualty Information June 2006

[14] Sverko D., "Hull Deflections Shaft Alignment Interaction, a Case Study", ABS Technical Papers 2005

[15] Mitsui J., Akutsu Y., "Analysis of Shaft Alignment Taking Oil Film Characteristics of Stern Tube Bearing into Consideration: Part 1, Theoretical Analysis", Bulletin of The Japan Society of Mechanical Engineers, 1984, 27(224), 317-324.

[16] Sverko D., "Shaft Alignment Optimization with Genetic Algorithms", ABS Technical Papers 2003.

[17] Sverko D., "A Solution to Robust Shaft Alignment Design", ABS Technical Papers 2006.

[18] Nikolakopouls P. G., Papadopoulos C. A., "A study of friction in worn misaligned journal bearings under severe hydrodynamic lubrication", Elsevier, Tribology International 41 (2008) 461–472

[19] Vassilopoulos L., "Static and Underway Alignment of Main Propulsion Shaft Systems", Naval Engineers Journal, May 1988.

[20] Nikolakopouls P. G., Papadopoulos C. A., "Non-linearities in misaligned journal bearings", Elsevier, Tribology International, Vol 27, 1994

[21] Bhusan B., "Modern Tribology Handbook", Boca Raton: CRC Press LLC, p. 1253, pp. 1262-1264, pp.1377-1378, 2001

[22] Ajith, Lakhmi J., "Evolutionary multiobjective optimization", London, Springer, 2005, pp. 1-6.

[23] Bodenhofer U., "Genetic Algorithms: Theory and Applications," Fuzzy.Logic.Lab.Linz, 2004

[24] Marseguerra M. and Zio E., "Genetic algorithms: Theory and applications in the safety domain," Trieste, 200, pp. 657-670.

[25] Nanopoulos S. A., "Development of optimization software using evolutionary algorithms. Applications in optimal machine design.", Athens: NTUA, 2016

[26] Coello C. Lamont G, "Evolutionary algorithms for solving multi-objective problems", Springer 2007

[27] Papadopoulos C. I., Nikolakopoulos P. G. & Kaiktsis L., "Elastohydrodynamic analysis and Pareto optimization of intact, worn and misaligned journal bearings," Meccanica, vol.46, pp.577-588, 2011
[28] Papadopoulos C.I., Efstathiou E.E., Nikolakopoulos P.G., Kaiktsis L., "Geometry Optimization of Textured 3-D Micro-Thrust Bearings", ASME Journal of Tribology, vol. 133, 041702, pp. 1-14, 2011.
[29] Vlachos O., "Elastic shaft alignment of marine vessel", Athens: NTUA, 2015.
[30] Koukoulopoulos E., "Software development for the solution of hydrodynamic lubrication problems in piston rings of two-stroke marine Diesel engines," Athens: NTUA, 2014.
[31] Raptis L., "Software development for the solution of hydrodynamic lubrication problems in main bearings of marine Diesel engines," Athens: NTUA, 2014.
[32] Kontaras G. N., "Computational and experimental study of journal bearings", Athens: NTUA, 2016.
[33] Σταματελόπουλος Δ., "Πειραματική μελέτη υδροδυναμικής λίπανσης σε ακτινικά έδρανα," Athens: NTUA, 2013
[34] "Test rig for journal bearings," Gdansk Univesristy of Technology Faculty of Mechanical Engineering Machine Design and Maintenace Department, pp. PG-II 1L.
[35] "Bearings and bearing metals", www.mae.ncsu.edu/eischen/courses/mae415/docs/JournalBearingDesign.pdf, Oct. 2013.
[36] Jha A.R., "Fundamentals of Finite Difference Methods", http://www.leb.eei.uni-erlangen.de/winterakademie/2011/report/content/course02/pdf/0203.pdf, Dec. 2013.
[37] Dufrane KF, Kannel JW, McCloskey TH, "Wear of steam turbine journal bearings at low operating speeds", J. Lubrication Technology, 105(3): 313-7, 1983
[38] Papadopoulos C.I., Kaiktsis L., Fillon M., Computational Fluid Dynamics Thermohydrodynamic Analysis of Three-dimensional Sector-Pad Thrust Bearings with Rectangular Dimples, ASME Journal of Tribology, Vol 136 (2014), pp. 011702-1-11, doi:10.1115/1.4025245.
[39] Sverko D. Sestan A., "Experimental determination of stern tube journal bearing behavior", BRODOGRANDNJA 61, pp. 130-141, 2010
[40] Kuroiwa R., Oshima A., Nishioka T, "Reliability improvement of stern tube bearing considering propeller shaft forces during ship turning", Mitsubishi Heavy Industries, Ltd, Sep. 2007
[41] Boedo S., Booker J. F., "Classical bearing misalignment and edge loading: A numerical study of limiting cases", Journal of Tribology, Vol. 126 / 535-541, July 2004
[42] Pinkus O., Bupara S. S., "Analysis of misaligned grooved journal bearings", Journal of Lubrication Tribology by ASME, vol. 101/503-509, 1979
[43] Ebrat O., Mourelatos Z., "Calculation of journal bearing dynamic characteristics including journal misalignment and bearing structural deformation", Taylor & Francis group, Trib. Transactions, 2003
[44] Chasalevris A., "A journal bearing with variable geometry for the reduction of the maximum amplitude during passage through resonance", Journal of Vibration & Acoustics, vol 134, 2012
[45] Andres L. S., "Hydrodynamic fluid film bearings and their effect on the stability of rotating machinery", RTO-EN-AVT-143, pp.10-1 –10-36, 2006
[46] Hirani H., Suh N.P., "Journal bearing design using multiobjective genetic algorithm and axiomatic design approaches", Elsevier ltd, Tribology International, 2005
[47] He T., Zou X. "Mixed –lubrication analysis of marine stern tube bearing considering bending deformation of stern shaft and cavitation", Elsevier ltd, Tribology international, 2014